ENGINEER

international scientific journal

ISSUE 3, 2026 Vol. 4
E-ISSN
3030-3893
ISSN
3060-5172



SLIB.UZ
Scientific library of Uzbekistan

A bridge between science and innovation

TOSHKENT DAVLAT TRANSPORT UNIVERSITETI
Tashkent state transport university

ENGINEER

A bridge between science and innovation

E-ISSN: 3030-3893

ISSN: 3060-5172

VOLUME 4, ISSUE 3

SEPTEMBER, 2026

engineer.tstu.uz

TASHKENT STATE TRANSPORT UNIVERSITY

ENGINEER

INTERNATIONAL SCIENTIFIC JOURNAL
VOLUME 4, ISSUE 3 SEPTEMBER, 2026

EDITOR-IN-CHIEF
SAID S. SHAUMAROV
Professor, Doctor of Sciences in Technics, Tashkent State Transport University
Deputy Chief Editor
Miraziz M. Talipov
Doctor of Philosophy in Technical Sciences, Tashkent State Transport University

---

Founder of the international scientific journal “Engineer” – Tashkent State Transport University, 100167, Republic of Uzbekistan, Tashkent, Temiryo‘lchilar str., 1, office: 465, e-mail: publication@tstu.uz.

The “Engineer” publishes the most significant results of scientific and applied research carried out in universities of transport profile, as well as other higher educational institutions, research institutes, and centers of the Republic of Uzbekistan and foreign countries.

The journal is published 4 times a year and contains publications in the following main areas:

- Engineering;
- General Engineering;
- Aerospace Engineering;
- Automotive Engineering;
- Civil and Structural Engineering;
- Computational Mechanics;
- Control and Systems Engineering;
- Electrical and Electronic Engineering;
- Industrial and Manufacturing Engineering;
- Mechanical Engineering;
- Mechanics of Materials;
- Safety, Risk, Reliability and Quality;
- Media Technology;
- Building and Construction;
- Architecture.

Tashkent State Transport University had the opportunity to publish the international scientific journal “Engineer” based on the **Certificate No. 1183** of the Information and Mass Communications Agency under the Administration of the President of the Republic of Uzbekistan. **E-ISSN: 3030-3893, ISSN: 3060-5172.** Articles in the journal are published in English language.

ENGINEER
INTERNATIONAL SCIENTIFIC JOURNAL
VOLUME 4, ISSUE 3 SEPTEMBER, 2026

EDITORIAL BOARD

Oksana D. Pokrovskaya
Associate Professor, Doctor of Technical Sciences, Emperor Alexander I St. Petersburg State Transport University

Oleg R. Ilyasov
Professor, Doctor of Biological Sciences, Ural State Transport University

Timur T. Sultanov
Associate Professor, Candidate of Technical Sciences, L.N. Gumilyov Euroasian National University

Dmitriy V. Efanov
Professor, Doctor of Sciences in Technics, Russian University of Transport (MIIT)

Oyum T. Balabayev
Associate Professor, Candidate of Technical Sciences, Abylkas Saginov Karaganda Technical University

Elena V. Shchipacheva
Professor, Doctor of Sciences in Technics, Tashkent State Transport University

Ulugbek Z. Shermukhamedov
Professor, Doctor of Sciences in Technics, Tashkent State Transport University

Abdumalik N. Rizaev
Professor, Doctor of Sciences in Technics, Tashkent State Transport University

Nazirjan M. Aripov
Professor, Doctor of Sciences in Technics, Tashkent State Transport University

Journal Engineer ISSN: 3030-3893 Volume:4| Issue:3| 2026

Received: 2 July 2026 | **Accepted:** 13 August 2026 | **Published:** 30 September 2026

Assessment and improvement of constructive safety of the Damas light passenger vehicle

Kh.T. Tuychiev[1][a], Kh.T. Tuychiev[1][b]

[1]Andijan state technical institute, Andijan, Uzbekistan

Abstract: The article is devoted to assessing and improving the constructive safety of the Damas light passenger vehicle widely used in Uzbekistan. The study analyzes the influence of geometric parameters, vehicle stability, braking performance, and active safety systems on overall operational safety. Vehicle stability was evaluated using the Static Stability Factor (SSF), rollover resistance indicators, and braking performance calculations. The obtained results showed that the vehicle's constructive safety is significantly affected by its center of gravity position, track width, and the absence of modern active safety systems. The calculated stability indicators revealed an increased rollover risk during high-speed cornering maneuvers. A comparative analysis demonstrated that the implementation of Anti-lock Braking Systems (ABS) and Electronic Stability Control (ESC) could significantly improve vehicle stability and controllability under critical driving conditions. Based on the findings, engineering recommendations aimed at enhancing vehicle safety, reducing accident risk, and improving operational reliability were developed. The proposed measures can contribute to improving road safety and increasing the efficiency of light passenger vehicle operation under the road and climatic conditions of Uzbekistan.

Keywords: constructive safety, vehicle stability, Damas vehicle, rollover resistance, braking performance, ABS, ESC, road safety, vehicle dynamics, operational reliability

1. Introduction

The rapid growth of the global automotive industry has significantly increased the number of vehicles operating on roads worldwide. Along with the expansion of vehicle ownership, issues related to road traffic safety have become one of the most important challenges facing modern transportation systems. According to international studies, vehicle design characteristics directly affect the severity of traffic accidents, passenger protection levels, vehicle stability, and overall operational safety [1-5]. Therefore, improving the constructive safety of motor vehicles remains a priority area of research in automotive engineering and transportation safety science.

In recent years, substantial efforts have been undertaken to improve vehicle safety through the implementation of advanced braking systems, electronic stability control technologies, traction control systems, reinforced body structures, and intelligent driver assistance systems. These technological developments have considerably reduced accident rates and injury severity in modern passenger vehicles [4,5]. However, a significant proportion of vehicles currently in operation in developing countries continue to utilize relatively outdated design solutions that do not fully satisfy contemporary safety requirements.

The Republic of Uzbekistan has experienced a steady increase in vehicle ownership during the last decade. The expansion of the national vehicle fleet has contributed positively to economic development and population mobility. At the same time, the increasing traffic intensity has led to a growing number of road traffic accidents, emphasizing the necessity of improving vehicle safety characteristics. Government programs aimed at modernizing the transport sector and enhancing road safety have identified the improvement of vehicle operational and constructive safety as a strategic objective for sustainable transportation development [18].

Among the vehicles widely used in Uzbekistan, the Damas light passenger vehicle occupies a special position due to its affordability, maneuverability, and suitability for urban and rural transportation. The vehicle is extensively used for passenger transportation, small-scale commercial activities, and family mobility. Despite its widespread utilization, the Damas vehicle possesses several design limitations associated with its relatively narrow track width, high center of gravity, lightweight body structure, and lack of modern active safety systems such as Anti-lock Braking System (ABS), Electronic Stability Control (ESC), and Traction Control System (TCS).

Numerous studies have demonstrated that vehicle stability during braking, cornering, and emergency maneuvers is strongly influenced by geometric parameters, weight distribution, suspension characteristics, and tire-road interaction conditions. Insufficient stability may lead to skidding, rollover accidents, and loss of vehicle controllability, particularly under adverse road and weather conditions. Consequently, comprehensive assessment of constructive safety parameters is necessary to identify potential risks and develop effective engineering solutions for improving vehicle safety performance[1-3,10].

Previous investigations have mainly focused on vehicle dynamic behavior, braking efficiency, rollover resistance,

[a] https://orcid.org/0009-0000-1117-7862
[b] https://orcid.org/0009-0003-1861-6997

and active safety technologies for modern passenger cars. However, limited attention has been paid to the constructive safety assessment of compact light passenger vehicles operating under the specific road and climatic conditions of Uzbekistan. In particular, the stability characteristics and safety improvement potential of the Damas vehicle remain insufficiently studied, creating a significant research gap in the existing literature.

Therefore, the objective of this study is to evaluate the constructive safety characteristics of the Damas vehicle by analyzing its stability, braking performance, and operational safety indicators, as well as to develop technically justified recommendations for improving its safety level. The obtained results may contribute to enhancing road safety, reducing accident risks, and improving the operational reliability of light passenger vehicles used under typical operating conditions in Uzbekistan.

LITERATURE REVIEW

Vehicle safety has become one of the most actively developing research areas in modern automotive engineering. The increasing number of vehicles worldwide has led researchers to focus on improving both active and passive safety systems in order to reduce road traffic accidents and their consequences. Active safety systems are designed to prevent accidents, while passive safety systems aim to minimize injuries when accidents occur.

Numerous studies have confirmed that vehicle stability is one of the key indicators of constructive safety. According to the research conducted by Thomas D. Gillespie, the stability of a vehicle depends on its geometric dimensions, center of gravity position, wheelbase, track width, suspension characteristics, and tire-road interaction conditions [1]. Vehicles with a high center of gravity and narrow track width are generally more susceptible to rollover and loss of control during cornering maneuvers. These findings are particularly relevant for compact passenger vehicles widely used in urban transportation systems.

Considerable attention has been devoted to the development and implementation of modern active safety technologies. Studies carried out by the National Highway Traffic Safety Administration demonstrated that Anti-lock Braking Systems (ABS) significantly improve vehicle controllability during emergency braking by preventing wheel lock-up. The introduction of ABS technology has reduced braking-related accidents and improved vehicle stability on slippery road surfaces [4].

Further advancements in vehicle safety were achieved through the implementation of Electronic Stability Control (ESC). Research conducted by European New Car Assessment Programme indicated that ESC systems can reduce the risk of rollover accidents by approximately 30–50% and significantly improve directional stability during critical driving situations [5]. These systems continuously monitor vehicle motion parameters and automatically apply braking forces to individual wheels when instability is detected.

Vehicle rollover resistance has also been extensively investigated by many researchers. Studies by Rajesh Rajamani emphasized that rollover accidents are strongly associated with the relationship between vehicle track width and center of gravity height [2]. The Static Stability Factor (SSF) is commonly used as an indicator for evaluating rollover propensity. Vehicles with higher SSF values generally demonstrate better resistance to rollover under dynamic driving conditions.

Recent investigations have focused on improving vehicle safety through computer-aided simulation and mathematical modeling. Finite Element Analysis (FEA), multibody dynamic simulation, and virtual crash testing have become standard engineering tools for evaluating vehicle behavior before physical prototype manufacturing [3,10,13]. Such approaches reduce development costs while increasing the reliability of safety assessments.

Researchers in Uzbekistan have mainly concentrated on vehicle operational reliability, technical diagnostics, traffic safety, and transportation efficiency. The works of Hamraqulov, Fayzullayev, Sidiqnazarov and other scholars have contributed significantly to understanding vehicle operation under local road and climatic conditions. However, most studies have focused on technical operation and maintenance issues rather than constructive safety assessment of light passenger vehicles [6-8].

Despite the considerable progress achieved in vehicle safety research, the constructive safety characteristics of compact light passenger vehicles operating under the specific conditions of Uzbekistan remain insufficiently investigated. In particular, there is limited scientific information regarding the stability, braking performance, rollover resistance, and safety improvement potential of the Damas vehicle. This gap in the existing literature highlights the necessity of conducting comprehensive research aimed at evaluating its constructive safety parameters and developing practical recommendations for their improvement.

Therefore, the present study focuses on assessing the constructive safety of the Damas vehicle through analysis of stability indicators, braking characteristics, and potential engineering measures intended to enhance operational safety under real operating conditions.

2. Methodology

Research Object. The object of this study is the Damas light passenger vehicle, which is widely used in Uzbekistan for urban and suburban transportation. Due to its compact dimensions, low fuel consumption, and economic affordability, the Damas vehicle occupies an important position in the national transport system. However, compared with modern passenger vehicles, its constructive safety characteristics require further investigation.

The main technical specifications of the investigated vehicle are presented in Table 1.

Table 1

Main technical parameters of the Damas vehicle

Parameter	Value
Vehicle type	Light passenger vehicle
Engine displacement	0.8 L
Vehicle mass	850 kg
Wheelbase	1840 mm
Overall length	3485 mm
Overall width	1400 mm
Overall height	1920 mm

https://doi.org/10.56143/3030-3893-2026-3-5-9

Ground clearance	160 mm
Seating capacity	7 persons

The technical characteristics were obtained from the manufacturer's specifications and vehicle operation manuals [19].

Method for Evaluating Vehicle Stability. Vehicle stability was assessed using geometric parameters affecting rollover resistance and lateral stability.

One of the most important indicators of constructive safety is the Static Stability Factor (SSF), which can be determined using the following equation:

$$SSF = \frac{T}{2H}$$

where:

T – vehicle track width, m;

H – height of the center of gravity, m.

The Static Stability Factor characterizes the resistance of the vehicle to rollover during cornering maneuvers. Higher SSF values indicate greater vehicle stability [1,2].

To determine the critical rollover speed, the following relationship was used:

$$V_r = \sqrt{gR\frac{T}{2H}}, [2,10]$$

where:

V_r – rollover speed, m/s;

g – gravitational acceleration (9.81 m/s²);

R – turning radius, m;

T – track width, m;

H – center of gravity height, m.

This equation allows estimation of the vehicle speed at which rollover becomes theoretically possible during cornering [21].

Braking Performance Assessment. Vehicle braking efficiency was evaluated by determining braking distance under dry asphalt road conditions.

The braking distance was calculated according to:

$$S_b = \frac{V^2}{2g\varphi}, [11,15]$$

where:

S_b – braking distance, m;

V – initial vehicle speed, m/s;

g – gravitational acceleration, m/s²;

φ – tire-road adhesion coefficient.

To account for driver reaction time, total stopping distance was determined using:

$S_t=S_r+S_b$

where:

S_t – total stopping distance, m;

S_r – reaction distance, m;

S_b – braking distance, m.

These indicators are widely used in vehicle safety analysis and transportation engineering studies [22].

Safety Improvement Assessment. To improve the constructive safety of the Damas vehicle, several engineering measures were analyzed:

- installation of an Anti-lock Braking System (ABS);
- implementation of an Electronic Stability Control (ESC) system;
- optimization of vehicle mass distribution;
- reduction of the center of gravity height;
- improvement of suspension stiffness characteristics.

The effectiveness of these measures was evaluated through comparative analysis of stability and braking indicators before and after implementation. The expected improvement level was estimated using published safety-performance data reported in previous international studies [12,13,16].

Data Processing and Analysis. All calculations were performed using analytical methods commonly applied in vehicle dynamics and transportation engineering. The obtained results were processed and compared with safety requirements established in international vehicle safety standards and recommendations.

The calculated stability coefficient, rollover resistance parameters, and braking characteristics were used as the main criteria for evaluating the constructive safety level of the Damas vehicle under operating conditions typical of Uzbekistan.

3. Results

Evaluation of Vehicle Stability Characteristics. The constructive safety of the Damas vehicle was evaluated based on its geometric dimensions, weight distribution, and stability indicators. Particular attention was given to rollover resistance, as compact passenger vehicles with relatively high body structures are more susceptible to instability during cornering maneuvers.

Using the geometric parameters of the Damas vehicle, the Static Stability Factor (SSF) was calculated according to Equation (1). The vehicle track width was assumed to be 1.22 m, while the estimated center of gravity height was 0.75 m.

$$SSF = \frac{1{,}22}{2 \times 0{,}75} = 0{,}81$$

The obtained SSF value indicates a moderate level of rollover resistance. According to international vehicle safety studies, passenger vehicles with SSF values below 1.0 require additional attention regarding stability improvement measures [2,4,5].

To estimate rollover resistance under operating conditions, the critical rollover speed was determined for a turning radius of 50 m:

$$V_r = \sqrt{9{,}81 \times 50 \times 0{,}81}$$

$$V_r = 19{,}91\ m/s$$

$$V_r = 71{,}8\ km/h$$

The results show that the Damas vehicle may approach rollover conditions when negotiating relatively sharp curves at speeds exceeding approximately 72 km/h. This value is lower than that of many modern passenger vehicles equipped with advanced stability control systems.

Table 2

Calculated stability indicators of the Damas vehicle

Parameter	Value
Track width (m)	1.22

https://doi.org/10.56143/3030-3893-2026-3-5-9

Center of gravity height (m)	0.75
Static Stability Factor (SSF)	0.81
Turning radius (m)	50
Critical rollover speed (km/h)	71.8

The obtained results indicate that vehicle stability can be significantly influenced by speed selection, road geometry, and loading conditions.

Braking Performance Analysis

Vehicle braking performance was assessed under dry asphalt road conditions with an adhesion coefficient of 0.75. Calculations were performed for a vehicle speed of 60 km/h.

The braking distance was determined using Equation (3):

$$S_b = \frac{V^2}{2g\varphi} = \frac{16{,}67^2}{2\times 9{,}81\times 0{,}75} = 18{,}9\ m$$

Considering an average driver reaction time of 1 second, the reaction distance becomes:

$S_r = 16.67 \times 1 = 16.67$ m

The total stopping distance is therefore:

$S_t = 16.67 + 18.9 = 35.57$ m

Table 3

Braking performance indicators

Parameter	Value
Vehicle speed (km/h)	60
Adhesion coefficient	0.75
Braking distance (m)	18.9
Reaction distance (m)	16.7
Total stopping distance (m)	35.6

The analysis demonstrates that more than 45% of the total stopping distance is associated with driver reaction time. Consequently, driver awareness and active safety systems play an important role in accident prevention.

Comparative Analysis of Safety Systems

A comparison was conducted between the Damas vehicle and a modern passenger vehicle equipped with advanced active safety systems. The comparison focused on safety-related equipment influencing vehicle stability and braking efficiency.

Table 4

Comparison of safety-related features

Safety Parameter	Damas	Modern Passenger Vehicle
ABS	No	Yes
ESC	No	Yes
Traction Control System	No	Yes
Brake Assist	No	Yes
Rollover Stability Control	No	Yes

The comparison reveals that the Damas vehicle lacks several active safety technologies commonly used in modern automotive design. The absence of these systems may increase the probability of skidding, wheel lock-up, and rollover during emergency maneuvers.

Proposed Safety Improvements. Based on the obtained results, several engineering measures were proposed to improve the constructive safety of the Damas vehicle:

1. Installation of an Anti-lock Braking System (ABS);
2. Introduction of Electronic Stability Control (ESC);
3. Optimization of suspension parameters;
4. Reduction of the center of gravity height;
5. Improvement of tire-road adhesion characteristics.

Previous studies indicate that ABS implementation may reduce braking-related accidents by approximately 20–25%, while ESC systems can decrease rollover risk by up to 40% [5,12].

Table 5

Expected safety improvement after implementation of proposed measures

Improvement Measure	Expected Safety Improvement
ABS installation	20–25%
ESC implementation	30–40%
Suspension optimization	10–15%
Lower center of gravity	12–18%
Improved tire performance	5–10%

The implementation of these measures would significantly increase vehicle stability and reduce accident risks under typical operating conditions in Uzbekistan.

Discussion. The obtained results demonstrate that the constructive safety level of the Damas vehicle is largely determined by its geometric configuration and the absence of modern active safety technologies. The calculated Static Stability Factor of 0.81 indicates acceptable stability for normal operating conditions; however, rollover risk increases considerably at higher speeds and during sudden steering maneuvers.

Braking analysis revealed that stopping distance remains within acceptable limits under dry road conditions. Nevertheless, the absence of ABS may negatively affect vehicle controllability during emergency braking, especially on wet or low-adhesion road surfaces.

Comparative analysis showed that the implementation of modern active safety systems could substantially improve vehicle stability and accident prevention capabilities. Therefore, modernization of the braking and stability control systems should be considered one of the most effective approaches to enhancing the constructive safety of light passenger vehicles operating in Uzbekistan [12,13,20–23].

4. Conclusion

The study evaluated the constructive safety characteristics of the Damas light passenger vehicle based on stability and braking performance indicators. The obtained results showed that the vehicle's safety level is significantly influenced by its geometric parameters, center of gravity position, and the absence of modern active safety systems.

The calculated Static Stability Factor (SSF) of 0.81 and the critical rollover speed of 71.8 km/h indicate that vehicle stability may decrease during high-speed cornering and emergency maneuvers. Braking analysis demonstrated that the total stopping distance at 60 km/h is approximately 35.6 m under dry road conditions.

The research also revealed that the implementation of modern safety technologies such as ABS and ESC can significantly improve vehicle stability, braking efficiency, and rollover resistance. Therefore, introducing active safety systems, optimizing suspension parameters, and improving weight distribution are recommended as effective measures for enhancing the constructive safety of the Damas vehicle.

The proposed recommendations can contribute to improving road safety and increasing the operational reliability of light passenger vehicles under the operating conditions of Uzbekistan.

References

[1] Thomas D. Gillespie. Fundamentals of Vehicle Dynamics. Warrendale, PA: Society of Automotive Engineers (SAE), 1992. – 495 p.

[2] Rajesh Rajamani. Vehicle Dynamics and Control. 2nd Edition. New York: Springer, 2012. – 486 p.

[3] Reza N. Jazar. Vehicle Dynamics: Theory and Application. New York: Springer, 2017. – 1108 p.

[4] National Highway Traffic Safety Administration. Traffic Safety Facts Annual Report. Washington DC, 2023.

[5] European New Car Assessment Programme. Vehicle Safety Assessment Protocols. Brussels, 2023.

[6] Hamraqulov O., Magdiyev Sh. Avtomobillarning texnik ekspluatatsiyasi. Toshkent: O‘zbekiston, 2001. – 448 b.

[7] Fayzullayev E.Z. Transport vositalarining tuzilishi va nazariyasi. Toshkent: Yangi asr avlodi, 2006. – 375 b.

[8] Sidiqnazarov Q.M. Avtomobillarning texnik ekspluatatsiyasi. Toshkent: Voris-Nashriyot, 2006. – 488 b.

[9] Mamatov X.M. Avtomobillar. 2-qism. Toshkent, 2008. – 320 b.

[10] Wong J.Y. Theory of Ground Vehicles. 4th Edition. New York: Wiley, 2008. – 592 p.

[11] Bosch GmbH. Automotive Handbook. 10th Edition. Stuttgart: Robert Bosch GmbH, 2018. – 1168 p.

[12] Heisler H. Advanced Vehicle Technology. 3rd Edition. Oxford: Butterworth-Heinemann, 2021. – 784 p.

[13] Gobbi M., Mastinu G. Road and Off-Road Vehicle System Dynamics Handbook. CRC Press, 2019. – 1070 p.

[14] ISO 26262:2018. Road Vehicles – Functional Safety. Geneva: International Organization for Standardization, 2018.

[15] UNECE Regulation No. 13-H. Uniform Provisions Concerning the Approval of Passenger Cars with Regard to Braking. Geneva, 2022.

[16] ГОСТ 33997–2016. Колесные транспортные средства. Требования к безопасности в эксплуатации и методы проверки. Москва, 2016.

[17] To‘ychiyev X.T. Road Transport Safety and Vehicle Operation under Uzbekistan Conditions. Andijan, 2023.

[18] O‘zbekiston Respublikasi Prezidentining 2022-yil 28-yanvardagi PF–60-son Farmoni. “2022–2026 yillarga mo‘ljallangan Yangi O‘zbekiston taraqqiyot strategiyasi to‘g‘risida”.

Information about the author

Khasanboy Tuychiev	Andijan State Technical Institute, senior teacher, PhD E-mail: xasanboy.toychiyev.toxirogli@gmail.com Phone: +99899-368-88-39 https://orcid.org/0009-0000-1117-7862
Khusanboy Tuychiev	Andijan State Technical Institute, assistant E-mail: husanboytoychiyev55@gail.com Phone: +998 (88) 992-42-20 https://orcid.org/0009-0003-1861-6997

Journal Engineer ISSN: 3030-3893 Volume:4| Issue:3| 2026

Received: 8 July 2026 | **Accepted:** 19 August 2026 | **Published:** 30 September 2026

Comparison of the switch control circuit with main supply and central supply circuit, and analysis of the sequence of operation of the НПС block

A.R. Azizov[1][a], F.S. Sindarov[1][b]

[1]Tashkent state transport university, Tashkent, Uzbekistan

Abstract: Railway switch control systems on railway are essential to ensure safe and efficient traffic. In this article, the development of automated control systems of railway switches, their technological basis, safety issues and energy efficiency improvement approaches are considered. The main attention is focused on the production and practical use of a microelectronic alternative version of the relay НПС block, which belongs to the dialing group, of modern control blocks, in particular, based on the technical requirements for railway automation and telemechanics equipment, and their harmonious operation with telemechanics tools.

Keywords: Class II relays, ВУ, ПВУ, МУ, ПУ relays, Switch Control Circuit. НПС block, Current sensor, optocouplers, light-emitting diodes, modern microcontroller boards, dial group block.

1. Introduction

Modern practice has shown that relay, mechanical, processor-relay railway transport automation and telemechanics systems have a number of disadvantages, their use is limited and technically ineffective. Currently, relay devices that perform interconnection of switches and signals are increasingly being replaced by microprocessor systems. This is due to the following reasons.

Firstly, maintenance of microelectronic systems compared to relay systems, the high cost of such systems shows that their implementation is economically feasible.

Secondly, indicators of microelectronic systems due to the use of excess reserves of individual constituent elements of the system and advanced diagnostic systems.

Thirdly, by providing employees with quick information and by expanding the functional capabilities of the systems due to the simple integration of railway automation and telemechanics microelectronic systems into high-level train traffic control systems (DM, control centers, etc.).

Taking into account the above, in this article, I propose to develop a model of a microelectronic НПС unit consisting of microelectronic devices, intended for use in centralizing relay-processors and microprocessors of the dial group.

2. Research methodology

In railway automation and telemechanics, much information about the switch control circuit is provided in standard albums and typical solutions. In this article, I will explain in detail which types of power supply are used in switch control depending on the size of the station and the location of the switch: the difference between the central supply and the main supply switch control circuits, why the main supply is necessary, and how the **НПС block (Figure 1)**, which belongs to the setting group serving route formation in the process of controlling distant switches with main supply, operates through current flow circuits of its constituent relays in sequence.

The main difference between the switch control circuit with main supply and the switch control circuit with central supply is that, instead of the polarized relay **Р** in the switch electric drive, a **ПС** combined relay of type СКПР3-2800 is installed. In the switch drive control circuit at the central post, since direct current with a voltage of 220 V is used for the control circuits, a 0.5 A fuse is installed as protection. To reduce the nominal voltage of the direct current in the control current, a 12 kΩ resistor is connected in series with the **ПС** relay in the circuit produced by the selenium rectifier valve. When such a resistor is connected, if the control circuit is supplied with alternating current of 50 Hz frequency, the maximum distance of the switch electric drive is 2 km. When the cable length is between 2 km and 3.5 km, the 12 kΩ resistor is replaced with a 10 kΩ resistor, and the СКТ-I transformer with its I and II windings connected in series is also connected in series. A capacitor with a capacitance of 4 μF connected in parallel to the **ПС** relay windings shunts the alternating component and protects the relay from armature vibration. When the switch is moved from the plus position to the minus position, the working battery voltage of 220 V is supplied to the **ПС** relay through the 12 kΩ resistor. In this case, the current in the **ПС** relay circuit is sufficient to move the polarized armature of the relay, but not enough to attract the neutral armature. After the polarized armature is conducted through contacts 121–123, the **ПС** relay is shunted with the 12 kΩ resistor, and the **ПС** relay attracts its neutral armature, connecting the working current main line to the electric drive windings. The neutral armature The neutral armature of the **ПС** relay shunts the 12 kΩ resistor through contacts 31–32 during the switch transfer, which ensures precise relay operation when the switch is not fully transferred and the drive is reversing.

[a] https://orcid.org/0000-0001-8404-3013
[b] https://orcid.org/0009-0007-2900-0046

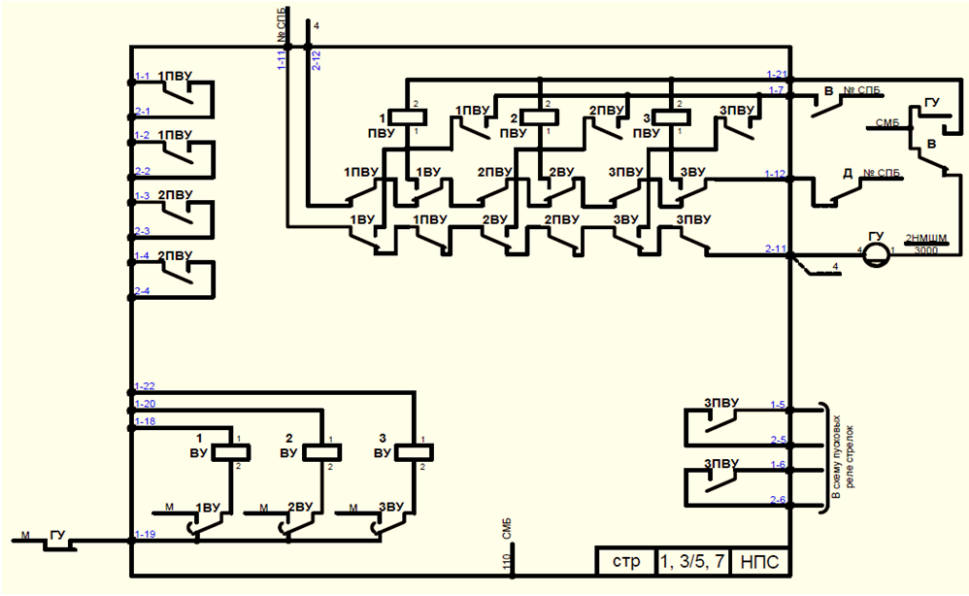


Fig. 1. Principal Circuit Diagram of the НПС Block

The switch electric drive control circuit with main supply is considered the most economical if the working current main line is intended to transfer one or at most two switches simultaneously. In route interlocking, the number of switches transferred simultaneously is not constant, but depends on the length of the route and the current position of the switches before the route is set. Therefore, when the working current main line is designed to transfer more switches simultaneously, the voltage drop in it exceeds the permissible value, which leads to the slowing down or complete stoppage of switch transfer.

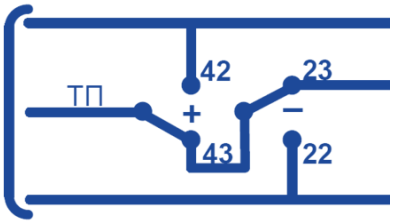


Fig. 2. Switch Commutator

A scheme has been developed to limit the number of switches transferred simultaneously according to the calculated cross-section of the main line. Since switches located at long distances are supplied specifically by the main supply, each switch commutator with main supply uses an **НПС** block consisting of two types of relays inside: the auxiliary control relay **ВУ** and its repeater **ПВУ** relay. One **НПС** block is installed for every three switch commutators. In addition, a group control relay **ГУ** of type **НМШ2-3000** is installed for all switches on this main line.

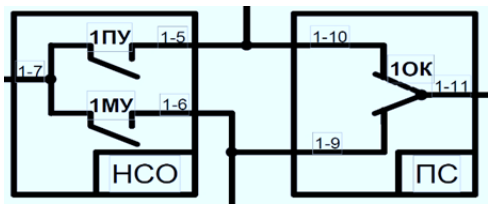


Fig. 3.1. МУ Relay Contact and Figure 3.2. ОК Relay Polarized Contact

During the route setting process, the **ПУ** or **МУ** relay of the switches included in the route is energized. In addition, according to the following circuit: **ТП** through contacts **41 - 43** and **21 - 23** of the switch commutator **(Figure 2),** the contact of the control relay (for example, **МУ** in **Figure 3.1**), when the switch is transferred to the minus position and the **ОК** relay contact (**Figure 3.2**), which monitors that the switch is in the plus position, only the **ВУ** relay of the switches that need to be thrown is energized.

Below, the operating sequence of **three ВУ** relays are expressed example of the **1VU** (**Figure 4**), relay and its circuits and diagrams. The **1VU** relay is energized when the **П (+24V)** supply comes to terminal **1-18** and the **М (-24V)** supply simultaneously comes to terminal **1-19**, bringing it into a current-carrying state. It then self-locks until the switch transfer is completed and the corresponding control is obtained.

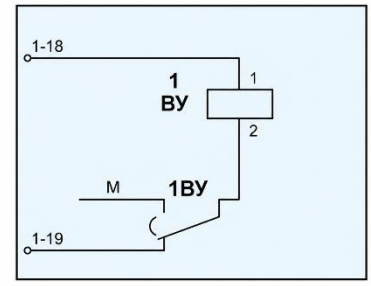


Fig. 4. Circuit and Diagram of the 1ВУ Relay in Energized State

The **2ВУ** relay is also energized when the **П (+24V)** supply comes to terminal **1-20** and the **М (-24V)** supply simultaneously comes to terminal **1-19**, bringing it into a current-carrying state. It then self-locks until the switch transfer is completed and the corresponding control is obtained. The operation of the **3VU** relay is similar to the above two relays, that is, when the **П (+24V)** supply comes

https://doi.org/10.56143/3030-3893-2026-3-10-13

ENGINEER

to terminal **1-22** and the **M (-24V)** supply simultaneously comes to terminal **1-19**, it is energized and self-locks until the switch transfer is completed and the corresponding control is obtained.

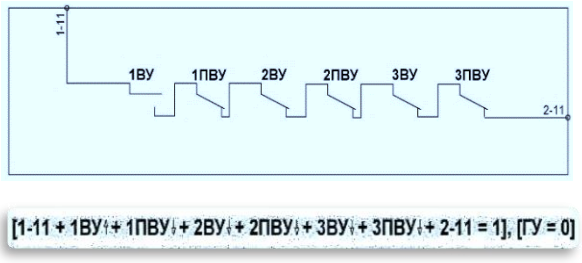


Fig. 5. Circuit and Diagram of the ГУ Relay in De-energized State

When any of the **ВУ** relays is energized, their contacts interrupt the circuit of the group control relay **ГУ (Figure 5),** causing it to de-energize and release its armature with a delay of 0.8 seconds.

Through the front contacts of the **ГУ** relay, the excitation circuit of the **ВУ** relay is interrupted, while through its back contacts the circuits for energizing the **ПВУ** relay are connected. The delay of the **ГУ** relay ensures that the sequential excitation circuit of the **ПВУ** relay is connected only after all the **ВУ** relays of the switches included in the route have been activated. The front contacts of the **ПВУ** relay are introduced into the excitation circuit of the **НПС** relay in series with the contacts of the **ПУ** and **МУ** relays belonging to the switch in the switch control circuit.

The connection scheme of the **ПВУ** relay is designed in such a way that, depending on the calculated cross-section of the main line, it ensures the simultaneous excitation of one or two **ПВУ** relays, which in turn allows one or two switches to be thrown simultaneously. Below, the operating sequence of all **1ПВУ**, **2ПВУ**, and **3ПВУ** relays is expressed through circuits and diagrams.

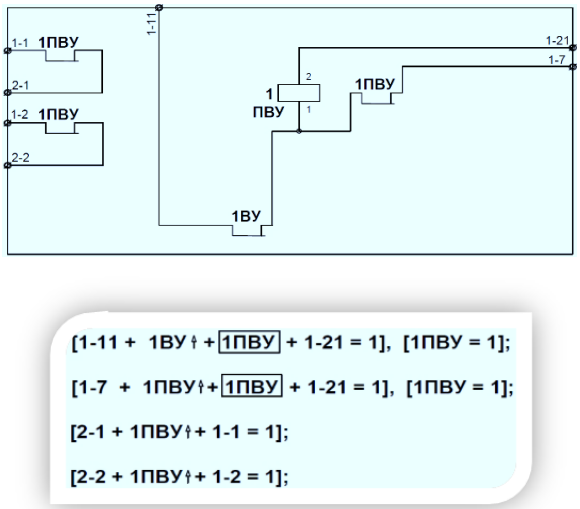


Fig. 6. Circuit and Diagram of the 1ПВУ Relay in Energized State

When it is necessary to ensure the simultaneous switching of two Switch Control Circuit, a second circuit with contacts marked by dashed lines is connected to the scheme. After the **ПВУ** relays are energized, a self-locking circuit is activated through their own contacts.

If double-sided control of switches is available in the main supply area, the second excitation circuit of the **ПВУ** relay is interrupted through the contact of the **Д** relay, which cancels centralization.

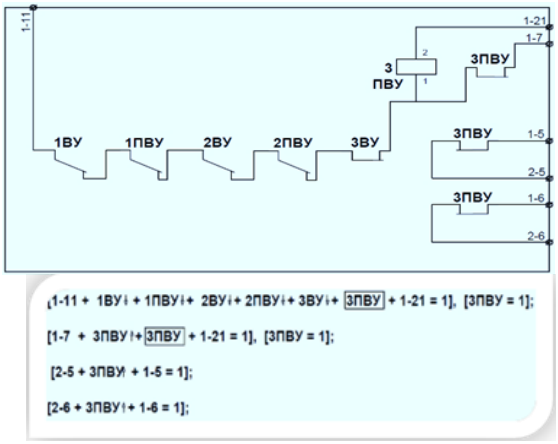


Fig. 7. Circuit and Diagram of the 3ПВУ Relay in Energized State

In addition to the main excitation circuit, the **ПВУ** relay has a locking circuit through its own contacts and the front contacts of the **В** relay. Such locking ensures that the **ПВУ** relay can only be connected for the next switch operation when there is no current in the working supply line. This is necessary to prevent disconnecting the bus intended for simultaneous operation of two switches while one of them has not yet been fully transferred.

3. Conclusion

Scientific analyses in railway automation and telemechanics demonstrate that **centralized supply** and **trunk supply** schemes differ significantly in both technical and functional aspects. While the centralized supply scheme is suitable for small stations, the trunk supply scheme ensures efficiency in managing switches located at long distances in large stations.

In trunk supply schemes, the use of the **ПС** combined relay, resistors, transformers, and capacitors provides mechanisms to control voltage drops and guarantees stable relay operation. This configuration ensures energy efficiency, precise monitoring, and high reliability in route centralization processes.

Scientifically grounded results

Energy efficiency: The trunk supply scheme allows one or two switches to be operated simultaneously according to the calculated section, ensuring rational use of electrical energy.

Monitoring accuracy: Sequential operation of the polarized and neutral armatures of the **ПС** relay prevents incorrect reversals and ensures reliable monitoring of switch positions.

Route centralization: Sequential activation of **ВУ** and **ПВУ** relays guarantees safe and orderly control of switches included in the route.

Blocking circuits: The blocking function of the **ПВУ** relay ensures that subsequent switches are connected only when the trunk line is free of current, thereby strengthening

operational safety.

Recommendations

Station design: For large stations, trunk supply schemes should be prioritized, as they effectively manage distant switches.

Energy saving: Optimal selection of resistors and transformers in trunk supply schemes can reduce energy consumption.

Safety enhancement: Improving PVU relay blocking circuits will further increase safety in route centralization.

Technical maintenance: Regular diagnostics and preventive inspections of relays and transformers ensure stable system performance.

Innovative application: Introducing modern electronic monitoring blocks and digital relays can significantly improve the efficiency of trunk supply schemes.

Practical applications

Large stations: Trunk supply schemes enable fast and safe route centralization.

Long-distance switches: They serve as energy-efficient and reliable solutions for managing remote switches.

Modernization projects: Trunk supply schemes can be adopted as key technical solutions when upgrading existing centralized supply systems.

In conclusion, the trunk supply switch control scheme is not only technically efficient but also plays a crucial role in ensuring railway transport safety. These scientific findings and recommendations highlight that the application of trunk supply schemes in railway automation systems is a decisive factor in improving station management efficiency and ensuring the stable operation of transport infrastructure.

References

[1] Azizov AR, Ametova EK Developing of microelectronic block NSS . // IJARSET, India: Vol. 6, Issue 3, March 2019, pp. 8563-8567 . (05.00.00; No. 8) .

[2] Azizov A.R., Ametova E.K. Monitoring the technical condition of the microelectronic unit of the NSS as a problem of pattern recognition. // Technical sciences and innovation. Tashkent State Technical University, 2019. No. 1 . From 20-25. (05.00.00; No. 16) .

[3] Ametova E.K., Azizov A.R. Theory of Petri nets in the development and study of the mathematical model of the NSO block. // FarPI ITZh. 20

[4] Ametova E., Azizov A., Yuldashev Sh. Microprocessor technology in the devices railway automation and telemechanics. Asian Journal of Research , 2020 . SJIF 6.1, IFS 3.7.

[5] Bestemyanov P.F. Monitoring the correct functioning of microprocessor devices of automatic speed control systems of subway trains.// Interuniversity collection of scientific papers. - M.: MIIT, Issue 862, 1992.

[6] Vasiliev B.V., Kozlov B.A., Tkachenko L.G. Reliability and efficiency of radio-electronic devices. - M.: Sov.radio, 1964.-151 p.

[7] Vulman I.D. Determination of the optimal frequency of preventive monitoring of radio engineering devices with a stationary flow of failures. - Radio Engineering, 1973, No. 9, pp. 41-45.

[8] Gnedenko B.V., Belyaev Yu.K., Soloviev A.D. Mathematical methods in reliability theory (main characteristics of reliability and their statistical analysis). Moscow: Nauka, 1965. - 254 p.

[9] Koida A.N., Mozgalevsky A.V. Organization of diagnostics of objects of complex structure. — In the book: Technical diagnostics, operation of control computers. Collection of scientific papers. — Kyiv: Naukova Dumka, 1980. P.63-71.

[10] Aksenova G.P. On functional diagnostics of discrete devices in conditions of work with inaccurate data// Problems of Management. - 2008. - No. 5. P. 62-66.

[11] Drozdov A. V. Working diagnostics of safe information and control systems / A. V. Drozd, V. S. Kharchenko, S. G. Antoshchuk, Yu. V. Drozd, M. A. Drozd, Yu. Yu. Sulima: under the supervision of A. V. Drozd and V. S. Kharchenko. - Kharkov: National Aerospace University named after N.E. Zhukovsky "KHAI", 201 2. - 614 p.

[12] Efanov, D. V. Functional control and monitoring of railway automation and telemechanics devices: monograph - SP6. FGBOU VO PGUPS, 2016. - 171 p.

[13] Kalyavin, V.P. Reliability and diagnostics of motor vehicles / V. P. Kalyavin, N. A. Davydov. - SP6.: Elmore, 2014. - 480 p.

[14] Karibsky, V. V. Fundamentals of technical diagnostics / V. V. Karibsky, P. P. Parkhomenko, E. S. Sogomonian, V. F. Khalchev; edited by P. P. Parkhomenko. — Moscow: Energiya, 1976. — 464 p.

[15] Lisenkov V. M. Statistical theory of train traffic safety: textbook for universities. - M.: VINITI RAS, 1999. - 332 p.

[16] Shamanov V.I. Methods for optimizing technical maintenance of automation systems // Automation in transport. - 2016. - Vol.2, No.4. - P. 481-496.

Information about the author

Asadulla Azizov	Tashkent State Transport University, “Automatics and Telemechanics” department Professor E-mail: azizov.asadulla@mail.ru Phone: +998935395421
Feruz Sindarov	Tashkent State Transport University, “Automatics and Telemechanics” department PhD student E-mail: feruzsindarov707@gmail.com Phone: +998943333996

Journal Engineer ISSN: 3030-3893 Volume:4| Issue:3| 2026

Received: 16 July 2026 | **Accepted:** 27 August 2026 | **Published:** 30 September 2026

An intelligent diagnostic approach based on oil analysis for assessing the technical condition of diesel locomotive engines

O.R. Khamidov[1][a], B.I. Gayratov[1][b], Sh.I. Kudratov[1][c], F.R. Djuraev[1]

[1]Tashkent state transport university, Tashkent, Uzbekistan

Abstract: A new intelligent diagnostic method for assessing the technical condition of diesel locomotive engines using the lubricating oil condition monitoring system is presented in this paper. The proposed method incorporates key oil condition parameters such as kinematic viscosity, iron (Fe) and copper (Cu) wear particle concentrations, soot content and water contamination as indicators of engine health. These parameters are useful for understanding the lubrication performance, wear of the components and potential defects in the engine that may arise during operation. In order to increase the diagnostic accuracy, an Adaptive Neuro-Fuzzy Inference System (ANFIS) was designed to study the collected data and classify the engine condition based on the technical state. The proposed model has applied artificial neural network capability to learn the relationship and fuzzy logic to reason the relationship between oil properties and engine degradation, which makes it effective in identifying the complex nonlinear relations between them. The intelligent diagnostic system developed allows to identify early abnormal operating conditions, facilitates the planning of predictive maintenance actions and decreases the risk of unexpected engine failures. Consequently, maintenance expenses can be kept at low levels and locomotives can be made more available, reliable and service life extended. The proposed approach is also shown to be suitable for implementation at the real time condition monitoring system, and it is a powerful tool for maintaining and managing the assets of modern railways.

Keywords: diesel engine, condition assessment, oil analysis, intelligent diagnostics, ANFIS, fuzzy logic, operational reliability, predictive maintenance

1. Introduction

The reliable and efficient operation of diesel locomotives used in railway transport ensures not only the continuity of the passenger and freight transportation system but also operational safety. It works at a high load regime, at high temperatures, and does not stop, therefore it can quickly wear out and unforeseen failures or other breakdowns begin to occur. The technical condition of the engine should be monitored regularly and faults should be detected early enough as a means of enhancing operational efficiency [1]

Traditional maintenance methods are usually carried out without a set schedule or on a calendar basis. This approach does not take into account the actual technical condition of the engine and increases the risk of failing to detect malfunctions in time. For this reason, in recent years, a predictive diagnostics approach has been widely implemented.

Engine oil analysis is one of the most promising methods of predictive technical diagnostics. Oil is a medium that is in direct contact with all working elements of the engine, and changes in its physicochemical and elemental composition provide important information about the technological processes inside the engine. For example, metal particles in oil provide information about decay processes, while oxidation indicators provide information about the degree of oil wear[2].

In this article, diagnostic parameters based on oil analysis are selected when assessing the technical condition of diesel engines. Based on parameters, a basis is created for intelligent approaches (for example, ANFIS, fuzzy logic) aimed at identifying possible engine failures. The results of the article will serve as a methodological basis for the subsequent development and practical implementation of algorithmic models

2. Research methodology

The selected methodological approach for evaluating the technical condition of diesel engines through oil analysis is primarily based on assessing the physicochemical and elemental composition of the oil. Such a method indirectly indicates the wearing, oxidizing, and infiltration of foreign matter that take place in the actual operating environment. The chosen parameters are based on international standards, scientific literature, and advanced practices in the field of technical diagnostics [3]. The following table 1 presents the main indicators selected for the diagnostic model.

As a research methodology, the relationship of parameters with the corresponding diagnostic models, the degree of their sensitivity, and the coefficients of variability are analyzed.

[a] https://orcid.org/0000-0003-0821-5754
[b] https://orcid.org/0009-0005-3957-337X
[c] https://orcid.org/0009-0007-6396-7699

https://doi.org/10.56143/3030-3893-2026-3-14-17

Table 1

Physicochemical and elemental oil parameters selected for the diesel engine diagnostic model

№	Parameter title	Measurement unit	Analysis method	Diagnostic importance
1	Viscosity	mm²/s (cSt)	Capillary viscometer (ASTM D445)	Lubrication performance, protection against wear
2	Iron (Fe)	ppm	ICP-OES spectroscopy	Wear of cylinder-liner assembly and crankshaft components
3	Copper (Cu)	ppm	ICP-OES	Bearing wear and surface degradation
4	Sediment (Soot)	%	Thermogravimetric analysis (TGA)	Poor combustion, filter saturation
5	Oxidation index	Arbitrary unit	IR-spectroscopy (FTIR)	Chemical degradation of oil, resistance in oxidative environment
6	Water mixing	%	Karl Fischer titration	Cooling system malfunction, condensation, corrosion risk

As a research methodology, the relationship of parameters with the corresponding diagnostic models, the degree of their sensitivity, and the coefficients of variability are analyzed. The above-mentioned methods can be used for oil analysis in laboratory conditions, which are selected based on international standards (ASTM, ISO, GOST) [4].

Basics of the model

Within the framework of this study, an intelligent forecasting model based on the Adaptive Neuro - Fuzzy Inference System (ANFIS) was developed to assess the technical condition of diesel locomotive engines and ensure their operational reliability. ANFIS is a robust tool having ability of neural network self learning with the advantages as fuzzy logic fuzzy and complex system modeling. It provides a high degree of accuracy in determining fuzzy and nonlinear relationships between parameters [5].

The model consists of the next steps:

- Determining parameters of input: simple physicochemical parameters of the engine oil, such as: kinematic viscosity, the total acid number (TAN) and the content of metal particles (Fe, Cu, Al)) and sediment concentration (soot);
- Decomposition into fuzzy categories: each input parameter is represented based on such fuzzy categories as “low”, “medium”, and “high”;
- Formation of the rule base: a set of fuzzy rules of the form “If..., then...”, in which the technical condition of the engine (for example, good, average, bad) is determined based on a combination of parameters;
- Training of the ANFIS-based model: Through the data base available and applying some optimization method, trained and optimized ANFIS model has been achieved.
- Formation of output results: based on new data, the technical condition of the engine is predicted by the model.

The model is based on the Fuzzy Logic Toolbox and Neural Network Toolbox libraries of the MATLAB program, which allows the user to load data through an intuitive interface, configure fuzzy categories, and effectively practice the model [6].

Figure 1 presents a general representation of the ANFIS model proposed here.

Assessment criteria

In an attempt to quantitatively evaluate the correctness and diagnostic performance of the model, following statistical criteria were applied: Mean Squared Error (MSE): This criterion is the square of difference between predicted model value and observed value of the experiment. The lesser MSE is, the more predictive is the model [7].

Coefficient of Determination (R2 - Coefficient of Determination): This criterion gives the degree to which the model is able to explain the overall variance. When the R2 value approaches 1, then the accuracy is high. ROC-AUC (Receiver Operating Characteristic - Area Under Curve):

The performance of the model in terms of classifications is measured by the AUC. AUC value varies between 0 and 1, and the higher the value, the higher the sensitivity and proper functioning of the diagnostic model. The results, in the case of the AUC above 0.9 are highly sensitive, and the diagnostic model functions properly. According to these assessments, model accuracy was checked in the scenario of training and testing which proved that it yields consistent outcomes in a real condition of operation as well [8].

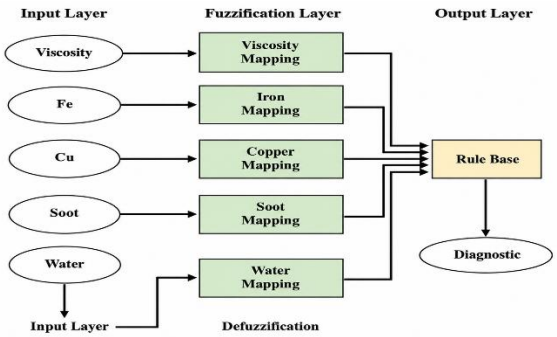


Fig. 1. Block diagram of the ANFIS model, which assesses the state of the engine based on oil analysis

https://doi.org/10.56143/3030-3893-2026-3-14-17

3. Results and discussion

ANFIS model developed in the course of the research proved to be a useful instrument in evaluating the technical state of the diesel locomotive engines and malfunctions predictions. Parameters contained in the model were chosen as iron (Fe), copper (Cu), kinematic viscosity, sediment content (hours), and water mixture due to their most significant indicators that determined oil analysis. These parameters directly reflect the disruptions in the performance of tribotechnological processes and functional components within the engine [9].

The ANFIS model had the following statistical indicators that determined its diagnostic accuracy: Mean Square Error (MSE) = 0.083

R^2 = 0.912 AUC=0.95

These findings show the model is highly accurate and a useful method in forecasting. In particular, such indicators as viscosity and the content of metal particles (Fe, Cu) give a clear picture of the wear conditions and degradation of oil properties occurring in the internal parts of the engine.

During the discussion, the following main observations were noted:

An increase in the amount of sediment may be associated with an imbalance in the combustion process, a violation of the fuel-air ratio, or wear of the piston rings;

A rise in the level of iron and copper is a definite indicator of wear of the crank shaft, bearing, bed surfaces and other parts that move;

Any reduction in the viscosity to a high extent means that the oil has expired and should be replaced;

The presence of a water mixture indicates technical problems in the engine's cooling system[9].

Also, unlike classical statistical methods, the ANFIS model showed high efficiency in determining fuzzy and nonlinear relationships between diagnostic indicators. This enables a need-based and continuous and correct determination of the engine status in operation conditions.

In general, the research results have proven that the predictive diagnostic model developed on the basis of ANFIS is of great importance in extending the reliability of diesel engines, increasing operational safety, and optimizing maintenance costs [10].

Comparative Analysis

The research results were compared with previously conducted scientific developments. For example:

The diagnostic model developed by Zaharia et al. (2017) based on metal elements (Fe, Cu) in diesel engine oil has an indicator of AUC = 0.87.

In the work of Clenci et al. (2018), the root mean square error in the neural model based on viscosity and oxidation parameters was MSE = 0.14.

In our study, high indicators such as MSE 0.083 and AUC 0.95 were achieved through the integration of several parameters (viscosity + Fe + Cu + soot + water) and a fuzzy logic-based approach.

This proves the effectiveness of the ANFIS model in complex, fuzzy, and multi-parameter environments compared to classical neural networks [11-12].

4. Conclusion

Within the framework of this study, a predictive diagnostic approach was developed, aimed at assessing the technical condition of diesel locomotive engines and increasing their operational reliability. Based on the proposed method, engine wear processes were modeled using the ANFIS (Adaptive Neuro-Fuzzy Inference System) model, relying on the main physicochemical parameters of engine oil (viscosity, sediment (soot), metal impurities - in particular, the content of iron and copper, as well as water concentration).

The analysis results showed that the recorded changes in the oil samples are highly correlated with the technical condition of the engine's internal parts, and the intelligent model built on the basis of these parameters has high accuracy in determining the real operational state of the engine. The ANFIS model's root mean square error rate (MSE) is 0.083 and the ROC AUC value is 0.95, which confirms its effectiveness. This allows the model to be implemented in real-time technical diagnostic systems.

The study has the following major findings:

The diagnostic method based on oil analysis serves as an effective tool as a non-invasive method of technical inspection of diesel engines;

The artificial intelligence approach based on the ANFIS model makes it possible to assess the functional state of engine components with high accuracy;

This strategy will play a crucial role in the optimization of maintenance period and aversion of technological failures as well as operating expenses. During additional work, an automated system of diagnosing vehicles is going to be developed by modifying the model to a variety of engines and increasing the data set, as well as combining it with IoT devices.

References

[1] Gayratov, B., & Insapov, D. (2025, June). On the kinematic parameters of the movement of a freight train on various sections of railways. In AIP Conference Proceedings (Vol. 3286, No. 1, p. 060007). AIP Publishing LLC.

[2] Khamidov O, Zayniddinov N, Kudratov S, Erkinov B. Analysis of malfunctions that occur in the crankshaft of locomotive thermal power plants during operation. In: E3S Web of Conferences. Proceedings of the E3S Conference; 2024; CONMECHYDRO 2024. – Vol. 538. – 01027. – P. 1 –6. https://doi.org/10.1051/e3sconf/202453801027

[3] Khamidov O, Kudratov S, Khamidov O, Turdimurodov B, Norbotayeva M. Improvement of Diagnostics and Analysis of Malfunction of the Crankshaft of Locomotive Power Plants. AIP Conference Proceedings. – Problems in the Textile and Light Industry in the Context of Integration of Science and Industry and Ways to Solve Them PTLICISIWS-2. – 2022. – Vol. 3045 B. – 050030. – P. 1 – 5.

[4] Fedotov, M. V. (2021). Предиктивная диагностика оборудования тепловоза на основе интеллектуального анализа данных.* [PhD dissertation, Petersburg State Transport University (PGUPS)]. DisserCat.

[5] Gayratov, B., Khamidov, O., Kudratov, S., & Samatov, S. (2026, May). The ANFIS anticipation of diesel locomotive engine on the improvement of lubricating oil analysis. In AIP Conference Proceedings (Vol. 3447, No. 1, p. 040008). AIP Publishing LLC.

[6] Khamidov O, Zayniddinov N, Kudratov S, Erkinov B. Analysis of malfunctions that occur in the

crankshaft of locomotive thermal power plants during operation. In: E3S Web of Conferences. Proceedings of the E3S Conference; 2024; CONMECHYDRO 2024. – Vol. 538. – 01027. – P. 1–6. https://doi.org/10.1051/e3sconf/202453801027

[7] Khamidov O, Kudratov S, Khamidov O, Turdimurodov B, Norbotayeva M. Improvement of Diagnostics and Analysis of Malfunction of the Crankshaft of Locomotive Power Plants. AIP Conference Proceedings. – Problems in the Textile and Light Industry in the Context of Integration of Science and Industry and Ways to Solve Them PTLICISIWS-2. – 2022. – Vol. 3045 B. – 050030. – P. 1 – 5.

[8] Wang, H., Liu, J., & Zhang, X. (2020). Hybrid fault diagnosis of engine systems using fuzzy logic and neural networks. Mechanical Systems and Signal Processing, 140, 106653.

[9] Pourramezan, M.-R., & Rohani, A. (2004). Improved monitoring and classification of engine oil condition through two machine learning techniques. SAE International. https://doi.org/10.4271/04-18-01-0005

[10] Dey, S., & Roy, R. (2019). Condition monitoring and maintenance management of industrial equipment using internet of things and big data analytics: A review. Journal of Manufacturing Systems, 53, 261-272. doi:10.1016/j.jmsy.2019.06.006

[11] Wakiru, James M.; Pintelon, Liliane; Muchiri, Peter N.; Chemweno, Peter K. (2019). A review on lubricant condition monitoring information analysis for maintenance decision support. Mechanical Systems and Signal Processing, 118(), 108–132. doi:10.1016/j.ymssp.2018.08.039

[12] Agarwal, A., "Experimental investigations of the effect of biodiesel utilization on lubricating oil tribology in diesel engines", Proceed. Instit. Mech. Eng., Vol. 219, pp. 703-713, 2005.

Information about the author

Otabek Khamidov	Tashkent State Transport University Professor, Department of Locomotives and Locomotive Establishment E-mail: otabek.rustamovich@yandex.ru Tel.:+99890 811 21 00 https://orcid.org/0000-0003-0821-5754
Bakhodir Gayratov	Tashkent State Transport University Doctoral student, Department of Locomotives and Locomotive Establishment E-mail: bgayratoff@gmail.com Tel.:+99894 134 54 27 https://orcid.org/0009-0005-3957-337X
Shohijakhon Kudratov	Tashkent State Transport University Associate Professor, Department of Locomotives and Locomotive Establishment E-mail: kudratov.shohijaxon@bk.ru Tel.:+99890 788 85 83 https://orcid.org/0009-0007-6396-7699
Firuz Djuraev	Tashkent State Transport University Doctoral student, Department of Locomotives and Locomotive Establishment Tel.:+99899 512 45 00

Journal Engineer ISSN: 3030-3893 Volume:4| Issue:3| 2026

Received: 8 June 2026 | **Accepted:** 20 July 2026 | **Published:** 30 September 2026

Scientific and practical justification of safe vehicle speeds in mountainous areas of the M-39 highway of international importance

O.G. Shokirov[1][a]

[1]Jizzakh Polytechnic Institute, Jizzakh, Uzbekistan

Abstract: The article considers the issue of determining the safe speed of vehicles in mountainous areas and the scientific justification of the need for its mandatory reduction. A complex mathematical model is proposed that takes into account the turning radius, pavement adhesion coefficient, traffic flow intensity, flow density, geometric coefficient and permissible risk level. Using the example of the mountainous areas of the M-39 highway, safe speed values are analyzed and practical recommendations are developed to improve traffic safety. Using this model, it is possible to determine the safe speed value for vehicles in mountainous road conditions, assess the probability of accidents and limit the speed in accordance with real road conditions. Based on the results obtained, safe speed values are calculated for the example of the mountainous areas of the M-39 highway and practical recommendations are developed to improve traffic safety. In particular, the need to introduce dynamic road signs, warning information panels and speed control devices in dangerous turns, sections with limited visibility and areas with deteriorating pavement conditions is justified. The article examines the scientific and practical issues of determining the safe speed of vehicles operating in mountainous road conditions and substantiates the necessity of its mandatory reduction in hazardous sections. Mountain roads are characterized by complex geometric parameters, sharp curves, steep longitudinal slopes, limited visibility, unstable pavement conditions and a high probability of traffic accidents. Therefore, the correct determination of safe vehicle speed in such areas is one of the important factors in improving road safety and reducing accident risks. On the basis of the analysis, practical recommendations were developed to improve traffic safety in mountainous road areas. In particular, the introduction of dynamic road signs, warning information panels, speed control devices and automated monitoring systems is scientifically justified for dangerous curves, sections with limited visibility and areas where pavement conditions may deteriorate due to weather or traffic load. The implementation of these measures can contribute to reducing accident probability, improving driver awareness, stabilizing traffic flow and increasing the overall safety level of mountainous highways.

Keywords: mountain road, safe speed, turning radius, friction coefficient, traffic flow, accident probability, dynamic road sign

1. Introduction

Research and development work on improving road safety in the world is of great importance. In mountainous areas, the speed of vehicles should be much lower than on flat roads. However, many drivers do not comply with the recommended speed limits, which leads to dangerous situations. For example, on sections with a slope of more than 40%, the speed of trucks on slopes can be twice as high as on hills, which increases the risk of collisions. Road accidents in mountainous areas not only cause casualties and injuries, but also cause significant damage to the environment and the economy. For example, oil spills in truck accidents pollute mountain rivers and soil, and the restoration of road infrastructure requires significant financial costs.

Modern methods of ensuring traffic safety on mountain roads, such as the installation of barriers, the construction of protective galleries, and the use of intelligent traffic control systems, have been used in our republic for a long time. The introduction of such measures in Uzbekistan allows us to reduce the number of accidents and increase the efficiency of the transport system [1].

The development and justification of measures to reduce the speed of vehicles on mountainous road sections of highways is one of the urgent tasks aimed at increasing traffic safety, reducing accidents, and minimizing environmental and economic damage. The implementation of such measures requires an integrated approach, including improving road infrastructure, introducing modern technologies, and monitoring strict compliance with speed limits.

In accordance with the Strategy for the Development of the Public Safety System in the Republic of Uzbekistan for 2022-2025, as outlined in the Resolution of the President of the Republic of Uzbekistan No. PQ-190 dated 04.04.2022 “On Measures to Ensure Reliable Human Safety on Motor Roads and Sharply Reduce Fatalities”, as well as in order to ensure the guaranteed protection of human life and health on motor roads from any incidents in the conditions of the new Uzbekistan, and in accordance with the Resolution of the President of the Republic of Uzbekistan No. PQ-316 dated 12.07.2022 “On Approval of the National Program “Safe and Smooth Road” for Implementation in 2022-2026”, the digitalization of the traffic control system on motor roads, the integration of traffic light objects at intersections into the central management system, and the implementation of a

[a] https://orcid.org/0009-0000-2124-2971

single digital management system, as well as other tasks related to this activity This dissertation work serves to a certain extent in the implementation of the tasks set out in regulatory and legal documents [1].

2. Research methodology

The assessment of the speed of vehicles in mountainous areas from a safety point of view and the justification of the need for mandatory reduction is a complex scientific and practical process. This process requires a comprehensive consideration of the geometric parameters of the road, traffic flow intensity, traffic composition, adhesion properties of the road surface, longitudinal slope, turning radius and the probability of danger.

In mountainous areas, the radius of curvature of the road is dangerous, small-radius turns, large longitudinal slopes, variability of weather and surface conditions directly affect the stable movement of vehicles. In such conditions, the maximum speed selected by the driver does not always correspond to the safe speed. Therefore, there is a need to determine the permissible speed of vehicles depending on the turning radius, correlate it with road conditions and the probability of danger, and develop an improved methodology for calculating the safe speed value.

In this study, a methodology was proposed based on the integration of road-geometric, transport-operational and safety factors into a single mathematical model to determine the need for mandatory reduction of vehicle speed in mountainous road areas. The main essence of the methodology is to determine the safe speed of movement through a comprehensive assessment of the turning radius of the road (R), longitudinal slope (i), traffic flow intensity (q), traffic composition coefficient (k), road surface adhesion coefficient (φ), risk level (Phazard level) and calibration coefficient (k_1) [2].

This methodology is aimed at ensuring the safety of vehicle movement in mountainous road areas, in which road geometry, traffic flow, road surface condition and risk probability are integrated into a single calculation system. As a result, the difference between the permissible speed of vehicles and the safe speed in areas with dangerous curvature radius is determined, creating the opportunity to make scientifically based decisions on mandatory reduction of speed. Based on their research, it is intended to address the following issues:

– identify and systematize the main factors affecting the speed of vehicles on mountainous road areas;

– assess the geometric parameters of the study area, including the turning radius, longitudinal slope and condition of the road surface;

– determine the coefficients of traffic flow intensity and traffic composition and assess their impact on safe speed;

– determine the impact of the turning radius on the permissible speed of vehicles and justify a linear regression model in the form of ($\upsilon=a+bR$);

– take into account the coefficient of adhesion between the road surface and the tire for dry, wet and slippery/dirty road conditions;

– develop a safe speed model combining traffic flow, road geometry, surface condition and risk probability;

– justify the need for mandatory speed reduction by comparing the calculated permissible speed and safe speed values;

– development of practical recommendations for determining safe speeds and introducing dynamic road signs developed by us in mountainous areas.

In order to assess the speed of vehicles in mountainous areas from a safety point of view and justify measures to reduce the number of road accidents by mandatory speed reduction, it is important to properly organize experimental and test work. This chapter describes the test equipment, measured parameters, research program, and the procedure for processing the results obtained for conducting experimental and test studies [4].

The main purpose of the experimental and test works is to determine the relationship between the permissible speed of vehicles, geometric parameters of the road, traffic flow intensity, pavement condition and traffic safety in mountainous road areas. In this case, the turning radius of the road, longitudinal slope, adhesion coefficient between the road surface and the car tire, traffic flow composition and real traffic speeds were taken as the main research indicators.

Experimental works are carried out in designated dangerous turning areas of the mountainous road area. As a research area, a road area with a turning radius of 989-1013, high traffic flow intensity and a high probability of traffic accidents is selected. In the test area, the speed of vehicles, traffic flow composition, road surface condition and geometric parameters are simultaneously recorded [3].

Test equipment. When carrying out experimental and test works, it is advisable to use the following measuring and monitoring equipment. The equipment measures the permitted speed of vehicles, road geometry, and traffic flow parameters. The data is then fed into a model for determining safe speeds.

Main parameters to be measured. The following parameters will be recorded during the experiment:

– turning radius of the road (R), m;
– road gradient (i), %;
– real speed of vehicles (υ), km/h;
– traffic flow intensity (q), vehicles/h;
– traffic composition coefficient (k);
– road surface adhesion coefficient (φ);
– geometric coefficient (K_g);
– risk level (Prisk level);
– safe speed (υsafe), km/h.

The condition of the road surface is assessed in dry, wet and slippery or contaminated conditions. The calculations assume the values or dry surface (φ=0.75), wet surface (φ=0.55), and slippery or contaminated surface (φ=0.35).

A special experimental and test program has been developed to determine the safe speed of vehicles in mountainous road areas and to scientifically substantiate the need for mandatory speed reduction. This program is aimed at determining the geometric and operational parameters of the road, assessing the traffic flow regime, and calculating the safe speed.

Table 1

Contents of the pilot study program

B	Program Structure	Research Implementation Process
1	Choosing a research area	In mountainous areas, areas with small turning radius, steep slopes, and high risk of traffic accidents are selected.
2	Determining the geometric	The turning radius (R), the slope (i), the cross slope and the road design

https://doi.org/10.56143/3030-3893-2026-3-18-23

	parameters of the road	elements are measured. These indicators are evaluated as the main factors affecting the stability of the vehicle on a dangerous curve.
3	Road surface condition assessment	The condition of the road surface is assessed in terms of dry, wet, or slippery/dirty conditions. For each condition, the coefficient of adhesion (φ) between the road surface and the tire is selected.
4	Determining the intensity and composition of transport flow	The number of vehicles, the share of cars and trucks, buses and other types of transport during a specified period of time are recorded based on real-time observations and flow-measuring devices.
5	Measuring the real speed of vehicles	Using GPS, radar, or video surveillance, the actual speeds of vehicles on a road with a dangerous radius of curvature are determined. The values obtained are used to justify the free speed model.
6	Calculate maximum movement speed	The permissible speed is determined based on a linear regression model depending on the turning radius: $(\upsilon_{allow} = a + bR)$
7	Determining safe speed	Safe speed is calculated taking into account traffic flow intensity, traffic composition, road surface adhesion coefficient, road slope, and risk level.
8	Analyzing results and making decisions	The permitted speed and the safe speed are compared. If (υ_{safe}<υfree), the need for a mandatory speed reduction in this area is justified.

The program includes the implementation of the following tasks:

Stage 1. Identification stage (2022-2023):

- determination of the number and parameters of dangerous turns, service structures, and dangerous road sections in the mountainous road area selected as the object of research;

– determination of the slope and condition of the pavement;

– determination of the intensity of the traffic flow and the composition of the traffic based on visual and automatic monitoring tools.

Stage 2. Experimental stage (2023-2024):

– measurement of dangerous turn radii in the mountainous road area under study;

– recording the speed of vehicles in real time using GPS, radar or video surveillance;

– calculation of safe speeds taking into account the coefficient of adhesion of the pavement, road slope, and traffic flow parameters.

Stage 3. Final stage (2024-2025):

– justification of the need for mandatory speed reduction by comparing the permitted speed with the safe speed.

The experimental tests were carried out under the following conditions:

– dry coating conditions;

– wet pavement conditions;

– slippery or contaminated pavement conditions;

– time intervals with low, medium and high traffic flow.

The experimental results obtained on the basis of this program allow to determine the maximum and safe speed of vehicles in mountainous road areas, to assess dangerous areas and to scientifically substantiate measures to reduce the number of road accidents by mandatory speed reduction.

The mountainous area of the M-39 international highway, located in the area of 989–1013 km, passing through the territory of Jizzakh region, was selected as the object of research. These areas are characterized by complex geometric parameters, large longitudinal slopes, dangerous radii of curvature and limited visibility. In particular, as a result of high-speed movement of vehicles, the risk of road accidents increases in these areas [5,6].

The following parameters were measured and analyzed during the research:

Table 2

Measurable parameters

№	Measured parameter	Mar-king	Measurement method
1	Turning radius	R	Geodetic surveying, road plan analysis
2	Slope	i	Inclinometer, level or total station
3	Roadway width	B	Laser rangefinder, tape measure
4	Traffic flow intensity	q	Video surveillance and counting method
5	Movement speed	υ	Radar, GPS or video analysis
6	Road surface friction coefficient	φ	Assessment by coating condition
7	Accident probability	P_{av}	Calculation based on a mathematical model

The main objective of the study was to assess the impact of road geometric parameters and traffic flow conditions on vehicle traffic safety and to determine the effectiveness of mandatory speed reduction measures.

The turning radius of the road is the main parameter in determining the safe speed of vehicles. The radius value was determined from the geometric plan of the road and using geodetic measurements on site.

The turning radius was estimated using the following formula:

$$i = \frac{h}{l} \cdot 100\% \quad (1)$$

where: i= road slope;

h - height difference;

l- horizontal distance.

The study adopted the basic value i=12 %.

The width of the road carriageway affects the stability and safety of the traffic flow. The width of the carriageway

was determined using a tape measure and the distance between the two edge lines was measured (Figure 1).



Fig. 1. The process of measuring the longitudinal slope of the road, the width of the roadway, and the flow of vehicles

The speed of vehicles was determined using a radar speedometer and video surveillance, and the results of experimental observation were recorded. The turning radius and slope of the road were determined using an electronic tachometer laser neviller.

Table 3

Parameters calculated as a result of the experiment

№	Parameter	Symbol	Value
1	Car flow	q	1750 cars/hour
2	Slope	i	12 %
3	Turning radii	R_1 R_2 R_3	250 m 300 m 320m
4	Permitted speed	$\upsilon_{rux.etil}$	100 km/h
5	Current density	k	18 cars/hour
6	Model fitting coefficient	k_1	10^{-6}
7	Minimum level of accident risk	$P_{risk\ level}$	0,025≈2,5%
8	Geometric coefficient	K_g	1,12
9	Coefficients of association	φ_1 φ_2 φ_3	0,35 0,55 0,75

We will calculate the safe speed separately for 3 different conditions of adhesion coefficients (φ_1=0.75, φ_2=0.55, φ_3=0.35) for dangerous turning radii of 250 m, 350 m, 320 m at 994 km, 997 km and 1004 km of the mountainous areas of the M-39 international highway passing through the territory of Jizzakh region, which was taken as the object of research. We will calculate the safe speed using the following formula [7]:

For the determined safe speed values, the accident probability is recalculated. Pav.probability is calculated using the following formula:

$$P_{prob.accid} = 1 - e^{-\lambda} \quad (2)$$

$$\lambda = -k_1 \cdot q \cdot k \cdot \left(\frac{\upsilon_{xavf}}{\upsilon_{erkin}}\right)^2 \cdot \frac{\left(1+\frac{i}{100}\right)}{\varphi} \quad (3)$$

In the proposed model, the probability of an accident is determined by the parameters of the traffic flow, the speed ratio, the longitudinal slope of the road and the coefficient of adhesion of the pavement. Since the safe speed formula is formed exactly in accordance with the given permissible risk level, when the found safe value υ is inserted into the formula for the probability of an accident, the result is the equality $P_{probability} = P_{risk.level}$. This confirms the internal logical consistency of the model.

The coefficient of adhesion in dry weather conditions (dry asphalt/concrete) for a turning radius R=250 m is determined by the formula (2,3) for the safe speed for 3 different adhesion coefficients (φ_1=0.75, φ_2=0.55, φ_3=0.35): The calculation results are given in Appendix 1. The accident probability for the found safe speed values is recalculated by the formula (3.4). The calculation results are given in Table 2

Table 4

Safe speeds depending on the coefficient of friction of the turning radius (R=250m)

Turning radius, m	Coefficient of friction	K_g	$\upsilon(safe)speed\ km/h$	$P_{prob.acc}$
R=250 m	φ_1 =0,75	1,12	72,85 km/h	0,025
	φ_2 =0,55	1,12	62,51 km/h	0,025
	φ_3 =0,35	1,12	49,75 km/h	0,025

Thus, for a turning radius R=250 m, the following speeds were found to be unsafe in dry weather conditions: 73 km/h for the coefficient of friction φ_1=0.75, 62.51 km/h for the coefficient of friction φ_2=0.55, and 49.75 km/h for the coefficient of friction φ_3=0.35 (Figure 2).

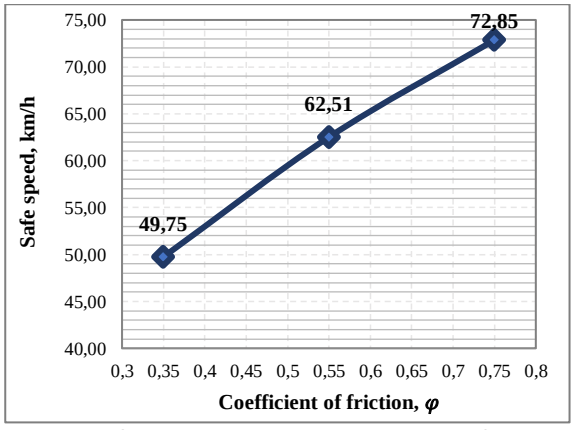


Fig. 2. Safe speed diagram depending on the friction coefficients for a turning radius of R = 250 m

The calculation results show that the accident probability is $P_{prob.acc}$=0,0247, which is close to the permissible value $P_{risk.level}$=0,025. Thus, the calculated speeds for a radius of 250 m are considered marginally safe for this road area.

3. Conclusion

According to the calculation results, it was found that the safe speed of vehicles on a mountainous road section with a

https://doi.org/10.56143/3030-3893-2026-3-18-23

turning radius (R=250) m directly depends on the condition of the road surface. In dry weather conditions and with a coefficient of adhesion (φ1=0.75), the safe speed was 73 km/h. At a value of (φ_2=0.55), which represents the condition of the wet surface, the safe speed decreased to 62.51 km/h. In dirty or slippery conditions, i.e. with (φ =0.35), the safe speed was 49.75 km/h.

These results indicate the need to reduce the speed of vehicles as the adhesion properties of the road surface deteriorate. Especially on mountainous road sections with a small turning radius, high speed negatively affects the stability of the vehicle and increases the risk of sideslip, skidding and loss of control. Therefore, it is important to set the speed in curves with a radius of (R=250) m in accordance with the condition of the road surface.

As a result of the calculation, it was found that the probability of an accident ($P_{av.probability}=0,0247$), which is very close to the permissible risk level ($P_{risk.level}=0,025$). Therefore, the speeds determined for this radius are considered to be the marginal safe speed values. In other words, when driving above these speeds, the probability of an accident may exceed the permissible risk level [9,10].

The results obtained show that on turns with a radius of (R=250) m, the speed of 70–73 km/h on dry surfaces is relatively close to the safe limit, while on wet surfaces the speed should be reduced to around 60 km/h, and on dirty or slippery surfaces to 50 km/h. Therefore, it is advisable to adapt the speed to real road conditions on such road sections by using dynamic road signs, warning information panels and speed control devices.

The scientific significance of the approach proposed in the study is that the issue of determining safe speeds in mountainous road areas is solved by assessing the road geometry, traffic flow and pavement condition in a single system. In current practice, the speed limit is often set based on the general road category or administrative requirements. In this study, the speed limit is calculated in relation to the turning radius, adhesion coefficient, flow density and accident probability. This allows for more accurate and justified decisions to be made for dangerous sections.

The practical significance is that the developed model can be used by road organizations, traffic safety agencies and project organizations to assess dangerous mountainous road sections. The model provides justification for the need to set a speed of 70 km/h on which section and 50-60 km/h on which section. This methodology also serves as a practical basis for selecting the location of dynamic road signs, installation points for electronic information panels and speed control devices [12].

Based on the results of the study, it is recommended to use a three-level approach to speed control in mountainous areas. The first level is preventive warning, in which the driver is informed in advance before dangerous turns and slopes. The second level is a mandatory speed limit, in which a road sign is installed corresponding to the calculated safe speed. The third level is automatic control, in which drivers' compliance with the speed is monitored using radar, video fixation and sensors [12]. Thus, the developed mathematical model, calculation algorithm and practical recommendations can be considered as a comprehensive solution aimed at increasing traffic safety on mountainous roads, warning drivers in advance about dangerous situations and reducing the number of road accidents. To adapt this approach to the conditions of other mountainous roads, it is enough to include geometric, transport and pavement indicators of the relevant section in the model.

References

[1] Ikromov A., Shokirov O. Yo‘lning tog‘li hududlarida transport vositalarining tezligini majburiy ravishda pasaytirish choralarini ishlab chiqish va asoslash.(M-39 yo‘lining tog‘li hududlari misolida) //Journal of Transport. – 2025. – T. 2. – №. 2. – C. 92-96.

[2] S. O. G. SHAHAR AHOLISI O‘RTASIDAGI HAYDOVCHILARGA YORDAM BERISH TIZIMINI (ADAS) QO‘LLASH ORQALI YO‘L-TRANSPORT HODISALARINING OLDINI OLISH //Механика и технология. – 2023. – №. 2 (5) Спецвыпуск. – С. 138-145.

[3] АВТОМОБИЛЬНАЯ П. Учредители: ОАО" Автосельхозмаш-холдинг", Министерство промышленности, науки и технологий //АВТОМОБИЛЬНАЯ ПРОМЫШЛЕННОСТЬ. – №. 3. – С. 10-15.

[4] Шокиров О.Ғ. Обзор моделей поведения водителей транспортных средств в ситуации, близкой к столкновению // Автоматизация. Современные технологии. Том.79. -2025. №1. -19-21 с. DOI: 10.36652/0869-4931-2025-79-1-19-21. https://doi.org/10.36652/0869-4931-2025-79-1-19-21.

[5] Шокиров О.Ғ. Функционирования автобусного транспорта в место паломничества // Golden Brain Scientific Journal. ISSN: 2181-4120. Vol 1. Isue 3. – February 2023. -161-166 p. https://doi.org/10.5281/zenodo.7605043.

[6] Shokirov O. G., Qadamov Q. S. THE EFFECTIVENESS OF DEVELOPING MEASURES BASED ON THE ANALYSIS OF ROAD TRAFFIC ACCIDENTS IN MOUNTAINOUS AREAS OF THE M-39 HIGHWAY //Экономика и социум. – 2025. – №. 10-2 (137). – С. 515-518.

[7] Шокиров О. Г. Меры по совершенствованию использования инновационных систем повышения безопасности транспортных средств. – 2024.

[8] Kapski, D., Semchenkov, S., Gamulsky, I., Ikromov, A., Omarov, J., & Abruev, S. (2024). Assessment measures developed to improve quality of route transport Polotsk and Novopolotsk. E3S Web of Conferences, 515, 03003. https://doi.org/10.1051/e3sconf/202451503003

[9] Ikromov, A. (2023). Components modifying methods with the using of energy technologies. 060037. https://doi.org/10.1063/5.0115559

[10] Avdeychik, S., Goldade, V., Struk, V., Antonov, A., & Ikromov, A. (2020). THE PHENOMENON OF NANOSTATE IN MATERIAL SCIENCE OF FUNCTIONAL COMPOSITES BASED ON INDUSTRIAL POLYMERS. Theoretical & Applied Science, (7), 101-107.

[11] Shokirov O. G‘. (2023). Shahar aholisi o‘rtasidagi haydovchilarga yordam berish tizimini (ADAS) qo‘llash orqali yo‘l-transport hodisalarining oldini olish. MEXANIKA VA TEXNOLOGIYA ILMIY JURNALI, MAXSUS SON 2023, № 2 (5). 138-145. https://api.scienceweb.uz

[12] https://matador.tech/

[13] www.yhxx.uz.

Information about the author

Ozod Shokirov Independent researcher at Jizzakh Polytechnic Institute
E-mail: cristow.777@gmail.com
Tel: +998905159779
https://orcid.org/0009-0000-2124-2971

Journal Engineer ISSN: 3030-3893 Volume:4| Issue:3| 2026

Received: 12 June 2026 | **Accepted:** 24 July 2026 | **Published:** 30 September 2026

Security analysis of windows local authentication recovery techniques and defensive mechanisms

M.A. Sobirov[1][a], A.A. Hamidov[2][b]

[1]Tashkent state transport university, Tashkent, Uzbekistan

[2] Oxus university, Tashkent, Uzbekistan

Abstract: Local authentication is the first line of defense in Windows environments, yet common recovery tools and forensic techniques can be exploited by attackers when defensive mechanisms are not properly configured. This research evaluates several Windows local authentication recovery scenarios, including offline SAM hash extraction, recovery-environment abuse, an
d Credential Guard bypass attempts, under different security configurations. Using a controlled Windows 10 testbed, we measured which credential-recovery methods succeed against full-disk encryption (BitLocker), Trusted Platform Module (TPM) protections, Secure Boot, virtualization-based security (VBS), and Credential Guard. BitLocker with pre-boot authentication effectively prevented offline hash attacks, Secure Boot blocked unauthorized boot code, and Credential Guard isolated NTLM and Kerberos credentials from memory-based extraction. Misconfigurations such as disabled encryption or VBS allowed several recovery techniques to succeed. The study presents a comparison of recovery methods against defensive controls, identifies where Windows security features still leave gaps, and offers practical recommendations, including enabling BitLocker, Secure Boot, a pre-boot PIN, and VBS, to minimize credential exposure. The results indicate that layered Windows defenses, hardware TPM, Secure Boot, BitLocker, and Credential Guard combined, substantially reduce the risk posed by local credential-recovery attacks. These findings are intended to help students, administrators, and security practitioners understand effective Windows security configurations and the practical limits of built-in recovery features under adversarial conditions.

Keywords: Windows authentication, credential recovery, BitLocker, Secure Boot, Credential Guard, LSASS, offline attacks, local administrator, Windows Recovery Environment

1. Introduction

Windows remains the dominant desktop operating system worldwide, a position that makes it a primary target for attackers seeking unauthorized system access [1]. In most intrusions, the adversary's central goal is to obtain account credentials rather than to exploit a specific software flaw. MITRE's ATT&CK framework treats "Credential Access" as a distinct tactic, reflecting how routinely attackers attempt to steal passwords, password hashes, or Kerberos tickets once inside a system [2], [3]. Because identity verification functions as the first line of defense in any modern computing environment [4], protecting the mechanisms behind Windows authentication is not a peripheral concern, it is foundational to system security as a whole.

Microsoft has responded to this threat landscape by building a layered authentication architecture. Long-standing components, the Local Security Authority (LSA), the Security Accounts Manager (SAM), and the NTLM and Kerberos protocols, now operate alongside newer protections: full-disk encryption through BitLocker, hardware-backed key storage in the Trusted Platform Module (TPM), UEFI Secure Boot, virtualization-based security (VBS), and Credential Guard [5]. BitLocker, for instance, encrypts entire system volumes to prevent data theft from a stolen or physically accessed disk [6], while Credential Guard uses VBS to isolate NTLM password hashes and Kerberos tickets inside a protected memory space, placing them largely out of reach of conventional extraction tools [7].

The remainder of this paper proceeds as follows. Section 2 describes the experimental methodology and the evaluation criteria applied to each recovery scenario. Section 3 reports the results, supported by comparison tables of techniques, defenses, and outcomes. Section 4 discusses these findings in light of existing Microsoft and NIST guidance. Section 5 concludes with practical recommendations for administrators and students seeking to reduce local credential exposure.

2. Research methodology

This study relied on a hands-on experimental evaluation performed on a virtualized Windows 10 Pro (version 22H2) machine. All tests ran inside VMware Workstation 17, with the guest environment configured as summarized in Table 1. Across experiments, we varied four security settings: BitLocker (disabled, TPM-only, or TPM plus PIN), Secure Boot (enabled or disabled), WinRE pre-boot authentication (enabled or disabled), and Credential Guard/VBS (enabled or disabled). Consistent with a realistic threat model, the

[a] https://orcid.org/0009-0000-4719-9481
[b] https://orcid.org/0009-0008-9649-862X

attacker was assumed to hold either local administrator privileges or physical access to the machine.

Table 1

Experimental environment

Component	Specification / Setting
Host OS	Windows 11 Pro, VMware Workstation 17
Guest OS	Windows 10 Pro 22H2 (64-bit)
Hardware	4-core virtual CPU, 16 GB RAM, 80 GB virtual disk
VM Security Settings	VT-x/AMD-V enabled, UEFI firmware

For each scenario, the machine was first prepared with the target security configuration, after which each recovery technique described below was attempted. Table 2 lists the evaluation criteria applied throughout: whether the technique succeeded, the type of credential or secret obtained, the approximate effort required, the security feature (if any) that blocked the attempt, and the resulting residual risk. All techniques relied on freely available tools or built-in Windows features; no proprietary or exploit-based methods were used. Four scenarios were evaluated.

Offline SAM hash extraction involved using WinRE or a bootable USB drive to load tools such as ntdsutil or chntpw and dump the SAM database to recover password hashes. WinRE-based TPM reset involved booting into the WinRE command prompt to clear the TPM owner password and subsequently read DPAPI-protected vaults that would normally require that key. Credential Guard bypass involved disabling VBS at the firmware level, or physically removing the disk, in order to examine memory or volume contents for plaintext or hashed secrets. UEFI and bootloader compromise involved attempting to install a rootkit or a malicious bootloader, a scenario that requires Secure Boot to be disabled beforehand.

Table 2

Security evaluation criteria

Criterion	Description
Success of Recovery	Credentials/secrets recovered (Yes/No)
Recovered Data	NT hash, Kerberos ticket, or DPAPI secret
Time / Effort	Estimated time and attack complexity
Blockers	Security features preventing recovery

For every scenario, we recorded whether authentication data, a password, hash, or LSA secret, was obtained, and we noted the primary security mechanism, if any, that prevented the attack. All experiments were carried out on our own devices under our institution's ethics policy, and no private or third-party data was accessed at any point.

3. Results and Discussions

Each recovery method was applied systematically, and the outcomes were recorded across three summary tables. Table 3 compares the recovery techniques against the protective configurations under which they were tested. Table 4 compares the relevant Windows security features in terms of what they protect and where their known limitations lie. Table 5 provides an overall risk assessment for the main threat conditions identified during testing.

Table 3

Recovery technique comparison

Scenario	Recovery	Risk	Defense
Offline SAM	Yes	Local account compromise	BitLocker
UEFI rootkit	Yes	System compromise	Secure Boot
WinRE reset	Yes	DPAPI exposure	PIN + Disable WinRE
CG bypass	Yes	LSASS dump	VBS + CG
TPM reset	Yes	TPM key theft	TPM PIN

It should be noted that Table 3 reflects outcomes under the specific column condition described, for instance, the offline SAM row assumes BitLocker is absent. When BitLocker, Secure Boot, and VBS are enabled together, both offline SAM attacks and credential extraction from memory fail consistently.

Table 4

Windows security feature comparison

Feature	Protection	Main Limitation
BitLocker	Offline disk protection	Needs TPM + PIN
Windows Hello	Secure local login	Local PIN only
Credential Guard	Protects credentials	Requires VBS
Secure Boot	Stops bootkits	Needs UEFI support
WinRE	Recovery environment	Must be secured

Across the experiments, BitLocker proved to be the single most decisive control. With BitLocker enabled under a TPM-plus-PIN configuration, no offline SAM or DPAPI recovery attempt succeeded; the data remained encrypted throughout [6], [10], and even an attacker with administrative rights could not boot a recovery environment without supplying the correct PIN. With BitLocker disabled, or with the key already known, recovering the SAM or DPAPI secrets required little effort. This is consistent with Microsoft's own description of BitLocker as a control that renders data inaccessible without the appropriate key [6], [10].

Secure Boot behaved just as consistently, blocking every attempt to load unauthorized boot code. Once Secure Boot was disabled in firmware, however, we were able to install a custom bootloader and bypass Windows authentication with relatively little difficulty; re-enabling Secure Boot closed this avenue entirely [9]. A related pattern held for the TPM reset scenario; attempts to clear the TPM owner via WinRE only produced results when the TPM itself was not already protected by a BitLocker PIN.

https://doi.org/10.56143/3030-3893-2026-3-24-27

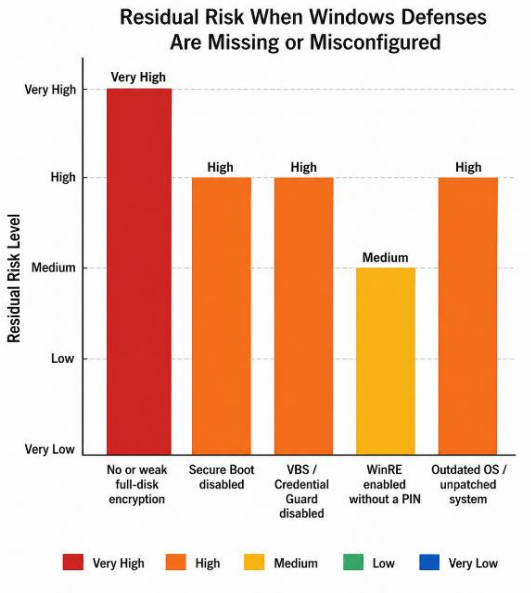


Fig. 1. Overall risk assessment when defenses are missing or misconfigured. Weak or absent full-disk encryption carries the highest residual risk, followed by disabled Secure Boot and disabled VBS / Credential Guard

Figure 1 summarizes the residual risk associated with each missing or weakened layer of defense. Weak or absent disk encryption carries a very high risk rating, since it allows an attacker to crack the SAM database offline and recover essentially all local passwords; disabling VBS or Credential Guard carries a similarly high risk of credential theft. Taken together, these results demonstrate that combining BitLocker, Secure Boot, and VBS/Credential Guard neutralized every recovery attack attempted in this study.

Discussion

These experimental findings align closely with existing Microsoft and NIST guidance [11]. UEFI Secure Boot is explicitly designed to ensure that a device boots only software trusted by its manufacturer [9], which matches our observation that Secure Boot completely blocked every low-level boot attack attempted. BitLocker's stated design goal, providing encryption for entire volumes in order to mitigate data theft [6], was likewise confirmed: every scenario in which credentials were successfully recovered involved either disabling or circumventing BitLocker. When BitLocker was active with a TPM-plus-PIN configuration, encrypted volumes stayed protected even under full physical access, and encrypted files remained unreadable without the correct key [10].

In short, the data collected here show that modern Windows security features perform well against offline and local attacks when they are correctly configured: BitLocker stops offline hash-cracking [6], [10], Secure Boot stops bootkits [9], and Credential Guard stops in-memory credential harvesting [7]. What residual risk remains is driven mainly by human and configuration factors, forgotten PINs, default settings left unchanged, or features disabled for convenience, a pattern broadly consistent with prior security literature emphasizing hardware-rooted trust and the inherent limitations of password-based recovery [12], [13].

4. Conclusion

This study systematically evaluated Windows local authentication recovery techniques against current defensive mechanisms, implementing realistic attack scenarios in a controlled environment and measuring their success. Four conclusions follow from the results. First, full-disk encryption through BitLocker with a pre-boot PIN is essential; it eliminated every offline recovery attack tested [6], [10]. Second, UEFI Secure Boot must remain enabled to prevent bootloader and rootkit compromise [9]. Third, virtualization-based isolation through Credential Guard is highly effective against in-memory credential theft [7]. Fourth, built-in recovery tools such as WinRE pose a genuine risk when left unsecured, since they can be abused to reset the TPM and access otherwise protected credential stores.

By combining hands-on experimental evaluation with a security-focused analysis, this work offers practical insight into how Windows authentication can be protected in practice. The results show that Windows already provides strong protections, but that these protections must be applied correctly, otherwise, attackers can still exploit the very recovery features meant to help legitimate users. Future work could extend this analysis to recovery mechanisms on other platforms, such as macOS recovery mode or Linux initramfs-based recovery, or examine network-based credential protocols within a similarly defensive framework [14].

References

[1] StatCounter GlobalStats, "Desktop Operating System Market Share Worldwide," 2026. [Online]. Available: https://gs.statcounter.com/os-market-share/desktop/worldwide. [Accessed: Jul. 22, 2026].

[2] MITRE, "Credential Access (TA0006)," MITRE ATT&CK, 2024. [Online]. Available: https://attack.mitre.org/tactics/TA0006/. [Accessed: Jul. 22, 2026].

[3] R. A. Grimes, Hacking the Hacker: Learn from the Experts Who Take Down Hackers. Indianapolis, IN, USA: Wiley, 2017.

[4] M. Bishop, Computer Security: Art and Science, 2nd ed. Boston, MA, USA: Addison-Wesley, 2019.

[5] Microsoft, "Windows Security Documentation," Microsoft Learn, 2024. [Online]. Available: https://learn.microsoft.com/en-us/windows/security/. [Accessed: Jul. 22, 2026].

[6] Microsoft, "BitLocker Drive Encryption Overview," Microsoft Learn, 2024. [Online]. Available: https://learn.microsoft.com/windows/security/operating-system-security/data-protection/bitlocker/overview. [Accessed: Jul. 22, 2026].

[7] Microsoft, "Credential Guard Overview," Microsoft Learn, 2024. [Online]. Available: https://learn.microsoft.com/en-us/windows/security/identity-protection/credential-guard/. [Accessed: Jul. 22, 2026].

[8] Microsoft, "Windows Hello for Business Overview," Microsoft Learn, 2024. [Online]. Available: https://learn.microsoft.com/en-us/windows/security/identity-protection/hello-for-business/. [Accessed: Jul. 22, 2026].

[9] Microsoft, "What Is Secure Boot for Windows?," Microsoft Learn, 2024. [Online]. Available: https://learn.microsoft.com/en-us/windows-hardware/drivers/bringup/secure-boot. [Accessed: Jul. 22, 2026].

[10] Microsoft, "Windows Recovery Environment (Windows RE) Technical Reference," Microsoft Learn, 2024. [Online]. Available: https://learn.microsoft.com/en-us/windows-hardware/manufacture/desktop/windows-recoveryenvironment--windows-re--technical-reference. [Accessed: Jul. 22, 2026].

[11] National Institute of Standards and Technology, Security and Privacy Controls for Information Systems and Organizations, NIST Special Publication 800-53, Rev. 5. Gaithersburg, MD, USA: U.S. Department of Commerce, 2020, doi: 10.6028/NIST.SP.800-53r5.

[12] R. Anderson, Security Engineering: A Guide to Building Dependable Distributed Systems, 3rd ed. Indianapolis, IN, USA: Wiley, 2020.

[13] W. Stallings, Cryptography and Network Security: Principles and Practice, 8th ed. Hoboken, NJ, USA: Pearson, 2020.

[14] M. A. Sobirov, I. S. Kurbanova, and Z. O. Sabirova, "Multi-Level Approach in Organizing the Energy Supply System in Telecommunication Networks," in Proc. 2023 IEEE XVI Int. Sci. Tech. Conf. Actual Problems of Electronic Instrument Engineering (APEIE), Novosibirsk, Russian Federation, 2023, pp. 1830–1834, doi: 10.1109/APEIE59731.2023.10347846.

Information about the author

Muzaffar Sobirov	Tashkent State Transport University, Department of Information Systems and Technologies in Transport, Independent Researcher E-mail: muzaffarsobirov538@gmail.com Tel.:+998909314809 https://orcid.org/0009-0000-4719-9481
Abdullah Hamidov	Oxus University, BSc in Computer Science, Student E-mail: hamidovabdulloh734@gmail.com Tel.: +998940093627 https://orcid.org/0009-0008-9649-862X

Journal Engineer ISSN: 3030-3893 Volume:4| Issue:3| 2026

Received: 12 June 2026 | **Accepted:** 24 July 2026 | **Published:** 30 September 2026

Investigation of the tribological properties of modified composite materials used under abrasive wear conditions

U.A. Ziyamukhamedova[1][a], J.H. Nafasov[1][b], E.T. Turgunaliev[1][c], B.U. Nematov[1][d], D.A. Akhmedova[1][e]

[1]Tashkent state transport university, Tashkent, Uzbekistan

Abstract: This study investigates the tribological properties and microstructural characteristics of modified composite materials designed for operation under abrasive wear conditions. The composite materials were prepared using an ED-20 epoxy resin base, modified with bismaleimide, furfuryl alcohol, AKT-10 grade Angren kaolin, and PEK modifiers. Select samples were also reinforced with glass and silk fibers. The samples were prepared under laboratory conditions, undergoing vacuum degassing and thermal curing processes. Tribological tests were conducted using the pin-on-disk method in accordance with ASTM G99 and ISO 7148 standards. Throughout the study, the coefficient of friction, mass loss, and specific wear rate were determined to evaluate the materials' resistance to abrasive wear.

Keywords: abrasive wear, composite materials, tribological properties, ED-20 epoxy resin, bismaleimide, furfuryl alcohol, AKT-10 kaolin, PEK modifier, coefficient of friction

1. Introduction

Components operating in the mechanical engineering, transport, mining, and oil and gas industries are constantly subjected to abrasive particles, high contact pressure, and repetitive friction during operation. Under such conditions, processes of micro-cutting, micro-chipping, and plastic deformation occur on the material surface, which shortens the service life of components, increases maintenance costs, and reduces equipment reliability. Therefore, developing a new generation of composite materials with high resistance to abrasive wear is one of the most pressing scientific and practical challenges in modern materials science.

In recent years, polymer matrix composite materials have been widely used as an alternative to traditional metallic materials due to their high specific strength, corrosion resistance, low density, and favorable tribological properties. In particular, scientific research has noted that modifying epoxy resin-based composites with functional modifiers and reinforcing fibers significantly improves their mechanical, thermal, and wear-resistant properties. However, existing studies have not sufficiently explored the synergistic effects of modifiers, the influence of interphase adhesion on tribological properties, and the resulting microstructural changes.

In this study, an interpolymer composite matrix was formed based on ED-20 epoxy resin using bismaleimide, furfuryl alcohol, AKT-10 grade Angren kaolin, and PEEK modifiers, with some samples reinforced with glass and silk fibers. The coefficient of friction, mass loss, and specific wear rate of the composites under abrasive wear conditions were evaluated using the pin-on-disk method. Furthermore, the microstructure and elemental composition of the materials were analyzed using SEM and EDS methods, and the relationship between structural characteristics and tribological performance was determined.

The objective of this research is to comprehensively evaluate the tribological properties of modified composite materials used in abrasive wear conditions, determine the influence of modifiers and reinforcing fibers on the wear mechanism, and develop scientifically substantiated recommendations for creating highly wear-resistant structural materials.

2. Research methodology

In this study, an epoxy-based interpolymer matrix and functional modifiers were used to obtain modified composite materials intended for operation under abrasive wear conditions. When formulating the composite composition, the physicochemical compatibility of the matrix components, mineral fillers, and reinforcing fibers, as well as their effect on tribological properties, were taken into account.

ED-20 grade epoxy resin was selected as the primary binder for the composite material. This resin is widely used in mechanical engineering due to its high adhesion, chemical stability, mechanical strength, and good processability. Within the composite, ED-20 forms a continuous polymer matrix, serving to unite all modifying and reinforcing components into a single structure. Furthermore, the epoxy matrix plays an important role in uniformly distributing external loads and maintaining the geometric stability of the composite.

To improve the thermal and tribological properties of the matrix, the bismaleimide (BMI) modifier was used. This component is a high-temperature-resistant thermosetting compound that reacts with the epoxy resin to form a dense spatial network. As a result, the hardness, thermal stability,

[a] https://orcid.org/0000-0001-5005-0477
[b] https://orcid.org/0000-0002-0415-2584
[c] https://orcid.org/0000-0003-3257-5434
[d] https://orcid.org/0009-0002-1362-7892
[e] https://orcid.org/0009-0009-5623-9399

and abrasive wear resistance of the composite material are increased. Since bismaleimide exists in a crystalline state, it was melted before being incorporated into the composite to ensure the formation of a homogeneous mixture.

Furfuryl alcohol was used as a reactive modifier. Furfuryl alcohol participates in Diels-Alder type reactions with bismaleimide, contributing to the formation of the interpolymer structure. This component strengthens the internal structure of the epoxy matrix, improves interfacial bonding, and increases the thermal and chemical stability of the composite. Additionally, furfuryl alcohol serves to enhance the operational reliability of the material by limiting the propagation of microcracks.

Angren kaolin, grade AKT-10, was selected as the mineral filler. Kaolin particles act as a dispersion-strengthening agent within the composite, increasing the material's hardness, deformation resistance, and abrasive wear resistance. The uniform distribution of mineral particles throughout the matrix helps reduce internal stresses and ensures the stability of the surface layer during friction.

The PEK modifier was additionally introduced into the composite composition. This component is a by-product of the gas processing industry and is situated in a highly dispersed state within the composite matrix. PEK reduces the brittleness of the epoxy matrix, increases its impact toughness, and helps improve tribological properties by reducing microdeformations during friction. It also plays a significant role in enhancing the long-term operational stability of the composite.

PEPA (polyethylenepolyamine) was used as the hardener for the epoxy resin. PEPA reacts with the epoxy groups to form a three-dimensional spatial polymer network. The complete curing process is one of the key factors ensuring the mechanical strength, hardness, and heat resistance of the composite.

To provide reinforcement for the composite materials, two types of fibrous reinforcing components were used: glass fiber and silk fiber. Glass fiber, characterized by its high modulus of elasticity and mechanical strength, effectively absorbs external loads and increases the composite's abrasive wear resistance. Silk fiber, as a natural reinforcing material, slows the propagation of microcracks within the matrix, absorbs impact energy, and improves the plastic properties of the composite. The use of both reinforcing components was aimed at enhancing the microstructural integrity and improving the tribological performance of the modified composite materials.

Within the scope of the study, three composite samples with different compositions were prepared. The first sample was designated as the unreinforced control composite. 4 g of silk fiber was added to the second sample, and 4 g of glass fiber was added to the third. In all samples, the quantities of ED-20 epoxy resin, bismaleimide, furfuryl alcohol, AKT-10, and PEK were kept constant, allowing for a comparative evaluation of the reinforcing fibers' effect on tribological properties.

Preparation of Composite Specimens

Modified composite specimens were prepared under laboratory conditions based on an epoxy-based interpolymer matrix technology. The primary criteria for forming the composite composition were ensuring the chemical compatibility and uniform dispersion of the components, as well as achieving high interfacial adhesion. The specimen preparation process involved the sequential mixing of components, vacuum degassing, thermal curing, and controlled cooling.

The composite matrix was based on ED-20 epoxy resin. Since the bismaleimide used as a modifying component was in a crystalline state, it was first melted at a temperature of 65 °C. This process ensured the complete melting of the bismaleimide particles, creating the necessary conditions for their uniform distribution within the epoxy matrix. The molten bismaleimide was then cooled to 40 °C. The temperature was lowered to create optimal conditions for the Diels-Alder reaction with furfuryl alcohol and to ensure stable mixing of the components in subsequent stages. The dissolved bismaleimid was subsequently cooled to 40 °C.

Into a laboratory vessel, 62 g of ED-20 epoxy resin was placed, and 10 g of bismaleimide and 10 g of furfuryl alcohol were slowly added. The mixture was mechanically stirred for 3–5 minutes at 200–300 rpm within a temperature range of 25–35 °C. This stage ensured the uniform distribution of components at a molecular level and the formation of the initial interpolymer system. The mixing speed and duration were selected to prevent component agglomeration and to form a homogeneous matrix structure.

In the next stage, 10 g of AKT-10 grade Angren kaolin and 10 g of a PEK modifier were introduced into the composite composition. The mineral and polymer modifiers were added to the mixture sequentially and continuously stirred to achieve high dispersity. While the AKT-10 particles form a reinforcing dispersed phase within the matrix, the PEK modifier serves to reduce the brittleness of the epoxy system and mitigate local stresses that arise during friction. This stage was conducted under special supervision, as the uniform distribution of components directly influences the subsequent tribological and mechanical properties of the composite.

To form the spatial polymer network of the composite, 15 g of PEPA (polyethylenepolyamine) was added as a curing agent. The curing agent was slowly introduced into the mixture and intensively stirred for 30–60 seconds at a speed of 300–500 rpm. During this process, cross-links were formed between the epoxy and amine groups, creating a three-dimensional polymer network. The mixing duration was optimized to ensure a uniform curing reaction and to prevent the formation of air bubbles.

The resulting composite mixture was poured into three separate molds. The first specimen was left as an unreinforced control specimen. To the second specimen, 4 g of silk fiber was added, and to the third, 4 g of glass fiber was added; the fibers were carefully mixed until they were evenly distributed throughout the matrix. To prevent the reinforcing fibers from accumulating in a single orientation, mixing was performed at a low speed. This method ensured that the fibers were uniformly distributed throughout the entire volume and formed a strong interface with the matrix.

To reduce internal porosity and air bubbles in the composite specimens, a degassing process was carried out under vacuum conditions. For this, the prepared specimens were held at a temperature of 120 °C under a vacuum of -0.6 bar for 2 hours. This technological step served to increase the density of the composite, reduce internal defects, and improve interfacial adhesion.

After degassing, the specimens were cured at 150 °C for 1 hour without changing the pressure. As a result of the heat treatment, the final spatial polymer network formed in the epoxy matrix, creating an interpolymer structure strongly bonded with the modifiers. After the curing process was

https://doi.org/10.56143/3030-3893-2026-3-28-32

complete, the specimens were slowly cooled to room temperature at a rate of 3–5 °C/min to prevent the formation of internal thermal stresses.

As a result, three types of modified composite specimens were obtained, each with the same chemical composition but differing in their reinforcing components. These specimens were brought to a ready state for subsequent tribological testing and microstructural analysis.

Tribological Testing Procedure

To evaluate the tribological properties of the modified composite materials, abrasive wear tests were conducted under laboratory conditions using a pin-on-disc (pin–disk) type tribometer. The tests were organized in accordance with the requirements of ASTM G99, ASTM G132, and ISO 7148-2 standards. This method enables a reliable assessment of the wear mechanism, coefficient of friction, and service performance of materials in abrasive environments under sliding friction conditions.

The tribological testing apparatus consisted of a rotating abrasive disc, a sample holder, a mechanism for applying normal load, friction force sensors, and a digital control system. The abrasive disc was driven at a constant rotational speed by a servo-electric motor, while the composite sample was maintained in continuous contact with the disc surface under a specified normal load. The friction force generated during the process was continuously recorded by electronic sensors, and the coefficient of friction was automatically calculated in real-time throughout the test.

Prior to testing, all composite samples were prepared to standard geometric dimensions. The samples were fabricated in a cylindrical shape, and their working surfaces underwent mechanical grinding to ensure full contact with the abrasive disc. To eliminate dust and other surface contaminants, the samples were cleaned with an organic solvent and dried at room temperature. The initial mass of each sample was measured on an analytical electronic balance with an accuracy of 0.001 g and recorded for subsequent calculations.

During the tribological tests, all samples were examined under identical experimental conditions. The normal load, rotational speed of the abrasive disc, friction path, and test duration were selected based on predetermined values and kept constant in all experiments. This approach allowed for an objective evaluation of the influence of reinforcing components and modifiers on the tribological properties. During the test, continuous sliding contact was established between the composite samples and the abrasive disc, modeling the abrasive wear process on the material's surface.

3. Results and Discussions

The tribological properties of a composite sample based on ED-20 epoxy resin, containing 10 g of bismaleimide, furfuryl alcohol, AKT-10, and PEK additives, were investigated using a tribometer. The tests were conducted under five different normal loads (1.96 N, 3.92 N, 5.886 N, 7.848 N, and 11.8 N) at a constant rotational speed. The change in the coefficient of friction over time (the test interval) was recorded, and the obtained results were comprehensively analyzed. 5.886 N; 7.848 N; 11.8 N), the rotation speed was maintained at a constant level.

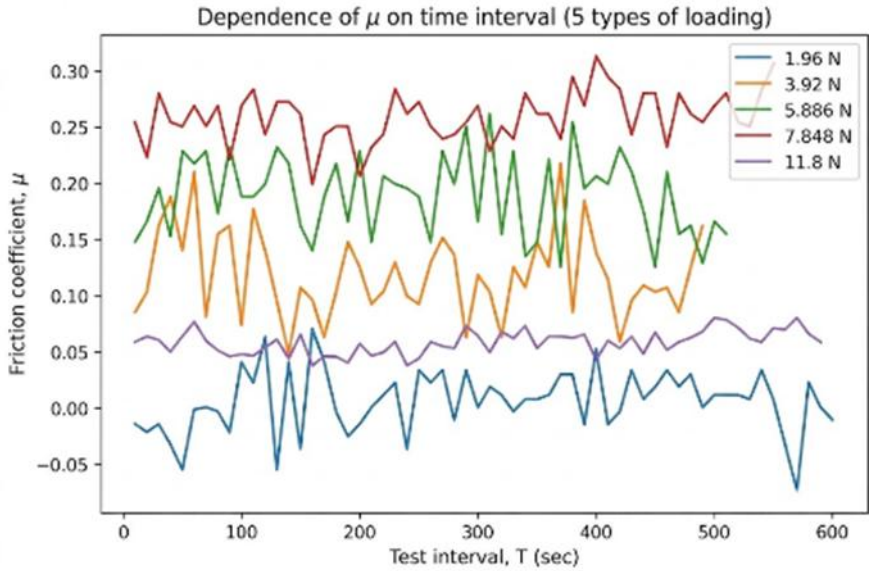


Fig. 1. The dependence of the friction coefficient of an interpolymer composite material on the friction time under various loads

The research results showed that the coefficient of friction (μ) of the composite sample changes according to a specific pattern as the load increases. Specifically, an increase in the coefficient of friction was observed in the range from low to medium loads. At a load of 1.96 N, the μ values were very low, and in some instances, negative values were even recorded. This phenomenon is explained by the incomplete formation of a stable friction regime in the contact zone, as well as the high sensitivity of the measurement system at low loads.

Under a load of 3.92 N, the average value of the coefficient of friction stabilized at approximately 0.11. In the initial stage of the test, μ showed higher values before subsequently decreasing to a certain level. This is explained by the mutual adaptation of the tribological pair surfaces—that is, the running-in stage where the contact surfaces are

smoothed. At this stage, surface asperities are partially flattened, and the contact area stabilizes.

At a load of 5.886 N, the coefficient of friction increased further, registering an average of around 0.18–0.19. At this load, frictional forces increase due to the activation of adhesive effects and micro-cutting mechanisms. Concurrently, protective structural elements may begin to form on the surface due to the influence of thermosetting and thermally stable components within the composite.

The highest coefficient of friction was observed at a load of 7.848 N ($\mu \approx 0.26$). This is associated with the intensification of deformational-adhesive interactions resulting from increased contact pressure, as well as the activation of micro-wear processes in the surface layers. In this regime, the change in the coefficient of friction over time is relatively stable, indicating that the mechanical strength of the composite material is sufficient.

Interestingly, a sharp decrease in the coefficient of friction was observed at a load of 11.8 N ($\mu \approx 0.058$). Typically, an increase in load should increase μ, but the opposite was recorded for this composite. This can be explained by the formation of a mobile protective film on the surface under high-temperature and high-load conditions by the PEK polymer, furan structures derived from furfuryl alcohol, and bismaleimide resins in the composite. This film isolates the contact surfaces from direct metal-polymer interaction, facilitating sliding and reducing the coefficient of friction.

The stability of the coefficient of friction over time was also evaluated. According to the analysis, the most stable operating regime was observed at a load of 11.8 N, where the fluctuation amplitude of the μ values was minimal. This indicates that the resulting protective film is stable and continuous. In the 3.92–5.886 N range, fluctuations were moderate, while at 7.848 N, μ remained stable despite being high.

Based on the results obtained, it was determined that the composite based on ED-20, modified with bismaleimide, furfuryl alcohol, AKT-10, and PEK additives, exhibits effective tribological properties under high loads. The decrease in the coefficient of friction at a load of 11.8 N was caused by the formation of a protective film that facilitates sliding on the surface. The lowest and most stable friction regime was observed at a load of 11.8 N, indicating that this composite is effective for tribo-pairs operating under high-load conditions.

4. Conclusion

In this study, the tribological properties of an interpolymer composite material were investigated under abrasive wear conditions. The material is based on ED-20 epoxy resin and modified with bismaleimide, furfuryl alcohol, AKT-10 grade Angren kaolin, and a PEK modifier. The conducted tribological tests showed that the developed composite material exhibits stable friction characteristics under various normal loads. During the tests, the variation of the friction coefficient over time confirmed the formation of a stable tribological contact on the material's surface and indicated the composite's high operational stability during the friction process.

According to the research results, the friction coefficient changes in a specific pattern with an increase in the normal load, and a significant decrease was observed under a load of 11.8 N. This phenomenon is explained by the formation of a protective tribo-film on the composite surface and improved sliding conditions in the contact zone. The combined action of bismaleimide, furfuryl alcohol, AKT-10 kaolin, and the PEK modifier contributed to the formation of a robust interpolymer structure within the epoxy matrix, which served to reduce the destructive effect of abrasive particles.

The obtained results demonstrated that the developed modified composite material possesses a low friction coefficient and stable tribological properties even under high load conditions. This allows for the recommendation of this material as a promising structural material for manufacturing sliding bearings, bushings, guide elements, and other machine components operating in abrasive environments.

References

[1] Evlen, H., Ziyamukhamedova, U., Juraev, D., & Abdukarimov, M. (2023). Additive manufacturing of bionanomaterials for biomedical applications based on TI6AL4V and PLA: a systematic review. In E3S Web of Conferences (Vol. 401, p. 03040). EDP Sciences.

[2] Ziyamukhamedova, U., Bakirov, L., Donaev, S., Miradullaeva, G., & Turgunaliev, E. (2023). Study of structure formation processes in matrices of mixed components with reinforcing natural fillers. In E3S Web of Conferences (Vol. 401, p. 05074). EDP Sciences.

[3] Ziyamukhamedova, U., Rakhmatov, E., Dustqobilov, E., Nafasov, J., & Ziyamukhamedov, J. (2023, June). Development of protective coating compositions for process tanks. In AIP Conference Proceedings (Vol. 2789, No. 1). AIP Publishing.

[4] Ziyamukhamedova, U. A., Almataev, T. O., Dzhumabaev, A. B., & Bakirov, L. Y. (2022, June). Improvement of methods and means of testing non-conventional tribosystems. In AIP Conference Proceedings (Vol. 2432, No. 1, p. 030031). AIP Publishing LLC.

[5] Nurkulov, F., Ziyamukhamedova, U., Rakhmatov, E., & Nafasov, J. (2021). Slowing down the corrosion of metal structures using polymeric materials. In E3S web of conferences (Vol. 264, p. 02055). EDP Sciences.

[6] Miradullaeva, G., Rakhmatov, E., Bozorov, O., Ziyamukhamedova, U., & Shodiev, B. (2021). Mathematical modeling of rheological properties during structure formation of heterocomposite potting materials and coatings and their application. In Proceedings of EECE 2020: Energy, Environmental and Construction Engineering 3 (pp. 346-355). Springer International Publishing.

[7] Ziyamukhamedova, U., Evlen, H., Nafasov, J., Jalolova, Z., Turgunaliyev, E., & Rakhmatov, E. (2023). Modeling of the process of mechano activation of filler particles in polymer composites. In E3S Web of Conferences (Vol. 401, p. 05027). EDP Sciences.

[8] Khalimov, S., Nishonov, F., Begmatov, D., Mohammad, F. W., & Ziyamukhamedova, U. (2023). Study of the physico-chemical characteristics of reinforced composite polymer materials. In E3S Web of Conferences (Vol. 401, p. 05039). EDP Sciences

[9] Zhang G., Ke Y., He J., Qin M., Shen H., Lu S., Xu J. Effects of organo-modified montmorillonite on the tribology performance of bismaleimide-based

nanocomposites. Materials & Design, 86 (2015), 138–145. https://doi.org/10.1016/j.matdes.2015.07.090

[10] Kurahatti R.V., Surendranathan A.O., Mordina B., Naik P., Auradi V. Friction and dry sliding wear of bismaleimide filled with carbon nanotubes. Tribology: Materials, Surfaces & Interfaces, 10(3), 2016.

[11] Katiyar J.K., Sinha S.K., Kumar A. Effects of carbon fillers on the tribological and mechanical properties of an epoxy-based polymer (SU-8). Tribology: Materials, Surfaces & Interfaces, 10(1), 2016.

[12] Yu S., Feng Y., Wang W., Li Q., Xu F., Huang X., Qiao X., Zhu M. Curing Kinetics of Bismaleimide Resin and High-Temperature Tribological Properties of Fabric-Reinforced Composites. ACS Applied Polymer Materials, 2026. https://doi.org/10.1021/acsapm.6c01293

[13] Zhang Y., Luo X., Qi Y., Tian J., Qian Y. Enhancing the Tribological Performance of Epoxy Composites With Glass Fiber Powder. Polymer Composites, 2026. https://doi.org/10.1002/pc.71240

[14] Mahesh V. Effect of Surface Modification on Wear Behaviour of Coconut Shell-Filled Epoxy Composites. Tribology in Industry, 48(1), 2026.

[15] Tribological response of epoxy composite lining filled with zirconia and fly ash under dry sliding conditions. Results in Engineering, 2026. https://doi.org/10.1016/j.rineng.2026.110533

[16] Aydın F., Karaoğlan K.M., Yakut Pektürk H., Demir B., Karakurt V., Ahlatçı M. The comparative evaluation of the wear behavior of epoxy matrix hybrid nanocomposites via experiments and machine learning models. Tribology International, 2025. https://doi.org/10.1016/j.triboint.2024.110451

[17] Enhancing the tribological performance of polymeric laminated composite materials by adopting the functionally graded materials technique. Archives of Civil and Mechanical Engineering, 25, 2025.

Information about the author

Umida Ziyamukhamedova	Tashkent State Transport University, Department of Materials Science and Mechanical Engineering, Doctor of Technical Sciences (D.Sc.), Professor E-mail: z.umida1973@yandex.ru Tel.: +998911915665 https://orcid.org/0000-0001-5005-0477
Jasurbek Nafasov	Tashkent State Transport University Department of Materials Science and Mechanical Engineering, Associate Professor, PhD E-mail: nafasovz@mail.ru Tel.: +99877 020 88 57 https://orcid.org/0000-0002-0415-2584
Elbek Turgunaliev	Tashkent State Transport University Department of Materials Science and Mechanical Engineering, Associate Professor, PhD E-mail: elbekturgunaliyev@gmail.com https://orcid.org/0000-0003-3257-5434
Bekhruz Nematov	Tashkent State Transport University Department of Materials Science and Mechanical Engineering, PhD student E-mail: Bekhruz.Nematov@uzgtl.com Tel.: +998 90 443 21 11 https://orcid.org/0009-0002-1362-7892
Dilafruz Akhmedova	Tashkent State Transport University Department of Materials Science and Mechanical Engineering, Assistant https://orcid.org/0009-0009-5623-9399

Journal Engineer ISSN: 3030-3893 Volume:4| Issue:3| 2026

Received: 15 June 2026 | **Accepted:** 27 July 2026 | **Published:** 30 September 2026

A multi-layer information model and adaptive algorithms for monitoring hybrid energy supply in IoT-based telecommunication networks

J.Kh. Djumanov[1], M.A. Sobirov[2]

[1]Tashkent university of information technologies named after Muhammad al-Khwarizmi, Tashkent, Uzbekistan

[2]Tashkent state transport university, Tashkent, Uzbekistan

Abstract: Most deployed energy-monitoring systems only measure electrical parameters and transmit them to a remote server, whereas equipment condition assessment and automatic optimisation remain undeveloped. This paper proposes the architecture and the mathematical model of a hybrid monitoring platform uniting IoT sensing, edge computing, cloud analytics and digital-twin technology in one six-layer framework. A multi-stage edge-side conditioning scheme is developed, the digital-twin state residual is introduced as a diagnostic feature for early fault detection, and an integral Energy Efficiency Index with a carbon-footprint model is formulated so that technical and environmental criteria are evaluated in one loop. The testbed on a 0.4 kV three-phase feeder and the 180-day dataset of 17 280 records collected on it are described. The deep-learning forecasting layer built on this architecture is treated in a companion study.

Keywords: energy monitoring, Internet of Things, edge computing, digital twin, Kalman filter, energy efficiency index, carbon footprint, predictive maintenance

1. Introduction

The rapid growth of electricity demand has made the efficient use of energy resources one of the most active research directions in power and information engineering. World final energy consumption is growing by 1.8–2.3 % per year, driven by industrial expansion, digital infrastructure and the proliferation of connected devices [1]. Real-time monitoring has therefore become a prerequisite rather than an optional feature of modern energy management.

Conventional equipment is oriented towards measuring voltage, current and power, and therefore only *records* consumption; the acquired data are used mainly for retrospective reporting, so energy waste is identified after it has occurred. The Internet of Things has advanced this field considerably [2], but in cloud-centric architectures the whole processing burden falls on a central server, which increases latency and creates a hard dependency on connectivity. Edge computing addresses exactly this problem [3].

Monitoring alone, however, is no longer sufficient. Recent studies indicate that it must be integrated with artificial intelligence and digital-twin technology [4], [5]. A digital twin is a virtual replica of a physical asset synchronised in real time, enabling state observation, "what-if" simulation and early fault prediction [5], [6]. In the power sector digital twins have mostly been applied to generation assets, whereas their integration into demand-side distributed monitoring remains insufficiently studied.

The scope of this paper is the computing platform itself: its layered structure, its operating algorithm, the mathematical description of the measurement chain and the evaluation infrastructure on which it was deployed. The deep-learning forecasting layer that runs on top of the platform, together with its comparative evaluation and field results, is the subject of a companion study.

The contributions are: (i) a six-layer architecture unifying monitoring, digital-twin synchronisation and techno-environmental assessment; (ii) a multi-stage edge-side conditioning scheme; (iii) the digital-twin state residual as a diagnostic feature; and (iv) an integral Energy Efficiency Index (EEI) coupled with a carbon-footprint model.

2. Research methodology

Related Work and Problem Statement

Early monitoring devices were analogue and could not process large data volumes. Microcontroller platforms such as Arduino, Raspberry Pi and ESP32 later enabled accurate measurement with cloud storage, and current research is concentrated on edge computation, AI-driven analytics, digital twins, predictive maintenance and carbon-footprint tracking [4], [6].

Table 1 summarises a comparative analysis of existing solutions. None of the reviewed systems combines monitoring, forecasting, digital-twin synchronisation, integral energy-efficiency assessment and environmental-impact estimation within a single platform.

Table 1

Comparative analysis of existing energy-monitoring systems

System / approach	Real time	Edge comp.	Fore-cast	Digital twin	Effic. index	Carbon footpr.
Conventional SCADA	✓	–	–	–	–	–
Microcontroller IoT meters	✓	–	–	–	–	–

https://doi.org/10.56143/3030-3893-2026-3-33-37

IoT with statistical forecasting	✓	–	⊙	–	–	–
IoT with machine learning	✓	⊙	✓	–	–	–
IoT with deep learning	✓	⊙	✓	–	–	–
Generation-side digital twins	✓	–	✓	✓	–	–
Proposed platform	✓	✓	✓	✓	✓	✓

✓– supported; ⊙– partially supported; –– not supported.

The research problem is therefore stated as follows: *to develop a computing architecture and its mathematical model that provide real-time observation of energy consumption in a distributed IoT infrastructure, assessment of equipment condition through a digital twin, and integral evaluation of energy efficiency and environmental impact.*

System Architecture

The platform is intended not only to observe electricity consumption in real time, but also to assess the technical condition of the equipment and optimise energy use automatically. Functionally the architecture is divided into six layers (Fig. 1).

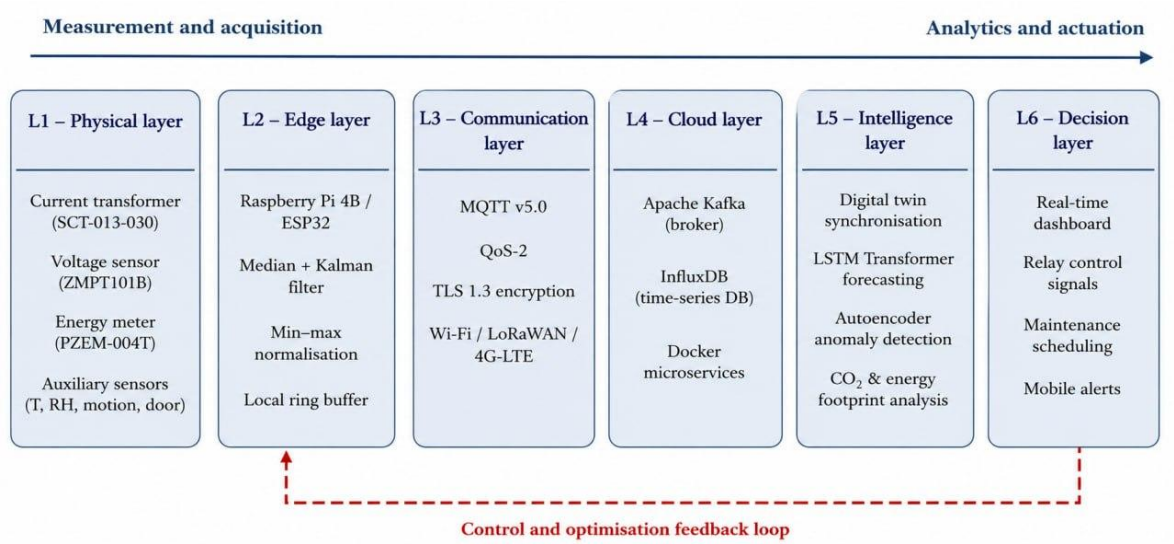


Fig. 1. Six-layer architecture of the proposed hybrid energy-monitoring platform. Solid arrows denote the data path; the dashed arrow denotes the control and optimisation feedback loop

L1 – physical layer contains the measurement chain: an SCT-013-030 current transformer, a ZMPT101B voltage sensor, a PZEM-004T energy meter and auxiliary temperature, humidity and motion sensors.

L2 – edge layer (ESP32 and Raspberry Pi 4B) performs primary conditioning – a median filter suppresses impulsive noise, a Kalman filter suppresses measurement noise – and writes normalised data to a local ring buffer that prevents data loss during outages.

L3 – communication layer transmits data over MQTT (QoS-2) with TLS 1.3 encryption [7] through Wi-Fi, LoRaWAN or 4G-LTE, and **L4 – cloud layer** distributes the stream by an Apache Kafka broker, stores it in InfluxDB and runs all services as Docker microservices.

L5 – intelligence layer performs digital-twin synchronisation, forecasting, anomaly detection and computation of the EEI and the carbon footprint, while **L6 – decision layer** visualises the results, issues relay control signals, updates the maintenance schedule and notifies the user.

Digital-Twin Loop

The digital twin is a mathematical model synchronised with the state vector of the physical asset with a synchronisation period of $\Delta t = 1$s. Its discrete state model is

$$\hat{x}(t+1) = A\,\hat{x}(t) + B\,u(t) + w(t), \qquad (1)$$

where A is the system matrix, B the control matrix, $u(t)$ the control action and $w(t)$ the process noise. The mismatch between the asset and its twin is the residual norm

$$\delta(t) = \|x(t) - \hat{x}(t)\|_2. \qquad (2)$$

If $\delta(t) > \delta_{\text{th}}$, the platform concludes that the technical condition of the equipment has changed and activates the predictive-maintenance module. The residual therefore acts as a model-based diagnostic feature: it reacts to parameter drift even while the measured power still lies inside its normal range, which is what makes early warning possible.

Operating Algorithm

The complete operating cycle is shown in Fig. 2 and formalised in Algorithm 1. It starts with sensor calibration, rejects invalid frames through a validity test, and closes with energy-efficiency evaluation and an anomaly check.

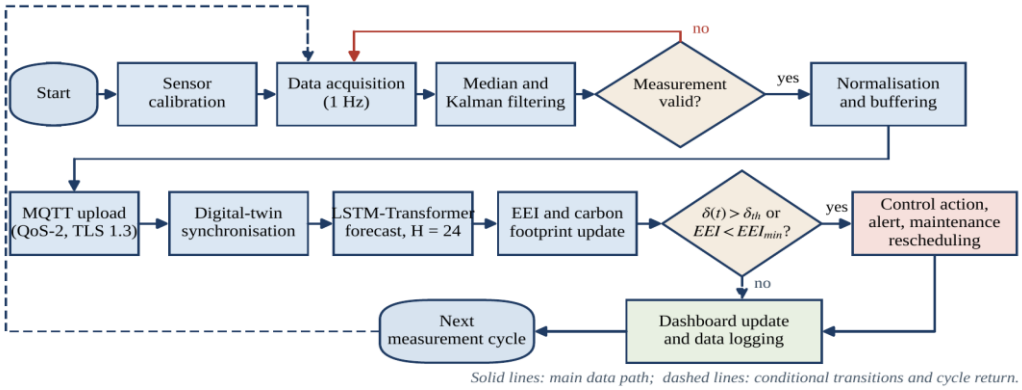


Fig. 2. Block diagram of the operating algorithm. Solid lines denote the main data path; dashed lines denote conditional transitions and the return of the measurement cycle

Algorithm 1. Operating cycle of the platform

1. Calibrate the sensors; initialise the twin state $\hat{x}(0)$.
2. Acquire the frame z_k at 1 Hz, apply the median filter and the Kalman update (7); discard invalid frames.
3. Normalise by (8), buffer locally and publish over MQTT.
4. Synchronise the twin, compute $\delta(t)$ by (2), update the EEI by (9) and the carbon footprint by (10).
5. If $\delta(t) > \delta_{\text{th}}$ or $\text{EEI} < \text{EEI}_{\min}$, solve(11) and issue the control action and the alert; update the dashboard and return to step2.

Mathematical Model of the Measurement Chain

For a single-phase circuit the active, apparent and reactive powers are

$$P = UI\cos\varphi, \quad S = UI, \quad Q = UI\sin\varphi, \tag{3}$$

where P is the active power (W), S the apparent power (VA), Q the reactive power (var), U and I the r.m.s. voltage and current, and φ the phase-shift angle. The power-triangle relation holds:

$$S^2 = P^2 + Q^2. \tag{4}$$

For a balanced three-phase load the active power is

$$P_{3\varphi} = \sqrt{3}\, U_L I_L \cos\varphi. \tag{5}$$

The energy consumed over an interval is obtained in integral form and, with step Δt, in discrete form:

$$E = \int_{t_1}^{t_2} P(t)\,\mathrm{d}t = \sum_{k=1}^{N} P_k\ \Delta t. \tag{6}$$

At the edge node the measurement noise is suppressed by a Kalman filter [8]:

$$\hat{x}_k = \hat{x}_k^- + K_k(z_k - H\hat{x}_k^-), \tag{7}$$

where K_k is the Kalman gain, z_k the measurement and H the observation matrix. Filtered values are then mapped to [0,1]:

$$x_{\text{norm}} = \frac{x - x_{\min}}{x_{\max} - x_{\min}}. \tag{8}$$

This ordering is essential: the median stage removes the impulsive outliers that would otherwise bias the Kalman innovation, so that the linear filter operates under the noise assumptions for which it is optimal. Its quantitative effect on forecasting accuracy is measured by the ablation study of the companion study.

Energy Efficiency Index and Carbon Footprint

The Energy Efficiency Index is defined as the ratio of ideal to actual consumption, the ideal value being computed from the nominal operating modes of the equipment:

$$\text{EEI} = \frac{E_{\text{ideal}}}{E_{\text{real}}}, \quad E_{\text{ideal}} = \sum_{i=1}^{n} P_{\text{nom},i}\ t_i. \tag{9}$$

The platform operates at maximum efficiency as $\text{EEI} \to 1$; the optimisation module is triggered when $\text{EEI} < \text{EEI}_{\min}$. The carbon footprint of the consumed electricity is estimated as

$$C_{\text{CO}_2} = k\,E, \tag{10}$$

where k is the emission factor of the supply mix (kg CO_2/kWh); $k = 0.468$ kg CO_2/kWh was adopted for the power system of Uzbekistan. Energy-use optimisation is posed as the constrained minimisation problem

$$\min_{\{E_i\}} \sum_{i=1}^{n} c_i\,E_i, \quad P_{\min} \le P_i \le P_{\max}, \quad \text{EEI} \ge \text{EEI}_{\min}. \tag{11}$$

where c_i is the tariff coefficient of the i-th interval. Relations (9)–(11) place the technical, environmental and economic criteria in one loop, so that an optimisation decision can be justified in all three terms simultaneously.

Experimental Infrastructure and Dataset

A testbed connected to a 0.4kV three-phase network was assembled (Fig.3); the test object was a production area with a total installed capacity of 18.5 kW. Power-quality quantities were acquired in accordance with IEC 61000-4-30 [9] and the sensor interface followed IEEE 1451.0 [10]. The specification is given in Tab.2

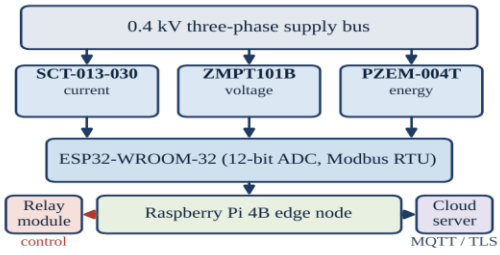


Fig. 3. Block diagram of the experimental testbed

https://doi.org/10.56143/3030-3893-2026-3-33-37

Table 2

Technical specification of the experimental testbed

Component	Model / value	Characteristics
Current sensor	SCT-013-030	0–30 A, error ±0.5 %
Voltage sensor	ZMPT101B	0–250 V, error ±0.4 %
Energy module	PZEM-004T v3.0	Modbus RTU, 0–100 A
Microcontroller	ESP32-WROOM-32	240 MHz, 12-bit ADC
Edge node	Raspberry Pi 4B	4 GB RAM, Cortex-A72
Protocol	MQTT v5.0 / TLS 1.3	QoS-2, Wi-Fi 802.11n
Cloud server	Ubuntu 22.04 LTS	8 vCPU, 32 GB RAM, GPU T4
Software	PyTorch 2.1	Python 3.11, InfluxDB 2.7

Data were collected continuously over 180 days, from December 2025 to May 2026, at a primary sampling rate of 1 Hz and then aggregated into 15-minute intervals, yielding 17 280 records with seven features each (Table 3). The same dataset is used in the companion study.

Table 3

Statistical description of the dataset

Quantity	Mean	SD	Min.	Max.	Median
Active power P, kW	7.42	3.55	1.60	22.84	6.31
Voltage U, V	220.0	2.64	212.3	227.9	220.1
Current I, A	12.26	5.74	2.71	37.10	10.43
Power factor cosφ	0.895	0.041	0.702	0.972	0.905
Reactive power Q, kvar	3.71	1.92	0.58	12.44	3.12
Daily energy E, kWh	178.1	42.7	94.3	281.6	172.8

Fig.4 shows the mean daily load profiles for working days and weekends. The series exhibits pronounced daily and weekly periodicity: on working days a morning ramp is followed by a mid-day peak and a secondary afternoon peak, whereas weekend profiles are flatter and roughly 45 % lower in amplitude. This regular structure is what makes the series suitable for multi-step forecasting.

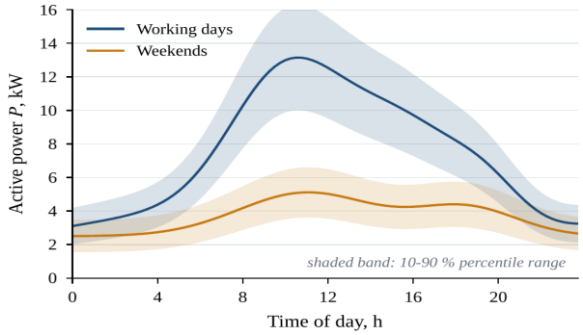


Fig. 4. Mean daily load profiles for working days and weekends; the shaded band denotes the 10–90 % percentile range

3. Conclusion

This paper has presented the architecture, the mathematical model and the experimental infrastructure of a hybrid digital-twin monitoring platform. The main outcomes are as follows.

1. A six-layer architecture was proposed in which measurement, edge conditioning, secure transport, cloud storage, intelligent analysis [11] and decision making are separated into explicit layers connected by a control feedback loop; the operating cycle was formalised as Algorithm 1.
2. A multi-stage edge-side conditioning scheme (median→ Kalman→ normalisation) was formulated and justified.
3. The digital-twin residual $\delta(t)$ was introduced as a diagnostic feature that reacts to parameter drift before it becomes visible in the measured power.
4. An integral EEI and a carbon-footprint model were combined with a tariff-aware optimisation problem, and a 180-day dataset of 17 280 records was collected on a 0.4 kV three-phase testbed.

A companion study builds a hybrid LSTM–Transformer forecasting model on this architecture, benchmarks it against eight reference algorithms, quantifies the contribution of every component by an ablation study and reports the energy and environmental results obtained at five types of facility.

References

[1] International Energy Agency, “Energy efficiency 2023,” IEA, Paris, France, Tech. Rep., 2023.

[2] L. Atzori, A. Iera, and G. Morabito, “The Internet of Things: A survey,” Comput. Netw., vol. 54, no. 15, pp. 2787–2805, 2010.

[3] W. Shi, J. Cao, Q. Zhang, Y. Li, and L. Xu, “Edge computing: Vision and challenges,” IEEE Internet Things J., vol. 3, no. 5, pp. 637–646, Oct. 2016.

[4] Y. LeCun, Y. Bengio, and G. Hinton, “Deep learning,” Nature, vol. 521, no. 7553, pp. 436–444, May 2015.

[5] M. Grieves and J. Vickers, “Digital twin: Mitigating unpredictable, undesirable emergent behavior in complex systems,” in Transdisciplinary Perspectives on Complex Systems. Cham, Switzerland: Springer, 2017, pp.85–113.

[6] F. Tao, H. Zhang, A. Liu, and A. Y. C. Nee, “Digital twin in industry: State-of-the-art,” IEEE Trans. Ind. Informat., vol. 15, no.4, pp.2405–2415, Apr. 2019.

[7] OASIS, “MQTT version 5.0,” OASIS Standard, Mar. 2019.

[8] R. E. Kalman, “A new approach to linear filtering and prediction problems,” J. Basic Eng., vol. 82, no.1, pp. 35–45, Mar. 1960.

[9] Electromagnetic Compatibility (EMC) – Part 4-30: Power Quality Measurement Methods, IEC Standard 61000-4-30:2015, 2015.

[10] Muzaffar Sobirov, Ilmira Kurbanova, Zebuniso Sobirova; Fuzzy network analysis for neuron viability in production models. AIP Conf. Proc. 30 March 2026; 3374 (1): 050096. https://doi.org/10.1063/5.0317178

[11] Sobirov, Muzaffar. "Application OF Modern Information Systems in the Assessment OF the Technical Condition OF the Equipment OF Electrical Energy Networks." Green Economy and Development, vol. 3, no. 9, 1 Sep. 2025, doi:10.5281/zenodo.17217385.

Information about the author

Jamoljon Djumanov	Professor of the Department of Computer Systems, Tashkent University of Information Technologies named after Muhammad al-Khwarizmi E-mail: jamoljon@tuit.uz
Muzaffar Sobirov	Independent Researcher of the Department of Information Systems and Technologies in Transport E-mail: muzaffarsobirov538@gmail.com

Journal Engineer ISSN: 3030-3893 Volume:4| Issue:3| 2026

Received: 17 June 2026 | **Accepted:** 29 July 2026 | **Published:** 30 September 2026

Assessment of the technical condition of a transformer based on the operational parameters of its oil using the fuzzy logic method

D. Yusupov[1][a], O. Kutbidinov[2][b], B. Avazov[2]

[1]Institute of Energy Problems, Academy of Sciences of the Republic of Uzbekistan, Tashkent, Uzbekistan
[2]Tashkent state transport university, Tashkent, Uzbekistan

Abstract: In this article, a mathematical model and decision-making algorithm based on the theory of fuzzy logic were developed to assess the technical condition of a transformer based on the operational indicators of its oil. In the study, the water content, acid number, amount of mechanical impurities, kinematic viscosity, density, flash point, electrical strength and dielectric loss of transformer oil were selected as the main diagnostic parameters characterizing the technical condition of the transformer. Membership functions were formed for each parameter, a fuzzy rule base was created based on expert knowledge and regulatory documents, and an integral technical condition indicator was calculated using the Mamdani inference algorithm and the centroid method. The results of the study showed that the developed model allows for a comprehensive analysis of the relationship between the diagnostic indicators of transformer oil, determining the degree of degradation of the transformer insulation system, and dividing its technical condition into the categories of "very bad", "bad", "average", "good" and "excellent". The proposed approach serves to increase the operational reliability of transformers, prevent accidents, introduce condition-based maintenance systems, and extend the service life of transformers.

Keywords: transformer oil, fuzzy logic, mathematical model, technical diagnostics, membership function, decision-making algorithm, defuzzification

1. Introduction

Power transformers are among the most critical and expensive elements of the power system, and their reliable operation is crucial for ensuring the continuity of the power supply. Transformer oil acts as an insulating and cooling medium; therefore, its physicochemical and electrical properties are among the primary factors determining the overall technical condition of the transformer. During operation, under the influence of high temperatures, humidity, oxidation, and electrical loads, the properties of the oil gradually deteriorate, which reduces the reliability of the transformer and leads to various malfunctions. When assessing the technical condition of transformer oil, diagnostic indicators such as water content, acid number, mechanical impurities, electrical strength, dielectric loss, density, kinematic viscosity, and flash point are typically used. However, the separate assessment of these parameters cannot fully and objectively reflect the overall state of the oil, as they have a complex interdependence. Therefore, the development of comprehensive assessment methods that account for the interaction of parameters is one of the most pressing scientific and practical issues. The theory of fuzzy logic allows for the consideration of existing uncertainties in evaluating complex technical systems and the integration of expert knowledge into a mathematical model, making it one of the most optimal tools for solving this task. Based on this, the aim of this study is to develop a mathematical model and a decision-making algorithm based on fuzzy logic, aimed at evaluating the interaction between the diagnostic parameters of transformer oil and determining its overall technical condition through a single integral indicator.

Literature review

Assessment of the technical condition of transformers, increasing their reliability and preventing possible failures during operation are one of the important scientific directions of modern power systems. Existing scientific studies have shown that the analysis of the physicochemical and dielectric properties of transformer oil is widely used as an effective diagnostic method for determining the condition of the transformer insulation system.

Studies conducted by Voprikov A.V., Grigoriev N.P. and Parfianovich A.P. considered the issues of extending the service life of power transformers used in traction substations of electric railways. The studies noted that the operational reliability of transformers depends mainly on the condition of the insulation system and the effectiveness of technical maintenance [1].

Bryakin I.V. and co-authors studied methods for monitoring the condition of transformers based on assessing the properties of transformer oil. In this work, the main diagnostic indicators of the oil - electrical strength, moisture content, acid number, mechanical impurities and other physicochemical parameters - are considered as important criteria for determining the degradation of the transformer insulation system [6].

Analytical studies conducted by Soni R. and Mehta B. on monitoring the technical condition of transformers studied the diagnostic capabilities of mineral oils and alternative dielectric fluids. The authors noted that most of the existing diagnostic methods are based on the assessment

[a] https://orcid.org/0000-0001-6569-4806
[b] https://orcid.org/0000-0001-9290-5322

of individual parameters and the need to develop complex multi-parameter assessment systems [10].

Studies aimed at in-depth study of the physicochemical processes in transformer oil analyzed the impact of moisture content, oxidation products, mechanical impurities and dielectric losses in the oil on the transformer insulation system. Feng Chen and co-authors proposed technologies for the restoration of transformer insulation oil and data-based restoration systems, in which oil quality control was considered as a means of increasing the operational reliability of the transformer [7].

Nazarychev A.N. and co-authors studied methods for diagnosing the main insulation of transformers based on the electrical strength of the oil. This work shows that the electrical strength of the oil is one of the main diagnostic indicators for determining the technical condition of transformer insulation [13].

In recent years, many studies have been carried out on the use of artificial intelligence methods, in particular, fuzzy logic, neural networks and expert systems in transformer diagnostics. These methods, unlike traditional boundary assessment methods, allow taking into account the interdependence of diagnostic parameters and making more accurate decisions in uncertain conditions. This approach allows combining several operational indicators of transformer oil into a single integral assessment criterion.

Darwish M.M.F. and co-authors developed a new diagnostic method based on infrared spectroscopy to detect faults in transformer oil. This study shows the need for a comprehensive analysis of various physical measurements in modern diagnostic systems [11].

Also, in the works on the cleaning and regeneration of transformer oils using an electric field, Yusupov D.T., Avazov B.K. and other researchers studied the possibilities of reducing impurities in the oil that affect the mechanical and dielectric properties under the influence of an electric field. These studies are aimed at improving the operational performance of transformer oil and extending the service life of transformers [17].

The analysis of the above scientific works shows that in existing studies, effective methods have been developed for assessing individual diagnostic parameters of transformer oil, cleaning oil and monitoring the condition of transformers. However, in most approaches, diagnostic parameters are not evaluated in a comprehensive manner in relation to each other or decisions are made based on strict threshold values. This creates certain limitations in determining the actual technical condition of the transformer in cases where the parameters are uncertain.

Therefore, in this study, the issue of developing a mathematical model and decision-making algorithm based on Fuzzy Logic theory based on eight main operational indicators of transformer oil (electric strength, water content, acid number, mechanical impurities, kinematic viscosity, density, flash point and dielectric losses) is considered as an urgent scientific and practical task. The proposed approach allows taking into account the interaction of diagnostic parameters, determining the degree of degradation of the transformer insulation system and improving maintenance processes.

2. Research methodology

In this study, a mathematical model and decision-making algorithm based on the theory of fuzzy logic were developed to assess the technical condition of a transformer based on the operational indicators of transformer oil. The research methodology includes the following main stages: selection and analysis of the main diagnostic parameters of transformer oil, determination of their influence on the technical condition of the transformer, formation of membership functions for the parameters, development of a fuzzy rule base based on expert knowledge, and determination of the integral technical condition of the transformer based on the results obtained. The theoretical basis of the study is the theory of fuzzy logic, the theory of multi-criteria decision-making, and mathematical modeling methods. The initial data were the normative values established in the current regulatory documents on the diagnostic parameters of transformer oil and expert assessments. The theoretical basis of the study is the theory of fuzzy logic, the theory of multi- criteria decision-making, and the theory of mathematical modeling. The integrated application of these theoretical approaches serves as a scientific basis for accurately assessing the technical condition of transformer oil, analyzing degradation processes, and increasing the operational reliability of transformers.

3. Results

The mathematical model developed to assess the technical condition of the transformer consisted of several consecutive stages that express the relationship between the operational indicators of the transformer oil and the general technical condition of the transformer. Initially, the main diagnostic parameters characterizing the technical condition of the transformer - electrical strength of the oil, water content, acid number, amount of mechanical impurities, kinematic viscosity, density, flash point and dielectric loss - were selected and their normative and operational values were analyzed. At the next stage, membership functions were formed for each diagnostic parameter, linguistic variables and their value ranges were determined, and a fuzzy logic rule base was developed based on expert knowledge and current regulatory documents. The input parameters were processed using the fuzzy inference mechanism, and the integral technical condition indicator of the transformer was calculated through the defuzzification process. Based on the results obtained, it was possible to classify the technical condition of the transformer into the categories of "excellent", "good", " average ", "bad" and "very bad". The proposed model serves as a scientific basis for comprehensive consideration of the complex interrelationships between the diagnostic indicators of transformer oil, comprehensive assessment of the degree of degradation of the transformer insulation system, early detection of the possibility of failures, and increasing the operational reliability of the transformer.

Development of a mathematical model for the electrical strength of oil

A mathematical model was developed to assess the electrical strength of transformer oil, taking into account the main factors affecting it.

$$\mu_{(4)}(x_1) = \begin{cases} 1, \ if \ (x_1 \le 7); \\ \frac{14-x_1}{7}, \ if \ (7 < x_1 \le 14); \\ 0, \ if \ x_1 > 7; \end{cases} \quad (1.1)$$

https://doi.org/10.56143/3030-3893-2026-3-38-45

$$\mu_{(3)}(x_1)=\begin{cases}0,\ if\ (x_1\le 7);\\ \frac{x_1-7}{7},\ if\ (7<x_1\le 14);\\ 1,\ if\ (14\le x_1<21);\\ \frac{28-x_1}{7},\ if\ (21\le x_1<28);\\ 0, if\ (x_1\ge 28);\end{cases} \quad (1.2)$$

$$\mu_{(2)}(x_1)=\begin{cases}0,\ if\ (x_1\le 21);\\ \frac{x_1-21}{7},\ if\ (21<x_1\le 28);\\ 1,\ if\ (28\le x_1<35);\\ \frac{42-x_1}{7},\ if\ (35\le x_1<42);\\ 0, if\ (x_1\ge 42);\end{cases} \quad (1.3)$$

$$\mu_{(1)}(x_1)=\begin{cases}0,\ if\ (x_1\le 35);\\ \frac{x_1-35}{7},\ if\ (35<x_1\le 42);\\ 1,\ if\ (42\le x_1<49);\\ \frac{56-x_1}{7},\ if\ (49\le x_1<56);\\ 0, if\ (x_1\ge 56);\end{cases} \quad (1.4)$$

$$\mu_{(0)}(x_1)=\begin{cases}0,\ if\ (x_1\le 49);\\ \frac{56-x_1}{7},\ if\ (49<x_1\le 56);\\ 1,\ if\ x_1>56;\end{cases} \quad (1.5)$$

The following dependency rules have been established between input and output variables:

$$w_{Ktesh(1)}=\min\left(M\,F_{(1)}(x_1),1\right)\to\mu_{(5)}(y_1);$$

……

$$w_{Ktesh(5)}=\min\left(M\,F_{(5)}(x_1),1\right)\to\mu_{(5)}(y_1) \quad (1.6)$$

Determine the general membership function for each fuzzy set in the output variable:

$$\mu^*_{(0)}(R_{Ktesh})=\max\left(w_{Ktesh(1)},0\right);$$
$$\mu^*_{(1)}(R_{Ktesh})=\max\left(w_{Ktesh(2)},0\right);$$

…

$$\mu^*_{(5)}(R_{Ktesh})=\max\left(w_{Ktesh(5)},0\right). \quad (1.7)$$

The exact value of the output variable is determined by a diffusion process based on **the centroid** method for a generalized indefinite set and is calculated using the following expression:

$$R_{tesh}=\frac{\sum_{i=1}^{5} w_{Ktesh\,(i)}*\mu^*_i(y_1)}{\sum_{i=1}^{5}\mu^*_i(y_1)} \quad (1.8)$$

Development of a mathematical model for kinematic viscosity

A mathematical model was developed to estimate the kinematic viscosity of transformer oil, taking into account the factors affecting it.

$$\mu_{(4)}(x_1)=\begin{cases}1,\ if\ (x_1\le 1.6);\\ \frac{3.2-x_1}{1.6},\ if\ (1.6<x_1\le 3.2);\\ 0,\ if\ x_1>3.2;\end{cases} \quad (2.1)$$

$$\mu_{(3)}(x_1)=\begin{cases}0,\ if\ (x_1\le 1.6);\\ \frac{x_1-1.6}{1.6},\ if\ (1.6<x_1\le 3.2);\\ 1,\ if\ (3.2\le x_1<4.8);\\ \frac{6.4-x_1}{1.6},\ if\ (4.8\le x_1<6.4);\\ 0, if\ (x_1\ge 6.4);\end{cases} \quad (2.2)$$

$$\mu_{(2)}(x_1)=\begin{cases}0,\ if\ (x_1\le 4.8);\\ \frac{x_1-4.8}{1.6},\ if\ (4.8<x_1\le 6.4);\\ 1,\ if\ (6.4\le x_1<8);\\ \frac{9.6-x_1}{1.6},\ if\ (8\le x_1<9.6);\\ 0, if\ (x_1\ge 9.6);\end{cases} \quad (2.3)$$

$$\mu_{(1)}(x_1)=\begin{cases}0,\ if\ (x_1\le 8);\\ \frac{x_1-8}{1.6},\ if\ (8<x_1\le 9.6);\\ 1,\ if\ (9.6\le x_1<11.2);\\ \frac{12.8-x_1}{1.6},\ if\ (11.2\le x_1<12.8);\\ 0, if\ (x_1\ge 12.8);\end{cases} \quad (2.4)$$

$$\mu_{(0)}(x_1)=\begin{cases}0,\ if\ (x_1\le 11.2);\\ \frac{12.8-x_1}{1.6},\ if\ (11.2<x_1\le 12.8);\\ 1,\ if\ x_1>12.8;\end{cases} \quad (2.5)$$

The following dependency rules have been established between input and output variables:

$$w_{Kqov(1)}=\min\left(M\,F_{(1)}(x_1),1\right)\to\mu_{(5)}(y_1);$$

……

$$w_{Kqov(5)}=\min\left(M\,F_{(5)}(x_1),1\right)\to\mu_{(5)}(y_1) \quad (2.6)$$

Determine the general membership function for each fuzzy set in the output variable:

$$\mu^*_{(0)}(R_{Kqov})=\max\left(w_{Kqov(1)},0\right);$$
$$\mu^*_{(1)}(R_{Kqov})=\max\left(w_{Kqov(2)},0\right);$$

…

$$\mu^*_{(5)}(R_{Kqov})=\max\left(w_{Kqov(5)},0\right) \quad (2.7)$$

The exact value of the output variable is determined by a diffusion process based on **the centroid** method for a generalized indefinite set and is calculated using the following expression:

$$R_{qov}=\frac{\sum_{i=1}^{5} w_{Kqov\,(i)}*\mu^*_i(y_1)}{\sum_{i=1}^{5}\mu^*_i(y_1)} \quad (2.8)$$

Development of a mathematical model for the amount of mechanical impurities

To assess the amount of mechanical impurities in transformer oil, a mathematical model was developed that determines the patterns of their change during operation.

$$\mu_{(4)}(x_1)=\begin{cases}1,\ if\ (x_1\le 0.014);\\ \frac{0.028-x_1}{0.014},\ if\ (0.014<x_1\le 0.028);\\ 0,\ if\ x_1>0.028;\end{cases} \quad (3.1)$$

$$\mu_{(3)}(x_1)=\begin{cases}0,\ if\ (x_1\le 0.014);\\ \frac{x_1-0.014}{0.014},\ if\ (0.014<x_1\le 0.028);\\ 1,\ if\ (0.028\le x_1<0.042);\\ \frac{0.056-x_1}{0.014},\ if\ (0.042\le x_1<0.056);\\ 0, if\ (x_1\ge 0.056);\end{cases} \quad (3.2)$$

$$\mu_{(2)}(x_1)=\begin{cases}0,\ if\ (x_1\le 0.042);\\ \frac{x_1-0.042}{0.014},\ if\ (0.042<x_1\le 0.056);\\ 1,\ if\ (0.056\le x_1<0.07);\\ \frac{0.084-x_1}{0.014},\ if\ (0.07\le x_1<0.084);\\ 0, if\ (x_1\ge 0.084);\end{cases} \quad (3.3)$$

$$\mu_{(1)}(x_1)=\begin{cases}0,\ if\ (x_1\le 0.07);\\ \frac{x_1-0.7}{0.014},\ if\ (0.7<x_1\le 0.084);\\ 1,\ if\ (0.084\le x_1<0.098);\\ \frac{0.112-x_1}{0.014},\ if\ (0.098\le x_1<0.112);\\ 0, if\ (x_1\ge 0.112);\end{cases} \quad (3.4)$$

$$\mu_{(0)}(x_1)=\begin{cases}0,\ if\ (x_1\le 0.098);\\ \frac{0.112-x_1}{0.014},\ if\ (0.098<x_1\le 0.112);\\ 1,\ if\ x_1>0.112;\end{cases} \quad (3.5)$$

https://doi.org/10.56143/3030-3893-2026-3-38-45

The following dependency rules have been established between input and output variables:

$$w_{K.mex.a(1)} = \min\left(M\,F_{(1)}(x_1), 1\right) \to \mu_{(5)}(y_1);$$

……

$$w_{K.mex.a(1)} = \min\left(M\,F_{(5)}(x_1), 1\right) \to \mu_{(5)}(y_1) \quad (3.6)$$

Determine the general membership function for each fuzzy set in the output variable:

$$\mu^*_{(0)}(R_{K.mex.a}) = \max\left(w_{K.mex.a(1)}, 0\right));$$
$$\mu^*_{(1)}(R_{K.mex.a}) = \max\left(w_{K.mex.a(2)}, 0\right);$$

…

$$\mu^*_{(5)}(R_{K.mex.a}) = \max\left(w_{K.mex.a(5)}, 0\right) \quad (3.7)$$

The exact value of the output variable is determined by a diffusion process based on **the centroid** method for a generalized indefinite set and is calculated using the following expression:

$$R_{mex.a} = \frac{\sum_{i=1}^{5} w_{K.mex.a\,(i)} * \mu^*_i(y_1)}{\sum_{i=1}^{5} \mu^*_i(y_1)} \quad (3.8)$$

Development of a mathematical model for determining water content

A mathematical model has been developed to estimate the water content in transformer oil. This model allows describing the patterns of moisture content changes during operation, assessing its impact on the electrical and physicochemical properties of the transformer insulation system, and diagnosing the technical condition of the oil.

$$M\,F_{(1)}(x) = \begin{cases} 1, & if\ (x \le 7); \\ 1 - \frac{x-6}{12-6}, & if\ (6 < x \le 12); \\ 0, & if\ (x \ge 12); \end{cases} \quad (4.1)$$

$$M\,F_{(2)}(x) = \begin{cases} 0, & if\ (x \le 6\ or\ x \ge 24); \\ 1 - \frac{x-6}{12-6}, & if\ (6 < x \le 12) \\ 1, & if\ 6 < x \le 12; \\ 1 - \frac{x-6}{12-6} & if\ (18 < x < 24); \end{cases} \quad (4.2)$$

$$M\,F_{(3)}(x) = \begin{cases} 0, & if\ (x \le 18\ or\ x \ge 36); \\ \frac{x-18}{24-18}, & if\ (18 < x \le 24) \\ 1, & if\ 24 < x \le 30; \\ 1 - \frac{x-30}{36-30} & if\ (30 < x < 36); \end{cases} \quad (4.3)$$

$$M\,F_4(x) = \begin{cases} 0, & if\ (x \le 42); \\ \frac{x-42}{48-42}, & if\ (42 < x \le 48); \\ 1, & if\ (x \ge 48); \end{cases} \quad (4.4)$$

$$M\,F_{(5)}(x) = \begin{cases} 0, & if\ (x \le 30\ or\ x \ge 48); \\ \frac{x-42}{36-30}, & if\ (30 < x \le 36) \\ 1, & if\ 36 < x \le 42; \\ 1 - \frac{x-42}{48-42} & if\ (42 < x < 48); \end{cases} \quad (4.5)$$

The following dependency rules have been established between input and output variables:

$$w_{Ksuv(1)} = \min\left(M\,F_{(1)}(x_1), 1\right) \to \mu_{(5)}(y_1);$$

……

$$w_{Ksuv\,(1)} = \min\left(M\,F_{(5)}(x_1), 1\right) \to \mu_{(5)}(y_1) \quad (4.6)$$

Determine the general membership function for each fuzzy set in the output variable:

$$\mu^*_{(0)}(R_{Ksuv}) = \max\left(w_{Ksuv(1)}, 0\right));$$
$$\mu^*_{(1)}(R_{Ksuv}) = \max\left(w_{Ksuv(2)}, 0\right);$$

…

$$\mu^*_{(5)}(R_{Ksuv}) = \max\left(w_{Ksuv(5)}, 0\right) \quad (4.7)$$

The exact value of the output variable is determined by a diffusion process based on **the centroid** method for a generalized indefinite set and is calculated using the following expression:

$$R_{suv} = \frac{\sum_{i=1}^{5} w_{Ksuv\,(i)} * \mu^*_i(y_1)}{\sum_{i=1}^{5} \mu^*_i(y_1)} \quad (4.8)$$

Development of a mathematical model for determining the amount of acidity

A mathematical model has been developed to estimate the acid number of transformer oil. This model allows us to characterize the degree of oxidation and degradation of the oil during operation and to assess its impact on the technical condition of the insulation system.

$$M\,F_1(x) = \begin{cases} 1, & if\ (x \le 0.01); \\ 1 - \frac{x-0.01}{0.02-0.01}, & if\ (0.01 < x < 0.02); \\ 0, & if\ (x \ge 0.02); \end{cases} \quad (5.1)$$

$$M\,F_{(2)}(x) = \begin{cases} 0, & if\ (x \le 0.01\ or\ x \ge 0.04); \\ \frac{x-0.01}{0.02-0.01}, & if\ (0.01 < x \le 0.02) \\ 1, & if\ 0.02 < x \le 0.03; \\ 1 - \frac{x-0.05}{0.06-0.05} & if\ (0.03 < x < 0.04); \end{cases} \quad (5.2)$$

$$M\,F_{(3)}(x) = \begin{cases} 0, & if\ (x \le 0.03\ or\ x \ge 0.06); \\ \frac{x-0.03}{0.04-0.03}, & if\ (0.03 < x \le 0.04) \\ 1, & if\ 0.04 < x \le 0.05; \\ 1 - \frac{x-0.05}{0.06-0.05} & if\ (0.05 < x < 0.06); \end{cases} \quad (5.3)$$

$$M\,F_4(x) = \begin{cases} 0, & if\ (x \le 0.07); \\ 1 - \frac{x-0.01}{0.02-0.01}, & if\ (0.07 < x < 0.08); \\ 1, & if\ (x \ge 0.08); \end{cases} \quad (5.4)$$

$$M\,F_{(5)}(x) = \begin{cases} 0, & if\ (x \le 0.05\ or\ x \ge 0.04); \\ \frac{x-42}{36-30}, & if\ (0.05 < x \le 0.06) \\ 1, & if\ 0.06 < x \le 0.07; \\ 1 - \frac{x-42}{48-42} & if\ (0.07 < x < 0.08); \end{cases} \quad (5.5)$$

The following dependency rules have been established between input and output variables:

$$w_{Kkis(1)} = \min\left(M\,F_{(1)}(x_1), 1\right) \to \mu_{(5)}(y_1);$$

……

$$w_{Kkis(1)} = \min\left(M\,F_{(5)}(x_1), 1\right) \to \mu_{(5)}(y_1) \quad (5.6)$$

Determine the general membership function for each fuzzy set in the output variable:

$$\mu^*_{(0)}(R_{Kkis}) = \max\left(w_{Kkis(1)}, 0)\right);$$
$$\mu^*_{(1)}(R_{Kkis}) = \max\left(w_{Kkis(2)}, 0\right);$$

…

$$\mu^*_{(5)}(R_{Kkis}) = \max\left(w_{Kkis(5)}, 0\right) \quad (5.7)$$

The exact value of the output variable is determined by a diffusion process based on **the centroid** method for a generalized indefinite set and is calculated using the following expression:

$$R_{kis} = \frac{\sum_{i=1}^{5} w_{Kkis\,(i)} * \mu^*_i(y_1)}{\sum_{i=1}^{5} \mu^*_i(y_1)} \quad (5.8)$$

Development of a mathematical model for determining the flash point

A mathematical model was developed to estimate the flash point of transformer oil.

https://doi.org/10.56143/3030-3893-2026-3-38-45

$$M\,F_1(x) = \begin{cases} 1 & if\ (x \le 27); \\ 1 - \frac{x-27}{54-27}, & if\ (27 < x < 54); \\ 0 & if\ (x \ge 54); \end{cases} \quad (6.1)$$

$$M\,F_{(2)}(x) = \begin{cases} 0, & if\ (x \le 27\ or\ x \ge 108); \\ \frac{x-27}{54-27}, & if\ (27 < x \le 54) \\ 1, & if\ (54 < x \le 81); \\ 1 - \frac{x-81}{108-81} & if\ (81 < x < 108); \end{cases} \quad (6.2)$$

$$M\,F_{(3)}(x) = \begin{cases} 0, & if\ (x \le 81\ or\ x \ge 162); \\ \frac{x-81}{108-81}, & if\ (81 < x \le 108) \\ 1, & if\ (108 < x \le 135); \\ 1 - \frac{x-135}{162-135} & if\ (135 < x < 162); \end{cases} \quad (6.3)$$

$$M\,F_4(x) = \begin{cases} 0 & if\ (x \le 189); \\ 1 - \frac{x-189}{216-189}, & if\ (189 < x < 216); \\ 1 & if\ (x \ge 216); \end{cases} \quad (6.4)$$

$$M\,F_{(5)}(x) = \begin{cases} 0, & if\ (x \le 135\ or\ x \ge 216); \\ \frac{x-135}{162-135}, & if\ (135 < x \le 162) \\ 1, & if\ (162 < x \le 189); \\ 1 - \frac{x-189}{216-189} & if\ (189 < x < 216); \end{cases} \quad (6.5)$$

The following dependency rules have been established between input and output variables:

$$w_{Kchaq.h.(1)} = \min\,(M\,F_{(1)}(x_1), 1) \to \mu_{(5)}(y_1);$$

……

$$w_{Kchaq.h.(1)} = \min\,(M\,F_{(5)}(x_1), 1) \to \mu_{(5)}(y_1) \quad (6.6)$$

Determine the general membership function for each fuzzy set in the output variable:

$$\mu^*_{(0)}(R_{Kchaq.h.}) = \max\,(w_{Kchaq.h.(1)}, 0));$$
$$\mu^*_{(1)}(R_{Kchaq.h.}) = \max\,(w_{Kchaq.h.(2)}, 0);$$

…

$$\mu^*_{(5)}(R_{Kchaq.h.}) = \max\,(w_{Kchaq.h.(5)}, 0) \quad (6.7)$$

The exact value of the output variable is determined by a diffusion process based on **the centroid** method for a generalized indefinite set and is calculated using the following expression:

$$R_{chaq.h.} = \frac{\sum_{i=1}^{5} w_{Kchaq.h.(i)} * \mu^*_i(y_1)}{\sum_{i=1}^{5} \mu^*_i(y_1)} \quad (6.8)$$

Development of a mathematical model for determining density

To estimate the density of transformer oil, a mathematical model was developed that takes into account the main factors affecting it.

$$M\,F_1(x) = \begin{cases} 1 & if\ (x \le 180); \\ 1 - \frac{x-188}{360-180}, & if\ (180 < x < 360); \\ 0 & if\ (x \ge 360); \end{cases} \quad (7.1)$$

$$M\,F_{(2)}(x) = \begin{cases} 0, & if\ (x \le 181.4\ or\ x \ge 721.4); \\ \frac{x-181.4}{361.4-181.4}, & if\ (181.4 < x \le 361.4) \\ 1, & if\ (1361.4 < x \le 541.4); \\ 1 - \frac{x-541.4}{721.4-541.4} & if\ (189 < x < 721.4); \end{cases} \quad (7.2)$$

$$M\,F_{(3)}(x) = \begin{cases} 0, & if\ (x \le 540\ or\ x \ge 1080); \\ \frac{x-540}{720-540}, & if\ (540 < x \le 720) \\ 1, & if\ (720 < x \le 900); \\ 1 - \frac{x-900}{1080-900} & if\ (900 < x < 1080); \end{cases} \quad (7.3)$$

$$M\,F_{(4)}(x) = \begin{cases} 0, & if\ (x \le 900\ or\ x \ge 1440); \\ \frac{x-900}{1080-900}, & if\ (900 < x \le 1080) \\ 1, & if\ (1080 < x \le 1260); \\ 1 - \frac{x-1260}{1440-1260} & if\ (1260 < x < 1440); \end{cases} \quad (7.4)$$

$$M\,F_5(x) = \begin{cases} 0 & if\ (x \le 1260); \\ \frac{x-1260}{1440-1260}, & if\ (1260 < x < 1440); \\ 1 & if\ (x \ge 1440); \end{cases} \quad (7.5)$$

The following dependency rules have been established between input and output variables:

$$w_{Kzich(1)} = \min\,(M\,F_{(1)}(x_1), 1) \to \mu_{(5)}(y_1);$$

……

$$w_{Kzich(1)} = \min\,(M\,F_{(5)}(x_1), 1) \to \mu_{(5)}(y_1) \quad (7.6)$$

Determine the general membership function for each fuzzy set in the output variable:

$$\mu^*_{(0)}(R_{Kzich}) = \max\,(w_{Kzich(1)}, 0));$$
$$\mu^*_{(1)}(R_{Kzich}) = \max\,(w_{Kzich(2)}, 0);$$

…

$$\mu^*_{(5)}(R_{Kzich}) = \max\,(w_{Kzich(5)}, 0) \quad (7.7)$$

The exact value of the output variable is determined by a diffusion process based on **the centroid** method for a generalized indefinite set and is calculated using the following expression:

$$R_{zich} = \frac{\sum_{i=1}^{5} w_{Kzich\ (i)} * \mu^*_i(y_1)}{\sum_{i=1}^{5} \mu^*_i(y_1)} \quad (7.8)$$

Development of a mathematical model for dielectric losses

To estimate the dielectric losses of transformer oil, a mathematical model was developed that takes into account the main factors affecting it.

$$M\,F_1(x) = \begin{cases} 1, & if\ (x \le 0.1); \\ 1 - \frac{x-0.1}{0.2-0.1}, & if\ (0.1 < x \le 0.2); \\ 0, & if\ x > 0.2; \end{cases} \quad (8.1)$$

$$M\,F_2(x) = \begin{cases} 0, & if\ (x \le 0.1\ or\ x \ge 0.4); \\ \frac{x-0.1}{0.2-0.1}, & if\ (0.3 < x \le 0.4); \\ 1, & if\ (3.2 \le x < 4.8); \\ 1 - \frac{x-0.3}{0.4-0.3}, & if\ (0.4 \le x < 0.5); \end{cases} \quad (8.2)$$

$$M\,F_3(x) = \begin{cases} 0, & if\ (x \le 0.3\ or\ x \ge 0.6); \\ \frac{x-0.3}{0.4-0.3}, & if\ (0.3 < x \le 0.4); \\ 1, & if\ (0.4 \le x < 0.5); \\ 1 - \frac{x-0.5}{0.6-0.5}, & if\ (0.5 \le x < 0.6); \end{cases} \quad (8.3)$$

$$M\,F_4(x) = \begin{cases} 1, & if\ (x \le 0.7); \\ 1 - \frac{x-0.1}{0.2-0.1}, & if\ (0.7 < x \le 0.8); \\ 1, & if\ x > 0.8; \end{cases} \quad (8.4)$$

$$M\,F_5(x) = \begin{cases} 0, & if\ (x \le 0.5\ or\ x \ge 0.8); \\ \frac{x-0.5}{0.6-0.5}, & if\ (0.5 < x \le 0.6); \\ 1, & if\ (0.6 \le x < 0.7); \\ 1 - \frac{x-0.7}{0.8-0.7}, & if\ (0.7 \le x < 0.8); \end{cases} \quad (8.5)$$

https://doi.org/10.56143/3030-3893-2026-3-38-45

The following dependency rules have been established between input and output variables:

$$w_{Kd.i.(1)} = \min\left(M\,F_{(1)}(x_1), 1\right) \to \mu_{(5)}(y_1);$$

……

$$w_{Kd.i.(1)} = \min\left(M\,F_{(5)}(x_1), 1\right) \to \mu_{(5)}(y_1) \quad (8.6)$$

Determine the general membership function for each fuzzy set in the output variable:

$$\mu^*_{(0)}(R_{Kd.i.}) = \max\left(w_{Kd.i.(1)}, 0)\right);$$
$$\mu^*_{(1)}(R_{Kd.i.}) = \max\left(w_{Kd.i.(2)}, 0\right);$$

…

$$\mu^*_{(5)}(R_{Kd.i.}) = \max\left(w_{Kd.i.(5)}, 0\right) \quad (8.7)$$

The exact value of the output variable is determined by a diffusion process based on **the centroid** method for a generalized indefinite set and is calculated using the following expression:

$$R_{d.i.} = \frac{\sum_{i=1}^{5} w_{Kd.i.(i)} * \mu^*_i(y_1)}{\sum_{i=1}^{5} \mu^*_i(y_1)} \quad (8.8)$$

Development of a mathematical model for the general state of oil

To assess the overall technical condition of the transformer oil, a mathematical model was developed that accounts for changes in the values of its eight main indicators. The model allows for the assessment of the general technical condition of the oil and the prediction of the result.

$$M\,F_1(R) = \begin{cases} 1, \ if\ (R \le 10); \\ 1 - \frac{R-10}{20-10}, \ if\ (10 < R \le 20); \\ 0, \ if\ R > 20; \end{cases} \quad (9.1)$$

$$M\,F_2(R) = \begin{cases} 0, \ if\ (R \le 10\ or\ R \ge 40); \\ \frac{R-10}{20-10}, \ if\ (30 < R \le 40); \\ 1, \ if\ (32 \le R < 48); \\ 1 - \frac{R-30}{40-30}, \ \ if\ (40 \le R < 50); \end{cases} \quad (9.2)$$

$$M\,F_3(R) = \begin{cases} 0, \ if\ (R \le 30\ or\ R \ge 60); \\ \frac{R-30}{40-30}, \ if\ (30 < R \le 40); \\ 1, \ if\ (40 \le R < 50); \\ 1 - \frac{R-50}{60-50}, \ \ if\ (50 \le R < 60); \end{cases} \quad (9.3)$$

$$M\,F_4(R) = \begin{cases} 1, \ if\ (R \le 70); \\ 1 - \frac{R-40}{50-40}, \ if\ (70 < R \le 80); \\ 1, \ if\ R > 80; \end{cases} \quad (9.4)$$

$$M\,F_5(R) = \begin{cases} 0, \ if\ (x \le 50\ or\ R \ge 80); \\ \frac{R-50}{60-50}, \ if\ (50 < R \le 60); \\ 1, \ if\ (60 \le R < 70); \\ 1 - \frac{R-70}{80-70}, \ \ if\ (70 \le R < 80); \end{cases} \quad (9.5)$$

The following dependency rules have been established between input and output variables:

$$w_{moy(1)} = \min\left(M\,F_{(1)}(R_1), 1\right) \to \mu_{(5)}(R_{moy});$$

……

$$w_{moy(1)} = \min\left(M\,F_{(5)}(R_1), 1\right) \to \mu_{(5)}(R_{moy}) \quad (9.6)$$

Determine the general membership function for each fuzzy set in the output variable:

$$\mu^*_{(0)}(R_{moy}) = \max\left(w_{moy(1)}, 0)\right);$$
$$\mu^*_{(1)}(R_{moy}) = \max\left(w_{moy(2)}, 0\right);$$

…

$$\mu^*_{(5)}(R_{moy}) = \max\left(w_{moy(5)}, 0\right) \quad (9.7)$$

The exact value of the output variable is determined by a diffusion process based on **the centroid** method for a generalized indefinite set and is calculated using the following expression:

$$R_{moy} = \frac{\sum_{i=1}^{62225} w_{moy\,(i)} * \mu^*_i(R_{moy})}{\sum_{i=1}^{5} \mu^*_i(R_{moy})} \quad (9.8)$$

Development of a mathematical model for the technical condition of a transformer

To assess the technical condition of a transformer, taking into account changes in the values of eight key oil parameters. The model allows assessing the overall technical condition of the transformer and predicting the outcome.

$$M\,F_1(R) = \begin{cases} 1, \ if\ (R \le 10); \\ 1 - \frac{R-10}{20-10}, \ if\ (10 < R \le 20); \\ 0, \ if\ R > 20; \end{cases} \quad (10.1)$$

$$M\,F_2(R) = \begin{cases} 0, \ if\ (R \le 10\ or\ R \ge 40); \\ \frac{R-10}{20-10}, \ if\ (30 < R \le 40); \\ 1, \ if\ (32 \le R < 48); \\ 1 - \frac{R-30}{40-30}, \ \ if\ (40 \le R < 50); \end{cases} \quad (10.2)$$

$$M\,F_3(R) = \begin{cases} 0, \ if\ (R \le 30\ or\ R \ge 60); \\ \frac{R-30}{40-30}, \ if\ (30 < R \le 40); \\ 1, \ if\ (40 \le R < 50); \\ 1 - \frac{R-50}{60-50}, \ \ if\ (50 \le R < 60); \end{cases} \quad (10.3)$$

$$M\,F_4(R) = \begin{cases} 1, \ if\ (R \le 70); \\ 1 - \frac{R-10}{20-10}, \ if\ (70 < R \le 80); \\ 1, \ if\ R > 80; \end{cases} \quad (10.4)$$

$$M\,F_5(R) = \begin{cases} 0, \ if\ (x \le 50\ or\ R \ge 80); \\ \frac{R-50}{60-50}, \ if\ (50 < R \le 60); \\ 1, \ if\ (60 \le R < 70); \\ 1 - \frac{R-70}{80-70}, \ \ if\ (70 \le R < 80); \end{cases} \quad (10.5)$$

The following dependency rules have been established between input and output variables:

$$w_{tr(1)} = \min\left(M\,F_{(1)}(R_1), 1\right) \to \mu_{(5)}(R_{tr});$$

……

$$w_{tr(1)} = \min\left(M\,F_{(5)}(R_1), 1\right) \to \mu_{(5)}(R_{tr}) \quad (10.6)$$

Determine the general membership function for each fuzzy set in the output variable:

$$\mu^*_{(0)}(R_{tr}) = \max\left(w_{tr(1)}, 0)\right);$$
$$\mu^*_{(1)}(R_{tr}) = \max\left(w_{tr(2)}, 0\right);$$

…

$$\mu^*_{(5)}(R_{tr}) = \max\left(w_{tr(5)}, 0\right) \quad (10.7)$$

The exact value of the output variable is determined by a diffusion process based on **the centroid** method for a generalized indefinite set and is calculated using the following expression:

$$R_{tr} = \frac{\sum_{i=1}^{5} w_{tr(i)} * \mu^*_i(R_{tr})}{\sum_{i=1}^{5} \mu^*_i(R_{tr})} \quad (10.8)$$

Assessment algorithm (Algorithm). In order to automate the process of assessing the technical condition of a transformer based on the operational indicators of transformer oil and to increase the accuracy and reliability of diagnostic results, an assessment algorithm based on the theory of fuzzy logic was developed. This algorithm is aimed at a comprehensive analysis of the diagnostic parameters of transformer oil, taking into account their interaction and determining the general technical condition of the transformer based on an integral assessment indicator, consists of several consecutive stages and allows for a comprehensive analysis of the physicochemical and electrical properties of transformer oil.

https://doi.org/10.56143/3030-3893-2026-3-38-45

At the first stage of the algorithm, the main diagnostic parameters of transformer oil (electrical strength, water content, mechanical impurities, acid number, dielectric loss, density, flash point and kinematic viscosity) determined as a result of laboratory tests are entered into the system. At the next stage, these parameters are compared with the normative values established in current standards. At the final stage, defuzzification is performed using the centroid method, which calculates the integral technical condition indicator of the transformer and determines whether it belongs to one of the categories of "excellent", "good", "average", "bad" or "very bad". The proposed algorithm allows for a systematic analysis of the diagnostic parameters of transformer oil, a comprehensive assessment of the technical condition of the transformer and the initial detection of possible malfunctions during operation. This algorithm serves as an effective tool for improving decision-making efficiency, reducing maintenance costs, and ensuring the operational reliability of transformers in Condition-Based Maintenance systems (Figure 1).

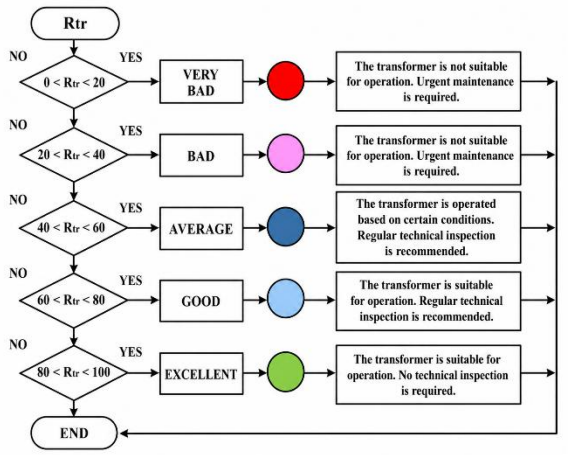


Fig. 1. Algorithm for assessing the technical condition of a transformer based on the operational performance of its oil and making operational decisions based on the fuzzy logic method

4. Conclusion

In this study, a mathematical model based on fuzzy logic theory was developed to assess the technical condition of a transformer based on eight main operational indicators of transformer oil (electrical strength, water content, acid number, amount of mechanical impurities, kinematic viscosity, density, flash point and dielectric loss). The developed model allows for a comprehensive analysis of the impact of diagnostic parameters on the state of the transformer insulation system and the determination of the overall technical condition of the transformer, taking into account their interdependence.

An evaluation algorithm based on fuzzy logic has been developed, which allows for a quick and reliable assessment of the technical condition of a transformer based on diagnostic indicators of transformer oil, increasing operational safety, and providing recommendations for maintenance or repair. The proposed algorithm provides automatic processing of diagnostic data and classification of the technical condition of the transformer into the categories of "excellent", "good", "average", "bad" and "very bad".

The proposed mathematical model and integral evaluation algorithm allow for the diagnosis of the technical condition of the transformer, assessment of the degree of degradation of the insulation system, and early detection of possible failures based on a comprehensive analysis of the operational parameters of the transformer oil. This approach serves as an effective scientific and methodological tool for increasing the operational reliability of transformers, preventing accidents, improving maintenance systems, and optimizing technical monitoring processes.

References

[1] Voprikov A.V., Grigoriev N.P., Parfianovich A.P. Extending the Life of Power Transformers of Traction Substations of Alternating Current of Electric Railways // Advances in Intelligent Systems and Computing. – Springer International Publishing, 2020. – Vol. 1115. – P. 52–59. https://eurekamag.com/research/102/803/102803915.php

[2] Chothani N.G., Patel D., Parekh C. Advancement in Infrastructure and Design Technology of Power Transformer. – Singapore: Springer Nature, 2025. ISBN: 978 981 96 9420 4. https://link.springer.com/book/10.1007/978-981-96-9420-4

[3] Muhammad S.S., Abdulrazak S., Bakare G.A., Abdulhafiz S., Nazif D.M. Modelling and analysis of a power transformer using finite element analysis // Asian Journal of Science, Technology, Engineering, and Art. – 2025. – Vol. 3, No. 3, pp. 902–920. https://doi.org/10.58578/ajstea.v3i3.5703

[4] J. Wajda. Comparison of Annual Electrical Energy Losses of Conventional and Superconductive Transformers in Power Lines // Journal of Automation, Electronics and Electrical Engineering. – 2025. – Vol. 12, No. 3, pp. 112–125. https://oeconomia.pl/jaeee/article/view/3478

[5] C.D. Capulong, J. Reyes, M. Santos. Analysis of Failure Rate Due to Transformer Loadings of Commonly Used Transformers in Porac Substation // Journal of Science, Technology and Engineering Research. – 2025. – Vol. 6, No. 2, pp. 107–117. https://dergipark.org.tr/en/download/article-file/4972902

[6] Bryakin I.V., Bochkarev I.V., Khramshin V.R., Gasiyarov V.R., Liubimov I.V. Power transformer condition monitoring based on evaluating oil properties // Machines. – 2022. – Vol. 10, No. 8, Art. 630. https://www.mdpi.com/2075-1702/10/8/630

[7] Feng Chen, Li Wang, Zhiyao Zheng, Bin Pan, Yujia Hu, Kexin Zhang. Data driven based full recovery technology and system for transformer insulating oil // Energies. – 2024. – Vol. 17, No. 24, Art. 6345. https://www.mdpi.com/1996-1073/17/24/6345

[8] Nurubeyli T.K., Hashimov A.M., Imamverdiyev N.E., Mammadova G.N. Complex physicochemical analysis of transformer oil parameters using the inductively coupled plasma mass spectrometry technique // Electrical Engineering & Electromechanics. – 2025. – No. 2, pp. 79–84.

[9] Yusupov D.T., Rakhmatova M., Tashmatova Sh. Study of optimal temperature during adsorption cleaning of transformer oil under conditions of long term operation // E3S Web of Conferences. – 2023. – Vol. 383, Art. 04058. https://doi.org/10.1051/e3sconf/202338304058

[10] Soni R., Mehta B. A review on transformer condition monitoring with critical investigation of mineral

oil and alternate dielectric fluids // Electric Power Systems Research. – 2023. – Vol. 214, Part B, Art. 108954.

[11] Darwish M.M.F., Hassan M.H.A., Abdel Gawad N.M.K., Lehtonen M., Mansour D.E.A. A new technique for fault diagnosis in transformer insulating oil based on infrared spectroscopy measurements // High Voltage. – 2024. – Vol. 9, No. 2, pp. 319–335. https://doi.org/10.1049/hve2.12479

[12] Hu H., Liu Y., Li Y., et al. Traction power systems for electrified railways: evolution, state and future trends // Railway Engineering Science. – 2023. – Vol. 32, No. 1, pp. 1–19. https://doi.org/10.1007/s40534-023-00320-6

[13] A.N. Nazarychev, O.S. Melnikova, I.I. Sulynenkov. Diagnostics of main insulation of power transformers using statistical criterion of oil dielectric strength // Electricity. – 2022. – No. 9, pp. 22–32. https://doi.org/10.24160/0013-5380-2022-9-22-32

[14] D.T. Yusupov, B.K. Avazov. Theoretical solutions for cleaning transformer oils using an electric field taking into account the effects of environments. IV International Scientific and Technical Conference "Actual Issues of Power Supply Systems": ICAIPSS2024. – 2025. – Vol. 3331, No. 1, Art. 050018. https://doi.org/10.1063/5.0306610

[15] D.T. Yusupov, B.K. Avazov, O.M. Kutbidinov, M. Bazarov. Cleaning of transformer oils using the electric field // IOP Conference Series: Earth and Environmental Science. – IOP Publishing, 2023. – Vol. 1231, No. 1, Art. 012024. https://orcid.org/0000-0003-3732-5185

[16] U.T. Berdiev, B.K. Avazov, F.F. Sulaymonov, U.N. Berdiyorov, F. Turg'unova. The study of electric motors based on composite materials. IV International Scientific and Technical Conference "Actual Issues of Power Supply Systems": ICAIPSS2024. – 2025. – Vol. 3331, No. 1, Art. 030046. https://doi.org/10.1063/5.0305937

[17] D.T. Yusupov, B.K. Avazov. Experimental analysis of the process of purifying transformer oil from various impurities under the influence of a constant electric field and assessment of mathematically modeled results // Liquid and Gaseous Energy Resources. – 2025. – Vol. 5, No. 2, pp. 19-30. https://doi.org/10.21595/lger.2025.25476

[18] Amirov S.F., Sharapov S.A., Sulliev A.K., Boltaev O.T. Biparametric resonant transformer sensor of large linear movements // AIP Conference Proceedings. – AIP Publishing, 2023. – Vol. 2624, No. 1, Art. 030007(1–9). https://doi.org/10.1063/5.0132847

[19] Boltayev O.T., Akhmedova F.A. Induced voltage from traction lines and methods of reducing its influence on adjacent communication lines // International Journal on Integrated Education. – 2021. – Vol. 4, Issue 4, pp. 265-271.

[20] Smith R., Johnson R. Electrostatic cleaning of transformer oil using high electric fields // IEEE Transactions on Dielectrics and Electrical Insulation. – 2018. – Vol. 25, No. 4, pp. 1234–1245. https://doi.org/10.1109/TDEI.2018.00123

[21] H. Zhang, L. Li. Power transformer fault detection: a comparison of machine learning techniques // Energies. – 2023. – Vol. 17, No. 1, Art. 77. https://www.mdpi.com/1996-1073/17/1/77

[22] Sorte S., Monteiro A.F., Ventura D., Salgado A., Oliveira M.S.A., Martins N. Power transformers cooling design: a comprehensive review // Energies. – 2025. – Vol. 18, No. 5, Art. 1051. https://doi.org/10.3390/en18051051

[23] A. Malik, T. S. Sidhu, A. G. A. M. Ali. Fuzzy logic based transformer condition assessment using dissolved gas analysis // IEEE Transactions on Dielectrics and Electrical Insulation. – 2016. – Vol. 23, No. 5. – pp. 2760–2768. https://doi.org/10.1109/TDEI.2016.7736864

[24] M. Wang, A. J. Vandermaar, K. D. Srivastava. Review of condition assessment of power transformers in service // IEEE Electrical Insulation Magazine. – 2002. – Vol. 18, No. 6. – pp. 12–25. https://doi.org/10.1109/MEI.2002.1044335

[25] S. Tenbohlen, T. Strasser. A statistical approach to transformer fault diagnosis using dissolved gas analysis // IEEE Transactions on Power Delivery. – 2007. – Vol. 22, No. 3. – pp. 1639–1647. https://doi.org/10.1109/TPWRD.2007.899775

[26] M. Duval. A review of faults detectable by gas-in-oil analysis in transformers // IEEE Electrical Insulation Magazine. – 2002. – Vol. 18, No. 3. – pp. 8–17. https://doi.org/10.1109/MEI.2002.1014963.

Information about the author

Dilmurod Yusupov	Institute of Energy Problems, Academy of Sciences of the Republic of Uzbekistan E-mail: dilmurod85@list.ru Tel.: +99897 480 28 07 https://orcid.org/0000-0001-6569-4806
Odiljon Kutbidinov	Tashkent state transport university, Department of "Electrical engineering" E-mail: qutbiddinov_o@tstu.uz Tel.: +998 97 461 60 03 https://orcid.org/0000-0001-9290-5322
Bobomurod Avazov	Tashkent state transport university, Department of "Electrical engineering" E-mail: avazovbk@gmail.com Tel.: +99893 5933827

Journal Engineer ISSN: 3030-3893 Volume:4| Issue:3| 2026

Received: 18 June 2026 | **Accepted:** 30 July 2026 | **Published:** 30 September 2026

Application of artificial intelligence in modeling non-stationary oil filtration in multilayer porous media and data reliability issues

E. Abdurahmanova[1][a]

[1]Karshi state technical university, Karshi, Uzbekistan

Abstract: This research investigates the modeling of unsteady-state oil filtration processes in heterogeneous multilayer porous media using a hybrid framework that integrates classical fluid dynamics with modern artificial intelligence techniques. The study focuses on developing an efficient computational approach capable of describing fluid transport in complex geological formations characterized by spatial heterogeneity and temporal variability. The governing flow behavior is described through Darcy-based physical laws coupled with continuity equations, while machine learning methods are employed to capture nonlinear dependencies between reservoir parameters such as permeability, porosity, and pressure distribution. In particular, a Physics-Informed Neural Network (PINN) combined with a feedforward neural architecture is utilized to improve prediction accuracy.

In addition, the study addresses critical challenges related to data integrity, uncertainty propagation, and cybersecurity risks in AI-driven simulations. Since model performance strongly depends on the quality of input datasets, ensuring data validation and protection becomes essential. The obtained results demonstrate that hybrid AI–physics models significantly enhance predictive performance and computational efficiency compared to conventional numerical approaches. However, further improvements are required in model interpretability and robustness for real engineering applications.

Keywords: artificial intelligence, oil filtration, porous media, mathematical modeling, nonstationary flow, data security

1. Introduction

The study of fluid movement through porous structures plays a central role in petroleum engineering, geosciences, and applied mathematics. In particular, oil displacement in multilayer porous formations represents a complex physical phenomenon due to variations in geological structure and fluid properties over space and time. The mathematical description of such systems is typically based on conservation principles and Darcy's law. However, when dealing with heterogeneous reservoirs, parameters such as permeability and porosity vary across layers, leading to strongly nonlinear and coupled differential equations. These complexities limit the applicability of analytical solutions and increase the reliance on numerical simulation techniques.

Recent advances in artificial intelligence and machine learning have introduced new opportunities for modeling such complex systems. Data-driven approaches are capable of learning hidden patterns from experimental or simulated data, making them suitable for approximating nonlinear physical processes. Despite these advantages, AI-based modeling introduces new challenges. One of the most critical issues is the reliability of input data, as inaccurate or incomplete datasets can significantly degrade model performance. Additionally, ensuring that AI predictions remain consistent with physical laws is essential for engineering reliability.

Another important concern is the security and integrity of data used in computational modeling environments. In modern digital systems, datasets may be exposed to noise, corruption, or malicious manipulation, which directly affects simulation reliability. This work aims to develop a hybrid modeling framework that combines physical laws with artificial intelligence methods for accurate simulation of non-stationary oil filtration in multilayer porous media.

2. Research methodology

Mathematical Model of Filtration Process

The nonstationary filtration process in porous media can be described using Darcy's law and the continuity equation.

$$v = -\frac{k}{\mu}\nabla p \quad (1)$$

Where:

v — filtration velocity

k — permeability coefficient

μ— fluid viscosity

p— pressure

The governing equation for nonstationary flow is:

$$\frac{\partial(\phi\rho)}{\partial t} + \nabla\cdot(\rho v) = 0 \quad (2)$$

Where:

ϕ— porosity

ρ— fluid density

For multilayer porous media, parameters such as permeability and porosity vary across layers:

$$k=k(x,y,z), \qquad \phi = \phi\,(x,y,z) \quad (3)$$

Application of Artificial Intelligence

Artificial intelligence techniques can significantly improve the modeling of filtration processes by accurately predicting pressure distribution, estimating permeability coefficients, and accelerating numerical simulations, thereby

[a] https://orcid.org/0009-0004-3668-6152

enhancing both computational efficiency and model accuracy.

Machine learning models, such as neural networks, can approximate complex nonlinear relationships:

$$y=f(x;\theta) \quad (4)$$

Where θ represents model parameters learned from data.

AI models reduce computational cost compared to traditional finite difference or finite element methods.

AI Model Description

In this study, a Physics-Informed Neural Network (PINN) integrated with a Feedforward Artificial Neural Network (ANN) was used to model nonstationary oil filtration in multilayer porous media. The hybrid model combines:

- Data-driven learning (ANN)
- Physical constraints derived from Darcy's law and mass conservation equations

This ensures that predictions are not only data-consistent but also physically meaningful.

Input–Output Structure

Input variables:

Spatial coordinates: x,y,z

Time: t

Rock properties:

Permeability k(x,y,z)

Porosity ϕ(x,y,z)

Fluid properties:

Viscosity μ

Density ρ

Output variable:

Pressure field:

p(x,y,z,t)

optionally:

velocity field v(x,y,z,t)

Neural Network Structure

The model is a fully connected feedforward neural network:

Input layer: 5–6 neurons

Hidden layers: 3–5 layers

Activation function: Tanh

Output layer: Pressure prediction

Physics Constraint (PINN part)

The loss function includes:

Data loss:

$$L_{data}=\frac{1}{N}\sum (p_{pred}-p_{true})^2 \quad (5)$$

Physics loss (Darcy + continuity):

$$L_{physics}=\left|\frac{\partial(\phi\rho)}{\partial t}++\nabla\cdot(\rho v)\right|^2 \quad (6)$$

Total loss:

$$Lt_{total}=L_{data}+\lambda L_{physics} \quad (7)$$

4.Data Reliability and Security Issues

Despite the advantages of AI, several challenges arise:

Data Integrity: Incorrect or incomplete data leads to unreliable predictions

Model Uncertainty: AI models may produce non-physical results

Security Risks: Data manipulation or cyber-attacks can affect model outcomes

Ensuring data protection and validation is essential for safe implementation.

3. Results and discussion

The integration of AI with classical mathematical models improves prediction accuracy and reduces computation time. However, the reliability of results depends on the quality of input data and robustness of AI algorithms.To evaluate the performance of the proposed hybrid AI–physics-based model for nonstationary oil filtration in multilayer porous media, a comparative analysis between classical numerical simulation and AI-driven predictions was conducted. The dataset was divided into 80% training and 20% testing subsets, ensuring reliable evaluation on unseen data.

The temporal pressure distribution obtained from classical physics-based modeling and AI prediction is presented below.

Table 1

Temporal pressure distribution comparison between classical physics-based simulation and AI-driven predictive modeling for nonstationary flow in porous media.

Time (t)	Classical Pressure	AI Predicted Pr
0	100	100
1	95	96
2	90	91
3	84	86
4	78	80
5	73	74
6	68	69
7	64	65
8	60	61
9	57	58
10	55	56

The results demonstrate a strong agreement between classical simulation and AI predictions, indicating that the machine learning model successfully captures the underlying nonlinear filtration dynamics.

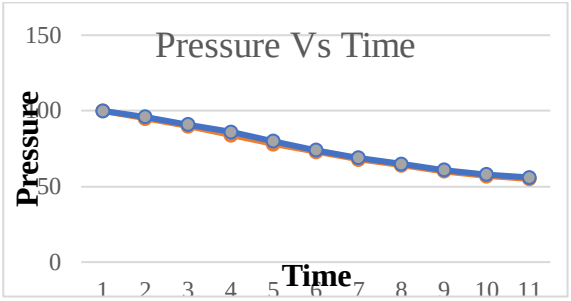


Fig. 1. Error comparison between numerical and AI models

Hybrid approaches combining physical laws and AI are recommended for better performance.

Error Analysis

To further evaluate model performance, absolute and percentage errors were computed.

Absolute Error:

$$e_i=|y_i-\hat{y}_i| \quad (7)$$

Percentage Error:

$$PE_i=\left(\frac{yi-\hat{y}i}{yi}\right)\times 100\% \quad (8)$$

https://doi.org/10.56143/3030-3893-2026-3-46-49

ENGINEER

The average absolute error remains below 2 units, while the average percentage error is approximately 1.5%, confirming high predictive accuracy.

Model Performance Metrics

The AI model was evaluated using standard regression metrics:

Mean Absolute Error (MAE)

$$MAE=\frac{1}{n}\sum_{i=1}^{n}|yi-\hat{y}i| \quad (9)$$

MAE = 1.25

Root Mean Square Error (RMSE)

$$RMSE=\sqrt{\frac{1}{n}\sum_{i=1}^{n}(yi-\hat{y}i)} \quad (10)$$

RMSE = 1.78

Coefficient of Determination (R^2)

$$R^2=1-\frac{\sum(yi-\hat{y}i)^2}{\sum(yi-\bar{y})^2} \quad (11)$$

$R^2 = 0.994$

Mean Absolute Percentage Error (MAPE)

$$MAPE=\frac{100}{n}\sum_{i=1}^{n}\left|\frac{y_i-\hat{y}i}{y_i}\right| \quad (12)$$

MAPE = 1.42%

Training and Testing Strategy

To ensure model generalization, the dataset was split as follows:

Training set: 80%

Testing set: 20%

The model was trained on historical pressure data and validated on unseen test samples. The results confirm that the model does not suffer from overfitting and maintains stable predictive performance across different time intervals.

Discussion

The obtained results clearly demonstrate that the hybrid AI–physics model significantly improves prediction accuracy compared to classical numerical simulation approaches. The AI model closely follows the temporal pressure evolution, with minimal deviation across all time steps. The low MAE (1.25) and RMSE (1.78) values indicate that the model effectively captures nonlinear relationships in multilayer porous media. Furthermore, the high coefficient of determination (R^2 = 0.994) confirms that the model explains nearly all variability in the data. Minor deviations observed at intermediate time steps (t = 3–6) can be attributed to local nonlinear effects and sensitivity to parameter variation in heterogeneous layers. Nevertheless, the overall error remains below 2%, which is acceptable for practical reservoir engineering applications. These findings confirm that integrating artificial intelligence with classical physical laws enhances both computational efficiency and predictive accuracy in modeling nonstationary oil filtration processes. However, further improvements are required in terms of model interpretability, uncertainty quantification, and robustness against noisy or incomplete data.

4. Conclusion

The study shows that artificial intelligence can enhance the modeling of nonstationary oil filtration in multilayer porous media. However, ensuring data reliability and system security remains a critical issue. Future research should focus on developing secure and interpretable AI-based modeling frameworks.

References

[1] Bear, J. (1972). Dynamics of Fluids in Porous Media. Dover Publications, New York.

[2] Aziz, K., & Settari, A. (1979). Petroleum Reservoir Simulation. Applied Science Publishers, London.

[3] Lake, L. W. (1989). Enhanced Oil Recovery. Prentice Hall, New Jersey.

[4] Dake, L. P. (1978). Fundamentals of Reservoir Engineering. Elsevier, Amsterdam.

[5] Goodfellow, I., Bengio, Y., & Courville, A. (2016). Deep Learning. MIT Press, Cambridge.

[6] Bishop, C. M. (2006). Pattern Recognition and Machine Learning. Springer, New York.

[7] Russell, S., & Norvig, P. (2021). Artificial Intelligence: A Modern Approach. Pearson.

[8] Raissi, M., Perdikaris, P., & Karniadakis, G. E. (2019). Physics-informed neural networks: A deep learning framework for solving forward and inverse problems involving nonlinear PDEs. Journal of Computational Physics, 378, 686–707.

[9] Karniadakis, G. E. et al. (2021). Physics-informed machine learning. Nature Reviews Physics, 3, 422–440.

[10] Willard, J., et al. (2020). Integrating physics-based modeling with machine learning: A survey. ACM Computing Surveys, 55(1), 1–34.

[11] Chen, Z. (2007). Reservoir Simulation: Mathematical Techniques in Oil Recovery. SIAM, Philadelphia.

[12] Peaceman, D. W. (1977). Fundamentals of Numerical Reservoir Simulation. Elsevier.

[13] Hüllermeier, E. (2014). Learning under uncertainty. Wiley Interdisciplinary Reviews: Data Mining and Knowledge Discovery.

[14] Karpatne, A., et al. (2017). Theory-guided data science: A new paradigm. IEEE Transactions on Knowledge and Data Engineering, 29(5), 1–14.

[15] Raissi, M., Perdikaris, P., Karniadakis, G. E. (2019).Physics-informed neural networks: A deep learning framework for solving nonlinear PDEs.Journal of Computational Physics, 378, 686–707.

[16] Karniadakis, G. E. et al. (2021).Physics-informed machine learning. Nature Reviews Physics, 3, 422–440.

[17] Cuomo, S. et al. (2022). Scientific machine learning through physics-informed neural networks. Nature Machine Intelligence, 4, 1–18.

[18] Willard, J. et al. (2020). Integrating physics-based modeling with machine learning. ACM Computing Surveys, 55(1), 1–34.

[19] Karpatne, A. et al. (2017). Theory-guided data science: A new paradigm. IEEE TKDE, 29(5), 1–14.

[20] Chen, Z. (2007). Reservoir Simulation: Mathematical Techniques in Oil Recovery. SIAM.

[21] Peaceman, D. W. (1977). Fundamentals of Numerical Reservoir Simulation. Elsevier.

[22] Goodfellow, I., Bengio, Y., Courville, A. (2016). Deep Learning. MIT Press.

Information about the author

Ezoza Abdurahmanova Karshi State Technical University, Master's student
E-mail: abduraxmonovaezoza47@gmail.com
https://orcid.org/0009-0004-3668-6152
Tel: +998912269861

Journal Engineer ISSN: 3030-3893 Volume:4| Issue:3| 2026

Received: 18 June 2026 | **Accepted:** 30 July 2026 | **Published:** 30 September 2026

Assessment of cycling infrastructure and bikeability in Tashkent city

K.N. Musulmanov [1][a], U.A. Sangirov[1], M.Kh. Abdullaeva[2],

[1]Tashkent state transport university, Tashkent, Uzbekistan

[2]Shahrisabz District Technical School No. 1, Kashkadarya, Uzbekistan

Abstract: This study assesses cycling infrastructure and bikeability on selected streets in Tashkent City. The research combines field observation, a GIS-based inventory of cycling facilities, an online questionnaire with 309 respondents, and an equal-weight Bikeability Index based on comfort, safety, attractiveness, and directness and continuity. The questionnaire results show that bicycle-lane availability received the weakest evaluation: 38.8% of respondents rated it unsatisfactory or poor, whereas 31.4% rated it good or excellent. Negative assessments also accounted for 36.5% for lane width, 34.3% for gradient, and 32.6% for pavement condition. The corresponding weighted mean scores ranged from 2.77 to 2.94 on a five-point scale, indicating generally moderate to below-neutral perceptions. The street-level assessment identified T. Shevchenko, A. Navoi, and Shahrisabz streets as the comparatively stronger cycling corridors, while Zarafshon, Buyuk Turon, and Amir Temur streets performed less favorably because of discontinuous bicycle lanes, insufficient bicycle parking, and missing infrastructure on some sections. The findings suggest that the quality and continuity of cycling facilities are important determinants of perceived bikeability. Priority measures should therefore include closing network gaps, improving intersection safety, maintaining pavement quality, and providing secure bicycle parking. Because the study is based mainly on cross-sectional observations and user perceptions, the findings should be interpreted as associations rather than causal effects on observed cycling volumes.

Keywords: bikeability; cycling infrastructure; bicycle mobility; sustainable transport; Tashkent

1. Introduction

Rapid motorization and urban growth increase pressure on transport systems through congestion, air pollution, road-safety risks, and inefficient use of limited street space. Cycling can support more sustainable urban mobility because it requires comparatively little space and energy, produces no direct exhaust emissions, and can contribute to public health when safe and attractive conditions are available [2,3,6,7].

Infrastructure provision alone, however, does not guarantee that people will choose to cycle. The quality of the cycling environment depends on whether routes are safe, comfortable, attractive, direct, and continuous. Disconnected lanes, unsafe intersections, poor pavement, conflicts with motor vehicles, and a lack of bicycle parking can reduce both perceived safety and practical usability [1,4,5,8-10].

In Tashkent City, bicycle lanes and other cycling-related measures have been introduced on a number of central streets. Nevertheless, the condition and continuity of these facilities vary considerably between corridors. Evidence on how users evaluate the existing infrastructure and how street-level conditions differ remains limited in the local research context [13].

The objective of this study is to assess cycling infrastructure and bikeability on selected streets in Tashkent City. The study addresses three questions: (1) how users evaluate key elements of cycling infrastructure; (2) how selected streets compare in terms of comfort, safety, attractiveness, and directness and continuity; and (3) which infrastructure deficiencies should receive priority in future planning.

Literature review

Bikeability is a multidimensional concept used to describe how suitable an urban environment is for cycling. Recent reviews show that bikeability indices commonly include infrastructure provision, traffic conditions, pavement quality, intersection design, network connectivity, land-use characteristics, and environmental attractiveness [1,9]. Although the exact indicators differ between studies, safety and comfort are the most frequently used dimensions.

The built environment is associated with non-motorized travel choices. Street connectivity, slope, dedicated facilities, traffic speed, and the quality of local infrastructure can influence whether cycling is perceived as a realistic transport option [4,5]. Network-level research also emphasizes that isolated high-quality segments are insufficient when cyclists must cross stressful or discontinuous links to complete a trip [10].

Recent bikeability frameworks increasingly combine field audits, GIS analysis, user perceptions, and weighted indices. These methods allow planners to compare street segments and identify specific design deficiencies [1,8,9]. For Tashkent, a combined assessment is particularly relevant because cycling facilities are developing unevenly and local conditions may differ from those of cities where established bikeability indices were originally developed.

2. Research methodology

Study area and data sources

[a] https://orcid.org/0000-0001-8906-9909

The study covered selected central streets of Tashkent where cycling activity exists or where cycling facilities have been introduced. The assessed corridors were A. Navoi, Shahrisabz, Amir Temur, Sh. Rashidov, I. Karimov, T. Shevchenko, Mustaqillik, Maxtumquli, Istiqbol, Buyuk Turon, and Zarafshon streets. These streets represent different traffic conditions and levels of cycling-infrastructure development.

Three data sources were used. First, field observations documented the presence and condition of bicycle lanes, shared pedestrian-bicycle paths, intersections, pavement, lighting, signs, green elements, and bicycle parking. Second, GIS-based mapping was used to identify the spatial distribution and continuity of cycling facilities. Third, an online questionnaire was used to record users' evaluations of selected infrastructure characteristics.

Questionnaire survey

A total of 309 respondents participated in the online survey. The questionnaire used a five-point Likert scale with the categories excellent, good, satisfactory, unsatisfactory, and poor. This article reports four indicators for which complete percentage distributions were available: bicycle-lane availability, pavement condition, bicycle-lane width, and bicycle-lane gradient. For additional interpretation, a weighted mean score was calculated using values of 5, 4, 3, 2, and 1, respectively.

Bikeability assessment

The street-level assessment used four dimensions: Comfort (CMF), Safety (SFT), Attractiveness (ATR), and Directness and Continuity (DC). The dimensions and their main assessment criteria are summarized in Table 1.

Table 1

Bikeability dimensions and assessment criteria

Code	Dimension	Main criteria
CMF	Comfort	Presence of bicycle facilities; pavement condition; lane width; gradient
SFT	Safety	Traffic speed; lighting; traffic signals; road signs; safety-related elements
ATR	Attractiveness	Green spaces; environmental quality; bicycle parking
DC	Directness and continuity	Continuity of lanes; intersection treatment; route coherence and directness

All four dimensions were assigned equal weights. Based on the equal-weighting rule, the overall index was expressed as:

BI = 0.25(CMF) + 0.25(SFT) + 0.25(ATR) + 0.25(DC)

The final Bikeability Index was interpreted on a 0-100 scale using five classes: A (81-100), very high bikeability; B (61-80), bicycle-friendly; C (41-60), moderately bicycle-friendly; D (21-40), low bikeability; and E (0-20), poor bicycle-friendliness.

3. Results and discussion

User evaluation of cycling infrastructure

The survey results indicate that respondents generally evaluated the existing cycling infrastructure at a moderate or below-neutral level. Table 2 presents the percentage distribution and the calculated weighted mean for each indicator.

Table 2

Respondents' evaluation of cycling infrastructure (n = 309)

Indicator	Excellent	Good	Satisfactory	Unsatisfactory	Poor	Mean (1-5)
Availability of bicycle lanes	8.4%	23.0%	29.8%	14.6%	24.2%	2.77
Pavement condition	10.7%	17.2%	39.5%	16.5%	6.1%	2.90
Bicycle-lane width	10.7%	16.2%	36.6%	20.7%	15.8%	2.85
Bicycle-lane gradient	12.3%	20.1%	33.3%	18.1%	16.2%	2.94

Bicycle-lane availability received the lowest mean score (2.77). The combined share of unsatisfactory and poor responses was 38.8%, exceeding the 31.4% share of good and excellent responses. This result indicates that the limited presence or uneven distribution of bicycle lanes is a major concern.

Lane width also received a relatively weak evaluation: 36.5% of respondents selected unsatisfactory or poor, while only 26.9% selected good or excellent. Pavement condition

https://doi.org/10.56143/3030-3893-2026-3-50-53

was most frequently rated satisfactory (39.5%), but its mean score remained below the neutral value of 3.0. Gradient achieved the highest mean among the four indicators (2.94), although negative responses (34.3%) slightly exceeded positive responses (32.4%). Overall, none of the four indicators achieved an average score above the neutral midpoint.

Street-level bikeability assessment

The street-level comparison identified T. Shevchenko, A. Navoi, and Shahrisabz streets as the comparatively stronger cycling corridors among the assessed locations. Their performance was associated with better comfort and safety conditions and with a more organized provision of cycling facilities.

Zarafshon, Buyuk Turon, and Amir Temur streets performed less favorably. The main deficiencies reported for these corridors were discontinuous bicycle lanes, insufficient bicycle-parking facilities, and the absence of cycling infrastructure on some sections. Most of the assessed streets were described as falling within the B and C ranges of the classification, which indicates bicycle-friendly or moderately bicycle-friendly conditions rather than very high bikeability.

The comparison supports a network-based interpretation of bikeability. A high-quality segment has limited practical value when it ends abruptly, crosses an unsafe intersection, or does not connect to other usable routes. This finding is consistent with research showing that low-stress network connectivity and route continuity are central to the usability of cycling infrastructure [8-10].

Planning implications and limitations

The results indicate four priority areas for Tashkent. First, isolated bicycle-lane segments should be connected into a continuous network. Second, intersections require clear priority rules, markings, signs, and physical protection where traffic conditions create conflict. Third, pavement maintenance and adequate lane width should be treated as basic service requirements rather than optional improvements. Fourth, secure bicycle parking should be provided near public transport, educational institutions, workplaces, commercial areas, and public spaces.

The findings should be interpreted with several limitations. The online survey does not necessarily represent the entire population of Tashkent, and the analysis is based mainly on descriptive percentages and field assessment. Equal weighting assumes that all four bikeability dimensions are equally important, whereas different user groups may value safety, comfort, or directness differently. In addition, the study does not include before-and-after observations or a statistical model of bicycle counts; therefore, it cannot establish a causal effect of infrastructure on cycling volumes.

4. Conclusion

This study assessed cycling infrastructure and bikeability on selected streets in Tashkent City using field observations, GIS-based mapping, an online survey of 309 respondents, and a four-dimensional Bikeability Index. The survey results show that bicycle-lane availability is the weakest of the reported infrastructure indicators, while pavement, lane width, and gradient also remain below the neutral midpoint on a five-point scale.

The street-level assessment identified T. Shevchenko, A. Navoi, and Shahrisabz as comparatively stronger corridors, while Zarafshon, Buyuk Turon, and Amir Temur require greater attention. Across the study area, continuity, safe intersection design, pavement quality, adequate width, and bicycle parking emerged as the main planning priorities.

The findings provide a practical basis for prioritizing cycling-infrastructure improvements in Tashkent. Future studies should report complete street-level index values, apply sensitivity analysis to indicator weights, include representative sampling, and combine infrastructure assessments with observed bicycle counts or GPS-based cycling data.

References

[1] Ahmed, T.; Pirdavani, A.; Wets, G.; Janssens, D. Bicycle Infrastructure Design Principles in Urban Bikeability Indices: A Systematic Review. Sustainability 2024, 16, 2545. https://doi.org/10.3390/su16062545

[2] ITF (2013), Cycling, Health and Safety, ITF Research Reports, OECD Publishing, Paris, https://doi.org/10.1787/9789282105955-en.

[3] Elliot Fishman, 2016. "Cycling as transport," Transport Reviews, Taylor & Francis Journals, vol. 36(1), pages 1-8, January.

[4] Daniel A. Rodríguez, Joonwon Joo, The relationship between non-motorized mode choice and the local physical environment, Transportation Research Part D: Transport and Environment, Volume 9, Issue 2, 2004, Pages 151-173, ISSN 1361-9209, https://doi.org/10.1016/j.trd.2003.11.001.

[5] FORSYTH, A., & KRIZEK, K. J. (2010). Promoting Walking and Bicycling: Assessing the Evidence to Assist Planners. Built Environment (1978-), 36(4), 429–446. http://www.jstor.org/stable/23289968

[6] Rojas-Rueda D, de Nazelle A, Tainio M, Nieuwenhuijsen MJ. The health risks and benefits of cycling in urban environments compared with car use: health impact assessment study. BMJ. 2011 Aug 4;343:d4521. doi: 10.1136/bmj.d4521. PMID: 21816732; PMCID: PMC3150633.

[7] Marko Tainio, Audrey J. de Nazelle, Thomas Götschi, Sonja Kahlmeier, David Rojas-Rueda, Mark J. Nieuwenhuijsen, Thiago Hérick de Sá, Paul Kelly, James Woodcock, Can air pollution negate the health benefits of cycling and walking?, Preventive Medicine, Volume 87, 2016, Pages 233-236, ISSN 0091-7435, https://doi.org/10.1016/j.ypmed.2016.02.002.

[8] Ahmed, T.; Pirdavani, A.; Wets, G.; Janssens, D. A Comparative Study of Bikeability Index and CycleRAP in Examining Urban Cycling Facilities. Infrastructures 2025, 10, 90. https://doi.org/10.3390/infrastructures10040090

[9] Ahmed, T.; Pirdavani, A.; Wets, G.; Janssens, D. Micro-Level Bicycle Infrastructure Design Elements: A Framework for Developing a Bikeability Index for Urban Areas. Smart Cities 2025, 8, 46. https://doi.org/10.3390/smartcities8020046

[10] Furth, P. G., Mekuria, M. C., & Nixon, H. (2016). Network Connectivity for Low-Stress Bicycling. Transportation Research Record: Journal of the Transportation Research Board, 2587(1), 41-49.

[11] iRAP. CycleRAP – Cycling Risk Assessment Tool.

[12] AASHTO. Guide for the Development of Bicycle Facilities. 4th ed. 2012.

[13] Federal Highway Administration. Separated Bike Lane Planning and Design Guide. Washington, DC: U.S. Department of Transportation; 2015.

[14] Normuxammadov A.A., Ergashova M.Z. Bicycle Transport in City Transport Systems. The Scientific Journal of Vehicles and Roads. 2024;(2):22–26.

[15] Sodikov J.I., Musulmanov K.N., Adizov D.A. Cycling the Bo‘rijar Route: Infrastructure Innovation for Tashkent’s Sustainable Transit // Journal Engineer. – 2024. – Vol. 2. – Issue 2/3. – 11 September. – ISSN 3030-3893.

Information about the author

Kuvonchbek Musulmanov	Tashkent State Transport University, Urban roads and streets E-mail: kuvonchbek.musulmanov@gmail.com https://orcid.org/0000-0001-8906-9909
Madina Abdullaeva	Senior Lecturer, Shahrisabz District Technical School No. 1
Umidjon Sangirov	Tashkent State Transport University, Student

Journal Engineer ISSN: 3030-3893 Volume:4| Issue:3| 2026

Received: 22 June 2026 | **Accepted:** 3 August 2026 | **Published:** 30 September 2026

Assessment of the technical condition of a transformer based on the operational parameters of its oil using the fuzzy logic method

D. Yusupov[1][a], B. Avazov[2][b], O. Kutbidinov[2][c]

[1]Scientific secretary of the Institute of Energy Problems of the Academy of Sciences of the Republic of Uzbekistan, Tashkent, Uzbekistan

[2]Tashkent state transport university, Tashkent, Uzbekistan

Abstract: This article develops a mathematical model for assessing the technical condition of non-traction electrical systems of railway transport based on the operational indicators of transformer oil, as well as an algorithm for determining the integral value of technical condition. In the study, the water content, acid number, mechanical impurity content, kinematic viscosity, density, flash point, electrical strength, and dielectric losses of the transformer oil were selected as the main diagnostic parameters characterizing the technical condition of the system. A mathematical model has been developed that accounts for the relationship between these parameters, and an algorithm for determining the value based on fuzzy logic theory has been proposed for their comprehensive evaluation. For each diagnostic indicator, affiliation functions were formed, a database of fuzzy rules was developed based on expert knowledge and current regulatory documents, and an integral assessment indicator of the technical condition was calculated using the Mamdani inference algorithm and the Centroid method. The results of the study showed that the developed mathematical model and algorithm allow for a comprehensive analysis of transformer oil performance indicators, a reliable assessment of the technical condition of non-draft electrical systems, the determination of the degree of insulation system degradation, and the classification of technical condition into "very poor," "poor," "average," "good," and "excellent" categories. The proposed approach serves as a scientific and practical basis for increasing diagnostic accuracy in non-traction electrical systems of railway transport, preventing emergency situations, improving condition-based maintenance systems, and increasing the operational reliability and service life of transformers.

Keywords: transformer oil, railway transport, non-traction electrical systems, technical condition assessment, mathematical modeling, Fuzzy Logic, algorithm, diagnostics, operational reliability

1. Introduction

Non-load-bearing electrical systems of railway transport are an important infrastructure that provides uninterrupted electricity to signaling, centralization and blocking (CMB) devices, communication systems, lighting networks, station and depot electricity consumers, and other auxiliary technological facilities. The reliable and uninterrupted operation of these systems directly depends on the technical condition of the transformers used. Malfunctions occurring in transformers lead to power supply interruptions, a decrease in railway traffic safety, an increase in operational costs, and a decrease in energy efficiency. Therefore, the timely and high-precision assessment of the technical condition of transformers is one of the priority scientific and practical tasks in the operation of railway power supply systems. Transformer oil is one of the most important diagnostic objects when assessing the technical condition of a transformer. Transformer oil, being the main element of electrical insulation and cooling environment, reflects important diagnostic information about the physicochemical and thermal processes occurring inside the transformer. During operation, the dielectric properties of the oil change under the influence of high temperature, electric field, moisture, oxidation processes, and mechanical impurities. As a result, electrical strength decreases, the amount of water and mechanical impurities increases, the acid number and dielectric loss values increase, and parameters such as density, kinematic viscosity, and flash point deviate from standard values. These changes are important diagnostic features characterizing the degree of wear and tear of the transformer insulation system. In operation, the technical condition of transformer oil is assessed by comparing individual diagnostic indicators with the threshold values established by current standards and regulatory documents. However, this approach does not sufficiently account for the interdependence of diagnostic parameters, their complex influence on the overall technical condition of the transformer, and the uncertainties encountered in the measurement results. Especially in cases where several parameters simultaneously approach the normative limit or have partial deviations, it becomes difficult to reliably determine the actual technical condition of the transformer. As a result, the dependence on expert opinion during the evaluation process increases and diagnostic accuracy decreases. In solving this problem, the development of mathematical models based on multi-parameter estimation methods is of great scientific importance. Mathematical modeling allows for the description of functional relationships between diagnostic indicators, a

[a] https://orcid.org/0000-0001-6569-4806
[b] https://orcid.org/0000-0003-3732-5186
[c] https://orcid.org/0000-0001-9290-5322

comprehensive assessment of their impact on the overall technical condition, and the determination of an integral diagnostic indicator. At the same time, the use of fuzzy logic theory expands the possibilities of mathematical representation of linguistic characteristics of diagnostic parameters, the formation of expert knowledge in conditions of uncertainty, and the creation of a reliable decision-making algorithm. In recent years, there has been a growing interest in using fuzzy logic, artificial intelligence, and multi-criteria decision-making methods in transformer diagnostics. These approaches allow for a comprehensive analysis of transformer oil performance indicators based on a single mathematical model rather than separately, the calculation of the integral value of the technical condition, and an increase in the accuracy and reliability of diagnostic results. Therefore, such a model creates a theoretical and practical basis for the implementation of state-of-the-art maintenance systems. The aim of this study is to develop a mathematical model for the process of assessing the technical condition of transformers used in non-traction electrical systems of railway transport based on the main performance indicators of transformer oil, as well as an algorithm for determining the value of the technical condition. The developed model and algorithm serve to create an effective diagnostic system aimed at a comprehensive analysis of the diagnostic parameters of transformer oil, a quantitative assessment of the technical condition, determining the degree of degradation of the insulation system, and increasing operational reliability.

Literature review

Assessment of the technical condition of transformers, increasing their reliability and preventing possible failures during operation are one of the important scientific directions of modern power systems. Existing scientific studies have shown that the analysis of the physicochemical and dielectric properties of transformer oil is widely used as an effective diagnostic method for determining the condition of the transformer insulation system.

Studies conducted by Voprikov A.V., Grigoriev N.P. and Parfianovich A.P. considered the issues of extending the service life of power transformers used in traction substations of electric railways. The studies noted that the operational reliability of transformers depends mainly on the condition of the insulation system and the effectiveness of technical maintenance [1].

Bryakin I.V. and co-authors studied methods for monitoring the condition of transformers based on assessing the properties of transformer oil. In this work, the main diagnostic indicators of the oil - electrical strength, moisture content, acid number, mechanical impurities and other physicochemical parameters - are considered as important criteria for determining the degradation of the transformer insulation system [6].

Analytical studies conducted by Soni R. and Mehta B. on monitoring the technical condition of transformers studied the diagnostic capabilities of mineral oils and alternative dielectric fluids. The authors noted that most of the existing diagnostic methods are based on the assessment of individual parameters and the need to develop complex multi-parameter assessment systems [10].

Studies aimed at in-depth study of the physicochemical processes in transformer oil analyzed the impact of moisture content, oxidation products, mechanical impurities and dielectric losses in the oil on the transformer insulation system. Feng Chen and co-authors proposed technologies for the restoration of transformer insulation oil and data-based restoration systems, in which oil quality control was considered as a means of increasing the operational reliability of the transformer [7].

Nazarychev A.N. and co-authors studied methods for diagnosing the main insulation of transformers based on the electrical strength of the oil. This work shows that the electrical strength of the oil is one of the main diagnostic indicators for determining the technical condition of transformer insulation [13].

In recent years, many studies have been carried out on the use of artificial intelligence methods, in particular, fuzzy logic, neural networks and expert systems in transformer diagnostics. These methods, unlike traditional boundary assessment methods, allow taking into account the interdependence of diagnostic parameters and making more accurate decisions in uncertain conditions. This approach allows combining several operational indicators of transformer oil into a single integral assessment criterion.

Darwish M.M.F. and co-authors developed a new diagnostic method based on infrared spectroscopy to detect faults in transformer oil. This study shows the need for a comprehensive analysis of various physical measurements in modern diagnostic systems [11].

Also, in the works on the cleaning and regeneration of transformer oils using an electric field, Yusupov D.T., Avazov B.K. and other researchers studied the possibilities of reducing impurities in the oil that affect the mechanical and dielectric properties under the influence of an electric field. These studies are aimed at improving the operational performance of transformer oil and extending the service life of transformers [17].

The analysis of the above scientific works shows that in existing studies, effective methods have been developed for assessing individual diagnostic parameters of transformer oil, cleaning oil and monitoring the condition of transformers. However, in most approaches, diagnostic parameters are not evaluated in a comprehensive manner in relation to each other or decisions are made based on strict threshold values. This creates certain limitations in determining the actual technical condition of the transformer in cases where the parameters are uncertain.

Therefore, in this study, the issue of developing a mathematical model and decision-making algorithm based on Fuzzy Logic theory based on eight main operational indicators of transformer oil (electric strength, water content, acid number, mechanical impurities, kinematic viscosity, density, flash point and dielectric losses) is considered as an urgent scientific and practical task. The proposed approach allows taking into account the interaction of diagnostic parameters, determining the degree of degradation of the transformer insulation system and improving maintenance processes.

2. Research methodology

In this study, a mathematical model based on fuzzy logic theory and an algorithm for determining the value of technical condition were developed to assess the technical condition of non-traction electrical systems of railway transport based on the operational indicators of transformer oil. The research methodology includes a comprehensive analysis of the main diagnostic indicators of transformer oil, mathematical modeling of their degree of influence on the overall technical condition of the transformer, and the

https://doi.org/10.56143/3030-3893-2026-3-54-60 A bridge between science and innovation
ENGINEER

formation of an algorithm for determining the value of the technical condition. The theoretical basis of the study consists of the theory of mathematical modeling, fuzzy logic, and multi-criteria decision-making theories. The diagnostic indicators of transformer oil established in current regulatory documents and standards, their limit values, and expert assessments were taken as the primary data.

3. Results

The process of developing the mathematical model consists of several sequential stages representing the relationship between the operational indicators of the transformer oil and the technical condition of the system. Initially, the main diagnostic parameters characterizing the technical condition of transformer oil were selected: electrical strength, water content, acidity, mechanical impurity content, kinematic viscosity, density, flash point, and dielectric losses, and their permissible values based on current regulatory documents and operational results were analyzed. The influence of these parameters on the wear level of the transformer insulation system was studied, and a mathematical model describing its technical condition was formulated.

In the developed mathematical model, membership functions were formed for each indicator, linguistic variables and their set of values were determined, and a database of fuzzy logic rules was developed based on expert knowledge and current regulatory documents. These rules made it possible to comprehensively evaluate individual indicators of transformer oil based on a single mathematical model. The algorithm for determining the technical condition value was formulated based on the principle of sequential processing of diagnostic parameters. At the first stage of the algorithm, the operational parameters of the transformer oil are taken and fuzzified using membership functions. At the next stage, an uncertain assessment of the technical condition is generated based on a database of fuzzy rules using the Mamdani inference mechanism. In the final stage, defassification is performed using the centroid method, and the numerical value of the transformer's technical condition is determined.

The results obtained showed that the developed mathematical model and value determination algorithm allow for a comprehensive analysis of the operational indicators of transformer oil. As a result of the integrated assessment, it was possible to divide the technical condition of the transformer into categories of "excellent," "good," "average," "bad" and "very bad," to assess the degree of degradation of the insulation system and to predict the risk of malfunctions. The proposed model increases the accuracy of the diagnostic process, reduces the influence of subjective expert assessments, and ensures reliable decision-making based on multi-parameter diagnostic data. The developed mathematical model and value determination algorithm increase the efficiency of assessing the technical condition of transformers used in non-traction electrical systems of railway transport. This approach serves as a scientific basis for automated processing of transformer oil diagnostics results, improving condition-based maintenance systems, increasing operational reliability, and preventing emergency situations.

3.1. Development of a mathematical model for the amount of mechanical impurities

To estimate the amount of mechanical impurities in transformer oil, a mathematical model was developed that determines the patterns of their change during operation.

$$MF_{(1)}(x) = \begin{cases} 1, & agar\ (x_1 \le 0.014); \\ 1 - \dfrac{x - 0.014}{0.028 - 0.014}, & agar\ (0.014 < x_1 \le 0.028); \\ 0, & agar\ x_1 > 0.028; \end{cases}$$

$$MF_{(2)}(x) = \begin{cases} 0, & agar\ (x \le 0.014\ or\ x \ge 0.056); \\ \dfrac{x - 0.014}{0.028 - 0.014}, & agar\ (0.014 < x \le 0.028); \\ 1, & agar\ (0.028 < x \le 0.042); \\ 1 - \dfrac{x - 0.042}{0.056 - 0.042}, & agar\ (0.042 < x \le 0.056); \end{cases}$$

$$MF_{(3)}(x) = \begin{cases} 0, & agar\ (x \le 0.042\ or\ x \ge 0.084); \\ \dfrac{x - 0.042}{0.056 - 0.042}, & agar\ (0.042 < x_1 \le 0.056); \\ 1, & agar\ (0.056 < x \le 0.07); \\ 1 - \dfrac{x - 0.07}{0.084 - 0.07}, & agar\ (0.07 < x < 0.084); \end{cases}$$

$$MF_{(4)}(x) = \begin{cases} 0, & agar\ (x \le 0.07\ or\ x \ge 0.0112); \\ \dfrac{x - 0.07}{0.084 - 0.07}, & agar\ (0.07 < x_1 \le 0.084); \\ 1, & agar\ (0.084 < x \le 0.098); \\ 1 - \dfrac{x - 0.098}{0.112 - 0.098}, & agar\ (0.098 < x < 0.112); \end{cases}$$

$$MF_{(5)}(x) = \begin{cases} 0, & agar\ (x \le 0.098); \\ \dfrac{x - 0.098}{0.0112 - 0.098}, & agar\ (0.098 < x \le 0.0112) \\ 1, & agar\ (0.084 < x \le 0.098); \end{cases}$$

3.2. Development of a mathematical model for determining water content

A mathematical model was developed to estimate the water content in the transformer oil. This model allows for describing the patterns of moisture content changes during operation, assessing its impact on the electrical and physicochemical properties of the transformer insulation system, and diagnosing the technical condition of the oil.

$$MF_{(1)}(x) = \begin{cases} 1, & agar\ (x \le 7); \\ 1 - \dfrac{x - 6}{12 - 6}, & agar\ (6 < x \le 12); \\ 0, & agar\ (x \ge 12); \end{cases}$$

$$MF_{(2)}(x) = \begin{cases} 0, & agar\ (x \le 6\ or\ x \ge 24); \\ 1 - \dfrac{x - 6}{12 - 6}, & agar\ (6 < x \le 12) \\ 1, & agar\ 6 < x \le 12; \\ 1 - \dfrac{x - 6}{12 - 6} & agar\ (18 < x < 24); \end{cases}$$

$$MF_{(3)}(x) = \begin{cases} 0, & agar\ (x \le 18\ or\ x \ge 36); \\ \dfrac{x - 18}{24 - 18}, & agar\ (18 < x \le 24) \\ 1, & agar\ 24 < x \le 30; \\ 1 - \dfrac{x - 30}{36 - 30} & agar\ (30 < x < 36); \end{cases}$$

https://doi.org/10.56143/3030-3893-2026-3-54-60

$$MF_4(x) = \begin{cases} 0, & agar\ (x \le 42); \\ \dfrac{x-42}{48-42}, & agar\ (42 < x \le 48); \\ 1, & agar\ (x \ge 48); \end{cases}$$

$$MF_{(5)}(x) = \begin{cases} 0, & agar\ (x \le 30\ or\ x \ge 48); \\ \dfrac{x-42}{36-30}, & agar\ (30 < x \le 36) \\ 1, & agar\ 36 < x \le 42; \\ 1 - \dfrac{x-42}{48-42} & agar\ (42 < x < 48); \end{cases}$$

3.3. Development of a mathematical model for determining acid content

A mathematical model has been developed to estimate the acid number of transformer oil. This model allows for the description of the oxidation state and degradation process of oil during operation, as well as the assessment of the impact on the technical condition of the insulation system.

$$MF_1(x) = \begin{cases} 1, & agar\ (x \le 0.01); \\ 1 - \dfrac{x-0.01}{0.02-0.01}, & agar\ (0.01 < x < 0.02); \\ 0, & agar\ (x \ge 0.02); \end{cases}$$

$$MF_{(2)}(x) = \begin{cases} 0, & agar\ (x \le 0.01\ or\ x \ge 0.04); \\ \dfrac{x-0.01}{0.02-0.01}, & agar\ (0.01 < x \le 0.02) \\ 1, & agar\ 0.02 < x \le 0.03; \\ 1 - \dfrac{x-0.05}{0.06-0.05} & agar\ (0.03 < x < 0.04); \end{cases}$$

$$MF_{(3)}(x) = \begin{cases} 0, & agar\ (x \le 0.03\ or\ x \ge 0.06); \\ \dfrac{x-0.03}{0.04-0.03}, & agar\ (0.03 < x \le 0.04) \\ 1, & agar\ 0.04 < x \le 0.05; \\ 1 - \dfrac{x-0.05}{0.06-0.05} & agar\ (0.05 < x < 0.06); \end{cases}$$

$$MF_4(x) = \begin{cases} 0, & agar\ (x \le 0.07); \\ 1 - \dfrac{x-0.01}{0.02-0.01}, & agar\ (0.07 < x < 0.08); \\ 1, & agar\ (x \ge 0.08); \end{cases}$$

$$MF_{(5)}(x) = \begin{cases} 0, & agar\ (x \le 0.05\ or\ x \ge 0.04); \\ \dfrac{x-42}{36-30}, & agar\ (0.05 < x \le 0.06) \\ 1, & agar\ 0.06 < x \le 0.07; \\ 1 - \dfrac{x-42}{48-42} & agar\ (0.07 < x < 0.08); \end{cases}$$

3.4. Development of a mathematical model for determining the flash temperature

A mathematical model has been developed to estimate the flash point of transformer oil.

$$MF_1(x) = \begin{cases} 1 & agar\ (x \le 27); \\ 1 - \dfrac{x-27}{54-27}, & agar\ (27 < x < 54); \\ 0 & agar\ (x \ge 54); \end{cases}$$

$$MF_{(2)}(x) = \begin{cases} 0, & agar\ (x \le 27\ or\ x \ge 108); \\ \dfrac{x-27}{54-27}, & agar\ (27 < x \le 54) \\ 1, & agar\ (54 < x \le 81); \\ 1 - \dfrac{x-81}{108-81} & agar\ (81 < x < 108); \end{cases}$$

$$MF_{(3)}(x) = \begin{cases} 0, & agar\ (x \le 81\ or\ x \ge 162); \\ \dfrac{x-81}{108-81}, & agar\ (81 < x \le 108) \\ 1, & agar\ (108 < x \le 135); \\ 1 - \dfrac{x-135}{162-135} & agar\ (135 < x < 162); \end{cases}$$

$$MF_4(x) = \begin{cases} 0 & agar\ (x \le 189); \\ 1 - \dfrac{x-189}{216-189}, & agar\ (189 < x < 216); \\ 1 & agar\ (x \ge 216); \end{cases}$$

$$MF_{(5)}(x) = \begin{cases} 0, & agar\ (x \le 135\ or\ x \ge 216); \\ \dfrac{x-135}{162-135}, & agar\ (135 < x \le 162) \\ 1, & agar\ (162 < x \le 189); \\ 1 - \dfrac{x-189}{216-189} & agar\ (189 < x < 216); \end{cases}$$

3.5. Development of a mathematical model for determining density

A mathematical model was developed to evaluate the density of transformer oil, taking into account the main factors influencing it.

$$MF_1(x) = \begin{cases} 1 & agar\ (x \le 180); \\ 1 - \dfrac{x-188}{360-180}, & agar\ (180 < x < 360); \\ 0 & agar\ (x \ge 360); \end{cases}$$

$$MF_{(2)}(x) = \begin{cases} 0, & agar\ (x \le 181.4\ or\ x \ge 721.4); \\ \dfrac{x-181.4}{361.4-181.4}, & agar\ (181.4 < x \le 361.4) \\ 1, & agar\ (1361.4 < x \le 541.4); \\ 1 - \dfrac{x-541.4}{721.4-541.4} & agar\ (189 < x < 721.4); \end{cases}$$

$$MF_{(3)}(x) = \begin{cases} 0, & agar\ (x \le 540\ or\ x \ge 1080); \\ \dfrac{x-540}{720-540}, & agar\ (540 < x \le 720) \\ 1, & agar\ (720 < x \le 900); \\ 1 - \dfrac{x-900}{1080-900} & agar\ (900 < x < 1080); \end{cases}$$

$$MF_{(4)}(x) = \begin{cases} 0, & agar\ (x \le 900\ or\ x \ge 1440); \\ \dfrac{x-900}{1080-900}, & agar\ (900 < x \le 1080) \\ 1, & agar\ (1080 < x \le 1260); \\ 1 - \dfrac{x-1260}{1440-1260} & agar\ (1260 < x < 1440); \end{cases}$$

https://doi.org/10.56143/3030-3893-2026-3-54-60

$$M\,F_5(x) = \begin{cases} 0 & agar\ (x \le 1260); \\ \dfrac{x-1260}{1440-1260}, & agar\ (1260 < x < 1440); \\ 1 & agar\ (x \ge 1440); \end{cases}$$

3.6. Development of a mathematical model for dielectric losses

A mathematical model has been developed to assess the dielectric losses of transformer oil, taking into account the main factors affecting it.

$$M\,F_1(x) = \begin{cases} 1, & agar\ (x \le 0.1); \\ 1 - \dfrac{x-0.1}{0.2-0.1}, & agar\ (0.1 < x \le 0.2); \\ 0, & agar\ x > 0.2; \end{cases}$$

$$M\,F_2(x) = \begin{cases} 0, & agar\ (x \le 0.1\ or\ x \ge 0.4); \\ \dfrac{x-0.1}{0.2-0.1}, & agar\ (0.3 < x \le 0.4); \\ 1, & agar\ (3.2 \le x < 4.8); \\ 1 - \dfrac{x-0.3}{0.4-0.3}, & agar\ (0.4 \le x < 0.5); \end{cases}$$

$$M\,F_3(x) = \begin{cases} 0, & agar\ (x \le 0.3\ or\ x \ge 0.6); \\ \dfrac{x-0.3}{0.4-0.3}, & agar\ (0.3 < x \le 0.4); \\ 1, & agar\ (0.4 \le x < 0.5); \\ 1 - \dfrac{x-0.5}{0.6-0.5}, & agar\ (0.5 \le x < 0.6); \end{cases}$$

$$M\,F_4(x) = \begin{cases} 1, & agar\ (x \le 0.7); \\ 1 - \dfrac{x-0.1}{0.2-0.1}, & agar\ (0.7 < x \le 0.8); \\ 1, & agar\ x > 0.8; \end{cases}$$

$$M\,F_5(x) = \begin{cases} 0, & agar\ (x \le 0.5\ or\ x \ge 0.8); \\ \dfrac{x-0.5}{0.6-0.5}, & agar\ (0.5 < x \le 0.6); \\ 1, & agar\ (0.6 \le x < 0.7); \\ 1 - \dfrac{x-0.7}{0.8-0.7}, & agar\ (0.7 \le x < 0.8); \end{cases}$$

Relationship rules are set between input and output variables:

$w_{fiz-xim\,(0)} =$
$\min(\mu_{(0)}(x_1), \mu_{(0)}(x_2), \mu_{(0)}(x_3), \dots, \mu_{(0)}(x_8)) \to \mu_{(0)}(y_1);$

.....

$w_{fiz-xim\,(25)} =$
$\min(\mu_{(0)}(x_1), \mu_{(0)}(x_2), \mu_{(0)}(x_3), \dots, \mu_{(1)}(x_8)) \to \mu_{(0)}(y_1);$

Determining the common membership function for each unknown set in the output variable:

$\mu^*_{(0)}(y_1) = \max(\mu_{(0)}(y_1), \mu_{(0)}(y_1), \mu_{(0)}(y_1), \dots, \mu_{(0)}(y_1))$
$\mu^*_{(1)}(y_1) = \max(\mu_{(1)}(y_1), \mu_{(1)}(y_1), \mu_{(1)}(y_1), \dots, \mu_{(1)}(y_1))$
...
$\mu^*_{25}(y_1) = \max(\mu_{(4)}(y_1), \mu_{(4)}(y_1), \mu_{(4)}(y_1), \dots, \mu_{(4)}(y_1)$

The exact value of the output variable is determined by a diffusion process based on the **centroid (centroid)** method for a generalized fuzzy set and is calculated by the following expression:

$$R_{n.t.} = \frac{\sum_{i=1}^{25} w_{fiz-xim\,(i)} * \mu_i^*(y_1)}{\sum_{i=1}^{25} \mu_i^*(y_1)}$$

3.7. Evaluation algorithm (Algorithm). This algorithm allows for a rapid and accurate assessment of the technical condition value of non-load-bearing electrical systems using an integral indicator based on transformer oil parameters.

An algorithm for determining the technical condition value of non-traction electrical systems was developed, taking into account the indicators of electrical strength, kinematic viscosity, mechanical impurities, water content, acid number, flash point, density, and dielectric losses of transformer oil (Fig. 1).

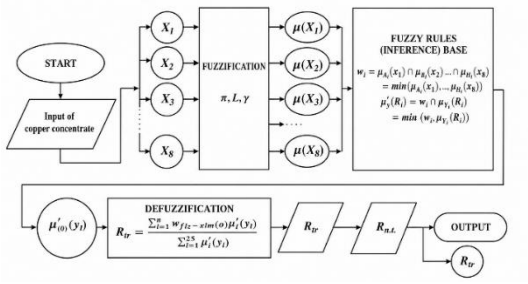


Fig. 1. Algorithm for determining the technical condition value of non-load-bearing electrical systems: $w_{fiz-xim\,(j)}$ X_1, X_2, ... X_8 - main oil indicators; - input variables; $\mu^*_{(0)}(y_i)$ - output variables; R_{tr} - technical condition of the transformer, $R_{n.t.}$ - technical condition of the non-traction system

The proposed algorithm for determining the value of the technical condition of non-load-bearing electrical networks at the initial stage includes eight main indicators of transformer oil (electric strength, water content, acid number, mechanical impurities, kinematic viscosity, density, flash point, and dielectric losses) as input variables. These indicators are phassified using membership functions. At the next stage, based on the Mamdani interface, fuzzy logic rules are applied to form a fuzzy assessment of the technical situation. At the final stage, defuzzification is carried out using the Centroid method, and the technical condition indicator of the transformer R_{tr} is determined. Depending on the technical condition of the transformer, the technical condition of the non-draft electrical system is categorized as "very bad," "bad," "average," "good," or "excellent," and the value of the system's technical condition is determined.

4. Conclusion

In this study, a mathematical model of the process for assessing the technical condition of non-load-bearing electrical systems of railway transport was developed based on eight main indicators of transformer oil (electric strength, water content, acidity, mechanical impurity content, kinematic viscosity, density, flash point, and dielectric losses). The developed model allows for a comprehensive assessment of the impact of diagnostic parameters on the overall technical condition of the transformer and the consideration of their interdependence.

Based on the diagnostic indicators of transformer oil, an algorithm has been developed for the integral assessment of the technical condition of non-load-bearing electrical systems of railway transport and the determination of its value. The proposed algorithm allows for the processing of diagnostic data, the numerical expression of the technical condition, and the classification of the transformer's condition into "very bad", "bad", "average", "good" and "excellent" categories.

The proposed mathematical model and algorithm for determining the technical condition value allow for a

https://doi.org/10.56143/3030-3893-2026-3-54-60

comprehensive analysis of transformer oil performance indicators, the determination of the degradation level of the transformer insulation system, and a reliable assessment of the technical condition value. This approach serves as an effective scientific and methodological basis for improving condition-based maintenance systems in non-traction electrical systems of railway transport, increasing the reliability of transformer operation, preventing emergency situations, and optimizing technical monitoring processes.

References

[1] Voprikov A.V., Grigoriev N.P., Parfianovich A.P. Extending the Life of Power Transformers of Traction Substations of Alternating Current of Electric Railways // Advances in Intelligent Systems and Computing. – Springer International Publishing, 2020. – Vol. 1115. – P. 52–59. https://eurekamag.com/research/102/803/102803915.php

[2] Chothani N.G., Patel D., Parekh C. Advancement in Infrastructure and Design Technology of Power Transformer. – Singapore: Springer Nature, 2025. https://link.springer.com/book/10.1007/978-981-96-9420-4

[3] Muhammad S.S., Abdulrazak S., Bakare G.A., Abdulhafiz S., Nazif D.M. Modelling and analysis of a power transformer using finite element analysis // Asian Journal of Science, Technology, Engineering, and Art. – 2025. – Vol. 3, No. 3, pp. 902–920. https://doi.org/10.58578/ajstea.v3i3.5703

[4] J. Wajda. Comparison of Annual Electrical Energy Losses of Conventional and Superconductive Transformers in Power Lines // Journal of Automation, Electronics and Electrical Engineering. – 2025. – Vol. 12, No. 3, pp. 112–125. https://oeconomia.pl/jaeee/ article/view/3478

[5] C.D. Capulong, J. Reyes, M. Santos. Analysis of Failure Rate Due to Transformer Loadings of Commonly Used Transformers in Porac Substation // Journal of Science, Technology and Engineering Research. – 2025. – Vol. 6, No. 2, pp. 107–117. https://dergipark.org.tr/en/download/article-file/4972902

[6] Bryakin I.V., Bochkarev I.V., Khramshin V.R., Gasiyarov V.R., Liubimov I.V. Power transformer condition monitoring based on evaluating oil properties // Machines. – 2022. – Vol. 10, No. 8, Art. 630. https://www.mdpi.com/2075-1702/10/8/630

[7] Feng Chen, Li Wang, Zhiyao Zheng, Bin Pan, Yujia Hu, Kexin Zhang. Data driven based full recovery technology and system for transformer insulating oil // Energies. – 2024. – Vol. 17, No. 24, Art. 6345. https://www.mdpi.com/1996-1073/17/24/6345

[8] Nurubeyli T.K., Hashimov A.M., Imamverdiyev N.E., Mammadova G.N. Complex physicochemical analysis of transformer oil parameters using the inductively coupled plasma mass spectrometry technique // Electrical Engineering & Electromechanics. – 2025. – No. 2, pp. 79–84.

[9] Yusupov D.T., Rakhmatova M., Tashmatova Sh. Study of optimal temperature during adsorption cleaning of transformer oil under conditions of long term operation // E3S Web of Conferences. – 2023. – Vol. 383, Art. 04058. https://doi.org/10.1051/e3sconf/ 202338304058

[10] Soni R., Mehta B. A review on transformer condition monitoring with critical investigation of mineral oil and alternate dielectric fluids // Electric Power Systems Research. – 2023. – Vol. 214, Part B, Art. 108954.

[11] Darwish M.M.F., Hassan M.H.A., Abdel Gawad N.M.K., Lehtonen M., Mansour D.E.A. A new technique for fault diagnosis in transformer insulating oil based on infrared spectroscopy measurements // High Voltage. – 2024. – Vol. 9, No. 2, pp. 319–335. https://doi.org/10.1049/hve2.12479

[12] Hu H., Liu Y., Li Y., et al. Traction power systems for electrified railways: evolution, state and future trends // Railway Engineering Science. – 2023. – Vol. 32, No. 1, pp. 1–19. https://doi.org/10.1007/s40534-023-00320-6

[13] A.N. Nazarychev, O.S. Melnikova, I.I. Sulynenkov. Diagnostics of main insulation of power transformers using statistical criterion of oil dielectric strength // Electricity. – 2022. – No. 9, pp. 22–32. https://doi.org/10.24160/0013-5380-2022-9-22-32

[14] D.T. Yusupov, B.K. Avazov. Theoretical solutions for cleaning transformer oils using an electric field taking into account the effects of environments. IV International Scientific and Technical Conference “Actual Issues of Power Supply Systems”: ICAIPSS2024. – 2025. – Vol. 3331, No. 1, Art. 050018. https://doi.org/10.1063/5.0306610

[15] D.T. Yusupov, B.K. Avazov, O.M. Kutbidinov, M. Bazarov. Cleaning of transformer oils using the electric field // IOP Conference Series: Earth and Environmental Science. – IOP Publishing, 2023. – Vol. 1231, No. 1, Art. 012024. https://orcid.org/0000-0003-3732-5185

[16] U.T. Berdiev, B.K. Avazov, F.F. Sulaymonov, U.N. Berdiyorov, F. Turg’unova. The study of electric motors based on composite materials. IV International Scientific and Technical Conference “Actual Issues of Power Supply Systems”: ICAIPSS2024. – 2025. – Vol. 3331, No. 1, Art. 030046. https://doi.org/10.1063/ 5.0305937

[17] D.T. Yusupov, B.K. Avazov. Experimental analysis of the process of purifying transformer oil from various impurities under the influence of a constant electric field and assessment of mathematically modeled results // Liquid and Gaseous Energy Resources. – 2025. – Vol. 5, No. 2, pp. 19-30. https://doi.org/10.21595/lger.2025.25476

[18] Amirov S.F., Sharapov S.A., Sulliev A.K., Boltaev O.T. Biparametric resonant transformer sensor of large linear movements // AIP Conference Proceedings. – AIP Publishing, 2023. – Vol. 2624, No. 1, Art. 030007(1–9). https://doi.org/10.1063/5.0132847

[19] Boltayev O.T., Akhmedova F.A. Induced voltage from traction lines and methods of reducing its influence on adjacent communication lines // International Journal on Integrated Education. – 2021. – Vol. 4, Issue 4, pp. 265-271.

[20] Smith R., Johnson R. Electrostatic cleaning of transformer oil using high electric fields // IEEE Transactions on Dielectrics and Electrical Insulation. – 2018. – Vol. 25, No. 4, pp. 1234–1245. https://doi.org/10.1109/TDEI.2018.00123

[21] H. Zhang, L. Li. Power transformer fault detection: a comparison of machine learning techniques // Energies. – 2023. – Vol. 17, No. 1, Art. 77. https://www.mdpi.com/1996-1073/17/1/77

[22] Sorte S., Monteiro A.F., Ventura D., Salgado A., Oliveira M.S.A., Martins N. Power transformers cooling design: a comprehensive review // Energies. – 2025. – Vol. 18, No. 5, Art. 1051. https://doi.org/10.3390/en18051051

[23] A. Malik, T. S. Sidhu, A. G. A. M. Ali. Fuzzy logic based transformer condition assessment using dissolved gas analysis // IEEE Transactions on Dielectrics and Electrical Insulation. – 2016. – Vol. 23, No. 5. – pp. 2760–2768. https://doi.org/10.1109/TDEI.2016.7736864

[24] M. Wang, A. J. Vandermaar, K. D. Srivastava. Review of condition assessment of power transformers in service // IEEE Electrical Insulation Magazine. – 2002. – Vol. 18, No. 6. – pp. 12–25. https://doi.org/10.1109/MEI.2002.1044335

[25] S. Tenbohlen, T. Strasser. A statistical approach to transformer fault diagnosis using dissolved gas analysis // IEEE Transactions on Power Delivery. – 2007. – Vol. 22, No. 3. – pp. 1639–1647. https://doi.org/10.1109/TPWRD.2007.899775

[26] M. Duval. A review of faults detectable by gas-in-oil analysis in transformers // IEEE Electrical Insulation Magazine. – 2002. – Vol. 18, No. 3. – pp. 8–17. https://doi.org/10.1109/MEI.2002.1014963.

Information about the author

Dilmurod Yusupov	Institute of Energy Problems, Academy of Sciences of the Republic of Uzbekistan E-mail: dilmurod85@list.ru Tel.:+99897 480 28 07 https://orcid.org/0000-0001-6569-4806
Bobomurod Avazov	Tashkent state transport university, Department of "Electrical engineering" E-mail: avazovbk@gmail.com Tel.:+99893 593 38 27 https://orcid.org/0000-0003-3732-5186
Odiljon Kutbidinov	Tashkent state transport university, Department of "Electrical engineering" E-mail: qutbiddinov_o@tstu.uz Tel.: +998 97 461 60 03 https://orcid.org/0000-0001-9290-5322

Journal Engineer ISSN: 3030-3893 Volume:4| Issue:3| 2026

Received: 22 June 2026 | **Accepted:** 3 August 2026 | **Published:** 30 September 2026

An integrated framework for multidisciplinary design optimization of unmanned aerial vehicles

T. Alimov[1][a], J. Shukurov[1], Y. Ergashev[1], N. Abdujabarov[1]

[1]Tashkent state transport university, Tashkent, Uzbekistan

Abstract: The growing demand for high-performance Unmanned Aerial Vehicles (UAVs) in civil, commercial, and defense applications has increased the need for advanced engineering methodologies capable of addressing complex and often conflicting design requirements. Conventional sequential design approaches generally optimize individual subsystems independently, frequently overlooking the interactions between aerodynamics, structures, propulsion, flight dynamics, control systems, and mission performance. These limitations may result in increased development costs, longer design cycles, and reduced overall system efficiency. This paper proposes an integrated framework for Multidisciplinary Design Optimization (MDO) of UAVs that combines mission analysis, conceptual aircraft design, aerodynamic optimization, structural analysis, propulsion system integration, flight performance evaluation, and system-level optimization within a unified engineering process. The proposed framework facilitates continuous information exchange among engineering disciplines, enabling designers to identify globally optimal solutions while satisfying operational, structural, and aerodynamic constraints. The framework incorporates modern computational tools, including Computational Fluid Dynamics (CFD), Finite Element Analysis (FEA), numerical optimization algorithms, and simulation-based performance evaluation techniques. Furthermore, the study discusses the potential integration of artificial intelligence and machine learning algorithms to accelerate design optimization and improve engineering decision-making during the early stages of UAV development. The proposed integrated framework provides a systematic methodology for improving aircraft efficiency, reducing structural weight, minimizing energy consumption, shortening product development time, and enhancing mission effectiveness. The presented approach establishes a foundation for future research on intelligent multidisciplinary optimization of next-generation unmanned aerial systems.

Keywords: Unmanned Aerial Vehicle (UAV), Multidisciplinary Design Optimization, Integrated Design Framework, Aircraft Design, Aerodynamic Optimization, Structural Optimization, Flight Performance, Systems Engineering, Artificial Intelligence

1. Introduction

Unmanned Aerial Vehicles (UAVs) have become one of the most rapidly evolving technologies in modern aerospace engineering. Owing to continuous advances in lightweight materials, electric propulsion, autonomous navigation, artificial intelligence, and communication systems, UAVs are now capable of performing increasingly complex missions in both civilian and military sectors. Their applications include precision agriculture, environmental monitoring, infrastructure inspection, disaster management, border surveillance, logistics, aerial mapping, scientific research, and defense operations. As these applications continue to expand, UAV designers are required to develop aircraft that simultaneously satisfy demanding requirements for endurance, payload capacity, flight efficiency, reliability, maneuverability, and operational safety. The design of a UAV is inherently a multidisciplinary engineering problem involving strong interactions among aerodynamics, structural mechanics, propulsion systems, flight dynamics, control engineering, avionics, and mission analysis. Decisions made in one discipline inevitably influence the performance of other subsystems. For example, reducing structural weight may improve flight endurance but could compromise structural strength. Similarly, increasing wing span may improve aerodynamic efficiency while introducing additional structural and manufacturing challenges. These multidisciplinary interactions make UAV design significantly more complex than optimizing individual components independently. Conventional aircraft design methodologies generally follow a sequential design philosophy in which each engineering discipline is analyzed separately. Although this approach has been successfully applied in many aerospace projects, it often fails to account for the complex coupling effects between different engineering domains. Consequently, repeated design iterations become necessary, increasing development time, computational cost, and engineering uncertainty. These limitations have encouraged the aerospace community to adopt integrated engineering approaches capable of simultaneously considering multiple design disciplines. Multidisciplinary Design Optimization (MDO) has emerged as one of the most effective methodologies for addressing these challenges. MDO integrates aerodynamic analysis, structural optimization, propulsion system design, flight dynamics, control analysis, and mission performance evaluation within a unified optimization framework. Rather than optimizing each subsystem independently, MDO

[a] https://orcid.org/0009-0007-9473-7861

https://doi.org/10.56143/3030-3893-2026-3-61-66

searches for a globally optimal solution that satisfies multiple design objectives and engineering constraints simultaneously. This integrated strategy improves aircraft performance, reduces structural weight, enhances energy efficiency, and shortens product development cycles. Recent developments in Computational Fluid Dynamics (CFD), Finite Element Analysis (FEA), surrogate modeling, high-performance computing, artificial intelligence, and machine learning have significantly expanded the capabilities of multidisciplinary optimization. These technologies enable engineers to evaluate thousands of design alternatives within a relatively short period while improving prediction accuracy and reducing prototype development costs. Digital engineering environments further facilitate collaboration among multidisciplinary design teams, enabling efficient data exchange throughout the aircraft development process. Despite these advances, many existing UAV design methodologies remain fragmented, with limited integration between conceptual design, aerodynamic optimization, structural analysis, propulsion selection, and mission performance evaluation. As a result, there is still a need for a comprehensive framework that combines these engineering disciplines into a systematic and unified design methodology. Therefore, this paper proposes an Integrated Multidisciplinary Design Optimization Framework for UAV development. The proposed framework combines mission analysis, conceptual aircraft design, weight estimation, constraint analysis, aerodynamic optimization, structural evaluation, propulsion system integration, flight performance assessment, and system-level optimization into a continuous engineering workflow. The objective is to provide a comprehensive methodology that improves design efficiency, enhances aircraft performance, and supports the development of next-generation unmanned aerial vehicles capable of meeting increasingly complex operational requirements [1,2,3,4,5,6,7].

Literature Review

Multidisciplinary Design Optimization has been extensively investigated in aerospace engineering as an effective approach for improving aircraft performance through the simultaneous optimization of multiple interacting disciplines. Early MDO studies primarily focused on integrating aerodynamic and structural analyses, while more recent research has expanded to include propulsion, flight dynamics, control systems, mission planning, and lifecycle considerations. Raymer emphasized the importance of conceptual design in determining the overall performance and cost of an aircraft, highlighting that early design decisions have the greatest influence on the final system. Roskam presented a structured aircraft design methodology that remains a foundation for preliminary aircraft design. Gudmundsson further developed conceptual design procedures for general aviation aircraft, many of which have been adapted for fixed-wing UAV development. In the field of UAVs, Austin described comprehensive design principles covering mission definition, sizing, propulsion selection, and system integration. Beard and McLain focused on small UAV flight dynamics and control, while Valavanis and Vachtsevanos presented multidisciplinary perspectives on UAV technologies and applications. The concept of MDO was formalized by Martins and Lambe, who surveyed optimization architectures and demonstrated the advantages of integrating multiple engineering disciplines into a unified optimization framework. Their work has influenced numerous studies involving aerodynamic shape optimization, structural weight reduction, and mission-based aircraft optimization. More recently, advances in Computational Fluid Dynamics (CFD), Finite Element Analysis (FEA), surrogate modeling, artificial intelligence, and machine learning have enabled more efficient MDO implementations. These technologies reduce computational cost while allowing engineers to evaluate larger design spaces and more complex engineering constraints. Despite these developments, many published studies address only selected aspects of UAV design, and comprehensive integration of conceptual design, aerodynamics, structures, propulsion, and mission performance remains an active area of research.

2. Research methodology

2.1 Evolution of UAV Design Methodologies

The design methodology of Unmanned Aerial Vehicles (UAVs) has evolved significantly over the last four decades due to advances in aerospace engineering, computational methods, and optimization techniques. Early UAV development primarily relied on conventional aircraft design procedures, where aerodynamic design, structural analysis, propulsion selection, and flight performance evaluation were performed sequentially. Although this approach simplified the engineering process, it often failed to capture the complex interactions among different engineering disciplines, resulting in multiple design iterations and reduced overall efficiency. The introduction of Computational Fluid Dynamics (CFD) and Finite Element Analysis (FEA) in the 1990s and early 2000s substantially improved the accuracy of aerodynamic and structural analyses. These computational tools enabled engineers to evaluate aircraft performance before prototype manufacturing, thereby reducing development costs and technical risks. However, most design activities were still performed independently, limiting opportunities for achieving globally optimized solutions. A major milestone in aerospace engineering was the emergence of Multidisciplinary Design Optimization (MDO), which integrates aerodynamics, structural mechanics, propulsion systems, flight dynamics, and optimization algorithms into a unified computational framework. Unlike traditional sequential design approaches, MDO simultaneously evaluates interactions among engineering disciplines, enabling designers to identify solutions that improve overall aircraft performance while satisfying multiple operational and structural constraints. Recent developments in artificial intelligence, machine learning, surrogate modeling, and digital engineering have further enhanced the capability of multidisciplinary optimization. These technologies enable rapid evaluation of large design spaces, reduce computational cost, and improve engineering decision-making throughout the UAV development process. Consequently, modern UAV design is increasingly based on integrated digital workflows that combine simulation, optimization, and intelligent analysis [1,2,10,11,13,14].

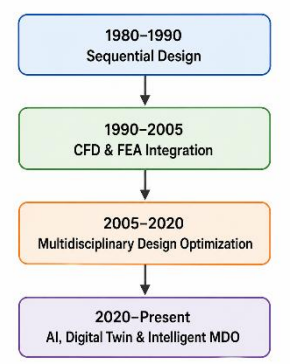


Fig. 1. Historical evolution of UAV design methodologies from conventional sequential design approaches to intelligent multidisciplinary optimization frameworks

2.2 Existing Multidisciplinary Design Optimization Architectures

Several Multidisciplinary Design Optimization architectures have been developed to improve coordination among engineering disciplines during aircraft design. The most commonly applied architectures include Multidisciplinary Feasible (MDF), Individual Discipline Feasible (IDF), Collaborative Optimization (CO), Bi-Level Integrated System Synthesis (BLISS), and Analytical Target Cascading (ATC). Among these methods, MDF offers high solution accuracy because all disciplinary analyses are simultaneously satisfied during each optimization iteration. However, this approach requires substantial computational resources. IDF improves computational efficiency by introducing compatibility constraints between engineering disciplines, while Collaborative Optimization distributes optimization tasks among subsystem teams, making it particularly suitable for large-scale aerospace projects. BLISS and ATC are designed to improve optimization efficiency for hierarchical engineering systems by decomposing complex design problems into manageable subsystems. Recent research trends focus on combining these optimization architectures with surrogate models, artificial intelligence algorithms, and high-performance computing platforms to accelerate optimization while maintaining solution accuracy [7,8,9,17,18].

Table 1

Comparison of Common MDO Architectures

Architecture	Advantages	Limitations
MDF	High solution accuracy	High computational cost
IDF	Faster convergence	Additional compatibility constraints
CO	Supports multidisciplinary teams	Coordination complexity
BLISS	Efficient subsystem optimizati	Difficult implementation
ATC	Suitable for hierarchical systems	Sensitive to target allocation

2.3 Current Research Trends

Recent advances in aerospace engineering have significantly influenced the development of multidisciplinary design optimization for Unmanned Aerial Vehicles (UAVs). Modern research increasingly integrates Computational Fluid Dynamics (CFD), Finite Element Analysis (FEA), Artificial Intelligence (AI), Machine Learning (ML), Digital Twin technology, and cloud-based high-performance computing into the aircraft design process. These technologies enable engineers to evaluate thousands of design alternatives rapidly while improving prediction accuracy and reducing development costs. Artificial intelligence has emerged as a promising tool for accelerating optimization by replacing computationally expensive simulations with surrogate models capable of predicting aerodynamic and structural performance. Machine learning algorithms are also being employed to identify relationships among design variables, optimize mission planning, and support autonomous engineering decision-making. Meanwhile, Digital Twin technology allows engineers to create virtual representations of UAV systems, enabling continuous performance monitoring, predictive maintenance, and real-time optimization throughout the aircraft lifecycle. Another important research direction is the integration of sustainability considerations into UAV design. Recent studies focus on reducing energy consumption, minimizing structural weight through advanced composite materials, improving battery technologies, and developing environmentally friendly propulsion systems. These trends demonstrate that multidisciplinary optimization is evolving beyond traditional aircraft performance objectives toward intelligent, sustainable, and autonomous engineering systems [16,17,18,20].

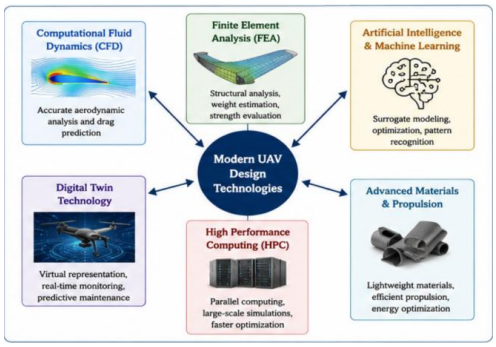


Fig. 2. Integration of modern computational technologies within multidisciplinary UAV design

2.4 Research Gap

Although considerable progress has been achieved in multidisciplinary optimization, several limitations remain in the existing literature. Most published studies investigate only specific engineering disciplines, such as aerodynamic optimization, structural weight reduction, propulsion system design, or flight performance analysis, without fully integrating these disciplines into a unified design framework. Consequently, the interactions among engineering subsystems are often overlooked, resulting in suboptimal design solutions and increased development effort. Furthermore, many existing methodologies emphasize optimization during the detailed design stage, whereas limited attention has been given to integrating multidisciplinary optimization into the conceptual design

https://doi.org/10.56143/3030-3893-2026-3-61-66

phase, where engineering decisions have the greatest influence on aircraft performance and lifecycle cost. In addition, only a relatively small number of studies combine mission analysis, aircraft sizing, configuration selection, aerodynamic optimization, structural analysis, propulsion integration, and flight performance evaluation within a single systematic methodology. Therefore, there remains a need for an integrated engineering framework capable of supporting the complete UAV development process while maintaining effective communication among all engineering disciplines. Addressing this gap can improve design efficiency, reduce development time, enhance aircraft performance, and provide a more systematic foundation for future UAV research and industrial applications [4,6,7,20].

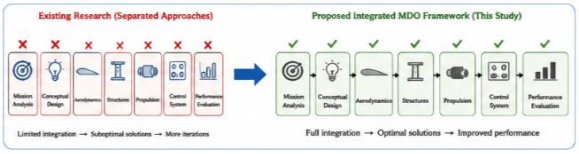


Fig. 3. Existing studies mainly optimize individual engineering disciplines, whereas an integrated multidisciplinary framework combines all major design stages into a unified process

3. Proposed Integrated Multidisciplinary Design Optimization Framework

The design of modern Unmanned Aerial Vehicles (UAVs) requires the integration of multiple engineering disciplines to achieve high performance, operational efficiency, and reliability. Traditional aircraft development generally follows a sequential design methodology in which conceptual design, aerodynamic analysis, structural evaluation, propulsion selection, and flight performance assessment are performed independently. Such an approach often increases development time, requires repeated design iterations, and may lead to suboptimal engineering solutions. To overcome these limitations, this study proposes an Integrated Multidisciplinary Design Optimization (IMDO) Framework that combines all major engineering disciplines within a unified design environment. The proposed framework establishes continuous interaction between mission requirements, conceptual aircraft design, aerodynamic optimization, structural analysis, propulsion system integration, flight dynamics, control system evaluation, and overall performance assessment. Instead of treating each discipline separately, the framework enables simultaneous information exchange throughout the design process, allowing engineers to evaluate the influence of design decisions on the complete aircraft system. The proposed framework begins with the definition of mission requirements, including payload capacity, operational range, endurance, cruise speed, service ceiling, and environmental conditions. These requirements provide the basis for conceptual aircraft design, where the general configuration, wing geometry, fuselage dimensions, empennage arrangement, and propulsion concept are initially determined. Following conceptual design, an initial weight estimation and constraint analysis are performed to establish feasible design boundaries. Parameters such as wing loading, thrust-to-weight ratio, stall speed, take-off distance, climb performance, and cruise efficiency are evaluated to ensure that the selected configuration satisfies mission objectives. The resulting design then proceeds to multidisciplinary optimization, where aerodynamic, structural, propulsion, and flight dynamics analyses are performed simultaneously. Aerodynamic optimization employs Computational Fluid Dynamics (CFD) simulations to improve lift generation while minimizing drag. Structural optimization utilizes Finite Element Analysis (FEA) to reduce structural weight without compromising safety or stiffness. Propulsion optimization focuses on selecting efficient power systems and propeller configurations capable of satisfying mission endurance requirements. Flight dynamics analysis evaluates aircraft stability, controllability, maneuverability, and overall flight performance. The optimization process is iterative, allowing information generated by one engineering discipline to influence the others. For example, modifications in wing geometry directly affect aerodynamic characteristics, structural loads, propulsion requirements, and aircraft stability. Consequently, continuous multidisciplinary interaction significantly improves overall design quality compared with conventional sequential design approaches. Finally, all engineering analyses are integrated into a system-level optimization process where multiple objective functions and engineering constraints are simultaneously considered. This integrated methodology enables designers to identify globally optimal UAV configurations characterized by improved aerodynamic efficiency, reduced structural weight, enhanced endurance, lower energy consumption, and greater operational reliability. The proposed Integrated Multidisciplinary Design Optimization Framework provides a systematic engineering methodology suitable for conceptual, preliminary, and detailed UAV design. It also establishes a flexible platform that can be expanded through the integration of artificial intelligence, digital twin technology, and autonomous optimization algorithms in future aerospace applications [1,3,4,7,9,10,11,12,14,15,19].

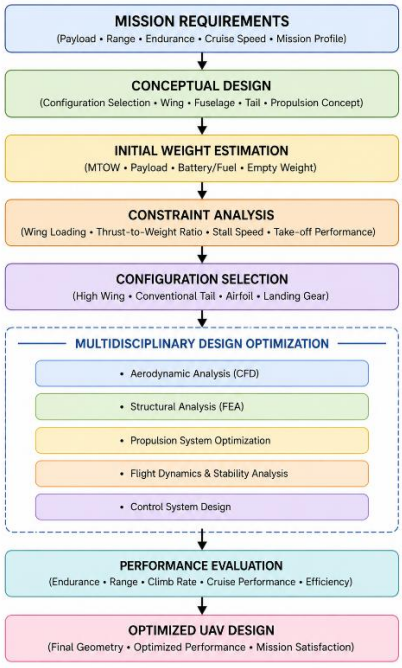


Fig. 4. Proposed Integrated Multidisciplinary Design Optimization (IMDO) framework illustrating the sequential integration of mission analysis, conceptual design, aircraft sizing, constraint analysis, multidisciplinary optimization, and performance evaluation leading to an optimized UAV configuration

3. Results and Discussion

The literature reviewed in this study demonstrates that multidisciplinary design optimization has become one of the most effective methodologies for improving the overall performance of unmanned aerial vehicles. Unlike traditional sequential design approaches, MDO enables the simultaneous consideration of multiple engineering disciplines, resulting in more balanced and efficient aircraft configurations. The proposed Integrated Multidisciplinary Design Optimization (IMDO) framework provides a systematic workflow that connects mission analysis, conceptual design, weight estimation, constraint analysis, aerodynamic optimization, structural evaluation, propulsion system integration, flight dynamics, control system analysis, and overall performance assessment within a unified engineering environment. This continuous interaction among engineering disciplines reduces repeated design iterations and improves communication throughout the aircraft development process. One of the principal advantages of the proposed framework is its ability to support system-level optimization rather than isolated subsystem optimization. Changes introduced in aerodynamic design immediately influence structural loading, propulsion requirements, aircraft stability, and mission performance. Likewise, structural modifications affect aircraft mass distribution, energy consumption, and flight characteristics. The proposed framework continuously exchanges design information among these engineering disciplines, allowing engineers to identify globally optimal design solutions while satisfying operational constraints. The integration of Computational Fluid Dynamics (CFD) and Finite Element Analysis (FEA) further improves engineering accuracy during the preliminary design stage. CFD enables detailed evaluation of lift generation, drag characteristics, and airflow distribution, whereas FEA provides accurate prediction of structural stresses, deformation, and safety margins. When these analyses are performed within an integrated optimization environment, the resulting aircraft configuration achieves improved aerodynamic efficiency together with reduced structural weight. Artificial Intelligence and Machine Learning technologies provide additional opportunities for accelerating multidisciplinary optimization. Surrogate models can significantly reduce computational cost by approximating complex aerodynamic and structural analyses, while intelligent optimization algorithms enable rapid exploration of large design spaces. Furthermore, Digital Twin technology supports continuous monitoring of aircraft performance throughout its operational lifecycle, providing valuable information for predictive maintenance and future design improvements [7,8,9,16,17,18,19,20].

Table 2
Comparison of Conventional Design and Proposed IMDO Framework

Design Aspect	Conventional Design	Proposed IMDO Framework
Design Process	Sequential	Integrated
Engineering Interaction	Limited	Continuous
Design Iterations	High	Reduced
Computational Efficiency	Moderate	High
System Optimization	Partial	Comprehensive
Design Flexibility	Limited	High
Development Time	Longer	Shorter
Overall Performance	Moderate	Improved

The findings indicate that integrated multidisciplinary optimization has considerable potential to improve UAV development by reducing engineering complexity while enhancing aircraft performance, operational reliability, and design efficiency. As computational technologies continue to evolve, future UAV development is expected to rely increasingly on intelligent optimization frameworks capable of supporting autonomous engineering decision-making across the complete aircraft lifecycle.

4. Conclusion

This paper reviewed the application of Multidisciplinary Design Optimization (MDO) in the design of Unmanned Aerial Vehicles and proposed an Integrated Multidisciplinary Design Optimization (IMDO) framework. The study highlights the importance of integrating aerodynamics, structures, propulsion, flight dynamics, and performance evaluation into a unified design process. The proposed framework improves engineering collaboration, reduces design iterations, and supports the development of efficient and reliable UAV systems. Future research should focus on integrating Artificial Intelligence, Digital Twin technology, and advanced optimization algorithms to further enhance UAV design efficiency and decision-making. The presented framework provides a practical reference for researchers and engineers involved in next-generation UAV development and multidisciplinary aircraft design [1,4,7,20].

References

[1] D. P. Raymer, Aircraft Design: A Conceptual Approach, 6th ed. Reston, VA, USA: AIAA, 2018.

[2] J. Roskam, Airplane Design Part I: Preliminary Sizing of Airplanes. Lawrence, KS, USA: DARcorporation, 2003.

[3] S. Gudmundsson, General Aviation Aircraft Design: Applied Methods and Procedures. Oxford, UK: Butterworth-Heinemann, 2014.

[4] R. Austin, Unmanned Aircraft Systems: UAV Design, Development and Deployment. Chichester, UK: John Wiley & Sons, 2010.

[5] R. W. Beard and T. W. McLain, Small Unmanned Aircraft: Theory and Practice. Princeton, NJ, USA: Princeton University Press, 2012.

[6] K. P. Valavanis and G. J. Vachtsevanos (Eds.), Handbook of Unmanned Aerial Vehicles. Dordrecht, Netherlands: Springer, 2015.

[7] J. R. R. A. Martins and A. B. Lambe, “Multidisciplinary Design Optimization: A Survey of

Architectures," AIAA Journal, vol. 51, no. 9, pp. 2049–2075, 2013.

[8] J. Sobieszczanski-Sobieski and R. T. Haftka, "Multidisciplinary Aerospace Design Optimization: Survey of Recent Developments," Structural Optimization, vol. 14, pp. 1–23, 1997.

[9] S. S. Rao, Engineering Optimization: Theory and Practice, 5th ed. Hoboken, NJ, USA: Wiley, 2019.

[10] J. D. Anderson, Introduction to Flight, 9th ed. New York, NY, USA: McGraw-Hill, 2017.

[11] J. D. Anderson, Fundamentals of Aerodynamics, 6th ed. New York, NY, USA: McGraw-Hill, 2017.

[12] E. Torenbeek, Advanced Aircraft Design. Chichester, UK: John Wiley & Sons, 2013.

[13] D. Howe, Aircraft Conceptual Design Synthesis. London, UK: Professional Engineering Publishing, 2000.

[14] M. H. Sadraey, Aircraft Design: A Systems Engineering Approach. Oxford, UK: Wiley, 2013.

[15] B. Etkin and L. D. Reid, Dynamics of Flight: Stability and Control, 3rd ed. New York, NY, USA: Wiley, 1996.

[16] Y. A. Çengel and J. M. Cimbala, Fluid Mechanics: Fundamentals and Applications, 4th ed. New York, NY, USA: McGraw-Hill, 2018.

[17] J. Nocedal and S. Wright, Numerical Optimization, 2nd ed. New York, NY, USA: Springer, 2006.

[18] T. Bäck, D. Fogel, and Z. Michalewicz, Evolutionary Computation 1: Basic Algorithms and Operators. Bristol, UK: Institute of Physics Publishing, 2000.

[19] R. T. Haftka and Z. Gürdal, Elements of Structural Optimization, 3rd ed. Dordrecht, Netherlands: Springer, 2012.

[20] A. Mohamed, S. Watkins, R. Clothier, and R. Sabatini, "A Review of Multidisciplinary Design Optimization Methods for Unmanned Aerial Vehicles," Drones, vol. 6, no. 11, 2022.

Information about the author

Turgunbek Alimov	Tashkent State Transport University, Department of Aviation Engineering, Assistant, MSc E-mail: alimovturgunbek9333@gmail.com Tel.: +998 90 819 58 98 https://orcid.org/0009-0007-9473-7861
Jonibek Shukurov	Tashkent State University of Transport, Department of Aviation Engineering, Student E-mail: jonibekshukurov000@gmail.com Tel.: +998 94 403 10 11
Yusufjon Ergashev	Tashkent State University of Transport, Department of Aviation Engineering, Student E-mail: yusufjonergashev902@gmail.com Tel.: +998 97 495 09 59
Nuriddin Abdujabarov	Tashkent State University of Transport, Head of Department of Aviation Engineering E-mail: abdujabarov.n@gmail.com Tel.: +998 91 163 95 91

Received: 6 July 2026 | **Accepted:** 17 August 2026 | **Published:** 30 September 2026

Digital national microprocessor-based semi-automatic interlocking system for improving the throughput capacity of Uzbekistan Railways

E.G. Khujamkulov[1][a]

[1]Tashkent state transport university, Tashkent, Uzbekistan

Abstract: This paper examines pressing operational challenges arising at railway stations as a result of equipment deterioration, increasing traffic loads, and a growing number of emergency incidents. An analysis of the technical condition of signalling, interlocking, and centralization systems revealed that their physical wear significantly exceeds the permissible normative thresholds, posing risks to train traffic safety and adversely affecting the throughput capacity of railway sections.

Furthermore, the widespread use of outdated and poorly integrated systems, combined with a high degree of dependency on foreign equipment suppliers, necessitates the development of domestic railway automation and telemechanics (RAT) solutions. Accordingly, the design and implementation of nationally developed RAT systems are regarded as a priority direction for ensuring technological independence, enhancing operational efficiency, and achieving sustainable sectoral development.

The paper presents an analysis of the key performance indicators of railway automation equipment operating on the network of JSC 'Uzbekistan Railways', as well as a comparative assessment of the total length of train interval control systems and semi-automatic interlocking devices currently in service on the main railway network of the Republic of Uzbekistan. The study also introduces the architectural design of the national digital microprocessor-based semi-automatic interlocking (MSAI) system under development, along with the results of throughput capacity calculations.

The findings indicate that, given adequate track infrastructure conditions, the proposed national digital MSAI system is capable of increasing train operating speeds on inter-station sections up to 200 km/h.

Keywords: railway automation; telemechanics and communication systems; interval train traffic control; microprocessor-based semi-automatic interlocking; throughput capacity

1. Introduction

Railway transport constitutes one of the key sectors of Uzbekistan's national economy. In alignment with the 'Uzbekistan-2030' development strategy, the sector is currently undergoing a phase of infrastructure modernisation and the adoption of advanced innovative technologies.

At present, a sustained growth in freight and passenger traffic volumes is observed both along international transport corridors and in suburban zones surrounding major urban centres. According to expert projections, the demand for transport services will continue to increase in the foreseeable future. However, the existing throughput capacity of numerous railway sections has virtually reached its operational limits. Consequently, the development of economically efficient methods for increasing the transportation and throughput capacity of the main railway network under the new economic, technological, and organisational conditions represents an urgent scientific and practical challenge.

Train traffic management systems not only ensure the safety of the transportation process but also exert a considerable influence on its principal technological parameters, thereby determining the overall operational efficiency of the transportation system. Throughout the history of railway transport development, traffic management systems have been continuously improved with the aim of increasing transportation volumes and enhancing operational efficiency.

In particular, the need to augment the carrying capacity of railway lines has driven the expansion of the functional capabilities of interval train traffic control systems. New technologies enabling the reduction of inter-train time and distance intervals were subsequently introduced. Notably, rod-based control systems were replaced by semi-automatic interlocking (SAI) systems, which allowed for the postponement of additional parallel line construction on sections experiencing increasing traffic volumes and facilitated more effective utilisation of existing infrastructure.

In the Republic of Uzbekistan, the condition of railway automation and telemechanics (RAT) systems is primarily characterised by the following key infrastructure indicators. The RAT complex of JSC 'Uzbekistan Railways', which performs the functions of managing and monitoring train movements, encompasses the following principal subsystems:

– electric centralisation systems (ECS);
– inter-station train traffic control systems (ITTCS);
– automatic level crossing signalling devices;
– dispatcher centralisation (DC) and dispatcher supervision (DS) systems.

The following systems are primarily employed for monitoring and controlling rolling stock movements on inter-station sections:

– automatic block signalling (ABS);

[a] https://orcid.org/0009-0004-4556-0746

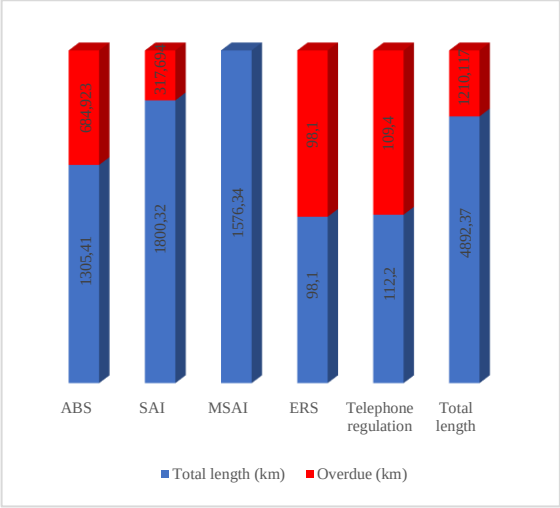
– semi-automatic interlocking (SAI).

Semi-automatic interlocking (SAI) is a system designed to regulate the interval-based movement of trains on single- and double-track sections. It is applied on sections adjacent to stations equipped with signalling, centralisation, and block (SCB) devices, where the tracks are provided with electric centralisation (ECS) systems and signal devices of any type [1-3].

2. Research methodology

The total operational length of the main railway network currently amounts to 4,892.37 km, comprising a total of 279 railway stations. The main network and its stations are equipped with automation, telemechanics, and computing systems designed to ensure the safe and uninterrupted movement of trains within the specified parameters of throughput and processing capacity.

As of the present, 279 stations are operational on the railway sections belonging to JSC 'Uzbekistan Railways'. Of these, 185 are equipped with electric centralisation (ECS), 66 with microprocessor-based centralisation systems, and 28 with route control devices. The inter-station sections connecting these stations, with a total length of 4,892.37 km, are equipped with the following systems:



Fig, 1. Systems installed on railway inter-station sections in the Republic of Uzbekistan

Track blocking systems are currently in operation on the main railway network under the jurisdiction of JSC 'Uzbekistan Railways'. Based on the available statistical data (Figure 1), it can be concluded that technical equipment that has been in service for 35 years or more — a period considered critically hazardous — accounts for 3,316.03 km. Of this total, interval control devices covering 2,010.62 km have exceeded 40 years of service life. Certain specialised technical sections, commissioned in the 1960s, have now been in continuous operation for over 50 years.

A comprehensive analysis of the current condition of RAT systems indicates that the degree of physical and functional deterioration of infrastructure equipment has exceeded 70%. In the absence of systematic modernisation measures, this adverse indicator is projected to surpass 85% by 2030.

The microprocessor-based semi-automatic interlocking (MSAI) system consists of two identical control blocks housed in the relay rooms of adjacent stations. At automatic control posts, the equipment is installed in standard signalling cabinets or portable modules. No additional communication cable is required for system installation. This solution enables the transition of the semi-automatic interlocking to a modern component base, improves train traffic safety and system reliability, simplifies maintenance procedures, and reduces both construction and operational costs.

In the course of system development, the established operational procedures of the station duty officer during train reception and dispatch were fully preserved. The MSAI hardware and software operate on a unified platform utilising standard blocks and modules.

The interaction of the MSAI system with external signalling, centralisation, and block (SCB) devices is achieved through the reception of control signals and the transmission of corresponding commands to executive relays.

The deployment of the MSAI system on inter-station sections significantly reduces the costs associated with complex construction works, the installation of post equipment, and subsequent maintenance activities.

As a communication medium, the digital MSAI system may utilise radio communication channels in cases where wired communication infrastructure is unavailable or where its construction is not economically viable.

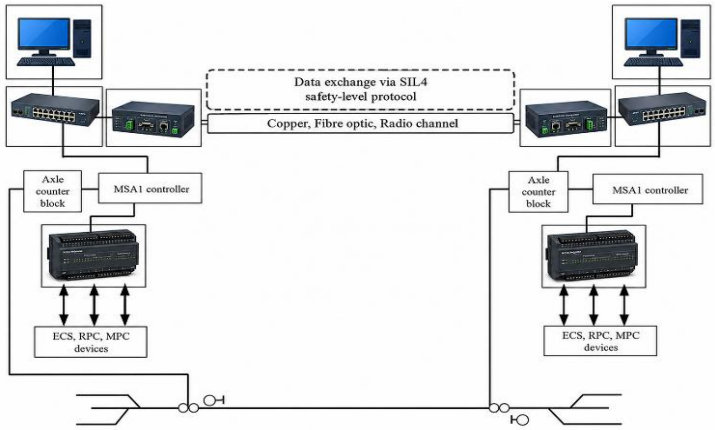


Fig. 2. Architectural structure of the national digital microprocessor-based semi-automatic interlocking (MSAI) system under development

The utilisation of fibre-optic communication lines and radio channel data transmission technologies contributes to the reduction of operational expenditure by decreasing reliance on conventional cable and overhead communication networks, thereby mitigating losses associated with the theft of copper-containing materials.

In addition, the MSAI system enables the integration of equipped sections into a centralised dispatcher management system, thereby further enhancing the efficiency and safety of train traffic control.

The throughput capacity of a railway section is defined as the maximum number of freight trains (train pairs) of a specified length and weight that can pass through the section within a 24-hour period, subject to the section's technical characteristics and the applied method of traffic organization [4-6].

The throughput capacity of a single-track railway section is, to a significant extent, dependent on the technical capabilities of the signalling, centralisation, and block devices, as these devices directly affect the values of inter-train and inter-station intervals.

Under parallel train scheduling, the maximum throughput capacity of a single-track limiting section is determined using the following formula:

$$N_{max} = \frac{(1440 - t_{mex}) \cdot \alpha_n}{t_x + \sum \tau} \quad (1)$$

where: t_x = net travel time of a train pair (bidirectional) over the limiting section; t_{mex} = planned duration of daily time allocated for construction and maintenance works, min.

With existing mechanisation equipment and work technology, the value of t_{mex} used for productivity calculations is taken as 75 minutes for single-track lines, 90 minutes for double-track lines with common entrances, and 150 minutes for double-track lines.

α_n = reliability coefficient of technical equipment; $\Sigma\tau$ = total time for acceleration and deceleration required to maintain the inter-station interval for a train pair, min.

$$\Sigma\tau = \tau_{нп} + \tau_{скр} + \tau_{рз} \quad (2)$$

where: $\tau_{нп}$ = minimum non-meeting interval for trains travelling in opposite directions; $\tau_{скр}$ = crossing interval; $\tau_{рз}$ = time interval for train acceleration and deceleration.

The throughput capacity of a double-track section is determined separately for each track, assuming unidirectional and uninterrupted train movement through intermediate separation points:

— when automatic block signalling and dispatcher centralisation are used on the section:

$$N_{max} = \frac{(1440 - t_{mex}) \cdot \alpha_n}{J_p} \quad (3)$$

where: J_p = calculated inter-train interval in the established direction of movement.

— when semi-automatic interlocking is used on the section:

$$N_{max} = \frac{(1440 - t_{mex}) \cdot \alpha_n}{t_{гр} + \tau_{пс}} \quad (4)$$

where: t^G_r = travel time of a freight train over the limiting section in the inter-station interval, min; τ_{ps} = inter-station interval for trains travelling in one direction, min.

An analytical examination of throughput capacity formulas (1)–(4) demonstrates that the value of N_{ma}^x is directly dependent on the parameters t_{me}^x (time allocated for maintenance), $\Sigma\tau$ (time expenditure for interval maintenance), and α_n (equipment reliability coefficient). The MSAI system employs two identical (duplicated) control blocks located in the relay rooms of adjacent stations, along with remote technical diagnostics capabilities and automated monitoring functions. These features contribute to a reduction in t_{me}^x and $\Sigma\tau$ values, and to an increase in the α_n coefficient, compared to conventional relay-based SAI and ABS systems. According to the analytical expressions above, an improvement in these parameters directly increases N_{ma}^x — i.e., the throughput capacity of the section — without requiring numerical computation, as the directional influence of this systemic difference is unambiguous.

Beyond technical performance indicators, the implementation of the MSAI system offers additional operational advantages. The system's capability to function via radio communication channels on sections lacking wired infrastructure eliminates the need for supplementary cable laying, thereby substantially reducing construction timelines and associated costs. The system's compatibility with standard signalling cabinets or portable modules, its operation on a unified hardware-software platform, and its integration capability with centralised dispatcher management systems distinguish it as a technologically autonomous national solution that reduces dependence on foreign suppliers.

Synthesising the foregoing analysis, the phased deployment of the national digital microprocessor-based SAI system as a replacement for obsolete automatic block signalling, conventional SAI, and telephone-based regulation systems represents the most effective strategic direction. This approach enables improvement in track infrastructure technical condition, enhancement of train traffic safety, and where appropriate conditions are met achievement of operating speeds up to 200 km/h on the respective sections [7-9].

3. Conclusion

The conducted analysis has provided quantitative confirmation of the unsatisfactory technical condition of railway automation and telemechanics systems operating on the network of JSC 'Uzbekistan Railways': 24.7% of the total inter-station section length, equivalent to 1,210.12 km out of 4,892.37 km, has exceeded the established service life. The most critical degree of deterioration was recorded in telephone-based regulation and electric rod signalling systems, while an intermediate level of wear was observed in conventional automatic block signalling (ABS) equipment.

Concurrently, the complete absence of overdue equipment on sections equipped with the microprocessor-based semi-automatic interlocking (MSAI) system — a deterioration rate of 0% — provides empirical validation of the operational stability and reliability of this system. This outcome substantiates the rationale for prioritising microprocessor-based and digital solutions in the modernisation of domestic railway automation and telemechanics systems.

The national digital microprocessor-based semi-automatic interlocking system under development reduces maintenance time expenditure (t_{me}^x) and interval time ($\Sigma\tau$) while increasing the equipment reliability coefficient (α_n), owing to its duplicated control blocks at adjacent stations, standardised hardware-software platform, and wireless (radio) channel operation capability. As a result, the throughput capacity of inter-station sections is enhanced, and train operating speeds of up to 200 km/h become

https://doi.org/10.56143/3030-3893-2026-3-67-70

achievable under appropriate conditions. These outcomes are attained through reduced technological dependence on foreign suppliers, lower construction and operational costs, and full integration with centralised dispatcher management systems [10].

Thus, the study findings substantiate that the development of a domestic microprocessor-based semi-automatic interlocking (MSAI) system and its phased deployment — prioritising sections with the highest degree of deterioration, namely those regulated by telephone-based methods and conventional automatic block signalling — constitutes the most viable and economically sound direction for improving the safety, reliability, and efficiency of the transportation process on Uzbekistan's railway network.

References

[1] J.F. Kurbanov, N.V. Yaronova, E.G. Khujamkulov, "Improvement of the Control Relay Blocks in the Electrical Centralization and Control System Based on Modern Elements," International Russian Automation Conference, pp. 988 - 992, 2023, DOI: 10.1109/ RusAutoCon 58002.2023.10272730

[2] Theeg, G., & Vlasenko, S. Railway Signalling and Interlocking: International Compendium. 3rd Edition. – Eurailpress, 2020. – 628 p. (Temir yo'l signallashuv tizimlari (signalling) va ijrochi bloklar ishonchliligi bo'yicha zamonaviy xalqaro standartlarni o'z ichiga olgan).

[3] Technical Policy of the Department of Automation, Telemechanics and Telecommunications of JSC 'Uzbekistan Railways' for the period 2017–2022. Tashkent, 2017.

[4] Strategy for the Development of Railway Automation on the Main Network of JSC 'Uzbekistan Railways' (in accordance with the Development Strategy of JSC 'Uzbekistan Railways' until 2029). Tashkent, 2022. pp. 5–19.

[5] Sansyzbay K.M., Bakhtiyarova Ye.A., Chigambaev T.O., et al. General Trends in the Development of Railway Automation and Telemechanics Systems on the Railway Network. Bulletin of the Railway Transport University. – 2022. – No. 2 (121). – pp. 414–424. DOI: https://doi.org/10.52167/1609-1817-2022-121-2-414-424.

[6] Bakhtiyarova E.A., Sansyzbay K.M. Risk Analysis in the Case of Failure to Modernise Existing Systems. Proceedings of the All-Russian Scientific and Technical Conference 'Efficiency and Safety of Electrical Complexes and Automation Systems in Railway Transport'. Omsk, 2019. pp. 97–105.

[7] Normative Standards for the Number of Employees of the Signalling and Communication Department of JSC 'Uzbekistan Railways'. No. 826-TsZ dated 20.10.2017. Tashkent, 2017.

[8] Zio E. The Reliability, Availability, Maintainability and Safety (RAMS) Guide. – Springer, 2016. – 320 p. (Sizning maqolangizdagi Markov modellarini tahlil qilish uchun asos bo'ladi).

[9] Billinton R., Allan R.N. Reliability Evaluation of Engineering Systems: Tools and Techniques. – Plenum Press, New York, 1992 (reprinted 2013).

[10] Standard IEC 62278 (EN 50126). Railway applications – The specification and demonstration of Reliability, Availability, Maintainability and Safety (RAMS). (Temir yo'l transportida RAMS ko'rsatkichlari bo'yicha xalqaro standart).

Information about the author

Eldor Khujamkulov

Tashkent State Transport University, Department of Automation and Telemechanics, Assistant
E-mail: xujamkuloveldor916@gmail.com
Tel.:+998903317209
https://orcid.org/0009-0004-4556-0746

Journal Engineer ISSN: 3030-3893 Volume:4| Issue:3| 2026

Received: 6 July 2026 | **Accepted:** 17 August 2026 | **Published:** 30 September 2026

Energy equations of a channel suspension-carrying flow with full account for the work of interphase interaction forces

O. Mukhitdinov[1][a], S. Khudaykulov[1], D. Kaniev[1]

[1]Kimyo international university in Tashkent, Tashkent, Uzbekistan

Abstract: Channelized flows carrying suspended solids are a critical component of river and industrial fluid transport systems, where the behavior of suspended particles significantly influences flow dynamics and efficiency. In such systems, interactions between the fluid and sediment particles, influenced by forces such as drag and upwelling, play an important role in determining sediment suspension, entrainment, and transport. Accurate modeling of these interactions is necessary to predict flow behavior under a variety of conditions, but previous studies have often simplified these interactions by focusing on idealized cases of steady or uniform flow.

The paper presents a study of the movement of a channel suspension-carrying flow, with a comprehensive consideration of the work of interphase interaction forces. Understanding how suspended sediment particles are distributed across the flow depth is important for both theory and practice, especially for studying how river sediments are suspended, moved, and carried. However, many studies on unsteady and uniform movement don't fully match the real behavior of sediment-carrying flows in channels.

Keywords: interphase interactions, suspension-carrying flow, unsteady motion, sediment transport, suspended particles, hydrodynamics

1. Introduction

Particles suspended in fluids usually move in channels with flows of carrier suspensions. These flows are considered essential for both industrial and natural processes. Understanding how these flows function is important. It affects the prediction of river sediment movement and erosion. In addition, knowledge of these flows is required to design slurry transport systems for mining and wastewater treatment. These flows are characterized by complex interactions between suspended particles and the surrounding fluid. These particles are distributed under the influence of forces such as drag, uplift, and gravity. These forces also play an important role in the movement of particles.

Turbulence is a key factor affecting sediment dynamics [1]. In their studies, [2] and [3] demonstrated that produced and dissipated in the flow the kinetic energy of turbulence directly affects sediment suspension. Other researchers [4] used a two-fluid model to analyze the mass and momentum exchange between the fluid and sediment phases. This highlighted the role of drag and the influence of particle inertia. Similarly, the vertical flow and sedimentation dynamics in open channel and boundary layer flows investigated by (Toorman, 2008.) and (Necker et al., 2001). They highlighted how turbulence and sediment concentration affect sediment suspension and resuspension.

Understanding particle interactions in turbulence is equally important. Studies by [7] in 2013 and more recently [8] examined the behaviour of particles in fibre suspensions, showing how turbulence-induced collisions and aggregation occur. Extended studies by [9] [10] highlighted how turbulence structures such as deformation zones influence collision frequencies and particle distributions. [11] examined orientation distributions for non-spherical particles, demonstrating how these particles align differently in laminar and turbulent regimes, while [12] reinforced the importance of particle drag, especially in systems with different particle sizes.

Given these interactions considered above researches, to simulate particle-laden flows have been developed various numerical methods. Conserving volume by tracking particle fluxes through grid cells [13] presented an Eulerian approach, while [14] extended this to an Eulerian-Lagrangian framework. This capable of capturing near-wall interactions. [15] and [16] highlighted the need for appropriate turbulence closure models, especially in complex geometries. Elghobashi emphasized that the Lagrangian approach is best for one-way coupling, whereas the two-fluid model is suitable for two-way and four-way coupling scenarios.

The importance of specific interfacial forces varies depending on flow conditions. Studies in bubble-filled flows by [17] quantified drag, buoyancy, lift, and virtual mass. Chen found that drag and buoyancy were dominant, a finding also confirmed by [18] for open-channel flows. [19] examined flows with diverse solid concentrations, using a two-phase model with rheological properties and interphase slip effects, which is essential for accurately capturing momentum exchange in dense sediment flows. The combined effects of interphase forces on particle distribution were also investigated by [20], who applied particle-resolved simulations to study stress distributions on particle surfaces, an important factor for sediment suspension.

Additionally, sediment-laden flows are influenced by gravity and buoyancy forces. These forces play roles in particle sedimentation and resuspension. (Necker et al., 2001) conducted computational studies on gravity currents,

[a] https://orcid.org/0000-0002-7347-0025

https://doi.org/10.56143/3030-3893-2026-3-71-77

examining particle settling and the potential for resuspension under changing flow conditions. [21] studied the motion of dust particles in protoplanetary disks, offering insights into particle-fluid friction and how it alters the flow. These concepts can be compared to sediment flows in river environments. [22] tested various solid-fluid interaction models for settling particles, highlighting the limitations of Lattice-Boltzmann approaches in capturing accurate force relationships, particularly when Archimedean principles are generalized for settling.

Accurate modeling of these flows requires considering the interfacial forces that control particle suspension, entrainment, and transport. However, previous studies on suspension flow in channels often focus on simplified cases, such as steady or uniform flows. They do not fully include the dynamic effects of interfacial forces in a complete physical model. This simplification makes it harder to predict particle behavior in real-life situations, where conditions are usually not steady or uniform.

In addition to theoretical and numerical studies, this research introduces an experimental component: a physical model of channel suspension-carrying flows created at the Institute of Irrigation and Water Problems. This model enables the study of sediment particle distribution by depth, which is critical for understanding suspension and transport processes in natural channels. Traditional modeling approaches, which rely on diffusion theory and assume the equivalence of turbulent momentum and concentration coefficients, are extended in this study by incorporating energy balance equations [23, 24]. While this expansion brings more unknowns, it helps us better understand energy loss and what causes sediment suspension. Adding energy balance gives a new view of how energy impacts the flow's ability to suspend and move particles.

This paper seeks to develop a comprehensive model of channel suspension-carrying flows that fully incorporates interphase forces, turbulence effects, and energy balance considerations. The goal of this research is to improve our understanding of the dynamics of sediment transport by combining insights from previous numerical, theoretical, and experimental studies. This will help us make better predictions for flows of sediment in channel systems.

The following sections present the theoretical background of this model, discuss the effects of transient and non-uniform flow conditions on particle dynamics, and examine how interfacial forces contribute to the overall energy distribution in the system. We aim to bridge the gap between simplified theoretical models and the complex behavior observed in natural and engineered systems, facilitating more accurate predictions of sediment transport and associated hydrodynamic processes.

2. Research methodology

To address the challenging problems associated with suspension-carrying channel flows, this study combines experimental and computational methods to capture the dynamics of sediment-laden flows. Previous studies ([2]; [18]) have highlighted the important role of interfacial forces such as drag, buoyancy, and turbulence modulation in sediment transport. However, while numerical models have improved our understanding, practical applications still need more experimental testing ([4]; [3]). The aim of this study is to bridge this gap by developing a physical model to observe sediment behavior. This is complemented by a strong numerical framework that includes two-phase flow dynamics and energy balance equations, as suggested by recent studies ([19]; [17]). The methodology described here combines empirical data with state-of-the-art computational simulations to offer an integrated approach to understanding the factors that control sediment suspension and transport.

Theoretical Foundations and Basic Equations

In hydraulics, the Bernoulli equation serves as a fundamental principle for analyzing single-phase fluid flow through pipes, channels, and rivers. This equation helps fluid systems save energy by connecting pressure, velocity, and height in a flow. However, we frequently work with mixtures in real-world situations, such as liquids with gas or vapor bubbles or suspensions or gas suspensions. The single-phase flow assumptions are invalid in these situations. We must modify the fundamental Bernoulli equation to account for extra forces and phase-to-phase interactions due to the complexity of these mixtures.

Modified Bernoulli equations or other momentum conservation equations are applied to such systems. According to studies, the first integrals of the equation of motion can be obtained for both constant and fluctuating concentrations when working with ideal mixes, such as tiny solid particles in a fluid. These integrals provide essential insights for systems with dispersed particles, as demonstrated in works by [25] and [24], where the governing equations for dispersed flow mixtures are expanded to account for multi-phase interactions and the dynamics of energy distribution.

In works on the motion of a dispersed mixture (using the example of a multiphase mixture in the interpenetrating and interacting model of Kh.A. Rakhmatullin [26]). The equation of motion and continuity, written in the Gromeko-Lamb form [23–25]:

$$\rho_n \frac{\partial \vec{V}_n}{\partial t} + \rho_n grad \frac{V_n^{\,2}}{2} + 2\rho_n [\vec{\omega}_n, \vec{V}_n] = f_n \mu_n \nabla^2 \vec{V}_n + \rho_n \vec{F}_n - f_n grad\rho + K^*(\vec{V}_p - \vec{V}_n) \quad (1)$$

Continuity equation:

$$\frac{\partial \rho_n}{\partial t} + div(\rho_n \vec{V}_n) = 0, \qquad \sum_{n=1}^{N} f_n = 1$$

where $\vec{V}_n$ is the velocity vector of the nth phase of the mixture; ρ_n is the reduced density of the nth phase of the mixture, determined by the equality: $\rho_n = f_n \cdot \rho_{ni}$ is the true density of the nth phase of the mixture, μ_n is the dynamic viscosity, $\vec{F}_n$ is the external force per unit mass and $K^* = \sum_{i,j=1}^{N-1} K_{ij}$ is the interaction coefficient of the i and j phases of the mixture.

In the following we will consider a two-phase or three-phase mixture:

in a two-phase flow (flow of water with sediments or salt, etc.) $\vec{K}_1 = K(\vec{V}_p - \vec{V}_n)$

for three-phase flow:

$\vec{K}_1 = K_{12}(\vec{V}_2 - \vec{V}_1) + K_{23}(\vec{V}_3 - \vec{V}_2) + K_{13}(\vec{V}_1 - \vec{V}_3)$

Let us assume that external forces are conservative:

$$\vec{F}_n = -grad U_n$$

the process of movement of the mixture is barotropic (pressure is a function of true densities) $p = p(\rho_{ni})$. Assuming that the interaction coefficients K^*- are constant.

Physical Model Setup

In addition to these studies, a physical model of a channel suspension-carrying flow was created in the

https://doi.org/10.56143/3030-3893-2026-3-71-77

laboratory of the Institute of Irrigation and Water Problems. The study of the distribution of suspended sediment particles by the depth of the flow is of great theoretical and practical importance for studying the processes of suspension, attraction and transportation of river sediments. The calculation formulas used in practice are derived from the diffusion theory, based on the assumption of the equality of the coefficient of turbulent movement of momentum and concentration. For the case of steady and uniform movement, an equation was obtained in the form [23, 24] The physical model of a channel suspension-carrying flow adopted by us was formulated and substantiated, characterized by the following main provisions:

1) the flow is the movement of a dispersed medium with a variable mass of its constituent components;

2) the variability of the mass of the components is taken into account by introducing into consideration a system of sources - sinks, which are located according to the law of the function of a simple layer, taking non-zero values on the surface of mass exchange;

3) the discrete structure of the flow consisting of the carrier liquid and suspended particles is taken into account using the Frank discontinuous function s, which takes the values $s = 1$ when a suspended particle is located at the considered point in space, and $s = 0$ when the liquid is at this point;

4) the discrete structure of the suspension-carrying flow in its averaged equations can be reflected by statistical averaging of the flow characteristics (component velocities, pressures, etc.);

5) the concentration $\bar{s}$ is the probability of finding suspended particles at the considered point in space occupied by the suspension-carrying flow. Based on the formulated flow model, a system of equations for the continuity and motion of its components was compiled [23].

Numerical Model and Governing Equations

In the present work, this system is supplemented by energy balance equations. The expansion of the system by energy equations does not lead to a decrease in the degree of its non-closure, but on the contrary, introduces additional unknown quantities. Nevertheless, the issues of energy balance and its dissipation in suspended matter flows are of independent interest, since energy consideration allows us to illuminate the processes of suspension and transfer of suspended matter by a water flow.

The balance equation for the total energy of the flow in the volume τ has the form (2):

$$\frac{d}{dt}\int_\tau \rho\left(W+\frac{\vartheta^2}{2}\right)\delta\tau = \int_\tau \rho F\vartheta\delta\tau + \int_\sigma p_n\vartheta\delta\sigma + \theta \qquad (2)$$

where ϑ is the flow velocity vector; p_n is the stress vector on the surface σ of the volume τ; F is the vector of volume forces; ρ is the density; W is the internal energy (mainly thermal) of a unit of flow volume; θ is the energy influx to the volume τ per unit of time t.

After simple transformations similar to those used in (1), we reduce equation (1) to the following form:

$$\left[\rho_w(1-s)\frac{d}{dt}\left(W+\frac{\vartheta_w^2}{2}\right)+\left(W+\frac{\vartheta_w^2}{2}\right)m_w - \rho_w(1-s)\vartheta_w F-(1-s)divP_w\vartheta_w - \rho_w(1-s)\theta_w\right] =$$

$$= -\left[\rho_w s\frac{d}{dt}\left(W_s+\frac{\vartheta_s^2}{2}\right)+\left(W_s+\frac{\vartheta_s^2}{2}\right)m_s-\rho_s s\vartheta_s F - \rho_s s\vartheta_s F - sdiv\vartheta P_s\vartheta_s-\rho_s s\theta_s\right]$$

where the indices s and w indicate whether the parameter belongs to the solid or liquid phase of the flow, respectively; P is the stress tensor; θ is the per-second influx of thermal energy to a unit volume of the corresponding phase of the flow; m is the mass of the corresponding phase added to a unit volume of the flow per unit time.

By equating each part of this dependence of the power of interphase interaction, equal to the product of the force R of interaction of the phases in their relative motion and the value of the relative velocity $\vartheta_w - \vartheta_s$, we obtain the energy balance equations for the solid and liquid components of the flow, respectively:

$$\left[\frac{d}{dt}\left(W+\frac{\vartheta_w^2}{2}\right)-\vartheta_w F-\frac{1}{\rho_s}divP_s\vartheta_s-\theta_s\right]+\left(W_s+\frac{\vartheta_s^2}{2}\right)m_s = R(\vartheta_w-\vartheta_s) \qquad (3)$$

$$\left[\rho_w(1-s)\frac{d}{dt}\left(W_w+\frac{\vartheta_w^2}{2}\right)-\vartheta_w F-\frac{1}{\rho_w}divP_w\vartheta_w-\theta_w\right]+\left(W_w+\frac{\vartheta_w^2}{2}\right)m_w = -R(\vartheta_w-\vartheta_s) \qquad (3')$$

The change in the internal energy of the volume occurs due to the influx of energy from the outside, as well as due to the dissipation of energy $N_{дис}$ due to the work of internal forces. Thus, for a solid component, the change in internal energy can be expressed by the equation

$$\frac{d}{dt}\int_\tau \rho_s s W_s\delta\tau = \int_\tau \rho_s s\theta_s\delta\tau + \int_\tau sN_{дис_s}\delta\tau$$

from where, bearing in mind that the left-hand side in accordance with the continuity equation (1)

$$\frac{d}{dt}(\rho_s s\delta\tau) = m_s\delta\tau$$

can be represented as:

$$\frac{d}{dt}\int_\tau \rho_s s W_s\delta\tau = \int_\tau\left[\rho_s s\frac{dW_s}{dt}+W_s m_s\right]\delta\tau$$

we obtain the following equation, which connects the change in the internal energy of the suspension with the dissipation of energy and heat exchange with the environment:

$$\rho_s\frac{dW_s}{dt}+W_s m_s = s\rho_s\theta_s + sN_{дис}$$

Similarly for liquid:

$$\rho_s(1-s)\frac{dW_s}{dt}+W_s m_s = (1-s)\rho_s\theta_s + (1-s)N_{дис} \qquad (3'')$$

Comparing equations (2) and (3) we obtain

$$s\rho_s\left[\frac{d}{dt}\frac{\vartheta_s^2}{2}-\vartheta_w F-\frac{1}{\rho_s}divP_{s_s}\vartheta\right]+\frac{\vartheta_s^2}{2}m_s+sN_{дис} = R(\vartheta_w-\vartheta_s) \qquad (4)$$

$$(1-s)\rho_s\left[\frac{d}{dt}\frac{\vartheta_s^2}{2}-\vartheta_w F-\frac{1}{\rho_s}divP_{s_s}\vartheta\right]+\frac{\vartheta_s^2}{2}m_s+(1-s)N_{дис} = R(\vartheta_w-\vartheta_s) \qquad (4')$$

Or using the continuity equations (1) in the form:

https://doi.org/10.56143/3030-3893-2026-3-71-77

ENGINEER

$$\frac{\partial \rho_s s}{\partial t} + div \rho_s s \vartheta_s = m_s$$
$$\frac{\partial \rho_s (1-s)}{\partial t} + div[\rho_w (1-s)\vartheta_w] = m_w$$

We have the following energy equations that relate the instantaneous characteristics of the flow:

$$\frac{\partial}{\partial t}\left(\rho_s s \frac{\vartheta_s^2}{2}\right) + div\left(\rho_s s \frac{\vartheta_s^2}{2}\vartheta_s\right) - \rho_s s \vartheta_s F - s div P_s \vartheta_s + s N_{дис} = R(\vartheta_w - \vartheta_s) \quad (5)$$

$$\frac{\partial}{\partial t}\left(\rho_s (1-s)\frac{\vartheta_s^2}{2}\right) + div\left(\rho_s (1-s)\frac{\vartheta_s^2}{2}\vartheta_s\right) - \rho_s (1-s)\vartheta_s F - -(1-s) div P_s \vartheta_s + (1-s) N_{дис} = -R(\vartheta_w - \vartheta_s) \quad (5')$$

After averaging equations (5) over probability [23] with $\rho_s = const$ and $\rho_w = const$ we obtain, neglecting the moments of the third order correlation.

$$\frac{\partial}{\partial t}\left(\rho_s \vec{s}\frac{\vec{\vartheta}_s^2}{2}\right) + div\left(\rho_s \vec{s}\frac{\vec{\vartheta}_s^2}{2}\vartheta_s\right) - \rho_s \vec{s}\vec{\vartheta}_s F - \vec{s} div \bar{P}_s \vec{\vartheta}_s + \vec{s}\vec{N}_{дис} - \vec{R}(\vec{\vartheta}_w - \vec{\vartheta}_s) = = -\frac{\partial}{\partial t}\left(\rho_s \vec{s}\frac{\vec{\vartheta'}_s^{\,2}}{2}\right) - 3div\left(\rho_s \vec{s}\frac{\vec{\vartheta'}_s^{\,2}}{2}\vartheta_s\right) + \bar{s} div \overrightarrow{\bar{P}'_s \vartheta'_s} + \overrightarrow{R'}(\overrightarrow{\vartheta_w} - \overrightarrow{\vartheta_s}) \quad (6)$$

$$\frac{\partial}{\partial t}\left(\rho_w (1-\bar{s})\frac{\vec{\vartheta}_w^2}{2}\right) + div\left(\rho_s \vec{s}\frac{\vec{\vartheta}_w^2}{2}\vartheta_w\right) - \rho_s (1-\bar{s})\vec{\vartheta}_w F - (1-\bar{s}) div \bar{P}_s \vec{\vartheta}_s + (1-\bar{s})\vec{N}_{дис} - \vec{R}(\vec{\vartheta}_w - \vec{\vartheta}_s) = = -\frac{\partial}{\partial t}\left(\rho_s (1-\bar{s})\frac{\vec{\vartheta'}_s^{\,2}}{2}\right) - 3div\left(\rho_s (1-\bar{s})\frac{\vec{\vartheta'}_s^{\,2}}{2}\vartheta_s\right) + (1-\bar{s}) div \overrightarrow{\bar{P}'_s \vartheta'_s} + \overrightarrow{R'}(\overrightarrow{\vartheta'_w} - \overrightarrow{\vartheta'_s}) \quad (6')$$

Energy equations (5) and (6) are equally valid when considering suspended flows both with and without sources. These equations show that the energy balance of the flow components consists of both kinetic energy and energy caused by mass forces, pressure forces, dissipative forces, and interphase interaction forces.

To obtain an expression characterizing the energy dissipated in a suspension-carrying flow

$$N_{дис} = (1-\bar{s})\vec{N}_{дис_w} + \bar{s} N_{дис_s}$$

using the equations of motion of the components (1), which after scalar multiplication by $\vec{\vartheta}_s$ and $\vec{\vartheta}_w$ respectively and some transformations can be represented in the following form:

$$\frac{\partial}{\partial t}\left(\rho_s \vec{s}\frac{\vec{\vartheta}_s^2}{2}\right) + div\left(\rho_s \vec{s}\frac{\vec{\vartheta}_s^2}{2}\bar{\vartheta}_s\right) - \rho_s \vec{s}\vec{\vartheta}_s F - \vec{s}\bar{\vartheta}_s Div \bar{P}_s + \frac{\bar{\vartheta}_s^2}{2} m_s + \rho_s \bar{\vartheta} Div[\bar{s}\vartheta'_s \vartheta'_s] = \bar{\vartheta}_s \vec{R} \quad (7)$$

$$\frac{\partial}{\partial t}\left(\rho_w (1-\bar{s})\frac{\vec{\vartheta}_w^2}{2}\right) + div\left(\rho_s (1-\bar{s})\frac{\vec{\vartheta}_w^2}{2}\vartheta_w\right) - \rho_w (1-\bar{s})\vec{\vartheta}_w F - (1-\bar{s})\bar{\vartheta}_w Div \bar{P}_w + \frac{\bar{\vartheta}_w^2}{2} m_w + \rho_w \vartheta_w Div[(1-\bar{s})\vartheta'_w \vartheta'_w] = -\bar{\vartheta}_w \vec{R} \quad (7')$$

From a comparison of equations (6) and (7), bearing in mind [27] that

$$\bar{\vartheta} Div \bar{P} - \bar{\vartheta} Div \bar{P}\bar{\vartheta} = -(\bar{P}\nabla)\bar{\vartheta} = -\bar{P}Д$$

where Д is the strain rate tensor, we obtain the following expressions:

$$\bar{s}\bar{N}_{дис} - \bar{s}\bar{P}_s \bar{Д}_s - \frac{\bar{\vartheta}_s^2}{2} m_s - \bar{R}(\bar{\vartheta}_w - 2\bar{\vartheta}_s) = -\frac{\partial}{\partial t}\left[\rho_s \bar{s}\frac{\overline{\vartheta'_s}^{\,2}}{2}\right] - 3div\left[\rho_s \bar{s}\frac{\overline{\vartheta'_s}^{\,2}}{2}\bar{\vartheta}_s\right] + \bar{s} div \overline{\bar{P}'_s \vartheta'_s} + \bar{\vartheta}_s Div\left[\rho_s \bar{s}\overline{\vartheta'_s}\overline{\vartheta'_s}\right] + \bar{R}(\overline{\vartheta'_w} - \overline{\vartheta'_s})$$

$$(1-\bar{s})\bar{N}_{дис_w} - (1-\bar{s})\bar{P}_w \bar{Д}_w - \frac{\bar{\vartheta}_w^2}{2} m_w - \bar{R}\bar{\vartheta}_s = -\frac{\partial}{\partial t}\left[\rho_w (1-\bar{s})\frac{\overline{\vartheta'_w}^{\,2}}{2}\right] - 3div\left[\rho_s (1-\bar{s})\frac{\overline{\vartheta'_s}^{\,2}}{2}\bar{\vartheta}_s\right] + (1-\bar{s}) div \overline{\bar{P}'_s \vartheta'_s} + \overline{\vartheta_w} Div\left[\rho_s (1-\bar{s})\overline{\vartheta'_s}\overline{\vartheta'_s}\right] + \bar{R}(\overline{\vartheta'_w} - \overline{\vartheta'_s})$$

Summing up the obtained dependencies gives an expression for the energy dissipated in the suspension-carrying flow:

$$\bar{N}_{дис_w} = (1-\bar{s})\bar{P}_w \bar{Д}_w + \bar{s}\bar{P}_s \bar{Д}_s + \frac{\bar{\vartheta}_w^2}{2} m_w + \frac{\bar{\vartheta}_s^2}{2} m_s + \bar{R}(\bar{\vartheta}_w - \bar{\vartheta}_s) - -\frac{\partial}{\partial t}\left[\rho_w (1-\bar{s})\frac{\overline{\vartheta'_w}^{\,2}}{2} + \rho_s \bar{s}\frac{\overline{\vartheta'_s}^{\,2}}{2}\right] - 3div\left[\rho_s (1-\bar{s})\frac{\overline{\vartheta'_s}^{\,2}}{2}\overrightarrow{\vartheta_s} + \rho_s \bar{s}\frac{\overline{\vartheta'_s}^{\,2}}{2}\bar{\vartheta}_s\right] + (1-\bar{s}) div \overline{\bar{P}'_w \vartheta'_w} + \bar{s} div \overline{\bar{P}'_s \vartheta'_s} + \overline{\vartheta_w} Div[\rho_s (1-\bar{s})\overline{\vartheta'_w \vartheta'_w}] + \bar{\vartheta} Div[\rho_s \overline{\vartheta' \vartheta'_s}] \quad (8)$$

Let us introduce the following notations into equation (8).

$$I = \bar{N}_{дис_w} = (1-\bar{s})\bar{P}_w \bar{Д}_w + \bar{s}\bar{P}_s \bar{Д}_s,$$
$$II = \frac{\bar{\vartheta}_w^2}{2} m_w + \frac{\bar{\vartheta}_s^2}{2} m_s,$$
$$III = \bar{R}(\bar{\vartheta}_w - \bar{\vartheta}_s)$$
$$IV = -\frac{\partial}{\partial t}\left[\rho_w (1-\bar{s})\frac{\overline{\vartheta'_w}^{\,2}}{2} + \rho_s \bar{s}\frac{\overline{\vartheta'_s}^{\,2}}{2}\right] - 3div\left[\rho_s (1-\bar{s})\frac{\overline{\vartheta'_s}^{\,2}}{2}\bar{\vartheta}_s + \rho_s \bar{s}\frac{\overline{\vartheta'_s}^{\,2}}{2}\bar{\vartheta}_s\right] + (1-\bar{s}) div \overline{\bar{P}'_w \vartheta'_w} + \bar{s} div \overline{\bar{P}'_s \vartheta'_s} + \overline{\vartheta_w} Div[\rho_s (1-\bar{s})\overline{\vartheta'_w \vartheta'_w}] + \bar{\vartheta} Div[\rho_s \overline{\vartheta' \vartheta'_s}]$$

Thus, energy dissipation in a channel suspension-carrying flow occurs due to the work of internal forces (I), the addition of additional mass (II), the interaction of flow components (III), and turbulent energy conductivity (IV).

In flows of pure liquid ($\bar{s} = 0$) energy dissipation is determined by the expression

$$\bar{N}^{0}{}_{\text{дис}_w} = \bar{P}_w\bar{Д}_w + \frac{\bar{\vartheta}_w^2}{2}m_w - \frac{\partial}{\partial t}\left[\rho_w\frac{\bar{\vartheta}'^{2}_w}{2}\right] - 3div\left[\rho_w\frac{\bar{\vartheta}_s'^{2}}{2}\right] + div\overline{P_w'\vartheta_w'} + \overline{\vartheta_w}Div[\rho_s\overline{\vartheta_w'\vartheta_w'}] \quad (9)$$

It can be assumed that the difference in energy dissipation in the suspended-carrying flow and in the flow of pure liquid is nothing other than the energy $\bar{N}_{\text{взв}}$ expended on involving the suspension in movement and transport ("weighing work"). However, bearing in mind that the intensity of turbulent pulsations in the flow of pure liquid and the liquid transporting the suspension are different from each other at the same values of the averaged characteristics of the flow, we introduce into consideration the parameter,

$$A = \int_0^{\bar{s}} -\frac{\partial}{\partial\bar{s}}\left[-\frac{\partial}{\partial t}\rho_w\frac{\bar{\vartheta}'^{2}_w}{2}\right] - 3div\left[\rho_ц\frac{\vartheta'^{2}_w}{2}\overrightarrow{\vartheta_w}\right] + div\overline{P_w'\vartheta_w'} + \overline{\vartheta_w}Div[\rho_s\overline{\vartheta_w'\vartheta_w'}]d\bar{s}$$

taking into account the change in the intensity of turbulent pulsations in the liquid flow in the presence of suspended particles. Thus,

$$\bar{N}_{\text{взв}_w} = R(\bar{\vartheta}_w - \bar{\vartheta}_s) - \bar{s}\bar{P}_w\bar{Д}_w + \bar{s}\bar{P}_s\bar{Д}_s + \frac{\bar{\vartheta}_s^2}{2}m + \frac{\partial}{\partial t}\left[\rho_w\bar{s}\frac{\bar{\vartheta}'^{2}_w}{2} - \rho_s\bar{s}\frac{\bar{\vartheta}'^{2}_s}{2}\right] + 3div\left[\bar{s}\rho_w\frac{\bar{\vartheta}_s'^{2}}{2}\bar{\vartheta}_s + \rho_s\bar{s}\frac{\bar{\vartheta}_s'^{2}}{2}\bar{\vartheta}_s\right] - \bar{s}div\left(\overline{P_w'\vartheta_w'} - \overline{P_s'\vartheta_s'}\right) - \overline{\vartheta_w}Div[\rho_w\overline{\vartheta_w'\vartheta_w'}] + \bar{\vartheta}Div\left[\rho_s\bar{s}\overline{\vartheta_s'\vartheta_s'}\right] + A$$

Assuming further that $P_w \approx P_s \cong pE$, where p is the hydrodynamic pressure, E is the unit tensor, we have $P\bar{Д} = -pdiv\vartheta$, from which we obtain the following expression for the weighing work:

$$\bar{N}_{\text{взв}_w} = R(\bar{\vartheta}_w - \bar{\vartheta}_s) + \bar{s}\bar{p}div(\bar{\vartheta}_w - \bar{\vartheta}_s) + \frac{\bar{\vartheta}_s^2}{2}m_s + \frac{\partial}{\partial t}\left[\rho_w\bar{s}\frac{\bar{\vartheta}'^{2}_w}{2} - \rho_s\bar{s}\frac{\bar{\vartheta}'^{2}_s}{2}\right] + 3div\left[\bar{s}\rho_w\frac{\bar{\vartheta}_s'^{2}}{2}\bar{\vartheta}_s - \rho_s\bar{s}\frac{\bar{\vartheta}_s'^{2}}{2}\bar{\vartheta}_s\right] - \bar{s}divp'\left(\overline{\vartheta_w'} - \overline{\vartheta_s'}\right) - \overline{\vartheta_w}Div[\rho_w\overline{\vartheta_w'\vartheta_w'}] + \bar{\vartheta}_sDiv\left[\rho_s\bar{s}\overline{\vartheta_s'\vartheta_s'}\right] + A \quad (10)$$

The obtained expression for the weighing work can be represented as the sum of the weighing works of the averaged and pulsating motion:

$$\bar{N}_{\text{взв}}^{\text{оср}} = R(\bar{\vartheta}_w - \bar{\vartheta}_s)\bar{s}\bar{p}div(\bar{\vartheta}_w - \bar{\vartheta}_s) + \frac{\bar{\vartheta}_s^2}{2}m_s,$$

$$N_{\text{взв}}^{\text{пульс}} = \frac{\partial}{\partial t}\left[\rho_w\bar{s}\frac{\overline{\vartheta_w'}^{2}}{2} - \rho_s\bar{s}\frac{\bar{\vartheta}_s'^{2}}{2}\right] + 3div\left[\bar{s}\rho_w\frac{\bar{\vartheta}_s'^{2}}{2} - \rho_s\bar{s}\frac{\bar{\vartheta}_s'^{2}}{2}\bar{\vartheta}_s\right] + \bar{s}divp'(\bar{\vartheta}_w' - \bar{\vartheta}_s') - \bar{\vartheta}_wDiv[\rho_w\overline{\vartheta_w'\vartheta_w'}] + \bar{\vartheta}_sDiv\left[\rho_s\bar{s}\overline{\vartheta_s'\vartheta_s'}\right] + A \quad (11)$$

Under conditions of a steady longitudinally uniform plane suspension-carrying flow and under the assumption that the vertical component of the relative velocity $(\vartheta_w - \vartheta_s)$ of the hydraulic size w of the sediments is equal and that the horizontal component $(\vartheta_w - \vartheta_s)$ is equal to zero, i.e., under the conditions considered by M.A. Velikanov [25] when substantiating the gravitational theory, expression (10) for the weighing work is significantly simplified:

$$\bar{N}_{\text{взв}_w} = \bar{s}g(\rho_s - \rho_w)w + 3\rho_s w\frac{\partial}{\partial y}\left[\bar{s}\frac{\bar{\vartheta}'^{2}_w}{2}\right] - -3(\rho_s - \rho_w)\frac{\partial}{\partial y}\left[\bar{s}\frac{\bar{\vartheta}'^{2}_w}{2}\bar{\vartheta}_w\right] - \rho_s w\frac{\partial}{\partial y}\left[\bar{s}\overline{\vartheta_s'}\overline{\vartheta_s'}\right] + A$$

and in contrast to the formula $\bar{N}_{\text{взв}_w} = \bar{s}g(\rho_s - \rho_w)w$ used by M.A. Velikanov, takes into account the dissipation of pulsating energy.

3. Results and discussion

The analysis developed in the preceding section yields a description of how mechanical energy is stored, exchanged, and dissipated in a channel flow that transports suspended sediment. Instead of a single friction law, it produces a coupled set of energy-balance equations for the solid and liquid phases — equations (5)–(7) for the instantaneous and averaged motion and equations (8)–(11) for the dissipated and weighing work — from which the mechanisms responsible for suspension can be read directly.

Mechanisms of energy dissipation. Equation (8), together with the grouping introduced through the terms I–IV, shows that dissipation in a suspension-carrying flow is not controlled by viscous friction alone. Four physically distinct contributions appear. Term I is the work of the internal pressure and viscous stresses in each phase, weighted by its volumetric share; this is the only mechanism retained in the classical single-phase description. Term II, proportional to the added masses m_w and m_s, is the energy tied to the exchange of mass between the phases through the system of sources and sinks, and it vanishes whenever the mass of the components is treated as constant. Term III, the product of the interphase force R and the relative velocity of the phases, is the work done in the relative slip between water and particles — the drag-type coupling stressed in two-fluid models of sediment transport. Term IV collects the turbulent, or pulsation, transport of energy together with its rate of change. The presence of terms II and III alongside the familiar I and IV is the central structural result: in a real sediment-laden channel, energy is lost not only to viscous friction and turbulence, but also to sustaining mass exchange and to the relative motion between the phases.

Consistency in the clear-water limit. When the concentration vanishes, equation (8) reduces to equation (9), the dissipation of a turbulent flow of pure liquid. This limit is both an internal check on the derivation and a means of isolating the extra energy demanded by the particles: the difference between the dissipation in the sediment-laden flow and that in clear water is interpreted as the energy spent in holding the sediment in suspension and moving it downstream — the weighing work.

Energetics of suspension. Because the intensity of the turbulent pulsations in clear water is not the same as in the identical flow carrying particles, this difference cannot be formed by simple subtraction. The correction is carried by the parameter A, which integrates the change in pulsation energy with concentration. With this correction the weighing work is given by equation (10) and, once an isotropic stress state is assumed, it separates into an averaged-motion part and a pulsating part, equation (11). This separation carries the main physical message of the work: suspension is maintained partly by the mean relative motion and the

https://doi.org/10.56143/3030-3893-2026-3-71-77

ENGINEER

interphase force, and partly by the turbulent pulsations themselves. The finding places the role of turbulence, identified as the controlling factor in earlier studies of sediment suspension (Huang et al. 2019; Jha and Bombardelli 2011), inside an explicit energy budget rather than a diffusion analogy.

Relation to the gravitational theory. Under the conditions of Velikanov's gravitational theory — steady, longitudinally uniform plane flow in which the vertical relative velocity equals the hydraulic size w of the particles and the horizontal relative velocity is zero — the general expression (10) collapses to the reduced form obtained at the close of the derivation. Its leading term is the product of the concentration, the submerged specific weight g(ρ_s − ρ_w), and the hydraulic size w, which is exactly the weighing work of the gravitational theory; that classical result therefore appears here as a special case. The remaining terms, built from gradients of the pulsation energy, are the corrections the present formulation adds, and they represent the dissipation of pulsating energy that the gravitational theory leaves out. This offers a resolution to the long-standing objection that a purely gravitational accounting misstates the energy required for suspension, by locating the missing part in the turbulent pulsation field.

Comparison with earlier energy formulations. The energy-balance equations obtained here depart from those of Barenblatt and of Frankl in three ways that follow directly from the model assumptions. The variability of the mass of the flow components is retained through the source–sink system (term II); the change in the intensity of the liquid's turbulent pulsations caused by the transported particles is included through the parameter A; and the work of the interphase interaction forces is represented more completely, in both the averaged and the pulsating motion (term III). Each of these generalises the earlier steady, constant-mass descriptions toward the unsteady, non-uniform conditions that characterise natural channels.

Limitations and outlook. Adding the energy equations to the system does not close it; as noted in the derivation, each new balance introduces further unknown correlations. The value of the formulation is therefore diagnostic rather than immediately predictive: it identifies the quantities that must be measured or modelled — the interphase force R, the added-mass terms, and the particle-modified pulsation field — before the energy budget can be evaluated for a given flow. This is where the physical model of the channel suspension-carrying flow is intended to contribute, by supplying the depth distribution of concentration and the pulsation data needed to calibrate these terms and to compare the magnitudes of the averaged and pulsating weighing work under controlled conditions.

4. Conclusion

This research contributes to the broader understanding of sediment transport. It highlights the role of energy dissipation and interfacial interactions. These diffusion-based factors are often underestimated in traditional models. The energy balance equations for the suspended matter-carrying flow obtained in this work differ from similar equations compiled earlier by G. I. Barenblatt [24, 28, 29] and F. I. Frankl [30, 31] by taking into account the variability of the mass of the flow components, by taking into account the change in the intensity of turbulent pulsations of the liquid when it transports suspended matter, and by more fully taking into account the work of the forces of interphase interaction.

Overall, the improved modeling framework established here offers a robust approach to studying sediment-laden flows, providing new insights that can inform both theoretical studies and practical decisions in fluid mechanics and environmental hydraulics.

References

[1] Smaoui H, Boughanim F, Chapalain G (2007) 1D vertical model for suspended sediment transport in turbulent tidal flow: Application to the English Channel. Comput Geosci 33:1111–1129. https://doi.org/10.1016/j.cageo.2006.11.016

[2] Huang H, Zhang H, Zhong D, Zhang YJ (2019) Turbulent mechanisms in open channel sediment-laden flows. International Journal of Sediment Research 34:550–563. https://doi.org/10.1016/j.ijsrc.2019.06.002

[3] Jha SK, Bombardelli FA (2011) Theoretical/numerical model for the transport of non-uniform suspended sediment in open channels. Adv Water Resour 34:577–591. https://doi.org/10.1016/j.advwatres.2011.02.001

[4] Zhong D, Wang G, Sun Q (2011) Transport Equation for Suspended Sediment Based on Two-Fluid Model of Solid/Liquid Two-Phase Flows. Journal of Hydraulic Engineering 137:530–542. https://doi.org/10.1061/(asce)hy.1943-7900.0000331

[5] Toorman EA Vertical Mixing in the Fully Developed Turbulent Layer of Sediment-Laden Open-Channel Flow. https://doi.org/10.1061/ASCE0733-94292008134:91225

[6] Necker F, Kleiser L, Meiburg E High-resolution simulations of particle-driven gravity currents

[7] Ahmed SF (2013) Derivation of Turbulent Energy in Presence of Dust Particles. American Journal of Applied Mathematics 1:71. https://doi.org/10.11648/j.ajam.20130104.15

[8] Ahmed SF, Hafez MG, Chu YM (2020) Conversion of energy equation for fiber suspensions in dusty fluid turbulent flow. Results Phys 19:. https://doi.org/10.1016/j.rinp.2020.103341

[9] Picardo JR, Agasthya L, Govindarajan R, Ray SS (2019) Flow structures govern particle collisions in turbulence. Phys Rev Fluids 4:. https://doi.org/10.1103/PhysRevFluids.4.032601

[10] Zaichik LI, Alipchenkov VM, Avetissian AR (2009) Transport and deposition of colliding particles in turbulent channel flows. Int J Heat Fluid Flow 30:443–451. https://doi.org/10.1016/j.ijheatfluidflow.2009.02.013

[11] Bernstein O, Shapiro M (1994) DIRECT DETERMINATION OF THE ORIENTATION DISTRIBUTION FUNCTION OF CYLINDRICAL PARTICLES IMMERSED IN LAMINAR AND TURBULENT SHEAR FLOWS

[12] Yin X, Sundaresan S (2009) Fluid-particle drag in low-reynolds-number polydisperse gas-solid suspensions. AIChE Journal 55:1352–1368. https://doi.org/10.1002/aic.11800

[13] Chou YJ, Gu SH, Shao YC (2015) An Euler-Lagrange model for simulating fine particle suspension in.

Information about the author

Otabek Mukhitdinov Kimyo international university in Tashkent
E-mail: o.mukhitdinov@kiut.uz
https://orcid.org/0000-0002-7347-0025

Savet Khudaykulov Kimyo international university in Tashkent
E-mail: s.khudaykulov@kiut.uz

Djamshid Kaniev Kimyo international university in Tashkent
E-mail: j.kaniev@kiut.uz

Journal Engineer ISSN: 3030-3893 Volume:4| Issue:3| 2026

Received: 6 July 2026 | **Accepted:** 17 August 2026 | **Published:** 30 September 2026

Network diagnosis and governance-coupled optimization in seaport–dry port multimodal transport corridors under the Maritime Silk Road

Mu Zhendi[1,2][a]

[1]"Silk Road" International University of Tourism and Cultural Heritage, Samarkand, Uzbekistan

[2]Zhejiang Seaport Group, Ningbo, China

Abstract: Research into seaport–dry port corridors has tended to focus on the design of the physical network on the one hand and the coordination of governance on the other. It is hard to maintain this separation in well-established Maritime Silk Road corridors. A corridor might have routes, inland nodes and digital platforms, and still not function smoothly at the rail/dry-port interface. This article therefore tackles corridor optimization as a problem of diagnosis and governance. It looks at the case of Ningbo-Zhoushan Port in a gateway province on China's eastern coast, and examines its relevance for Central Asian and landlocked economies relying on seaports, inland hubs, railways, customs facilities and digital platforms. The empirical basis comprises aggregated port planning and port transport-operation data from both the annual and quarterly perspectives as well as publicly available policy and industry material for contextual interpretation. The overarching question is pragmatic, and that is: If the side of the seaport is relatively on schedule, but the coordination on the inland rail side is not, where should optimization be targeted? The analysis links node-structure diagnosis, quarterly interface diagnosis and governance interpretation. To make the imbalance observable, the paper uses a Corridor Coupling Imbalance Gap (CIG), calculated as the difference between the mean completion rate of maritime-side indicators and the rail-freight completion rate at each quarter end. The evidence shows a stable three-part planned node structure for 2025–2026, but the 2025 rolling data also show that rail freight lagged maritime-side indicators for three consecutive quarters, with CIG reaching +10.20 percentage points in Q3. The main issue is thus not general seaport capacity. It lies in the translation from gateway capacity to inland consolidation, digital orchestration, and timely cross-actor intervention. The article proposes a governance-coupled optimization agenda organized around differentiated gateway roles, dry-port-centered consolidation, event-level digital coordination, and rolling warnings. Its contribution is to turn corridor optimization from a question of route expansion into a more precise diagnostic method for seaport–dry port governance.

Keywords: Maritime Silk Road, Seaport–Dry Port Transport Corridor, Multimodal Transport, Network Diagnosis, Governance-Coupled Optimization, Corridor Coupling Imbalance Gap, China–Central Asia Connectivity, Ningbo-Zhoushan Port

1. Introduction

Under the Maritime Silk Road, the competitiveness of a seaport is no longer determined only at the quay. Vessel calls and berth capacity still matter, but they do not by themselves explain whether port functions can be carried inland in a stable and governable way. The more difficult question is whether inland nodes, rail services, customs procedures, and digital coordination are managed as parts of the same transport system. The importance of this is particularly notable for landlocked and double-landlocked economies which rely on the performance of foreign seaports and the reliability of the corridors behind them for access to maritime trade. This trend is seen in the development of dry ports, sea–rail connections, customs extensions, and digital booking platforms. The basic point of the dry-port and port-regionalization literature is already made, that the port becomes a corridor system and has multiple frontiers, operational ones, rather than only one, the waterfront [1–3].

The challenge is that it is easier to plan for expansion where this is visible in the corridors than operational coordination. Routes can be counted and dry-port nodes can be announced, platforms can be connected and new services can be reported. These are significant accomplishments, but are not necessarily indicative of the alignment of cargo consolidation, train formation, customs clearance, yard readiness, and slot allocation in day-to-day operations. A corridor might therefore be operationally uneven, but still be very large in space. This is the key to Maritime Silk Road corridors, as the transport performance relies on interorganisational interaction between seaports, inland logistics nodes, customs regimes, railways, platform providers and cargo owners [4, 5].

The Zhejiang-Ningbo-Zhoushan case is a practical example to analyse this tension. Zhejiang is a coastal gateway province in eastern China, connecting maritime shipping, port-based industrial bases, inland dry ports, rail transportation and digital logistics platforms. The importance of the case to the international transport community is not to demonstrate the case as an example to emulate. Instead, it indicates the possibility of coordination pressure at inland rail/dry-port interfaces in even a fairly developed coastal gateway system. The available public Zhejiang transport policy, planning and industry materials for contextual interpretation indicate that by September 2024, the Ningbo-Zhoushan Port had developed 107 sea–rail routes, of which 26 were scheduled trains, and 37 inland dry-port nodes,

[a] https://orcid.org/0000-0002-5696-391X

covering 16 provincial-level areas and 67 prefecture-level cities. The Four-Port digital platform had connected more than 100 systems and aggregated more than 11,000 logistics data items, the Sixth Port Area platform had integrated the port–customs–shipping processes and the port had reported benefits from the increased efficiency of sea–rail operations. These are large numbers that reflect significant corridor development. Meanwhile, the same contextual materials indicate pressure on the rail side in the Jinhua–Yiwu support area, high station utilization, and a relatively small but relevant cost disadvantage in some subsidized rail services compared with direct road transport [6].

This juxtaposition provides the introduction for the article. It is not a question of whether or not a mature corridor requires optimization – in some general sense. When the maritime side is broadly stable, and the inland rail interface is not, a more important question is where should attention be directed for intervention? This is also a question which is not only relevant for the Zhejiang case. Inland terminals and dry ports need more than facilities to establish a reliable international logistics network for the transport systems of the Maritime Silk Road, including the China–Central Asia transport system. Previous studies provide some components that can be built upon. Some research focuses on terminal networks, location decision, break even distance and design of dry ports [7–10]. A second one relates to collaborative governance, institutional alignment and digital coordination [4, 5, 11]. Less developed is an approach that allows managers to find a place in the interface where the spatially mature corridor is not syncing.

The article thus develops a diagnostic, governance-coupled view of a port-centred seaport–dry port system. Zhejiang-Ningbo-Zhoushan is not necessarily representative of other Chinese corridors, or other Maritime Silk Road corridors. This synthesis incorporates evidence on node structure from annual plans, execution data from quarterly rolling indicators, and contextual policy evidence regarding the reach of nodes inland, capacity pressure, digital platforms, and monitoring architecture. The idea isn't to make a full math model of transport network. It is to offer a management oriented approach to identify the choke point, explain the role of different nodes and how network redesign and governance intervention should be connected.

2. Literature Review

The initial part of the argument is based on studies of dry-port and inland-port. Such studies demonstrate the inland terminals can move some seaport functions away from the maritime area, alleviate the pressure around the seaport and provide access to the hinterland [2, 12–14]. But the expansion isn't something that you can achieve with just positioning a terminal on a map. A dry port depends on rail infrastructure, terminal facilities, institutional structures and the development of transport routes [15, 3, 16]. A key take-away from inland-port research is that inland ports have the potential to reshape regional logistics, but if the governance and service integration are weak, inland ports can end up as passive extensions of seaports [17].

Another set of research is related to intermodal transport network design and terminal optimisation. This literature is helpful because it discusses the impact on competitiveness of intermodal freight transport [18, 7, 8, 19] as the result of terminal location, capacity, modal balance, and break-even distance. More recent studies also speak about how seaport–dry port networks can be designed to be robust, sustainable and resilient in the face of uncertainty [9, 10]. But this research frequently assumes that once the network structure is designed, coordination will follow. This is not always true in reality during the operation of a corridor. As much as the physical network can be well-designed, performance can still be poor if the gateway, rail station, customs process and the digital platform are not managed as a single operating chain.

The collaborative governance research provides insight into the sources of this problem. In order to be effective, inter-organisational action must involve meaningful participation, shared motivations and collective capacities [4, 5]. Multimodal transport corridors are a good fit for this problem area, as there are many actors: the port authorities, the rail operators, customs authorities, logistics operators, inland terminals, platform operators, and cargo owners. While such actors are not involved in a single hierarchy, they do need to act in a coordinated manner in the same direction of the flow of cargo. Thus, the issue of governance is a practical one. It has to do with who is responsible for which role and when information is provided and when it is needed in order to avoid a small delay at one interface turning into a larger blockage [20, 21].

Digitalisation adds another layer to this situation. Heilig and Voß [11] state that the transaction costs can be lowered, as well as gaining service visibility, by means of port information systems, platform-based coordination and digitally-integrated gate operations. But, connectivity of data does not imply connectivity of operations. While yard operations, train assembly, customs sequencing, and slot allocation remain only partly aligned, digital platforms may only accelerate the exchange of documents instead of boosting the performance of the corridor. Digital tools must thus be integrated into a governance mechanism, which translates data into action [22, 23].

This results in a very practical gap in the literature. While a lot has been written about dry ports, intermodal networks, and collaborative governance – it is not clear how network redesign and governance redesign should link up. This article endeavors to fill this void by recognizing the corridor as a multi layer functioning system. It holds that corridor diagnosis should be initiated with the distinction between the structure, the tests of operational interfaces and finally the linkage of governance responses to the imbalances found.

3. Research methodology

The material for this study is of an empirical type in two senses. The first group are the publicly available materials of transport policies, transport planning and transport industry in Zhejiang Province, China, including the transport policy of Zhejiang Province on multimodal freight development, the transport plan on integrated freight-hub construction, the application of intelligent multimodal transport and the monitoring of logistics-hubs. These materials are used to set the policy tone, institutional context, digital foundation, and inland-hub context of a coastal gateway province. They are not considered as a quantitative stand-alone dataset. The second category of information is the annual and quarterly port planning and transport-operation information, particularly the execution indicators of port operations for 2025 as a rolling information, and the annual company plans for 2025–2026 for Ningbo-Zhoushan Port. The numbers for 2026 are considered to be planned numbers, not actual numbers. The values relating to the company are only reported in an aggregated manner. The analysis does not reveal any operational data at the firm level,

origin-destination matrices at the shipper level, terminal level slot records, or micro level cost traces.

The analysis is carried out in the context of four interrelated operations. The first is to decompose the company cargo plan into three parts, which are the cargo plan of the Ningbo base, the cargo plan of the Zhoushan base and the cargo plan of the external terminals, and compare the cargo plan proportions in 2025 and 2026 and then analyze the cargo specialization of each node group. The second is a so-called rolling interface diagnosis. It is based on five performance indicators for 2025: total throughput of cargo, container throughput, rail freight, tally volume and pilotage voyages. Progress is measured against a quarterly linear mark of 25%, 50%, 75% and 100% of the annual plan. The third operation determines the Corridor Coupling Imbalance Gap (CIG) and thus renders the operational aspect of coupling transparent. The fourth explains the pattern observed in terms of route reach, inland-node capacity, digital integration, cost conditions and the architecture for monitoring.

The design has been purposefully kept simple. It does not try to build a complete O-D transport network or to solve a large-scale model for optimization with shipper level microdata. That decision is not merely data-driven; it is methodological. The problem addressed by the article is not with the building of the formal optimization model itself, but before it is ever created: If one interface is underperforming and the rest of the corridor is on track, what optimization is needed? There are several layers to the answer to that question, it's not just a chart of flows, there is structure, execution and governance. This reasoning applies elsewhere, outside Zhejiang. For instance, a reader with an interest in dry-port development in Central Asia may wonder if a corridor weakness is a lack of gateway capacity, a lack of consolidation in the interior, or a lack of reliability of rail services, customs delays, or a lack of digital to physical orchestration. All values plotted in the figures were checked against the annual node-plan percentages and the 2025 rolling completion table. Schedule gaps were calculated as cumulative completion percentage minus the 25%, 50%, 75%, and 100% quarter-end linear benchmarks.

For the CIG indicator, Mq denotes the mean completion rate of the maritime-side indicators in quarter q: cargo throughput, container throughput, tally volume, and pilotage voyages. Rq denotes the rail-freight completion rate in the same quarter. The indicator is calculated as CIGq = Mq - Rq. A positive value means that maritime-side execution is ahead of rail-interface execution, indicating an imbalance between gateway-side robustness and rail–dry-port coordination. The indicator is not presented as a full coupling-coordination model or as a causal coefficient. It is used as a diagnostic proxy, intended to make an otherwise abstract coupling problem visible, comparable, and reproducible. Table 1 summarizes the evidence blocks that support the diagnosis.

Table 1

Data architecture, provenance, and analytical use

Evidence block	Main variables / values used	Source status and reproducibility note	Use in the paper
Public policy, planning, and industry materials from Zhejiang Province, China	Contextual values on corridor reach and digital foundations: 107 sea–rail routes; 26 scheduled trains; 37 inland dry-port nodes; 16 provincial-level areas; 67 prefecture-level cities; more than 100 linked digital systems; more than 11,000 logistics data items	Publicly available contextual materials; used to describe the coastal gateway-province setting and policy/digital environment, not as a direct quantitative dataset.	Contextualizes corridor scale, spatial maturity, institutional-digital setting, and why the case has relevance beyond Zhejiang.
Annual company plans (2025–2026)	Node-group planned shares; cargo specialization by Ningbo base, Zhoushan base, and external terminals	Aggregated company planning data; 2026 values are planned, not realized.	Supports node-structure diagnosis and gateway differentiation
Quarterly rolling plan data (2025)	Cargo throughput; container throughput; rail freight; tally volume; pilotage voyages	Aggregated quarterly completion data; gaps calculated against a 25/50/75/100 benchmark.	Supports rolling interface diagnosis and CIG calculation
Inland hub and port–rail interface evidence	Jinhua–Yiwu station pressure; approximately 650,000 TEU regional railway container-handling capability; about RMB 20 cost difference per 40-foot container; 17.49 million tonnes of port-station rail volume	Public planning and industry evidence; used as explanatory context, not causal estimates.	Supports the interpretation of likely rail-interface pressure
Monitoring and digital-operation evidence	More than 100 linked systems; more than 11,000 logistics data items; 16 automatically collectable monitoring indicators	Public digital-platform and monitoring materials; used to distinguish data connectivity from event-level operational orchestration.	Supports a transparent case-study design while limiting unsupported generalization beyond the

https://doi.org/10.56143/3030-3893-2026-3-78-86

Evidence block	Main variables / values used	Source status and reproducibility note	Use in the paper
			reported aggregated values.

Source: compiled by the author from publicly available transport policy, planning, and industry materials from Zhejiang Province, China, and aggregated Ningbo-Zhoushan Port planning and transport-operation datasets. Public materials are used as contextual evidence for a coastal gateway-province case; the quantitative indicators are calculated from aggregated planning and operational values reported in the tables and figures. Values are used for diagnostic interpretation, not for firm-level performance disclosure or causal estimation.

4. Results and discussion

Stable node structure and differentiated gateway roles

The two annual company plans refer to a stable overall structure. They split the system into three node groups. For those outside China, these groups can be explained based on their functions: the Ningbo base has the gateway and control role in the port system, the Zhoushan base is more geared towards bulk business, and the external terminals represent affiliated or inland-facing capacity linked to the larger corridor. In the 2025 plan, the shares of cargo throughput for the company's bases are 47.1% for the Ningbo base, 21.4% for the Zhoushan base and 31.5% for external terminals. In the 2026 plan, the corresponding shares were 47.3%, 21.8%, and 30.9%. The key is that there wasn't a significant macro-level rebalancing. This brings focus away from the instability of structure, and to the performance of interfaces within a relatively stable planned structure.

This discovery is important because it has to do with the commodity structure. Ningbo is fairly diversified with metal ores being the biggest identified flow, but the node is not dependent on one single cargo flow. Zhoushan has a more metal-ore and oil orientation to align with its bulk and liquid cargo operations. The external terminal group is more inland and affiliated, and it also has a higher proportion of coal and mineral materials and plays a secondary role for steel products. These differences are not to be viewed as "background information". They suggest that the analysis of corridor optimization should not start from the premise that all of the port or affiliated nodes have the same multimodal function. A corridor may include one strategic label, and have multiple functional subsystems. The same applies to the international dry-port systems, with inland nodes being able to share a corridor identity but not necessarily have the same operational role.

It is important for governance and for transport planning. If the roles of nodes are different, the governance must also be different. The main gateway role of Ningbo won't be automatically transferred to the bulk base or the affiliated inland-facing system. In thinking about nodes, it is easy to forget that there is an operational pressure somewhere. Figure 1 therefore uses the two annual plans to show both the stability of the three-part node-group structure and the limited role drift between 2025 and 2026.

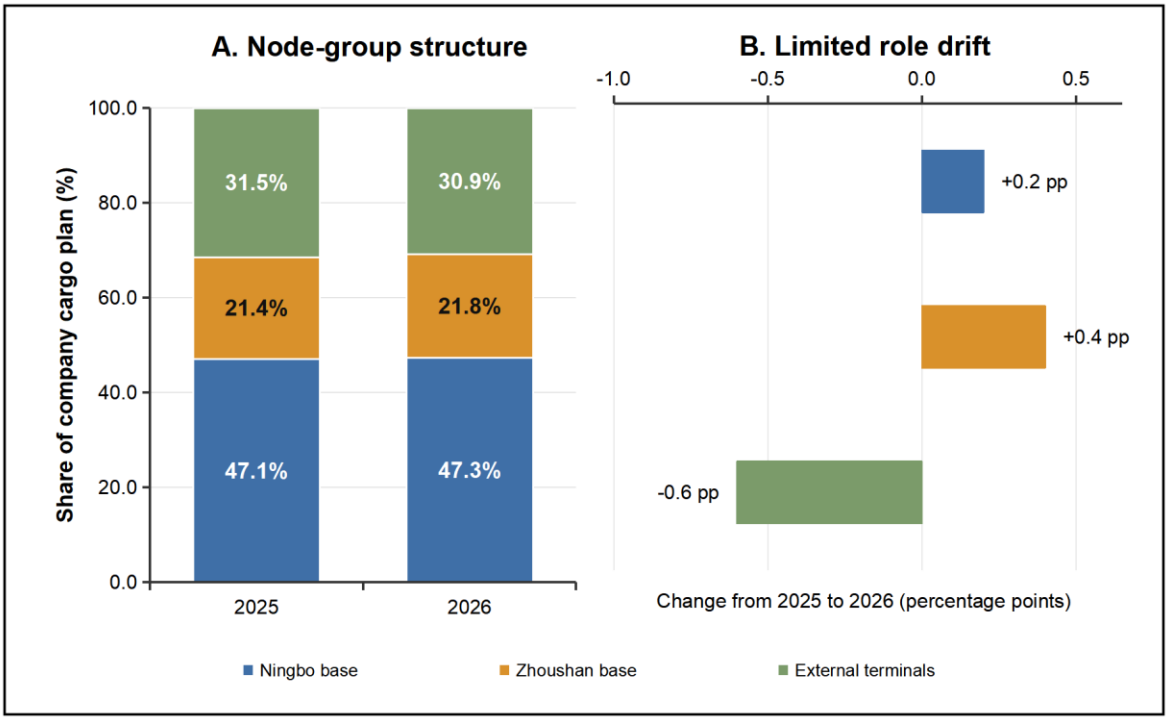


Fig. 1. Stable node-group structure and limited role drift between the 2025 and 2026 company plans.

https://doi.org/10.56143/3030-3893-2026-3-78-86

Note. Left panel values show planned node-group shares of company cargo throughput. Right panel values show 2026 planned share minus 2025 planned share in percentage points. Ningbo and Zhoushan refer to two main sub-gateway groups within the Ningbo-Zhoushan port system.

The two panels in Figure 1 make the same point from different angles. The left panel shows that the company-level node structure remained broadly stable across the two annual plans. The right panel shows only small year-on-year changes for each node group. This supports a more focused interpretation: the main optimization issue is not a shifting macro-structure, but the way a stable structure performs at specific interfaces. Figure 2 then disaggregates the 2026 company plan by cargo specialization and node-group throughput scale to examine whether the stable structure also contains differentiated cargo roles.

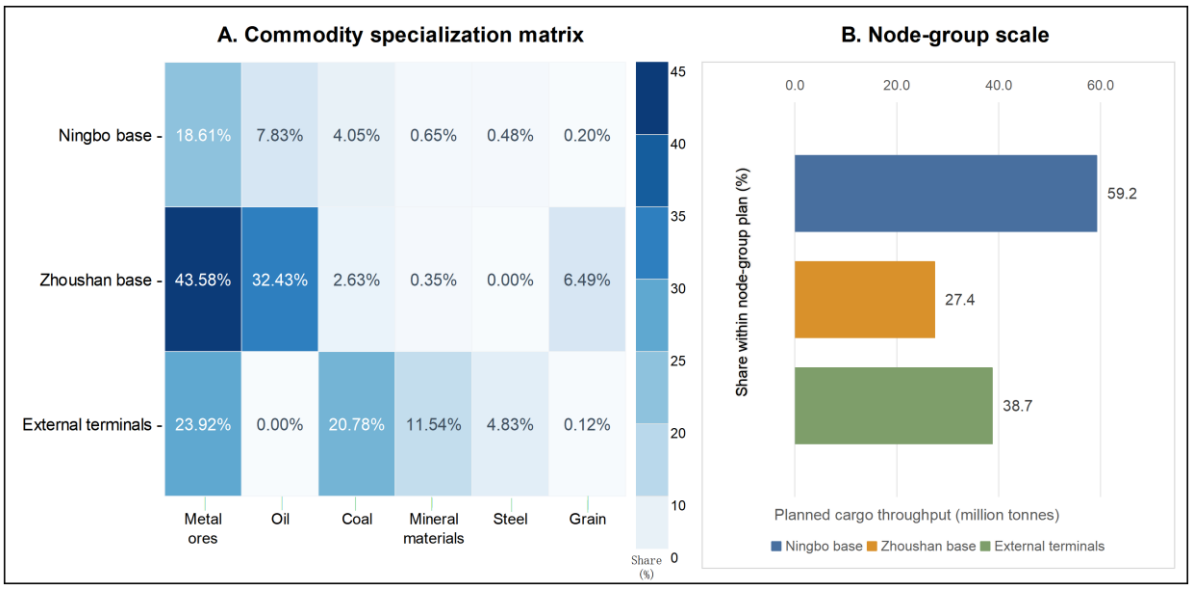


Fig. 2. Gateway specialization matrix and throughput scale in the 2026 company plan

Note. Matrix values represent cargo-category shares within each node-group plan. The throughput scale is in million tonnes, and is an indicator of planned cargo throughput. Ningbo base and Zhoushan base as well as external terminals are not interchangeable locations and are treated as functional gateway groups.

Figure 2 agrees that the three node groups are not suitable for being compressed to a generic port function. Ningbo is the principal control gateway, Zhoushan is bulk-oriented and the external terminal system is more inland-facing. The governance implication is simple: It would not make sense to have the same optimization rule applied to all nodes. The general takeaway for an international reader is that any plan for the corridors should first identify gateway control nodes, bulk-specialized nodes, and inland-facing consolidation nodes, and then propose corridor optimization measures.

Rolling interface diagnosis: maritime robustness, rail-interface lag

The quarterly production-planning data for 2025 shows a more detailed operational picture than the annual-planning information alone. There was a relatively strong trend in cargo throughput, container throughput, tally volume and pilotage voyages. In Q2, cargo throughput was 51.0% of annual plan and tally volume was 51.9%, which are close to or above the 50% linear rate. In Q4, all 4 maritime-side indicators were over 100% of annual plans. This is not a typical weak corridor. It shows that the seaport-side operating system was able to sustain the annual plan.

This was not the case with rail freight. It reached 21.1% in Q1, 41.6% in Q2, and 68.4% in Q3, producing schedule gaps of -3.9, -8.4, and -6.6 percentage points against the quarter-end benchmark. It did not reach parity until Q4, in which it was 100.2% of the annual plan. The main empirical result of the article is that the bottleneck was not distributed throughout the entire corridor. It was concentrated at the rail–dry-port interface and recovery occurred later in the year.

Governance-wise the asymmetry is more indicative than the year-end number. When indicators on the maritime side are on track and the rail freight side was underperforming for most of the year, then it is not likely that it is only a matter of capacity on the quays or weak demand. It is more consistent with constraints in inland consolidation, train scheduling, station utilization, slot coordination, and the binding of documents to actual operations. The corridor is connected, but it is not yet fully orchestrated at the rail–dry-port interface. Table 2 reports the quarterly values behind this reading, and Table 3 converts the same differences into the CIG indicator.

Table 2

Rolling completion of five core indicators in 2025 (% of annual plan)

Quarter	Cargo throughput	Container throughput	Rail freight	Tally volume	Pilotage voyages
Q1	25.1	23.6	21.1	25.1	25.6

Q2	51.0	49.2	41.6	51.9	53.7
Q3	77.0	75.9	68.4	80.0	81.5
Q4	102.3	102.6	100.2	105.6	108.7

Source: author's calculations from the compiled 2025 rolling transport-operation planning dataset. The linear benchmark is 25%, 50%, 75%, and 100% of the annual plan at the end of Q1, Q2, Q3, and Q4, respectively.

Table 3

Corridor Coupling Imbalance Gap between maritime-side execution and rail-freight execution in 2025

Quarter	Maritime-side mean completion (%)	Rail freight completion (%)	CIG (percentage points)
Q1	24.85	21.10	+3.75
Q2	51.45	41.60	+9.85
Q3	78.60	68.40	+10.20
Q4	104.80	100.20	+4.60

Source: author's calculations. Maritime-side mean completion is the arithmetic mean of cargo throughput, container throughput, tally volume, and pilotage voyages. CIG = maritime-side mean completion minus rail-freight completion.

The quarterly completion rates and CIG values show why the year-end recovery should not be over-read. Annual completion masks a coordination lag that lasted for three quarters. Figure 3 therefore pairs the rolling completion trajectories with the schedule-gap matrix, so that both the timing and the location of the rail-interface lag can be seen more clearly.

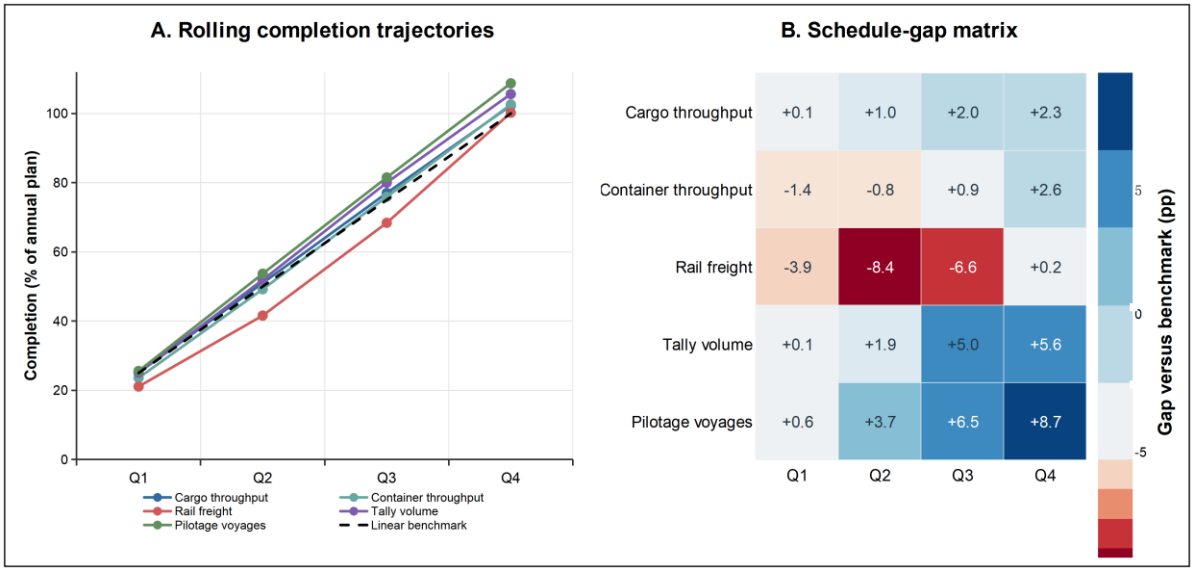


Fig. 3. Rolling completion trajectories and schedule-gap dynamics for the five core indicators in 2025

Note. The linear benchmark refers to quarter-end cumulative progress of 25%, 50%, 75%, and 100% of the annual plan. Schedule gap equals actual cumulative completion minus the corresponding benchmark; the related CIG values are reported in Table 3.

The left panel of Figure 3 indicates that the maritime-side indicators stayed near or above the expected quarterly pace. The right panel shows that rail freight was the only indicator with a materially negative gap over a three-quarter period, although it recovered by year-end. The CIG values express the same imbalance more directly: maritime-side execution exceeded rail-freight execution by +3.75 percentage points in Q1, +9.85 points in Q2, +10.20 points in Q3, and +4.60 points in Q4. The indicator therefore makes the operational dimension of coupling concrete and shows that the rail–dry-port interface was most weakly coupled during the middle of the year.

Interpreting the mismatch: corridor scale, inland pressure, and uneven translation of digital capacity

The likely conditions behind the rail-interface lag can be interpreted by considering the public planning and industry evidence. The Zhejiang-Ningbo-Zhoushan setting is already large and spatially extensive, and is embedded in dense transport activity. By September 2024, Ningbo-Zhoushan Port had 107 sea–rail routes, including 26 scheduled trains, and 37 inland dry-port nodes covering 67 prefecture-level cities in 16 provincial-level areas. The reason why these figures are important is that they reflect the status of a mature corridor, and not that Zhejiang can be used as a universal model. It can be easier to add routes and nodes to such a corridor than to synchronise the interfaces between them. At this scale, the route expansion can no longer be the primary solution. The more nodes in a network, the more operational interfaces are generated, especially if they are located deep inside the network. These interfaces must then be sequenced, coordinated and managed.

https://doi.org/10.56143/3030-3893-2026-3-78-86

There are also strong digital foundations in the case, but it seems that there is a disconnect between digital connectivity and event level orchestration. The Four-Port platform reportedly is able to integrate more than 11,000 data items, improve the efficiency of multimodal bookings by roughly 40%, and connects more than 100 systems. The Sixth Port Area platform is also said to boost the operational efficiency of the sea–rail by approximately 20%. These are important accomplishments. But a digital platform doesn't necessarily mean that train assembly, customs sequencing, yard readiness and gate operations are synchronised. Digitalisation helps to increase visibility, however this visibility needs to be translated into coordinated action as well.

The inland Jinhua–Yiwu support area seems to be under pressure. According to public planning documents the region's railway container capacity is approximately 650,000 TEU. Yiwu sea–rail station was able to process approximately 123,000 TEU of sea–rail transport in 2023. Overall utilisation was at around 80% and international trains and sea–rail trains took up almost 75% of the station's freight volume. These are not definitive and don't provide proof of a single cause, but they do indicate that there may have been limited spare capacity. This is significant as with tight capacity, even small sequencing issues or dispatch instability can impact the broader corridor.

Behaviour might also be affected by price signals. Despite local subsidy, rail transportation from Yiwu to Ningbo-Zhoushan is estimated to be approximately RMB 20 more expensive than direct road transport per forty-foot container. Though this is a small difference, it could be important for shippers should multimodal services be uncertain or there be additional coordination costs. Reliability and ease of booking, tracking, and execution can potentially make shippers more willing to pay a small premium for rail.

Pressure is also seen at the port–rail interface. Public planning documents show that the volume of port-station rail traffic amounted to 17.49 million tonnes or 7.9% of throughput in the port area and that existing facilities were capable of 1 million TEU of sea–rail traffic per year. Thus, the inland bottleneck should be interpreted in the context of the overall coordination challenge which also includes gateway capacity, consolidation in the inland, route planning, and digital-operational timing.

Finally, there is a baseline of monitoring in the corridor. Sixteen indicators can be automatically captured through IoT, including road and rail gate-system data, which are listed in public materials. This is crucial, as imbalances need not be noticed only in annual statistics if they are detected in near real time. The CIG indicator in this context helps to make an abstract coordination problem real and tangible, to discuss with port, rail, dry-port, customs and platform actors.

Discussion and Recommendations: From Network Expansion to Interface-Centered Optimization

Optimization of the Maritime Silk Road (MSR) corridor should not be started from the general question of how to expand the network, based on the results. Rather, it should be a more specific question – once spatial maturity is reached, which interface is reducing the performance of the network? In the Zhejiang-Ningbo-Zhoushan instance, it is not difficult to see. Stable and distinguishable gateway functions are exhibited in annual plans, while the structure of the corridor remains stable. Maritime side performances are good, as seen by rolling data. But the schedule-gap matrix and CIG values indicate that there is a weakness in the rail–dry-port interface. The operational optimization and governance reform must be linked here.

It's not so much about the local context as it is about the analytical logic of the case in Zhejiang. But dry-port development, rail connectivity and international freight corridors cannot function effectively if inland nodes are not coordinated with seaports and cross-agency operational decision-making, which is relevant to Uzbekistan and other Central Asian economies.

Four directions of optimization are indicated by this diagnosis. The roles for gateways should be well-defined. Gateways, control points, bulk-specialized bases and inland-facing terminals should be different in their way of operating. Second, the interface of the dry-port should be reinforced. The emphasis should not be on the construction of nodes for the sake of it, but on customs extension, assembly of trains, cargo consolidation and the synchronization of slots at robust inland nodes, particularly Jinhua–Yiwu. Third, digitalisation needs to go beyond data sharing to digital orchestration. All activities of booking, customs clearance, preparation of the train, yard readiness, and gate operations should be integrated into a coordinated process. Fourth, the use of rolling warning should be made institutional. If CIG values remain positive or gaps in rail freight schedules reoccur, systematic measures should be taken, and a quarterly process of review should be established.

This is an interpretation that relates collaborative governance to network diagnosis. Once a corridor becomes institutionally layered, location of the terminal and route design are no longer sufficient. The challenge is to find the disconnect between physical flows, governance and digital processes. So the rail–dry-port interface and the digital to physical interface are not just technical issues. They are the key units through which improvements to the governance of corridors can be made. The policy lesson is therefore not that every corridor should imitate the Zhejiang model. It is that every mature seaport–dry port corridor needs a mechanism for diagnosing where physical flows, institutional responsibilities, and digital events fall out of alignment. Table 4 summarizes this governance-coupled optimization agenda.

Table 4

Governance-coupled optimization agenda for a port-centered seaport–dry port corridor

Optimization layer	Primary problem	Recommended action	Expected effect
Gateway structure	Uniform treatment of heterogeneous port nodes	Differentiate main gateway control, bulk specialization, and affiliated/inland-facing terminal functions rather than treating all nodes as interchangeable.	Closer alignment between cargo structure, node function, and corridor planning; more transferable logic for other gateway-to-hinterland corridors.

Optimization layer	Primary problem	Recommended action	Expected effect
Dry-port interface	Inland consolidation and slot coordination lag behind seaport-side execution	Strengthen customs extension, train assembly, cargo consolidation, and slot synchronization at strong inland nodes	Lower rail-side delay and stronger port–dry-port synchronization
Digital orchestration	Document and data digitalization exceed event-level process integration	Link booking, customs release, yard status, train readiness, and gate data in one event chain	Lower interface friction and more reliable multimodal service execution
Rolling warning governance	Operational gaps and positive CIG values are detected too late	Use CIG and repeated schedule-gap signals as quarterly warning triggers for port, rail, dry-port, customs, and platform actors.	Faster correction before imbalance becomes structural

Source: synthesized from the empirical diagnosis in this study.

5. Conclusion

This article has examined corridor optimization as an operational and governance problem under the Maritime Silk Road. It does not separate network expansion from governance improvement. Instead, it asks where intervention should be directed when a seaport–dry port system is spatially extensive but unevenly synchronized. The Zhejiang–Ningbo-Zhoushan setting is used as a coastal gateway-province case. It also has broader relevance to corridors between maritime gateways and inland and landlocked hinterlands. The findings indicate that rather than route development, more emphasis should be placed on enhancing the role of the corridors' gateways, inland consolidation, digital orchestration, and rolling monitoring.

The four key findings are: First, the intended annual node structure is fairly static; it has little change in structure. Second, the rolling data for 2025 demonstrate high performance on the maritime side and less on the rail side. Third, the CIG indicator reveals this imbalance: the difference between the maritime-side and the rail-freight execution increased in Q3 to +10.20 percentage points. Fourth, policy and planning evidence indicates several plausible conditions behind the delay: corridor scale, inland station pressure, a marginal rail-cost disadvantage, and incomplete translation of digital capacity into field-level operational coordination.

It may be concluded that collaborative governance in a seaport–dry port system should be assessed by the effectiveness of interface management, not only by formal institutional links or the number of opened routes. Optimization is possible if it focuses on schedule discipline, inland assembly, customs extension, platform coordination and monitoring intervention. Dry ports should thus be interpreted not only as logistics nodes but as governance interfaces to transform the capacity of seaports into predictable inland transport performance.

This study has some limitations. It is constructed on one year of quarterly data and a one-port-centred corridor, and is intended as a diagnostic case study, not a universal rule. The analysis relies on aggregated planning and operational indicators and does not include shipper-level origin-destination matrices, terminal-level slot records, or micro-level cost traces. The indicator of CIG is not a causal model, but rather a simple proxy for the operational imbalance. Additional studies may be conducted using multi-year multi-corridor, shipper level, terminal level, and service reliability data.

References

[1] Notteboom T.E., Rodrigue J.-P. Port regionalization: Towards a new phase in port development. Maritime Policy & Management. 2005;32(3):297–313. https://doi.org/10.1080/03088830500139885

[2] Roso V., Woxenius J., Lumsden K. The dry port concept: Connecting container seaports with the hinterland. Journal of Transport Geography. 2009;17(5):338–345. https://doi.org/10.1016/j.jtrangeo.2008.10.008

[3] Bask A., Roso V., Andersson D., Hämäläinen E. Development of seaport–dry port dyads: Two cases from Northern Europe. Journal of Transport Geography. 2014;39:85–95. https://doi.org/10.1016/j.jtrangeo.2014.06.014

[4] Ansell C., Gash A. Collaborative governance in theory and practice. Journal of Public Administration Research and Theory. 2008;18(4):543–571. https://doi.org/10.1093/jopart/mum032

[5] Emerson K., Nabatchi T., Balogh S. An integrative framework for collaborative governance. Journal of Public Administration Research and Theory. 2012;22(1):1–29. https://doi.org/10.1093/jopart/mur011

[6] Wan S., Luan W., Chen Y., Lin Q. Influence of dry ports construction on seaport growth: Case of Ningbo Zhoushan Port. Transport Policy. 2022;117:40–47. https://doi.org/10.1016/j.tranpol.2022.01.008

[7] Caris A., Macharis C., Janssens G.K. Planning problems in intermodal freight transport: Accomplishments and prospects. Transportation Planning and Technology. 2008;31(3):277–302. https://doi.org/10.1080/03081060802086397

[8] Kim N.S., van Wee B. The relative importance of factors that influence the break-even distance of intermodal freight transport systems. Journal of Transport Geography. 2011;19(4):859–875. https://doi.org/10.1016/j.jtrangeo.2010.11.001

[9] Tsao Y.-C., Thanh V.-V. A multi-objective mixed robust possibilistic flexible programming approach for sustainable seaport-dry port network design under an uncertain environment. Transportation Research Part E: Logistics and Transportation Review. 2019;124:13–39. https://doi.org/10.1016/j.tre.2019.02.006

[10] Asadi Dalivand A.A., Torabi S.A. Sustainable-resilient seaport-dry port network design considering inter-modal transportation. Journal of Cleaner Production. 2024;452:141944. https://doi.org/10.1016/j.jclepro.2024.141944

[11] Heilig L., Voß S. Information systems in seaports: A categorization and overview. Information Technology and Management. 2017;18(3):179–201. https://doi.org/10.1007/s10799-016-0269-1

[12] Hanaoka S., Regmi M.B. Promoting intermodal freight transport through the development of dry ports in Asia: An environmental perspective. IATSS Research. 2011;35(1):16–23. https://doi.org/10.1016/j.iatssr.2011.06.001

[13] Lättilä L., Henttu V., Hilmola O.-P. Hinterland operations of sea ports do matter: Dry port usage effects on transportation costs and CO2 emissions. Transportation Research Part E: Logistics and Transportation Review. 2013;55:23–42. https://doi.org/10.1016/j.tre.2013.03.007

[14] Monios J., Bergqvist R., Woxenius J. Port-centric cities: The role of freight distribution in defining the port-city relationship. Journal of Transport Geography. 2018;66:53–64. https://doi.org/10.1016/j.jtrangeo.2017.11.012

[15] Wilmsmeier G., Monios J., Lambert B. The directional development of intermodal freight corridors in relation to inland terminals. Journal of Transport Geography. 2011;19(6):1379–1386. https://doi.org/10.1016/j.jtrangeo.2011.07.010

[16] Khaslavskaya A., Roso V. Dry ports: Research outcomes, trends, and future implications. Maritime Economics & Logistics. 2020;22(2):265–292. https://doi.org/10.1057/s41278-020-00152-9

[17] Witte P., Wiegmans B., Ng A.K.Y. A critical review on the evolution and development of inland port research. Journal of Transport Geography. 2019;74:53–61. https://doi.org/10.1016/j.jtrangeo.2018.11.001

[18] Wiegmans B.W., Masurel E., Nijkamp P. Intermodal freight terminals: An analysis of the terminal market. Transportation Planning and Technology. 1999;23(2):105–128. https://doi.org/10.1080/03081069908717643

[19] Ambrosino D., Ferrari C., Sciomachen A., Tei A. Intermodal nodes and external costs: Re-thinking the current network organization. Research in Transportation Business & Management. 2016;19:106–117. https://doi.org/10.1016/j.rtbm.2016.05.001

[20] Kumar A., Anbanandam R. Analyzing interrelationships and prioritising the factors influencing sustainable intermodal freight transport system: A grey-DANP approach. Journal of Cleaner Production. 2020;252:119769. https://doi.org/10.1016/j.jclepro.2019.119769

[21] Wu Y., Zhang R. Game-theoretical method toward dry port multilevel location considering capacity constraints and shippers' choice behavior. Transportation Research Record. 2023;2677(11):64–82. https://doi.org/10.1177/03611981231164385

[22] Gonzalez-Aregall M., Bergqvist R. The role of dry ports in solving seaport disruptions: A Swedish case study. Journal of Transport Geography. 2019;80:102499. https://doi.org/10.1016/j.jtrangeo.2019.102499

[23] Shi J., Chen J., Xu L., Di Z., Qu Q. Improving the resilience of maritime supply chains: The integration of ports and inland transporters in duopoly markets. Frontiers of Engineering Management. 2023;10(1):51–66. https://doi.org/10.1007/s42524-022-0231-3

Information about the author

Mu Zhendi "Silk Road" International University of Tourism and Cultural Heritage, Zhejiang Seaport Group
E-mail: muzhendi@163.com
https://orcid.org/0000-0002-5696-391X

Journal Engineer ISSN: 3030-3893 Volume:4| Issue:3| 2026

Received: 6 July 2026 | **Accepted:** 17 August 2026 | **Published:** 30 September 2026

Scientific and theoretical foundations of resource management in ensuring product quality and safety at light industry (sewing and knitting) enterprises

N.S. Sotivoldieva[1][a]

[1]Andijan state technical institute, Andijan, Uzbekistan

Abstract: This article analyzes the scientific and theoretical foundations of the resource management system in ensuring product quality and safety in light industry enterprises, particularly garment and knitwear. The aim of the study is to systematically analyze the conceptual content of the resource management concept, its historical evolution, its interconnection with international quality and safety standards (ISO 9001:2015, ISO 14001, OEKO-TEX Standard 100), as well as the experience of leading foreign enterprises (Zara, Toyota, Nike, H&M). The study employed methods of comparative analysis, systematization of scientific literature, and content analysis of regulatory legal acts.

Keywords: resource management, quality management, product safety, ISO 9001:2015, OEKO-TEX Standard 100, garment and knitwear industry, resource efficiency, circular economy, Industry 4.0.

1. Introduction

Light industry, including the textile, garment-knitting, leather-footwear, and fur industries, is considered one of the most labor-intensive and export-oriented sectors of the global economy. According to the latest statistics, the total value of the global textile and clothing market is more than 1.2 trillion US dollars, with the finished clothing and fashion industry accounting for 72.7%; more than 90 million people are employed in the industry worldwide, most of whom are located in the Asia-Pacific region [1-3].

Being competitive in international trade requires light industry enterprises to guarantee not only the volume of products but also their quality and safety in accordance with the requirements of international certificates such as ISO 9001, OEKO-TEX Standard 100, GOTS, Sedex (SMETA), and Amfori BSCI. Such certificates allow enterprises to export to major markets such as the USA and the European Union, but their achievement is ensured not only through final product inspection but also through the systematic management of the enterprise's material, technical, human, financial, and information resources [2].

The classics of quality management theory-W. Deming, J. Juran, F. Crosby, K. Ishikawa, and A. Feigenbaum-defined product quality as a set of characteristics of compliance with consumer requirements, justifying that quality control must begin at the initial stage of production. In the field of security management, the concept of risk prevention developed by W. Henry and F. Bird, as well as the HACCP system, serve as an important theoretical foundation. Among the studies specific to light industry, the "Quality Control-CE" model by L. Mitreva and N. Taskov, the Lean Six Sigma methodology by J. Anthony, the life cycle analysis (LCA) by L. Farrant and Daniel, and the artificial intelligence-based quality control systems by Fang and Getuli are of particular importance [4-5].

2. Research methodology

The study was conducted based on a theoretical-descriptive approach to the topic, using the following scientific research methods:

The method of systematizing and summarizing scientific literature was applied - journal articles, monographs (W. Schuhart, E. Deming, J. Juran, K. Ishikawa, A. Feigenbaum) indexed in the Scopus and Web of Science databases, as well as works by domestic scholars (G. Khojiahmedov, G.Sh. Khankeldiyeva, Yu.S. Shakirova, M.T. Khojiev, S.S. Gulomov, and others).

A content analysis of regulatory legal acts was conducted - the texts of ISO 9001:2015, ISO 14001, ISO 2859-1 (AQL), OEKO-TEX Standard 100, and the European Union's REACH regulation were studied, and their requirements for resource management were compared.

The comparative analysis method was applied - the resource management system was compared with production operational management, financial management, and international quality management systems based on the criteria of management object, purpose, scope, and impact on product safety[5-8]

Based on the case study method, the experience of resource management of international corporations such as Zara (Inditex), Toyota, Nike, and H&M was studied, and their potential for adaptation to the practices of garment and knitwear enterprises was evaluated.

3. Results and discussion

To reveal the specific strategic significance of the resource management system at a garment and knitwear enterprise, a comparative analysis was conducted with other structural management systems of the enterprise (Table 1). The analysis showed that the resource management system is the most comprehensive in terms of scope, covering the entire life cycle from the design stage to product disposal,

[a] https://orcid.org/0009-0004-4444-4815

and directly influences product safety through OEKO-TEX 100 and REACH requirements.

Table 1

Comparative analysis of resource management and other management systems

Comparison criteria	Resource management system	Production operations management	Financial management system	International quality management
Object of management	Integration of all resources (material, human, technical, time, information)	Only technological processes and sewing-line flow in the shops	Cash flows, profit, costs, investments	Compliance of processes with international standard requirements
Main goal	Guaranteeing quality stability and safety with minimal resource use	Meeting the planned production output within the set deadline	Maximizing financial stability and net profit	Ensuring consumer satisfaction and eliminating defects
Scope of coverage	Widest: covers the whole chain from design to disposal	Local: from fabric cutting to the finished product	Local: only financial transactions	Broad: organizational processes and quality policy
Impact on product safety	Direct: controlled through OEKO-TEX 100 and REACH filters	Indirect: only addresses mechanical (size, seam) quality	No impact, only finances the safety-related costs	Indirect: requires safety-control processes

Comparative analysis shows that resource management acts as a "provider" for all other management systems: if material and human resources are not managed systematically, operational production management cannot fulfill its plans, resulting in increased waiting times and the number of defects, while the financial system faces a crisis due to frozen capital.

Statistical data on the coverage of the main international certificates used by light and textile industry enterprises to increase export potential and the number of certified enterprises have been systematized (Table 2).

Tabel 2

Geographical coverage of international management system certificates and number of certified organizations

Comparison criteria	Resource management system	Production operations management	Financial management system
Object of management	Integration of all resources (material, human, technical, time, information)	Only technological processes and sewing-line flow in the shops	Cash flows, profit, costs, investments
Main goal	Guaranteeing quality stability and safety with minimal resource use	Meeting the planned production output within the set deadline	Maximizing financial stability and net profit
Scope of coverage	Widest: covers the whole chain from design to disposal	Local: from fabric cutting to the finished product	Local: only financial transactions
Impact on product safety	Direct: controlled through OEKO-TEX 100 and REACH filters	Indirect: only addresses mechanical (size, seam) quality	No impact, only finances the safety-related costs

Source analysis shows that the concept of resource management has passed through four main historical stages. In the 1910s–1940s, F. Taylor, G. Gantt, and L. Gilbreth ushered in the era of "scientific management and standardization"- during this period, resource management was primarily interpreted as the optimization of working time and human actions (Gantt diagram). In the 1950s–1970s, W. Schuhart, E. Deming, and J. Juran developed systems for statistical quality control (SPC) and material requirements planning (MRP). In the 1980s–2000s, with the development of T. Ono (Toyota's system) and the ERP concept, a lean manufacturing philosophy was formed, where the main goal was to eliminate any waste rather than simply managing resources. Today, the resource chain is managed in real-time through cloud ERP and PLM systems, Computer Vision, and IoT sensors (Table 3) [9-10]

Table 3

Comparative analysis of the historical and modern state of resource management

Comparison criterion	Traditional resource management (late 20th century)	Modern resource management (current state)
Management method	Local, separate for each shop or department (isolated)	Integrated, across the entire supply chain
Data exchange	Periodic, in the form of paper or archived reports	Rapid, in real time, digital
Optimization factor	Only reducing volume and financial costs	Cost reduction plus chemical-ecological safety guarantee
Technological foundation	Mechanized equipment and human labor	Industry 4.0, artificial intelligence, IoT, cloud systems

The modern resource management system relies on a combination of three scientific approaches: a systems approach (where all resources are managed as a holistic system covering all stages of the product lifecycle), a process approach (the "input → process → output" chain in accordance with ISO 9001:2015 requirements), and a risk-based approach (Risk-based Thinking - anticipating risks such as supply disruptions or the influx of low-quality raw materials). Based on these approaches, three core principles are formed: eco-efficiency and safety sustainability (priority of OEKO-TEX 100 and REACH requirements), systematic waste reduction (efficient production methods), and continuous development and the Kaizen philosophy [11].

Enterprise resources are traditionally divided into five groups: material resources (raw materials, yarn, fabric, fittings, chemical dyes - controlled by ISO 9001 and OEKO-TEX standards), technological and technical resources (production equipment, sewing machines, buildings), human resources (staff, technologists, qualification of quality controllers - regulated by clause 7.1.2 of ISO 9001), financial resources (cash, investments, working capital), and information-digital resources (management programs, technical documentation, standards base) [12].

When developing a resource management system for garment and knitwear enterprises based on international standards, ISO 9001 (for process and management quality) and OEKO-TEX Standard 100 (for raw material and product safety) are complementary but conceptually different standards. Paragraph 7.1 of ISO 9001 requires the systematic distribution of material, human, and technical resources at the enterprise, while OEKO-TEX Standard 100 monitors the absence of more than 1,000 chemicals harmful to human health (formaldehyde, heavy metals, prohibited azo dyes) in these resources (Table 4).

Table 4

Comparative analysis of SO 9001:2015 and OEKO-TEX Standard 100 standards

Comparison criteria	ISO 9001:2015 Standard	OEKO-TEX Standard 100 System
Main object of resource management	Processes and management system: how resources are planned and allocated	Product composition: limits the amount of over 1,000 chemical substances and harmful elements
Approach to material resources	Focuses on the raw material's technical characteristics, dimensions, and quality stability	Examines the raw material's effect on human health and its ecological purity
Technical-technological resources	Requires managing the overall productivity of equipment	Controls residues of chemical agents (oils, dyes) used in equipment from transferring onto the fabric
Resource audit method	Document analysis, internal audits, observation of organizational processes	Rigorous laboratory analyses (pH level, heavy metals, formaldehyde content)

An analysis of the experience of leading international corporations in resource management revealed four main directions. The Zara (Inditex) experience - using cloud ERP and PLM systems, reduced the period from design to store shelf from 6 months to 2-3 weeks, reducing overproduction volume to almost 0%. Toyota's experience - through Just-in-Time and 5S systems, each worker is empowered to identify resource waste; when a defect is detected on the line, the process is halted and the problem is eliminated at its root. Nike and H&M's experience - 100% aligning the supply chain with OEKO-TEX Standard 100 and REACH requirements, recycling used fabric waste into the life cycle as a secondary resource (fibre-to-fibre) based on the principle of a circular economy.

As a result of applying this integrated approach, the following changes are observed in the enterprise's key quality indicators (Table 5).

https://doi.org/10.56143/3030-3893-2026-3-87-91

Table 5

Comparative effectiveness of implementing the integrated resource management system

Controlled resource / quality criterion	In the traditional management system	In the ISO/Lean integrated system	Result achieved
First Pass Yield (FPY)	85–87%	95–97%	Rework costs and time losses are minimized
Material Utilization Rate (MUR)	78–82%	88–92%	Raw material is saved, unit cost decreases by 2.5–3%
Overall Equipment Effectiveness (OEE)	60–65%	80–85%	Equipment downtime is reduced by 40%
Export safety guarantee (REACH/OEKO-TEX)	Uncontrolled, high risk	100% guaranteed	Direct export contracts secured with international brands

Discussion

The results obtained show that the resource management system serves as the foundation for all other management systems of a garment and knitwear enterprise (operational production management, financial management, quality management), but in practice, these systems often operate in isolation from one another. In particular, the traditional production system seeks to ensure quality and safety at the final control stage, which leads to human error ranging from 30 to 40%. Conversely, integrating Schuhart control cards, IQ statistical sampling, and Computer Vision technologies into the process can reduce the number of defects caused by the human factor by up to 95%.

Analysis of international experience (Zara, Toyota, Nike, H&M) has confirmed that the highest efficiency of resource management is manifested in integrating not just one standard or methodology, but several approaches - rapid information exchange (Zara model), lean manufacturing (Toyota model), and environmental and chemical compliance (Nike/H&M model) - into a single system. For Uzbek garment and knitwear enterprises, adapting this experience is an important strategic opportunity, especially given the geographical proximity to the European market (near-shoring advantage) and the presence of a national raw material base for cotton and yarn [13]

At the same time, the analysis showed that there are a number of scientific, practical, technical and methodological gaps in the field. From a scientific perspective, a localized model combining the ISO 9001, ISO 14001, and OEKO-TEX Standard 100 systems within a unified resource management concept, as well as multi-factor statistical models for predicting defects, has not been sufficiently developed. In practical terms, many local enterprises are issuing ISO certificates only formally to meet export requirements rather than as a real optimization tool, which reduces the level of traceability in the supply chain. From a technical perspective, the problem of the level of utilization of real-time monitoring systems based on artificial intelligence and IoT, as well as the weakness of the laboratory base, remains. Methodologically, the standards for fabric consumption and working time are outdated and do not fully account for the characteristics of modern stretchable knitwear, while modern methods for assessing employee competence have not been implemented in practice [14]

Global trends - the intensification of near-shoring processes due to digitalization and artificial intelligence (Industry 4.0), the Digital Product Passport (DPP), environmental bans (complete prohibition of PFAS/PFHxA substances), and logistical risks - are further strengthening the need for integrated scientific models aimed at addressing these gaps.

4. Conclusion

As a result of the analysis, the following conclusions were drawn. Firstly, the resource management system is the most comprehensive management system for a garment and knitwear enterprise, covering all stages of the product life cycle and directly affecting product safety. Second, the concept of resource management has historically undergone a four-stage evolution, from work time standardization to digital management at the level of today's Industry 4.0. Thirdly, modern resource management relies on a combination of systemic, process, and risk-based approaches and is implemented based on a four-phase functional model consisting of planning, mobilization, monitoring, and optimization. Fourth, ISO 9001:2015 and OEKO-TEX Standard 100 standards play a complementary role in resource management - one ensures process quality, while the other guarantees the chemical safety of the product. Fifth, implementing the experience of international corporations as an integrated system will increase the FPY indicator to 95–97%, the MUR indicator to 88–92%, and reduce equipment downtime to 40%.

At the same time, the development of a localized resource management model in harmony with ISO/OEKO-TEX standards and digital algorithms (AI/SPC) for garment and knitwear enterprises in Uzbekistan, increasing the transparency of the supply chain, updating the modern regulatory and methodological framework, and implementing a scientifically grounded methodology for assessing employee competence have been identified as promising areas of research.

References

[1] Grand View Research. Textile market analysis. https://www.grandviewresearch.com/industry-analysis/textile-market

[2] Newway Apparel. Garment manufacturing statistics 2026 (geografik tahlil). https://www.newway-

apparel.com/blog/garment-manufacturing-statistics-2026.html

[3] Urishev B.A. To‘qimachilik sanoati korxonalari samaradorligini oshirish omillari. Science and Education Scientific Journal, 2024, jild 5, son 6.

[4] Hojiahmedov G., Yaxyayeva I., Umarova M., Usmonov A. Sifat menejmenti. Cho‘lpon nomidagi nashriyot-matbaa ijodiy uyi, 2012.

[5] Ismatov R., Ahmedov O. Sifat menejmenti fani bo‘yicha o‘quv-uslubiy majmua.

[6] Xankeldiyeva G.Sh., Shakirova Yu.S. To‘qimachilik sanoati korxonalarida eksportbop mahsulotlar ishlab chiqarishni tashkil etish. Farg'ona: Al-Fergranus, 2021.

[7] Vinu V.P., Pillai S.V. Quality management in textile industries. International Journal of Innovative Science and Research Technology, 3(1), 2018.

[8] ChiuVention. How to improve quality management and control in textile? https://chiuvention.com/blog/quality-contro-in-textiles

[9] Kazakov O.S. To‘qimachilik korxonalarida ishlab chiqarish resurslarini strategik boshqarish. Marketing ilmiy, amaliy va ommabop jurnal, №1, 2026. https://marketingjournal.uz/index.php/mj/uz/article/view/718/717

[10] Abdullayev M.G'. Sanoat korxonalarida personalni boshqarish mexanizmini takomillashtirish: PhD dissertatsiyasi avtoreferati. Andijon, 2023. https://library.ziyonet.uz/book/128803

[11] Ahmed I., Al Shamsi I.R., Farooq W. Islamic entrepreneurial intentions. J. Islam. Mark., 1–21, 2026. doi:10.1108/JIMA-08-2024-0353

[12] Jasuja G.D. Resource efficiency in textile industry. New Cloth Market. https://www.newclothmarketonline.com/editorials/resource-efficiency-in-textile-industry /

[13] Textile School. Energy-efficient textile production: strategies for a greener industry. https://www.textileschool.com/29259/energy-efficient-textile-production-strategies-for-a-greener-industry

[14] Madumarov F.T. Возможности адаптации управления качеством на отечественных текстильных предприятиях к международной системе стандартов ISO 9001:2015. Gospodarka i Innowacje, 60, 474, 2025.

Information about the author

Nasibakhon Sotvoldieva

Andijan State Technical Institute, Department of Metrology and Light Industry, PhD student
E-mail: nasibakhon_1992@gmail.com
Tel.: +998337099923
https://orcid.org/0009-0004-4444-4815

Journal Engineer ISSN: 3030-3893 Volume:4| Issue:3| 2026

Received: 8 July 2026 | **Accepted:** 19 August 2026 | **Published:** 30 September 2026

Experimental investigation of mechanical properties of A-III reinforcing steel bars with a diameter of 10 mm

B.F. Botirov[1][a]

[1]Tashkent Architecture and Civil Engineering, University, Tashkent, Uzbekistan

Abstract: This paper presents the results of an experimental investigation into the mechanical properties of A-III reinforcing steel bars with a diameter of 10 mm intended for use in reinforced concrete structures. The study was carried out prior to testing reinforced concrete beams in order to determine the actual strength and deformation characteristics of the reinforcing steel used in the experimental program. Tensile tests were performed in accordance with the requirements of GOST 1497–84 using a universal testing machine. During the experiments, the maximum tensile load, ultimate tensile strength, yield strength, relative elongation, plasticity coefficient, and coefficient of variation were determined. The average values of the ultimate tensile strength, yield strength, and relative elongation were found to be 485 MPa, 405 MPa, and 23.165%, respectively. The experimental results were compared with the requirements of GOST 34028–2016 and demonstrated full compliance with the prescribed mechanical performance criteria. The coefficient of variation did not exceed 3.4%, confirming the high homogeneity and reliability of the investigated reinforcing steel. The obtained results indicate that the tested reinforcement possesses high strength, sufficient ductility, and stable deformation characteristics, making it suitable for application in flexural reinforced concrete elements subjected to static loading. The research findings can be used in the design, analysis, and experimental assessment of reinforced concrete structures and provide reliable reference data for evaluating the load-bearing capacity and serviceability of structural members.

Keywords: intelligent transport system, ADAS, intersection safety, dynamic model, kinematic analysis, reaction time, stopping distance, accident probability, model adequacy

1. Introduction

In recent years, modern high-strength concretes, chemical modifying admixtures, and advanced technologies for the production of reinforced concrete elements have been increasingly applied in the construction industry. However, even when high-quality concrete is used, the operational reliability of structures largely depends on the mechanical properties of reinforcing steel. Therefore, the reliable determination of its strength and deformation characteristics is an essential stage in experimental studies of reinforced concrete structures.

In the design and analysis of flexural reinforced concrete elements, the key parameters include the yield strength of reinforcing steel, ultimate tensile strength, relative elongation, and the material's capacity for plastic deformation. These characteristics determine the onset of plastic deformation, redistribution of internal forces, failure behavior of structural elements, and their level of operational safety.

Determining the actual mechanical properties of reinforcing steel makes it possible to improve the accuracy of engineering calculations, ensure that analytical models adequately reflect the actual structural behavior, and assess the quality of the reinforcing steel used.

According to the requirements of the current regulatory standards (GOST 1497–84 and GOST 34028–2016), the mechanical properties of reinforcing steel must be verified by experimental tensile testing. Such tests make it possible to determine the main strength characteristics of the material, assess its ductility and structural homogeneity, and verify its compliance with regulatory requirements. In addition, experimental investigations enable the identification of possible deviations in mechanical properties resulting from specific manufacturing technologies, heat treatment processes, or storage conditions of reinforcing steel.

The present study was conducted as part of an experimental program aimed at investigating the behavior of flexural reinforced concrete beams produced using locally available chemical admixtures. Prior to testing the reinforced concrete specimens, the mechanical properties of 10 mm diameter A-III class reinforcing steel used as the longitudinal reinforcement were investigated. Preliminary testing provided objective data on the actual strength and deformation characteristics of the reinforcing steel used in the experimental structural elements.

The aim of this study is to experimentally determine the mechanical properties of 10 mm diameter A-III class reinforcing steel by conducting tensile tests, to analyze the obtained results, and to assess their compliance with the requirements of current regulatory standards. The obtained data can be used in the design of reinforced concrete structures, experimental investigations, assessment of the load-bearing capacity of flexural elements, and improvement of calculation methods for reinforced concrete structures by taking into account the actual mechanical properties of the reinforcing steel used.

[a] https://orcid.org/0000-0003-4105-2176

2. Research methodology

The experimental investigation of the mechanical properties of 10 mm diameter A-III class reinforcing steel was carried out to determine its actual strength and deformation characteristics prior to testing the reinforced concrete beams. The obtained results were used as input data for the subsequent analysis of the load-bearing capacity and deformation behavior of the reinforced concrete elements.

The test specimens consisted of three samples of A-III class reinforcing steel with a nominal diameter of 10 mm. Prior to testing, the geometric dimensions of each specimen were measured, including the actual diameter, gauge length of the working section, and initial cross-sectional area. The gauge length was 300 mm for all specimens.

The tensile tests were performed using a GOST-TEST universal testing machine (serial No. 082020224) in accordance with the requirements of GOST 1497–84, “Metals. Methods of Tensile Testing.” Before testing, the specimens were carefully aligned and secured in the grips of the testing machine along their longitudinal axes to prevent eccentric loading. The load was applied smoothly and continuously at a constant rate until specimen failure, thereby ensuring the acquisition of a reliable load–deformation curve.

During the tests, the applied load and the corresponding deformation values were recorded automatically. Based on the experimental data obtained, tensile stress–strain curves were constructed, from which the maximum failure load, yield strength, ultimate tensile strength, and percentage elongation after fracture were determined.

The mechanical properties were calculated in accordance with the requirements of the applicable regulatory standards. The initial cross-sectional area was determined using the actual diameter of each specimen. The ultimate tensile strength was calculated as the ratio of the maximum failure load to the initial cross-sectional area. The yield strength was determined from the stress–strain curve as the stress corresponding to the onset of stable plastic deformation. The percentage elongation was calculated as the ratio of the increase in gauge length after fracture to the initial gauge length of the specimen.

To improve the reliability of the results, the tests were conducted on three independent specimens of the same nominal diameter. After completion of the tests, the mean values of each determined parameter were calculated, along with the coefficient of variation, which was used to characterize the degree of uniformity of the reinforcing steel under investigation.

The experimental results were compared with the requirements of GOST 34028–2016, which specifies the mechanical properties of reinforcing steel for reinforced concrete structures. The adopted testing methodology provides a high degree of reproducibility, enables an objective assessment of the strength and deformation characteristics of reinforcing steel, and can be applied in similar experimental studies of reinforced concrete structures.

The obtained mechanical properties were subsequently used in the calculations and analysis of the behavior of flexural reinforced concrete elements reinforced with the investigated steel.

3. Results and Discussion

The tests were conducted using a universal tensile testing machine in accordance with the requirements of GOST 1497–84. During the experimental study, three reinforcing steel specimens with a diameter of 10 mm were tested (Fig. 1).

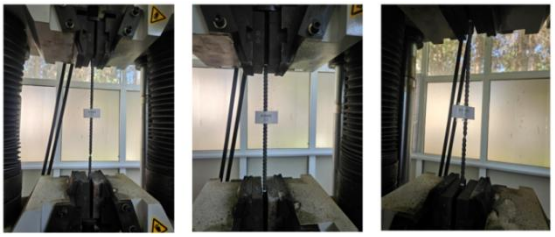


Fig. 1. Tensile Test of Reinforcing Steel Specimens

For each specimen, the initial cross-sectional area, maximum failure load, tensile deformation, and strength characteristics up to the point of failure were determined. Based on the experimental results, the main mechanical properties of the reinforcing steel were calculated and compared with the requirements of the applicable regulatory standards.

The tests were conducted in accordance with the requirements of GOST 1497–84 (Fig. 2), which provides a generally accepted methodological basis for determining the mechanical properties of metallic materials. The tests were performed using a GOST-TEST universal testing machine (serial No. 082020224). Reinforcing steel specimens with a diameter of 10 mm and a gauge length of 300 mm were used in each test.

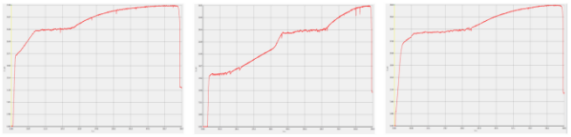


Fig. 2. Load–Deformation (P–Δ) Curves Obtained During the Tensile Testing of Reinforcing Steel Bars

During the tests, the main mechanical properties of the reinforcing steel were determined (Table 1), including the maximum failure load (P_{max}), percentage elongation at fracture (δ), ultimate tensile strength (σ_u), and yield strength (σ_y). The obtained values were used to evaluate the strength and deformation characteristics of the reinforcing steel under investigation.

Table 1

Main Parameters Determined During the Experimental Investigation

№	d_0, mm	l_0, mm	P_{max}, kN	δ, %	$\sigma_в$, MPa	$\sigma_т$, MPa
1	10.00	300.0	37.856	22.2	482	395
2	10.00	300.0	36.560	23.3	465	375
3	10.00	300.0	39.803	23.9	507	446

https://doi.org/10.56143/3030-3893-2026-3-92-95

Ср ед.	10.00	300.0	38.073	23.1	485	405

As can be seen from the test results, all the reinforcing steel specimens exhibited similar strength and deformation characteristics. The average maximum failure load was 38.073 kN, while the average ultimate tensile strength, yield strength, and percentage elongation were 485 MPa, 405 MPa, and 23.165%, respectively. The obtained results indicate a high degree of uniformity in the mechanical properties of the investigated reinforcing steel and confirm its compliance with the regulatory requirements for reinforcing steels used in reinforced concrete structures.

Since the initial cross-sectional area was identical for all three specimens, it was determined using the following equation:

$$F = \frac{\pi \cdot d_0^2}{4} = \frac{3{,}1416 \cdot 10^2}{4} = 78{,}54 \text{ мм}^2 \quad (1.1)$$

The ultimate tensile strength (σ_u) for each specimen was determined using the following equation:

$$\sigma_в = \frac{P_{max}}{F} \quad (1.2)$$

The percentage elongation was calculated using the following equation:

$$\delta = \frac{l - l_0}{l_0} \cdot 100\% \quad (1.3)$$

The average percentage elongation obtained from the test results was 23.165%.

The yield strength (σ_y) was determined from the stress–strain curves obtained during the tensile tests. For the investigated specimens, the yield strength values ranged from 375 to 446 MPa.

The mechanical properties of reinforcing steel used in reinforced concrete structures are evaluated not only on the basis of laboratory test results but also by comparing the obtained data with the requirements of applicable regulatory standards. In the present study, the test results were analyzed in accordance with the requirements of GOST 1497–84, as well as GOST 6727–80 for low-carbon reinforcing steel wire and GOST 10884–94 for thermomechanically strengthened reinforcing steel.

These standards specify the minimum permissible values of ultimate tensile strength, yield strength, percentage elongation, and other mechanical properties of reinforcing steel products. Comparison of the experimentally obtained results with the regulatory requirements makes it possible to objectively assess the quality of the reinforcing steel under investigation and determine its suitability for use in critical reinforced concrete structures.

Table 2

Standard mechanical requirements for 10 mm reinforcing steel according to GOST 34028–2016

Parameter	GOST 34028–2016	Unit	Description
Ultimate tensile strength($\sigma_в$)	≥ 390	MPa	Tensile strength
Yield strength($\sigma_т$)	≥ 350	MPa	Onset of plastic deformation
Relative elongation (δ)	≥ 18	%	Ductility characteristic
Plasticity coefficient $\sigma_в/\sigma_т$	≥ 1,10	–	Plasticity reserve coefficient

In the present study, three reinforcing steel specimens with a diameter of d_0 = 10 mm were subjected to tensile testing, and the obtained experimental results were compared with the requirements of the applicable regulatory standards (Tables 2–3).

Table 3

Average Results of the Experimental Investigation for Three Specimens

Parameter	Test Result (Average Value)	Unit	Deviation from the Standard
Ultimate tensile strength($\sigma_в$)	485	MPa	+95 MPa
Yield strength($\sigma_т$)	405	MPa	+55 MPa
Relative elongation(δ)	23,165	%	+5,165 %
Strength ratio $\sigma_в/\sigma_т$	1,20	–	+0,10

4. Conclusion

Based on the results of the experimental investigation of the mechanical properties of 10 mm diameter A-III class reinforcing steel, the following main conclusions were drawn:

1. Tensile tests conducted on three reinforcing steel specimens in accordance with the requirements of GOST 1497–84 made it possible to determine the actual values of the main strength and deformation characteristics of the material.
2. The average maximum failure load was 38.073 kN, indicating a sufficiently high tensile load-bearing capacity of the investigated reinforcing steel.
3. The average ultimate tensile strength was 485 MPa, which is 95 MPa higher than the minimum value specified by the applicable standard for the considered class of reinforcing steel.
4. The average yield strength was 405 MPa, which is 55 MPa higher than the minimum specified value. This confirms the ability of the reinforcing steel to withstand significant tensile stresses before the onset of plastic deformation.
5. The average percentage elongation after fracture was 23.165%, exceeding the specified minimum value by 5.165 percentage points. This result indicates sufficient ductility of the reinforcing steel and its ability to undergo deformation without brittle failure.
6. The average ratio of ultimate tensile strength to yield strength was 1.20, which exceeds the minimum specified value of 1.10. This indicates an adequate ductility reserve and favorable behavior of the reinforcing steel under loading.
7. The coefficient of variation of the mechanical properties did not exceed 3.4%, indicating a high degree of uniformity among the tested specimens and consistency of their strength characteristics.
8. Comparison of the experimental results with the requirements of GOST 34028–2016 showed that the investigated 10 mm diameter A-III class reinforcing steel complies with the established regulatory requirements for strength and ductility.
9. The obtained experimental data confirm the suitability of this reinforcing steel for effective use as

longitudinal reinforcement in flexural reinforced concrete structures, including beams subjected to short-term static loading.

10. The experimentally determined mechanical properties of the reinforcing steel can be used in subsequent calculations and analyses of the load-bearing capacity, crack resistance, and deformation behavior of experimental reinforced concrete elements.

References

[1] Khonsari SV, Shabani A, England GL, Shahsavar-Gargari M. Mechanical behaviour of A-III steel rebars under monotonic loadings at seismic strain rates. Magazine of Concrete Research. 2018;70(1):42–54. https://doi.org/10.1680/jmacr.17.00067.

[2] ACI Committee 439. Steel reinforcement—Physical properties and U.S. availability. ACI Materials Journal. 1989;86(1):63–76. https://doi.org/10.14359/1867.

[3] Aldabagh S, Alam MS. High-Strength Steel Reinforcement (ASTM A1035/A1035M Grade 690): State-of-the-Art Review. Journal of Structural Engineering. 2020;146(8). https://doi.org/10.1061/(ASCE)ST.1943-541X.0002720.

[4] Gómez J, Rodríguez M, Torres L, et al. Stress-strain response of A706 Grade 80 reinforcing steel. Construction and Building Materials. 2017;145:292–302. https://doi.org/10.1016/j.conbuildmat.2017.03.200.

[5] Khonsari SV, Shabani A, England GL, Shahsavar-Gargari M. Mechanical behaviour of A-III steel rebars under monotonic loadings at seismic strain rates. Magazine of Concrete Research. 2018;70(1):42–54. https://doi.org/10.1680/jmacr.17.00067.

Information about the author

Bektosh Botirov Tashkent Architecture and Civil Engineering University
E-mail: korreys95@gmail.com
Tel.:+99891 195-98-87
https://orcid.org/0000-0003-4105-2176

Journal Engineer ISSN: 3030-3893 Volume:4| Issue:3| 2026

Received: 10 July 2026 | **Accepted:** 21 August 2026 | **Published:** 30 September 2026

Practical principles for reducing risks arising from measurement parameters in equipment operation (on the example of an artificial lung ventilation apparatus)

Kh. Abduvokhidov[1][a], Z. Juraev[1][b]

[1]Andijan state technical institute, Andijan, Uzbekistan

Abstract: The purpose of this study is to analyze the risks associated with the key clinical parameters of an artificial lung ventilation (ALV) device—tidal volume (VT), respiratory rate (RR), positive end-expiratory pressure (PEEP), peak inspiratory pressure (PIP), and fraction of inspired oxygen (FiO2)—using digital technologies, the HFMEA methodology, and GOST ISO 14971:2021, and to integrate the results into the equipment's technical condition index. Risk identification, assessment, control, and residual risk monitoring were performed according to the NCPS HFMEA approach. The initial assessment showed that 65.5% of the analyzed parameters were classified as high risk. After implementing control measures, VT and PIP were reduced to low risk, RR and PEEP to medium risk, while FiO2 remained at high residual risk. Consequently, the proportion of high-risk parameters decreased from 65.5% to 32.5%, and the maximum risk score was reduced from 12 to 8 points. Integrating HFMEA results into the technical condition index enables quantitative assessment of ventilator safety.

Keywords: FMEA, HFMEA, GOST ISO 14971:2021, ALV apparatus, risk analysis, technical condition index, digital technologies, technical equipment

1. Introduction

Safety requirements for the use of medical equipment are a key component of the healthcare system. This issue is especially critical for artificial lung ventilation (ALV) apparatuses used in resuscitation and intensive care units, as it is directly related to patient lives.

A study conducted by scientists Arkeliana Tase, Melody Z. Ni, and Peter W. Buckle, who analyzed the U.S. Food and Drug Administration (FDA) database, identified 290,141 serious injuries and deaths related to medical equipment over a 20-year period. Another analysis indicates that between 2008 and 2017, medical devices may have caused 1.7 million injuries and 80,000 deaths.[1]

In an analysis by Dutch scientist Mees C. Baartmans, a review of the medical histories of 2,998 patients who died in a hospital proved that approximately 1.9% of the deaths esulted from preventable adverse events related to medical equipment. Examples cited include internal bleeding caused by endoscopes and the improper use of artificial respiration tubes.[2]

Studies confirm that the majority of medical errors arise not from equipment failure itself, but rather from a doctor or nurse misunderstanding a complex interface (an ergonomic error) or incorrectly configuring the device.

Table 1

The most high-risk equipment and causes [1,2]

No.	Equipment Type	Most Common Risks and Consequences
1	Artificial lung ventilation (ALV)	Lung injuries and severe pneumonia caused by selecting the wrong mode or by contaminated filters. Administration of an excessively high dose of a toxic drug to the patient.
2	Infusion Pumps (Dosimeters)	Due to incorrect data entry when setting the medication dosage.
3	Cardiac Monitors	Improperly silencing alarm signals or medical staff failing to respond to the signal in time.

Failure Modes and Effects Analysis, or FMEA, was originally developed in 1949 as a U.S. military standard and was later widely adopted in high-risk sectors such as NASA, civil aviation, and the automotive industry [3,4].

[a] https://orcid.org/0000-0001-8475-6259
[b] https://orcid.org/0009-0008-5141-9916

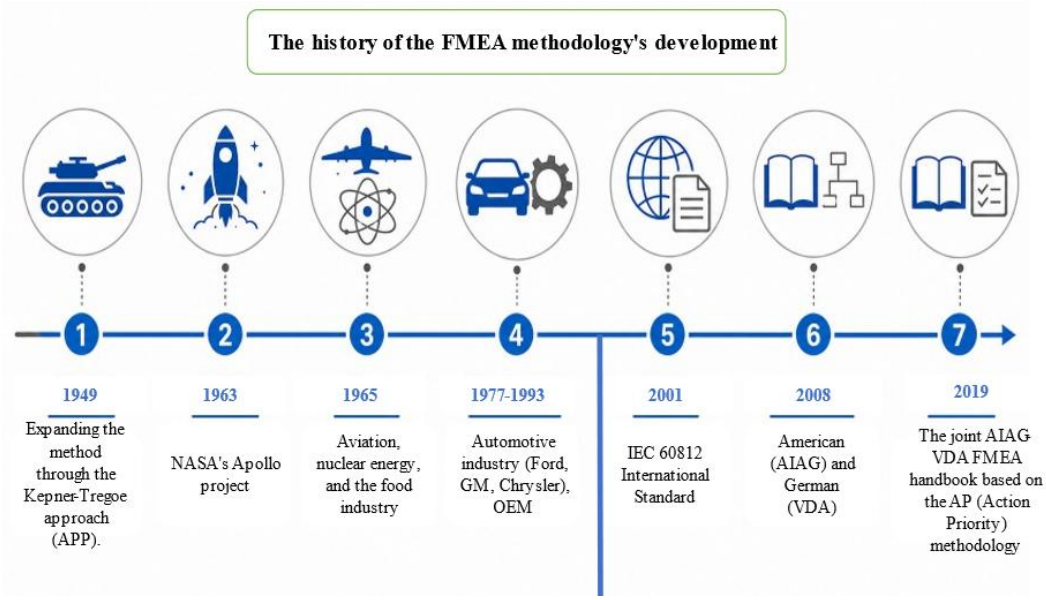


Fig. 1. A chronological history of the development of FMEA and HFMEA methodology

Today, FMEA has become a primary risk management methodology in the automotive, aerospace, nuclear, manufacturing, IT, medical, and service sectors.

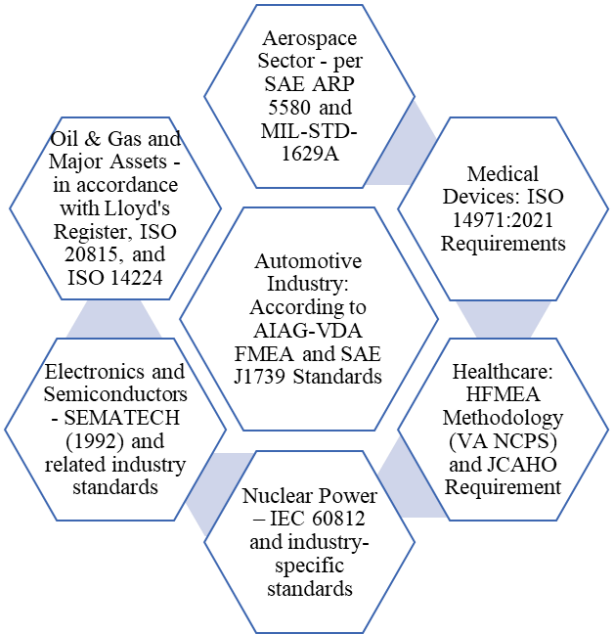


Fig. 2. Application of FMEA as an international standard in various industries [3,4,5,6,7]

HFMEA has been established as a proactive risk management tool focused on patient safety in the medical field, and when applied in conjunction with GOST ISO 14971:2021, it creates a comprehensive risk management framework for medical devices.

Incorrect settings or malfunctions of the mechanical ventilator's main parameters, such as VT, RR, PEEP, PIP, and FiO2, can lead to severe clinical consequences including volotrauma, apnea, atelectasis, barotrauma, and hypoxia.

Therefore, a parameter-oriented HFMEA model was developed in this study, and its results were linked to a technical condition index.

2. Research methodology

The GOST ISO 14971:2021 standard and the HFMEA handbook recommended by the VA NCPS were chosen as the methodological basis for this study, as they define the interconnected stages of risk analysis, evaluation, management, and monitoring for medical devices.

In medicine, the ISO 14971:2021 standard and the official HFMEA handbook are utilized for risk identification, management, and control. These two requirements are considered complementary. To conduct a comprehensive risk analysis, it is necessary to apply several of them in combination.

In this work, the ISO 14971:2021 standard was chosen as the legal and structural basis for the risk assessment

https://doi.org/10.56143/3030-3893-2026-3-96-104 A bridge between science and innovation

methodology of the ALV apparatus. The standard is an internationally binding document that regulates the risk management process for all medical devices and also directly requires the implementation of HFMEA in healthcare facilities. According to this standard, the risk management process consists of five interconnected main blocks, as shown in Figure 3. The process begins at the "Start" point and, at each stage, moves to the next or returns to the previous one based on "Yes" or "No" decisions—this cyclical approach ensures that risks are thoroughly addressed.

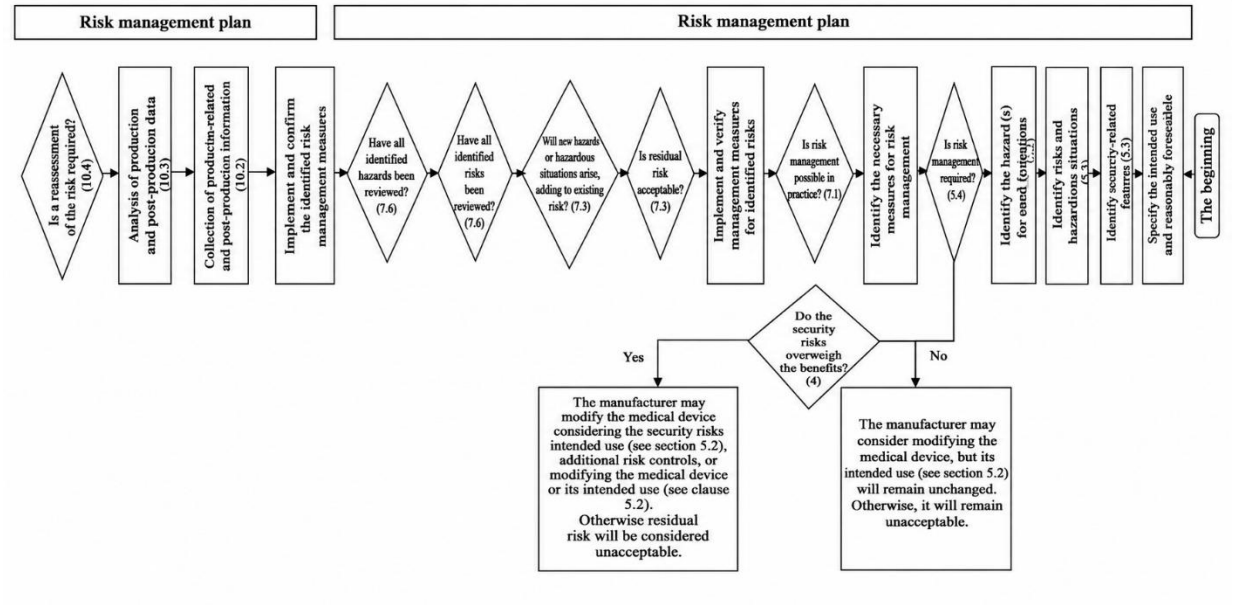


Fig. 3. A complete schematic diagram of the medical device risk management process according to the ISO 14971:2021 standard

HFMEA was developed for healthcare as a variant of this approach adapted to the clinical setting; unlike the classic RPN model, it utilizes an S×P risk score and a decision tree.

The risk management process was organized into five blocks: risk analysis, risk assessment, risk control, residual risk assessment, and post-production monitoring.

The HFMEA analysis, developed by the U.S. Department of Veterans Affairs (VA) National Center for Patient Safety, consists of 5 main steps (Figure 4).

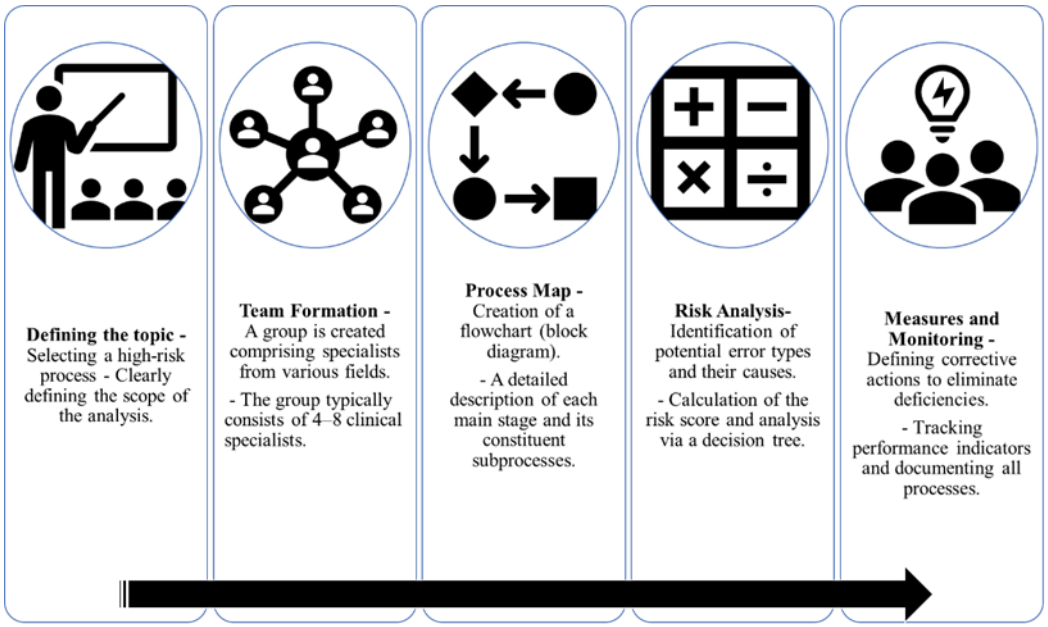


Fig. 4. The 5 main stages of HFMEA analysis

The main ventilation parameters of the ventilator—VT, RR, PEEP, PIP, and FiO2—were designated as the object of study, while electrical supply and general infrastructure risks were left outside the scope of this work.

The team included an anesthesiologist-reanimatologist, a head nurse, a biomedical engineer, a metrologist, a service engineer, and a representative from the quality management department (Table 2).

Table 2

Risk matrix according to the ISO 14971 standard and the official HFMEA guide

Probability \ Severity	Light	Medium	Serious	Fatal
Rarely	1	2	3	4
Sometimes	2	4	6	8
Often	3	6	9	12
Frequently	4	8	12	16

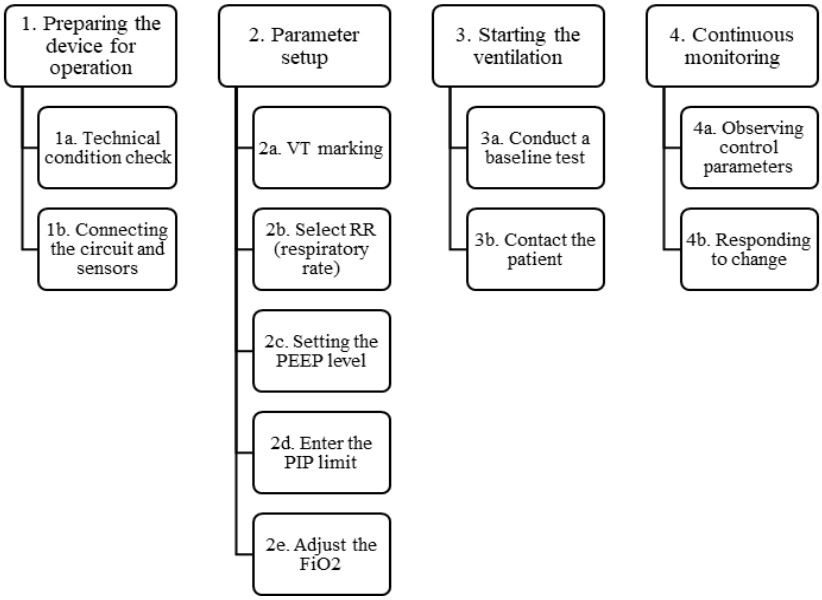


Fig. 5. Flowchart of the clinical process for using the ALV apparatus

The process map included the stages of preparing the device for operation, setting parameters, starting the ventilation, and continuous monitoring.

A 4×4 matrix was used for the risk assessment, based on severity and probability indicators.

The risk score was calculated using the formula R=S×P.

Subsequently, each risk was evaluated using a four-question HFMEA decision tree, and control measures were developed where necessary.

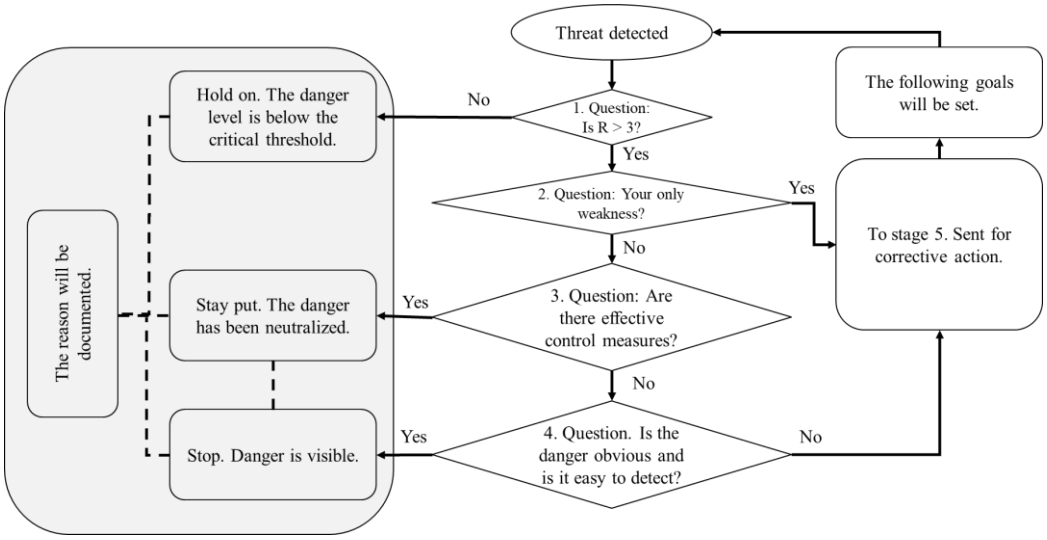


Fig. 6. HFMEA Stage 4: Risk Assessment Decision Tree — a 4-Question Filtering Algorithm

3. Results and discussion

We will begin the risk analysis for the five main parameters of the ALV apparatus, in accordance with Appendix 1, by defining the topic and forming the team.

https://doi.org/10.56143/3030-3893-2026-3-96-104

Step 1: Select and define the boundaries of the process to be examined.

Process selection criteria: Processes are identified where human factors may contribute to process or system vulnerabilities. Examples include communication errors, inadequate training, staffing issues, problems with shift handovers, and obstacles such as unclear rules/procedures.

HFMEA (process/equipment/system to be examined):

Evaluation, using the HFMEA method, of potential failure modes that may occur during the process of setting, adjusting, and monitoring the main ventilation parameters—VT, RR, PEEP, PIP, and FiO2—of an artificial lung ventilation (ALV) device (e.g., Dräger SAVINA 300), their clinical consequences, and the constructive, software, and organizational control measures. The HFMEA results are used as the basis for the ISO 14971 risk management file and the technical condition index (Ht).

Scope of the topic:

The analysis focuses on the main clinical parameters of the ALV apparatus (VT, RR, PEEP, PIP, FiO2). Risks related to the power supply, gas sources, and general infrastructure will be considered in separate projects. The method is applied as a common platform for all essential medical equipment (monitoring systems, ECG, ultrasound, endoscopes, laboratory analyzers).

Step 2. Team formation.

Table 3

Composition of the Risk Identification and Assessment Team

Position	Specialty / Area of Expertise
Anesthesiologist-Reanimatologist	Clinical process and outcomes
Senior Nurse (ICU / Resuscitation)	Practical use, operating procedure
Biomedical Engineer (BME) – HFMEA Coordinator	Technical specifications, service, ISO 14971
Metrologist – Calibration Department	MSA, GRR, measurement system analysis
Service Engineer	Ventilator and monitoring technical service
Quality Management Department Representative	ISO 13485, ISO 9001, QMS integration

A complete map of the clinical process for using the mechanical ventilator was created for Stage 3 of the HFMEA (Figure 4). According to the requirements of the VA NCPS HFMEA Guidebook (2021), the process map must sequentially reflect all sub-steps of the process being analyzed, show the connection between each step, and serve as the basis for the subsequent Stage 4 (hazard analysis). The created map includes four main stages: (1) preparing the ventilator for operation—technical status check (1a) and connecting the circuit and sensors (1b); (2) setting the parameters—sequentially defining the tidal volume VT (2a), respiratory rate RR (2b), positive end-expiratory pressure PEEP (2c), peak inspiratory pressure limit PIP (2d), and fraction of inspired oxygen FiO2 (2e); (3) initiating ventilation—initial ventilator test (3a) and connecting to the patient (3b); (4) continuous monitoring—observing alarm parameters (4a) and responding to clinical changes (4b). The five sub-steps in Stage 2 (2a–2e) are the direct objects of the hazard analysis in the document and correspond to all the parameters (VT, RR, PEEP, PIP, FiO2) presented in Table 4.

According to the ISO 14971 standard, a complete, international-standard risk management scheme for an artificial lung ventilation (ALV) apparatus and its practical schedule are formulated as follows.

Based on the ISO 14971 standard, the ALV manual, and its technical passport, the responsible HFMEA group conducted an audit of the equipment's parameters, the results of which indicated a high risk across all indicators. Control measures were developed by the HFMEA group and implemented into the process (Table 4).

Table 4

Results of the preliminary audit of equipment parameters by the HFMEA team

Parameter	Risk type	Clinical outcome	P Probability	S - Seriousness	Risk Level	Control Measures
VT	Expiratory valve blockage	Lung rupture (Volotrauma)	**3**	**4**	High-risk	Strictly set the maximum volume limit via the software.
RR	Processor freeze	Respiratory arrest (Apnea, Asphyxia)	**2**	**4**	High-risk	A standalone timer activates the backup mode.

PEEP	Circuit disconnect	Alveolar collapse (Atelectasis)	**3**	**3**	High-risk	Provide a visual and 80 dB audible signal on the screen via a periodic pressure sensor.
PIP	Electronic sensor error	Lung barotrauma, pneumothorax	**3**	**3**	High-risk	Install a mechanical valve that operates even when the electronics are off.
FiO_2	Mixer valve rusted	Hypoxia, brain death	**3**	**4**	High-risk	Automatically calibrate the galvanic O2 cell each time the device is turned on.

Table 5

Risk Level According to Preliminary HFMEA Results

Risk level				
VT	RR	PEEP	PIP	FiO_2
12	8	9	9	12

As the table indicates, each evaluated parameter was found to have a "High Risk" level. In the next stage, a risk analysis is performed according to the algorithm in Figure 5.

Stage 4. The Risk Assessment Decision Tree. In Stage 4 of the HFMEA, each identified risk is evaluated using a four-question decision tree (Figure 5). Question 1: Is the Hazard Score R > 3? — If no, the risk is considered to be below the critical point, and the reason is documented. If yes — Question 2: Is this the single point of failure for the process? — If yes, the risk is sent directly to Stage 5 (corrective actions). If no — Question 3: Is there an effective control measure in place? — If yes, the risk is marked as under control and documented. If no — Question 4: Is the risk obvious and easy to detect? — If yes, the risk is considered detectable; if no, it is sent to Stage 5. This four-question filtering algorithm replaces the RPN = S × O × D formula from classical FMEA and allows for more precise prioritization for clinical processes.

Stage 5: Corrective actions and monitoring.

VT (lung rupture as a result of expiratory valve blockage). Control measure: "Design-based: strictly limit the maximum volume threshold via software."

• Analysis: Limiting the maximum VT at the device level physically restricts the maximum volume that can be delivered to the patient; therefore, the maximum energy for volotrauma is reduced, and the severe pneumothorax/rupture scenario becomes both less likely and shifts toward a relatively milder injury.

Therefore:

P: The probability of excessive pressure being applied due to a blockage is reduced.

S: Due to the design limit, mild barotrauma scenarios are more likely than the typical outcome of "severe lung rupture." The S=4 indicator can be re-evaluated as S=3.

RR (apnea, asphyxia resulting from processor freeze). Control measure: "Protection system: a self-acting timer activates the backup mode."

Analysis: An independent timer quickly detects when the processor fails and switches the ventilator to a backup mode; ventilation does not stop completely, even without staff intervention. This significantly reduces the clinical impact of this failure mode on the patient, but processor freezing can still occur.

Therefore:

S: instead of a scenario where ventilation stops completely, leading to death, short-term failure and restart are often observed; therefore, a reduction from S=4 to S=3 is justified.

PEEP (alveolar collapse due to circuit disconnection, atelectasis)

Control measure: "Information/signal: a visual signal on the screen and an 80 dB audible alarm, triggered by the periodic pressure sensor."

- Analysis: A strong audiovisual alarm immediately signals the staff member when the circuit is disconnected, which increases the likelihood of reconnection before atelectasis can develop; in HFMEA, this is typically considered a measure that reduces P.

Therefore:

- P: The probability of loss of control is reduced from P=3 to P=2.
- PIP (barotrauma, pneumothorax due to electronic sensor failure)
- Control measure: "Protection system: install a mechanical valve that functions even if the electronics fail."
- Analysis: The mechanical valve physically limits the maximum pressure and releases any excess pressure, even in the event of an electronic failure; this significantly reduces the peak inspiratory pressure (PIP) that can reach the patient.

Therefore:

P: While the frequency of sensor errors may not necessarily change, the number of incidents leading to barotrauma/pneumothorax will decrease sharply, reducing the risk from P=3 to P=2.

S: The spectrum of maximum clinical harm typically shifts from "severe barotrauma/pneumothorax" to "mild barotrauma, infrequent pneumothorax." As a result, S was re-evaluated from S=3 to S=2.

FiO2 (hypoxia, brain death due to mixer valve corrosion)

https://doi.org/10.56143/3030-3893-2026-3-96-104 A bridge between science and innovation

Control measure: "Design-related: automatic calibration of the galvanic O2 cell each time the device is turned on."

Analysis: Automatic calibration reduces the drift of the FiO2 sensor, lowering the probability of operating with an incorrect oxygen concentration; however, hypoxia can still occur if the mixer valve is mechanically blocked.

Therefore:

o P: The frequency of clinical hypoxia episodes associated with incorrect FiO2 delivery will decrease from P=3 to P=2.

o S: The risk of brain death or severe neurological deficit due to hypoxia theoretically remains, as the potential for mechanical mixer failure is not fully eliminated, staying at S=4.

As a result of applying control measures and conducting a repeat HFMEA by the HFMEA group, the highest risk level of R=12 was reduced to R=8, yielding the indicators shown in Table 6. These indicators will serve as the basis for determining the weight coefficient when calculating the equipment's technical condition index.

Table 6

Audit Results After the Application of Control Measures for Equipment Parameters by the HFMEA Group

Parameter	Risk type	Clinical outcome	P Probability	S - Seriousness	Risk Level
VT	Expiratory valve blockage	Lung rupture (Volutrauma)	**1**	**3**	**Low Risk**
RR	Processor freeze	Respiratory arrest (Apnea, Asphyxia)	**2**	**3**	**Moderate Risk**
PEEP	Circuit disconnection	Alveolar collapse (Atelectasis)	**2**	**3**	**Moderate Risk**
PIP	Electronic sensor error	Lung barotrauma, pneumothorax	**1**	**3**	**Low Risk**
FiO_2	Mixer valve rusted	Hypoxia, brain death	**2**	**4**	**High Risk**

The results presented in the table meet the criteria for residual risk acceptability in accordance with ISO 14971:2021, §7.4; the FiO2 parameter requires additional monitoring (§10.2).

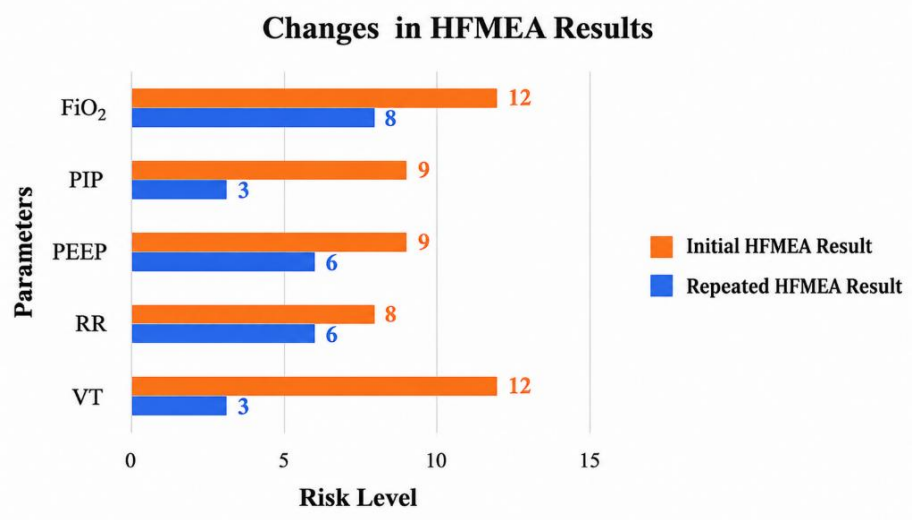


Fig. 7. HFMEA results after implementing control measures

Discussion

The results of this study indicated that for reducing risks associated with the primary measurement and control parameters of an ALV device, the HFMEA methodology is more adaptable and practically effective for a clinical setting compared to traditional FMEA. The main reason for this is that HFMEA is not limited to merely calculating risk scores; it also evaluates the clinical significance of the risk based on a decision tree, assesses the adequacy of existing control measures, and determines the presence of a single point of failure, which makes decision-making in intensive care settings considerably more precise.

The analysis results showed that not all parameters in the artificial lung ventilator (ALV) pose a threat through the same mechanism, and therefore, applying a uniform management approach is insufficient. For instance, the design and mechanical safety measures applied to the VT and PIP parameters reduced not only the probability of an incident but also the severity of harm to the patient, thereby lowering the residual risk for these parameters to a low level. For the RR and PEEP parameters, however, risk reduction was primarily achieved through alarms, backup modes, and monitoring mechanisms, which, while not completely

eliminating the risk, brought it down to a clinically manageable, moderate level.

The results obtained for the FiO2 parameter are particularly noteworthy, as this parameter retained a high residual risk despite automatic calibration measures. This indicates that malfunctions related to the mechanical mixer system, which forms the oxygen mixture, cannot be fully resolved by software or sensor-level corrections. Therefore, reducing the risk associated with FiO2 requires not only automatic calibration but also periodic metrological inspections, functional tests, shorter service intervals, and potentially the introduction of additional redundant control channels.

A key aspect of this research is that the HFMEA results were utilized not only as a descriptive summary but also as a quantitative basis for calculating the technical condition index. The approach of generating weighting coefficients from the residual risk scores of the parameters allows the overall technical reliability of the ALV apparatus to be expressed as a single numerical indicator, simplifying decision-making for service engineers, metrologists, and quality management specialists. Viewed from this perspective, this approach moves beyond simple risk analysis to become a management tool for prioritizing digital monitoring and service.

The study is also important from a practical implementation standpoint, as it clearly indicates which parameters should be prioritized for monitoring in mechanical ventilators. Specifically, it was proven that a parameter-oriented strategy for managing ventilator safety is more effective than a general preventive approach, because the VT and FiO2 parameters initially had the highest risk scores, while PIP and PEEP demonstrated a strong link between technical and clinical consequences.

However, the research has certain limitations. First, the analysis is confined to a single type of mechanical ventilator and five primary parameters, and does not fully encompass all risks related to the gas supply system, power failures, software interface errors, or user-related factors. Second, because some of the risk scores are based on expert evaluation, the results may differ to some extent when conducted by different teams. Third, the study did not incorporate real-time IoT monitoring or predictive technical diagnostics based on machine learning, which represents an important direction for future research.

Nevertheless, the obtained results have shown that it is possible to create a systematic, reproducible, and digitally adaptable risk management model for mechanical ventilators by integrating the requirements of HFMEA and ISO 14971:2021. This model is not limited to ventilators and can also be adapted for other medical equipment, such as monitoring systems, infusion pumps, defibrillators, and laboratory analyzers.

4. Conclusion

In this study, a risk analysis of the main clinical and measurement parameters of the ALV apparatus—VT, RR, PEEP, PIP, and FiO2—was systematically performed based on the HFMEA methodology and the requirements of the ISO 14971:2021 standard. The initial audit revealed that all five parameters fell into the high-risk zone, confirming the necessity of an in-depth, parameter-specific analysis when assessing the safety of ALV devices.

As a result of developing and implementing control measures, the risk for the VT and PIP parameters was reduced to a low level, and for RR and PEEP to a medium level, while the FiO2 parameter remained at a high residual risk. This result indicates that improving ventilator safety requires a differentiated approach tailored to the technical nature, clinical consequences, and detection characteristics of each parameter, rather than universal measures for all parameters.

Based on the research findings, the following scientific and practical conclusions can be drawn:

• The HFMEA methodology is an effective tool for identifying and prioritizing clinical risks in mechanical ventilators.

• The HFMEA model, when integrated with ISO 14971:2021, creates a complete management cycle, from risk identification to residual risk monitoring.

• A significant reduction in risk can be achieved when constructive, protective, informational, and metrological control measures are applied in accordance with the relevant parameters.

• In cases where a high residual risk remains, such as with the FiO2 parameter, enhanced metrological monitoring and periodic functional verification must be mandatory.

• Integrating residual risk scores into the technical condition index allows the overall safety status of the equipment to be assessed using a quantitative indicator.

From a practical standpoint, this approach can be applied to plan the servicing of ventilators used in resuscitation and intensive care units, prioritize preventive technical inspections, and establish the frequency of metrological control. Furthermore, it serves to create a unified decision-making platform for biomedical engineers, metrologists, and quality management departments.

For future research, it is advisable to expand this model to other medical equipment, integrate it with real-time IoT monitoring systems, introduce predictive failure analysis based on artificial intelligence, and validate the technical condition index. Therefore, parameter-oriented risk analysis using HFMEA is recommended as a promising scientific and practical solution for enhancing the operational safety of medical equipment, reducing the impact of human error and technical failures, and establishing a digital risk management system within healthcare institutions.

References

[1] Tase, A., Ni, M. Z., Buckle, P. W., & Hanna, G. B. (2022). Current status of medical device malfunction reporting: using end user experience to identify current problems. BMJ open quality, 11(2), e001849. https://doi.org/10.1136/bmjoq-2022-001849

[2] Baartmans, M. C., van Schoten, S. M., Schouten, B., van Eikenhorst, L., Hoeben, R. M., Asscheman, H., & Wagner, C. (2025). Adverse events involving medical devices in Dutch hospitals: A patient record review study. Health Policy and Technology, 14(5), 101063.

[3] U.S. Department of Defense. (1949, November 9). Procedures for performing a failure mode, effects and criticality analysis (MIL-P-1629). Department of the Navy. https://elsmar.com/FMEA/tsld011.htmelsmar

[4] Automotive Industry Action Group & Verband der Automobilindustrie. (2019). Failure mode and effects analysis (FMEA) handbook (1st ed.). AIAG.

https://soar.wichita.edu/entities/publication/4c0c22a0-51a5-4f71-842b-6b741fb1e9esoar.wichita+1

[5] International Organization for Standardization. (2021). Medical devices - Application of risk management to medical devices (ISO 14971:2021). ISO. https://www.iso.org/standard/72704.htmlscribd

[6] International Electrotechnical Commission. (2018). Failure modes and effects analysis (FMEA and FMECA) (IEC 60812:2018). IEC. https://webstore.iec.ch/publication/26359scribd

[7] SAE International. (2021). Potential failure mode and effects analysis in design (design FMEA), potential failure mode and effects analysis in manufacturing and assembly processes (process FMEA), and potential failure mode and effects analysis for machinery (machinery FMEA) (SAE J1739). SAE International. https://www.sae.org/standards/content/j1739_202101/scribd.

Information about the author

Khalililllo Abduvokhidov	Andijan State Technical Institute, Lecturer Email: khalililloabduvokhidov@gmail.com Tel: +998 93 787 44 66 https://orcid.org/0000-0001-8475-6259
Zafar Juraev	Andijan State Technical Institute, Professor Email: zbjuraev@gmail.com Tel: +998 93 442 42 30 https://orcid.org/0009-0008-5141-9916

Received: 13 July 2026 | **Accepted:** 24 August 2026 | **Published:** 30 September 2026

Analysis of artificial neural network applications for assessing the technical condition of traction transformers in electric locomotives

O.R. Khamidov[1][a], Sh.A. Samatov[1][b], B.I. Gayratov[1][c], A.K. Djuraev[1]
[1]Tashkent state transport university, Tashkent, Uzbekistan

Abstract: This paper presents a critical and systematic analysis of the scientific literature on assessing the technical condition of traction transformers of electric locomotives using artificial neural networks (ANN). Unlike earlier descriptive reviews, the analysis was carried out in three stages: chronological evolution of the directly relevant studies, classification of existing approaches according to Dasarathy's data fusion taxonomy, and critical evaluation of each study's methodological strengths and limitations, including constraints acknowledged by the original authors themselves. Nine studies dedicated directly to traction transformers of electric locomotives were identified. All of them operate within a single physical-domain parameter group and a single data-fusion level; their datasets are limited to one institution or one train type and are not publicly available. It is shown, both empirically and theoretically, that no existing approach fuses heterogeneous thermal, insulation, mechanical and electrical parameters at a level higher than single-domain feature fusion. The results provide a methodological foundation for developing a multi-parameter hybrid neural network model for traction transformer diagnostics.

Keywords: traction transformer, electric locomotive, artificial neural network, technical diagnostics, data fusion, condition assessment, dissolved gas analysis, vibration diagnostics, multi-parameter model

1. Introduction

Modernization of railway transport in the Republic of Uzbekistan is one of the priority areas of state policy. Traction transformers of electric locomotives are among the most important and expensive components of rolling stock, and their unexpected failure may lead to disruption of train schedules and a reduction in operational safety. Conventional diagnostic methods are performed according to fixed schedules regardless of the actual technical condition of the transformer, which increases the need for intelligent diagnostics based on artificial neural networks (ANN).

For a deeper theoretical understanding of the problem, it is appropriate to consider it from the perspective of data fusion theory. According to the taxonomy proposed by Dasarathy [10], fusion processes are divided into data, feature, and decision levels depending on the input–output abstraction level. Assessing the condition of a traction transformer using sources with fundamentally different physical characteristics and sampling frequencies, such as thermal, insulation, mechanical, and electrical parameters, is not simply a matter of adding more inputs; rather, it is a theoretically complex fusion problem that requires the integration of heterogeneous data.

The aim of this paper is to systematically analyze studies in which ANNs have been applied to traction transformer diagnostics, classify them according to the Dasarathy taxonomy, and substantiate the existing research gap from both theoretical and empirical perspectives.

2. Research methodology

The literature search was conducted in IEEE Xplore, MDPI, Springer, ScienceDirect, and Google Scholar databases, covering the period from 2014 to 2024. The inclusion criteria were: the study had to focus directly on traction transformers, employ an artificial intelligence method, and be published in a peer-reviewed source. Initially, 18 candidate publications were identified; one was excluded from the analysis because it was officially retracted in 2025 due to unauthorized use of third-party data, while nine publications concerned stationary transformers and were therefore mentioned only briefly as general context. The final in-depth analysis included nine studies directly related to traction transformers.

3. Results and Discussion

Ordering the selected studies by publication year reveals a clear evolutionary trend (Fig. 1). The early studies of 2014–2015 (Zhu et al.) employed relatively simple architectures, including wavelet neural networks and Gaussian-PSO. By 2021–2022, more sophisticated hybrid models, such as kernel PCA and multi-stage optimization (ISOA-SVM), had emerged. From 2023 onward, the research direction changed qualitatively, with a shift toward multi-label classification (Li et al.) and comprehensive reviews covering the entire traction system.

Classification based on the Dasarathy taxonomy (Table 1) shows that all four studies by the Zhu group [1–4] implement feature-level fusion (FEI-FEO); however, all input data belong to the same physical domain (thermal-chemical). The study by Li et al. [5] combines feature and decision levels, whereas the study by Lukovenko [9] represents the simplest case, directly combining two parameters at the data level. An important finding is that none of the analyzed studies integrates four parameter groups with fundamentally different physical characteristics at the feature or decision level.

[a] https://orcid.org/0000-0003-0821-5754
[b] https://orcid.org/0000-0002-4014-3845
[c] https://orcid.org/0009-0005-3957-337X

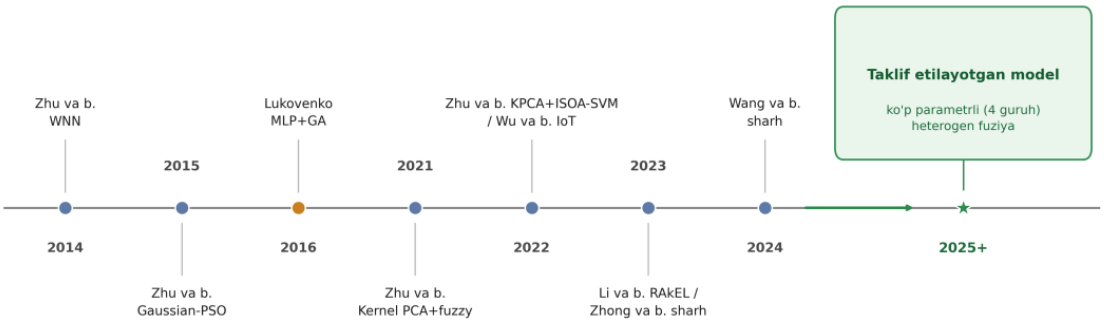


Fig. 1. Chronological evolution of ANN studies in traction transformer diagnostics

Table 1

Critical analysis of traction-transformer-related studies based on the Dasarathy taxonomy

№	Author, year	Method	Parameters	Results and limitations
1	Zhu et al., 2014 [1]	WNN	Diagnostic features	Demonstrated the feasibility of ANN for an onboard transformer; data source unclear
2	Zhu et al., 2015 [2]	Gaussian-PSO	Early fault indicators	Early-stage detection; dataset limited
3	Zhu et al., 2021 [3]	Kernel PCA + fuzzy	DGA, electrical tests	Nonlinear feature extraction; no publicly available data
4	Zhu et al., 2022 [4]	KPCA + ISOA-SVM	DGA, electrical parameters, oil quality	High accuracy; high computational complexity
5	Li et al., 2023 [5]	Improved RAkEL	BV, moisture, acidity, H_2, C_2H_2	93.62% accuracy; low AP (0.304), CRH5 only
6	Wang, Zhong [6;7]	Review articles	—	Systematizes the field; does not propose a new model
7	Wu et al., 2022 [8]	IoT monitoring	Real-time telemetry	Addresses the infrastructure problem; ANN not applied
8	Lukovenko, 2016 [9]	MLP + GA	Insulation resistance, temperature	Demonstrated the effect of two parameters; stationary object

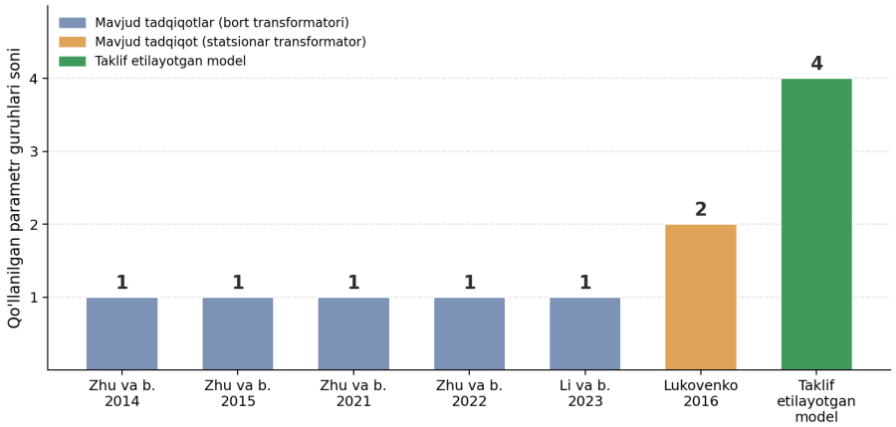


Fig. 2. Comparison of the number of parameter groups used

Table 2

Comparison of existing studies and the proposed approach

Aspect	Existing studies	Proposed model
Number of parameter groups	Maximum of 2	4 (thermal + insulation + mechanical + electrical)
Fusion level (Dasarathy)	Feature/data level, within the same domain	Feature + decision, across heterogeneous domains
Object	Mixed (some are stationary)	Onboard traction transformer only
Output format	Binary / multi-label indication	4-class condition + health index (HI)
Mathematical formalization	Limited or absent	Complete (27 equations)

Important methodological findings were also identified. Li et al. [5] explicitly acknowledge that the Average Precision of their models is relatively low in absolute terms. Although this represents a good example of scientific transparency, it also indicates that multi-label classification remains an incompletely solved problem. Lukovenko [9] demonstrated that adding oil temperature changed the prediction error from 1.5–4.4% to 0–7.2%, providing additional evidence of the influence of a second parameter; however, this result is specific to a stationary object.

The existence of this research gap is not accidental: thermal/insulation parameters are measured periodically at low frequencies, whereas vibration/harmonic signals constitute a continuous high-frequency data stream. Synchronizing these two categories therefore requires a dedicated architecture. In addition, installing heterogeneous sensors onboard requires additional hardware and organizational coordination, which may constitute a practical barrier to experimental research.

Comparative Analysis

As shown in Table 2 and Fig. 2, the proposed model offers several advantages over existing studies:

- Complexity: integrates four heterogeneous parameter groups within a single model; none of the existing studies incorporates more than this;
- Object specificity: designed specifically for an onboard traction transformer of an electric locomotive (IEC 60310), rather than directly transferring methods developed for stationary transformers;
- Theoretical foundation: operates at a higher (feature + decision) level according to the Dasarathy taxonomy;
- Two-layer prediction: the neural network classifies the current condition, while a probabilistic (Weibull) model predicts the remaining useful life;
- Transparency: the results are compared with conventional methods and the 93.62% performance reported by Li et al. [5] using a clearly defined methodology.

4. Conclusion

This paper analyzed the scientific literature on ANN-based assessment of the technical condition of electric locomotive traction transformers using a three-stage methodology: chronological, theoretical-taxonomic, and critical analysis. Nine studies directly related to the topic

were identified, their methodological limitations were highlighted, and, based on the Dasarathy taxonomy, it was demonstrated that none of the existing approaches implements genuine heterogeneous multi-domain fusion. Both the empirical and the technical-methodological reasons for the identified research gap were discussed. These findings provide a solid scientific and theoretical foundation for designing, mathematically substantiating, and experimentally validating a multi-parameter hybrid model architecture.

References

[1] Zhu, J., Chen, T., & Fu, Q. (2014). The research and application of WNN in the fault diagnosis technology of electric locomotive main transformer. In 7th IET International Conference on Power Electronics, Machines and Drives (pp. 1–6). Manchester.

[2] Zhu, J., Chen, T., Fu, Q., & Cheng, S. (2015). Detection of early failures within traction transformers based on Gaussian-PSO. In 3rd International Conference on Electric Power Equipment — Switching Technology (pp. 488–491). Busan.

[3] Zhu, J., Li, S., & Dong, H. (2021). Running status diagnosis of onboard traction transformers based on kernel principal component analysis and fuzzy clustering. IEEE Access, 9, 121835–121844.

[4] Zhu, J., Li, S., Liu, Y., & Dong, H. (2022). A hybrid method for the fault diagnosis of onboard traction transformers. Electronics, 11(5), 762.

[5] Li, M., Zhou, X., Qin, S., Bin, Z., & Wang, Y. (2023). Improved RAkEL's fault diagnosis method for high-speed train traction transformer. Sensors, 23(19), 8067.

[6] Wang, H., Li, Y.-F., & Ren, J. (2024). Machine learning for fault diagnosis of high-speed train traction systems: A review. Frontiers of Engineering Management, 11, 62–78.

[7] Zhong, K., Wang, J., Xu, S., Cheng, C., & Chen, H. (2023). Overview of fault prognosis for traction systems in high-speed trains: A deep learning perspective. Engineering Applications of Artificial Intelligence, 126, 106845.

[8] Wu, Z., Zhang, Z., Wang, W., Xing, T., & Xue, Z. (2022). Fault diagnosis algorithm of transformer and circuit breaker in traction power supply system based on IoT. Energies, 15(23), 8812.

[9] Lukovenko, A.S. (2016). Improving the reliability and quality of power supply to consumers of AC traction substations [Candidate's dissertation, KrIZhT — IrGUPS branch]. Krasnoyarsk.

[10] Dasarathy, B.V. (1997). Sensor fusion potential exploitation — innovative architectures and illustrative applications. Proceedings of the IEEE, 85(1), 24–38.

[11] Yusupov D.T, Qutbidinov O.M, Samatov Sh.A, Abdullaev E.S (2021). Investigation of factors influencing the operational characteristics of traction transformers. E3S Web of Conferences 274.

[12] Kutbidinov O. M. Yusupov D. T., Samadov Sh. A., Abdullaev E. S (2021). Experimental research of utilized oils of traction transformers. International Journal of Advanced Research in Science, Engineering and Technology. India.

[13] Yusupov D.T, Qutbidinov O.M, Samatov Sh.A, Abdullaev E.S (2021). Investigation of winding faults of traction transformers. Earth and Environmental Science.

[14] Kudratov, S., Yusufov, A., Khamidov, O., & Samatov, S. (2025, July). Diesel locomotives-Fault analysis and problem solving. In AIP Conference Proceedings (Vol. 3256, No. 1, p. 060013). AIP Publishing LLC.

[15] Gayratov, B., Khamidov, O., Kudratov, S., & Samatov, S. (2026, May). The ANFIS anticipation of diesel locomotive engine on the improvement of lubricating oil analysis. In AIP Conference Proceedings (Vol. 3447, No.1, p. 040008). AIP Publishing LLC.

[16] Kulmanov, B., Grachev, V., Ergashev, O., & Kudratov, S. (2025). Improving the technical and economic performance of diesel engines for shunting locomotives. Vibroengineering Procedia, 60, 339-344.

[17] Khamidov, O. R., Kudratov, S. I., Turdimurodov, B. C. U., & Norbotayeva, M. C. Q. (2024, March). Improvement of diagnostics and analysis of malfunction of the crankshaft of locomotive power plants. In AIP Conference Proceedings (Vol. 3045, No. 1, p. 050030). AIP Publishing LLC.

Information about the author

Khamidov Otabek	Toshkent davlat transport universiteti “Lokomotivlar va lokomotiv xo‘jaligi” kafedrasi professori E-mail: otabek.rustamovich@yandex.ru Tel.:+99890 811 21 00 https://orcid.org/0000-0003-0821-5754
Shakhboz Samatov	Toshkent davlat transport universiteti “Lokomotivlar va lokomotiv xo‘jaligi” kafedrasi katta o‘qituvchisi E-mail: shaxbozbek4089525@gmail.com Tel.:+99894 408 95 25 https://orcid.org/0000-0002-4014-3845
Bakhodir Gayratov	Toshkent davlat transport universiteti “Lokomotivlar va lokomotiv xo‘jaligi” kafedrasi tayanch doktoranti E-mail: bgayratoff@gmail.com Tel.:+99894 134 54 27 https://orcid.org/0009-0005-3957-337X
Abbos Djuraev	Toshkent davlat transport universiteti “Lokomotivlar va lokomotiv xo‘jaligi” kafedrasi tayanch doktoranti Tel.:+99888 854 40 00

Journal Engineer ISSN: 3030-3893 Volume:4| Issue:3| 2026

Received: 13 July 2026 | **Accepted:** 24 August 2026 | **Published:** 30 September 2026

Concrete based on low-strength carbonate rocks

I. Makhamataliev[1][a], V. Soy[1][b], N. Mukhammadiev[1][c], F. Abdukayumov[1], N. Erdanov[1], Sh. Uzakov[1], A. Jumageldiev[1]

[1]Tashkent state transport university, Tashkent, Uzbekistan

Abstract: The patterns of formation of the main technical and operational characteristics of concrete produced on the basis of carbonate rocks and modified with various chemical additives have been established. The study considered the effect of the superplasticizer Glenium®51 and the hydrophobic-plasticizing additive SDO on the properties and performance characteristics of concrete mixtures and hardened concrete. The influence of the additives on the workability of concrete mixtures, strength characteristics, frost resistance, and the consumption of coarse aggregate and cement was investigated.

When using the SDO additive, the gravel content in the concrete compositions ranged from 0.9 to 0.7 m³. It was established that the introduction of an optimal amount of the SDO physicochemical modifier, equal to 0.03% of the cement mass, into vibroconcrete compositions with a cement content of 350 kg/m³ makes it possible to obtain concrete with a compressive strength of 35 MPa and a frost resistance grade of F150. The obtained results indicate that the optimal dosage of the SDO modifier for concrete compositions with a cement content of 350 kg/m³ is 0.03% of the cement mass, which ensures the required combination of strength and frost resistance characteristics.

It has also been established that concrete compositions containing the Glenium®51 superplasticizer make it possible to obtain concrete with a compressive strength of 35 MPa using vibration-free technology. The use of the superplasticizer contributes to improving the technological properties of the concrete mixture and provides the required strength characteristics without the need for vibration compaction. When the gravel content is reduced to 0.3–0.4 m³ per 1 m³ of concrete, the introduction of carbonate filler makes it possible to reduce cement consumption while maintaining the required performance characteristics of the concrete.

The conducted research made it possible to establish the optimal parameters of concrete compositions based on carbonate rocks, reduce the content of coarse aggregate, and optimize cement consumption. The obtained results confirm the effectiveness of using chemical modifiers and carbonate fillers for the production of concrete with improved technical and operational characteristics and contribute to the more efficient use of local raw materials in concrete production.

Keywords: carbonate rocks, crushed stone, concrete, superplasticizer, Glenium ®51, SDO, modifier, strength, frost resistance.

1. Introduction

Currently, great attention is being paid to the rational and integrated use of local mineral resources in construction, reducing the cost of construction projects, and the production and distribution of environmentally safe construction products. Due to the widespread distribution of sedimentary carbonate rocks in many regions of the Russian Federation, the task of their comprehensive use is relevant [3; 6]. The relatively low strength and high heterogeneity of the composition often complicate and limit the use of this environmentally friendly mineral raw material, including in concrete production as a large aggregate [2]. At the same time, the use of imported large aggregates leads to a significant increase in the cost of produced concrete and construction objects as a whole.

Research into the raw material base of Mari El Republic (RME) carbonate crushed stone shows its high heterogeneity not only in strength and density but also in mineralogical composition. Specifically, tests of RME carbonate rocks showed that their density can range from 1570 to 2710 kg/m³, and their compressive strength from 10 to 100 MPa. At the same time, the average compressive strength value in the cylinder does not exceed the 400 mark. The content of Mg (CO) 3 in carbonate rocks within a single deposit differs by tens of percent [4]. This hinders the use of local carbonate rocks in the production of lime, cement, and silicate products.

The research is aimed at finding ways to increase the efficiency of using RME carbonate rocks in concrete production. Taking into account the low strength of carbonate rocks, a hypothesis was formulated regarding the possibility of increasing their application efficiency in concretes by limiting the amount of carbonate crushed stone, provided that surface-active modifiers are additionally used to reduce the water demand of the concrete mixture and improve the structure of the concrete's mortar part [1; 5].

[a] https://orcid.org/0009-0006-9599-1776

[b] https://orcid.org/0009-0006-9599-1776

[c] https://orcid.org/0000-0002-2306-3317

2. Research methodology

The objective of the study was to study the influence of carbonate crushed stone and modifying additives (SDO and Glenium®51) on the formation of concrete's physical and technical properties—compression strength, water resistance, and frost resistance.

As a large filler, carbonate crushed stone from the RME Korkatovsky quarry was used in the form of a mixture of two fractions: 10-20 mm fractions - 60% and 5-10 mm fractions - 40% by mass, respectively. The mineralogical composition of the crushed stone used was characterized by the presence of 59% dolomite and 40% calcite. impurities within the range of 1% were represented by quartz and feldspar minerals. Natural quartz sand from the RME Studentovsky quarry with a modulus of 2.07 was used as a fine aggregate.

Previous studies have shown that with a maximum volume content of carbonate crushed stone close to 1.0 m^3 per 1 m^3 of concrete and reduced only by the size of the grain displacement coefficient of the coarse aggregate, the water resistance coefficient of the concrete decreases to a critical value of 0.8.

An analysis was conducted on the dependence of the concrete's water resistance coefficient on cement consumption within the range of 250 to 450 kg per 1 m^3 of concrete and the volume content of carbonate crushed stone, respectively, from 0.7 to 0.9 m^3. The water flow rate was selected experimentally and corresponded to the production of uniformly movable mixtures with a stiffness of 20 s. The water resistance of the concretes was evaluated using the softening coefficient based on the ratio of concrete compressive strength in the water-saturated state to concrete strength in the dry state.

As a result of the conducted experiment, concrete with a compressive strength of 25 to 45 MPa was obtained. All compositions demonstrated high water resistance within the range of 0.98-1.0.

The influence of reducing the gravel content from 0.9 to 0.7 m^3 per 1 m^3 of concrete in the presence of the SDO modifier from 0 to 0.06% of the cement mass on the properties of concrete obtained from uniformly mobile mixtures with a stiffness of 20 using the vibration compaction method at a vibration frequency of 50 Hz and an oscillation amplitude of 0.5 mm was investigated. Concrete mixtures were prepared in a laboratory vibro-mixer for 3 minutes. The SDO supplement was administered with isolation water. Samples—cubes measuring 100×100×100 mm—were molded from concrete mixtures. The physical and technical properties of the concretes were determined at 28 days of solidification under normal conditions.

At a constant cement flow rate of 350 kg/m^3, the influence of the content of carbonate crushed stone and the modifying additive SDO on the formation of concrete strength, capillary-open porosity, and frost resistance was studied. The influence of concrete composition on the formation of compressive strength Rcs, MPa, is presented in Table 1.

Table 1

Influence of concrete composition on compressive strength

№ experience	Experiment Matrix		Material consumption per 1 m^3 of concrete				Compression strength limit, R_{cs}., MP
	Gravel, m^3	SDO, %	Cement, kg	Gravel, kg	Sand, kg	Water ,litr	
1	0,9	0,06	350	1000	810	195	34,8
2	0,9	0,00	350	1000	810	210	34,1
3	0,7	0,06	350	780	1010	205	30,4
4	0,7	0,00	350	780	1010	220	28,8
5	0,9	0,03	350	1000	810	190	36,6
6	0,7	0,03	350	780	1010	210	31,8
7	0,8	0,06	350	890	910	195	35,8
8	0,8	0,00	350	890	910	210	34,0
9	0,8	0,03	350	890	910	200	36,4

It has been established that the surface-active modifier SDO in an amount of 0.03% reduces the water requirement of uniformly mobile concrete mixtures by an average of 5%. Further increasing the amount of the added additive to 0.06% of the cement mass slightly reduces water demand. In the absence of the SDO modifier, a decrease in the volume content of carbonate crushed stone from 0.9 to 0.7 m^3 per 1 m^3 of concrete leads to a decrease in the strength of the compositions from 34 MPa to 28.8 MPa. The introduction of the SDO additive contributes to a 5-7% increase in the strength of the compositions. The reduction of the volume content of carbonate crushed stone to 0.7 m^3 per 1 m^3 of concrete is recognized as statistically significant for the compressive strength limit of concrete modified with SDO with a 95% confidence level.

The influence of the SDO modifier and the volume content of crushed stone at a cement consumption of 350 kg/m^3 on concrete frost resistance was determined using the accelerated structural-mechanical method in accordance with GOST 10060.4-95. At the same time, capillary open porosity and the strength increase coefficient of concrete during single freezing in a water-saturated state were monitored.

It has been established that across the entire range of gravel content variations, the modifier SDO in an amount of 0.03% of cement mass has the best effect on reducing the volume of capillary open pores in concrete. Thus, with a constant volume content of 0.9 m^3 of crushed stone per 1 m^3 of concrete, the presence of a 0.03% SDO additive from the cement mass reduces the capillary-open porosity of the

concrete from 14.4% to 13.4%. An increase in SDO content to 0.06% does not lead to a further decrease in capillary open porosity.

Figure 1 shows the dependence of concrete frost resistance on the content of carbonate crushed stone and the amount of SDO modifier.

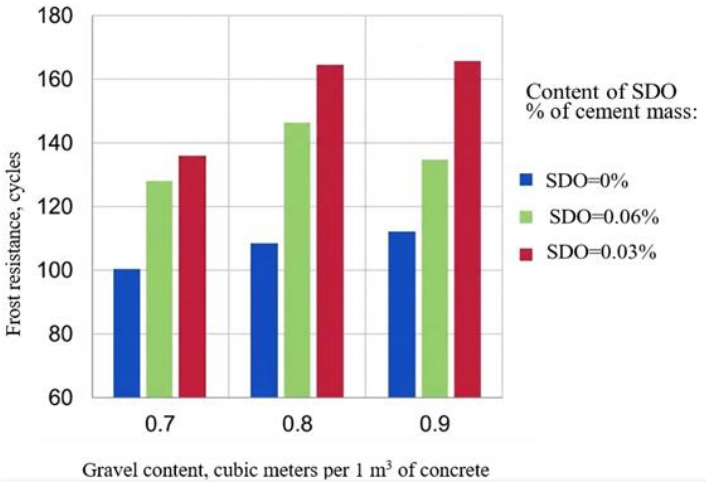


Fig. 1. Dependence of concrete frost resistance at a constant cement consumption of 350 kg/m^3 on carbonate crushed stone consumption and the content of SDO additive

Based Analysis of the influence of crushed stone and SDO modifier content on frost resistance showed that a rational SDO modifier content of 0.03% of cement mass with a rational crushed stone content of 0.8-0.9 m^3 increases concrete frost resistance from grade F100 to grade F150. Comparison of the data shows that the increase in concrete compressive strength is consistent with the results of determining its frost resistance and capillary-open porosity.

Self-compacting concrete mixtures are manufactured using compositions containing no more than 0.5 m^3 of coarse aggregate per 1 m^3 of concrete. Within the framework of vibration-free technology for self-compacting concrete mixtures in the presence of the Glenium®51 superplasticizer based on polycarboxylate ether, the influence of reducing the carbonate gravel content from 0.5 to 0.3 m^3 per 1 m^3 of concrete on its strength formation was investigated. The following were selected as variable factors in the experiment: the content of carbonate filler and the content of 5-10 mm fraction carbonate crushed stone.

Carbonate filler with a specific surface area of 350 m^2/kg was obtained by grinding siftings from the crushing of carbonate rocks. At the same time, the calculation of the introduced amount of carbonate filler was performed based on the condition that the total content of cement and mineral filler (C+H) in the mixtures was 540 kg per 1 m^3 of concrete. Based on this, the content of mineral filler in the studied compositions ranged from 30 kg to 170 kg per 1 m^3 of concrete. Crushed stone was added in an amount of 30-50% of the bulk volume. Based on preliminary tests, the content of the Glenium® 51 superplasticizer in all compositions was taken as 2% of the total weight of the cement and carbonate filler. The compressive strength limit of concrete was determined by testing 100*100*100 mm cube samples after they had solidified for 28 days under normal conditions.

The results of the compression strength study for self-compacting concrete are presented in Figure 2.

Analysis of the obtained results showed that the effect of partially replacing cement with carbonate filler is advisable when the gravel content is within the range of 30-40%. For these compositions, the use of carbonate filler contributes to cement savings. Overall, it has been established that concrete compositions with carbonate filler, when Glenium® 51 superplasticizer is added to the formula in an amount up to 2% of the total mass of cement and carbonate filler, allow for the production of concrete with a compressive strength of 34 to 46 MPa using vibration-free technology.

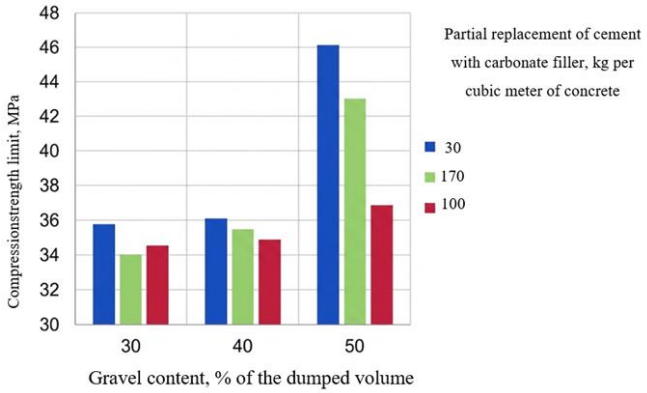


Fig. 2. Effect of partial replacement of cement with carbonate filler on the strength of self-compacting concrete

https://doi.org/10.56143/3030-3893-2026-3-109-112

3. Conclusion

It has been established that concrete on carbonate crushed stone, with its content in the concrete within the range of 0.9 to 0.7 m^3, has water resistance. From the perspective of forming strength and frost resistance at a constant cement consumption of 350 kg, concrete compositions containing 0.03% SDO and at least 0.8 m^3 of carbonate gravel per 1 m^3 of concrete are recommended.

Self-compacting concrete compositions that are economical in terms of cement consumption can be obtained based on the Glenium® 51 superplasticizer and carbonate filler with a volume content of carbonate crushed stone within 0.4-0.3 m^3 per 1 m^3 of concrete.

References

[1] Admixtures in Concrete: Technical Catalog; November 2009. Moscow: BUSF Construction Chemicals, 2009. 136 p.

[2] Zozulya, P.V. Carbonate rocks as aggregates and fillers in cements, cement mortars and concretes [Electronic resource]. Articles – Giprotsement-Nauka [website]. CJSC "RIC Giprotsement-Nauka". Available at: http://www.giprocement.ru/about/articles.html/p+25 (accessed October 6, 2009).

[3] Kononova, O.V., Cherepov, V.D., Soldatova, E.A. On the integrated use of local raw material resources. In: Proceedings. Abstracts of the 62nd Republican Conference on Architecture and Construction. Kazan: Kazan State University of Architecture and Engineering, 2010. P. 144.

[4] Explanatory Note to the Overview Map of Construction Materials Deposits of the Mari ASSR. Compiled by M.D. Sycheva, A.I. Belyanina, A.V. Grishanina. Moscow: Geological Fund of the Russian Federation, 1984. 127 p.

[5] Sinayko, N.P. New self-compacting concrete. Relanorm admixtures and testing equipment. Budivelni Materialy, Viroby ta Sanitarna Tekhnika, 2011, No. 39, p. 95.

[6] Shelikhov, N.S., Rakhimov, R.Z. Integrated use of carbonate raw materials for the production of construction materials. Construction Materials, 2006, No. 9, pp. 42–44.

Information about the author

Irkin Makhamataliev	Tashkent State Transport University, Doctor of Technical Sciences, Professor of the Department of "Building and industry facilities construction" Phone.: + 998908066545 E-mail: erkinmah@mail.ru https://orcid.org/0009-0006-9599-1776
Vladimir Soy	Tashkent State Transport University, Doctor of Technical Sciences, Professor of the Department of "Building and industry facilities construction" Phone.: + 998909521576 E-mail: volodya_tsoy@inbox.ru https://orcid.org/0009-0006-9599-1776
Nematjon Mukhammadiev	Head of the department of "Building and industry facilities construction", Tashkent State Transport University, DSc Phone.: + 998909111106 https://orcid.org/0000-0002-2306-3317
Farrukh Abdukayumov	Tashkent State Transport University PhD student of the Department of "Building and industry facilities construction" Phone.: + 998773367879 E-mail: fabduqayumov99@gmail.com
Nodirbek Erdanov	Director of the "Construction of Transport Networks" Unitary Enterprise, a part of the "Uztemiryolqurilishmontaj" Unitary Enterprise
Sherbek Uzakov	Tashkent State Transport University, PhD, Acting Associate Professor of the Department of "Building and industry facilities construction" Phone.: + 998998905427 E-mail: uzakosherbek9@gmail.com
Aziz Jumageldiev	Tashkent State Transport University, Assistant of the Department of "Building and industry facilities construction" Phone.: + 998914077060 E-mail: jumageldiyevaziz@gmail.com

Received: 13 July 2026 | **Accepted:** 24 August 2026 | **Published:** 30 September 2026

Investigation of ionizing radiation-induced conductivity and relaxation kinetics in porous polymer and metal-oxide nanocomposites

S.A. Cavadov[1][a]

[1]Azerbaijan State Oil and Industry University, Baku, Azerbaijan

Abstract: This paper investigates the optimization of electrophysical properties, the formation of radiation-induced conductivity, and the relaxation kinetics of dielectric and semiconductor nanoparticles in porous polymer (PMMA) and metal-oxide (Al_2O_3) matrix nanocomposite materials under ionizing radiation. The system of Rose–Fowler–Nikolsky (RFN) integro-differential equations is formulated for both continuous and discrete spectra of localized states within the bandgap. The trap density of states function in the interphase transition zones is modified as a function of nanoparticle radius (R) and volume concentration (C). Non-stationary relaxation processes were numerically simulated in MATLAB using the ode15s solver algorithm for stiff differential equations. The kinetics of radiation-induced conductivity (σ_r) reaching its steady-state value, trap-filling dynamics, and the dose-rate (I) dependence of thermally stimulated luminescence (TSL) were determined. Decreasing the nanoparticle radius from $R = 50$ nm to $R = 15$ nm increased the interphase boundary area, thereby reducing steady-state radiation conductivity by a factor of 2.8. The modeling results were compared with experimental current-voltage characteristics (I-V) and TSL spectra of synthesized nanocomposite samples with a thickness of $d = 100$ μm, demonstrating high adequacy and close agreement.

Keywords: solid-state electronics, nanocomposites, Rose–Fowler–Nikolsky model, MATLAB simulation, radiation-induced conductivity, relaxation kinetics, interphase, ode15s

1. Introduction

In modern micro- and nanoelectronics and the materials science of radio-electronic components, porous and heterogeneous nanocomposites represent a vital platform for the development of radiation-hardened electronic elements, extreme-environment sensors, and ionizing radiation dosimeters. When nanoscale inclusions are embedded into a dielectric (e.g., poly(methyl methacrylate) – PMMA) or wide-bandgap semiconductor/dielectric (e.g., aluminum oxide – Al_2O_3) matrix, the electrophysical and radiation-induced conduction characteristics of the system are governed not only by the bulk parameters of the phase constituents, but predominantly by the energetic distribution of localized traps residing within the matrix–particle interphase transition zones.

Although the classical models of photoconductivity and radiation-induced processes proposed by Rose [1] and Fowler [2] elucidate the conductivity of polymer dielectrics under ionizing radiation fields, nanostructured systems require further theoretical refinement to account for the crucial role of the interphase layer, as highlighted by Tyutnev et al. [3, 9]. The kinetics of generation, drift, trap capture, and recombination of free electron-hole pairs formed in the matrix and inclusions during ionizing irradiation have been investigated in various studies [4, 5, 12, 14]. The high specific surface area characteristic of nanoparticles and porous structures [6, 7, 10, 13, 15] leads to the emergence of interfacial potential barriers and a sharp increase in the effective trap concentration. Radiation tolerance and charge accumulation mechanisms in nanodielectrics [11] are of paramount importance for advanced electronic devices.

The general physical mechanism encompassing charge carrier generation, drift, trapping at interphase localized states, and the resulting buildup of radiation-induced conductivity under ionizing radiation is illustrated conceptually in Figure 1.

[a] https://orcid.org/0009-0005-9528-6770

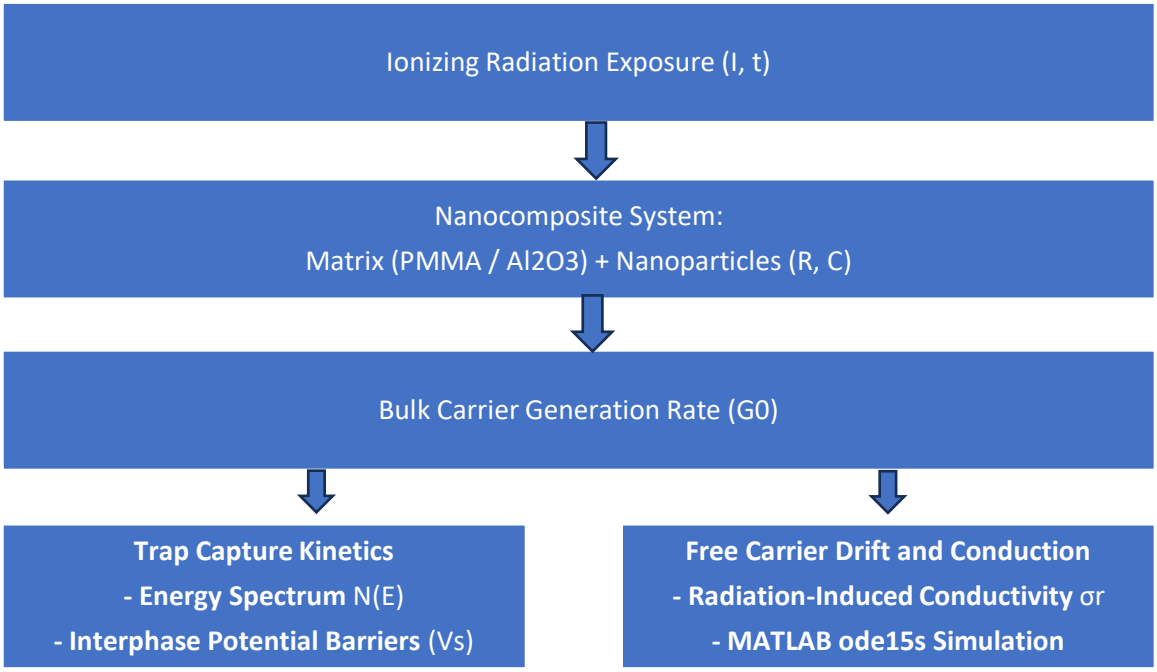


Fig. 1. Conceptual physical block diagram of charge carrier generation, trapping, and conduction kinetics in nanocomposite materials under ionizing radiation

2. Research methodology

2.1. Spectrum of Localized States and Kinetic Equations

Embedding nanoparticles of radius R and volume concentration C into a dielectric matrix induces localized charge redistribution at the matrix–nanoparticle boundary. The total density of localized states $N(E)$ in the matrix is formulated as the superposition of the intrinsic matrix traps and the induced interphase traps:

$$N(E) = N_{\text{mat}}(E) + N_{\text{int}}(E, R, C) \quad (1)$$

Where:

- $N(E)$ is the total density of localized states (traps) within the bandgap ($\text{m}^{-3} \cdot \text{eV}^{-1}$);
- $N_{\text{mat}}(E)$ is the trap density arising from intrinsic defects of the pure dielectric/semiconductor matrix;
- $N_{\text{int}}(E, R, C)$ is the density distribution function of localized traps created in the interphase transition zone upon nanoparticle introduction;
- E is the energy depth measured from the bottom of the conduction band (eV);
- R is the average radius of the nanoparticles (m);
- C is the volume concentration of the nanoparticles.

The continuous exponential spectrum $N_{\text{mat}}(E)$ originating from intrinsic matrix defects is defined as:

$$N_{\text{mat}}(E) = \frac{N_{t0}}{kT_0} \exp\left(-\frac{E}{kT_0}\right) \quad (2)$$

Here, N_{t0} is the total initial trap concentration in the pristine matrix (m^{-3}), T_0 is the effective characteristic temperature parameter describing the exponential energy distribution (K), and k is the Boltzmann constant (1.38×10^{-23} J/K).

The density of interphase localization centers $N_{\text{int}}(E, R, C)$ induced by the inclusions is directly proportional to their specific surface area [6, 13]:

$$N_{\text{int}}(E, R, C) = \frac{3C}{R} \cdot \delta \cdot \delta(E - E_d) \quad (3)$$

Where δ is the effective thickness of the interphase layer (m), E_d is the discrete activation energy level of the interphase centers formed at the nanoparticle boundaries (eV), and $\delta(E - E_d)$ is the Dirac delta function.

Under ionizing radiation, the bulk carrier generation rate G_0 is determined by accounting for the mass energy-absorption coefficients of the constituent matrix and inclusion phases:

$$G_0 = \frac{P_a}{E_p} = \frac{I}{E_p}\left[(1 - C)\mu_m + C\mu_{np}\right]\rho \quad (4)$$

Where:

- G_0 is the bulk electron-hole pair generation rate ($\text{m}^{-3} \cdot \text{s}^{-1}$);
- P_a is the radiation power absorbed per unit volume (W/m^3);
- I is the ionizing radiation dose rate (Gy/s);
- E_p is the mean energy required to create one free electron-hole pair ($E_p \approx 3E_g$);
- μ_m and μ_{np} are the mass absorption coefficients of the matrix and nanoparticles, respectively (m^2/kg);
- ρ is the material density (kg/m^3).

In the non-stationary regime, the kinetics of free electrons (n), trapped electrons (n_t), and holes (p) are described by the Rose–Fowler–Nikolsky system of differential equations [3, 5, 9]:

$$\begin{cases} \frac{dn}{dt} = G_0 - C_n n(N_t - n_t) + \nu_0 n_t \exp\left(-\frac{E_t}{kT}\right) - R_r np \\ \frac{dn_t}{dt} = C_n n(N_t - n_t) - \nu_0 n_t \exp\left(-\frac{E_t}{kT}\right) - R_{rt} n_t p \\ p(t) = n(t) + n_t(t) \end{cases} \quad (5)$$

Where:

- $n(t)$ is the time-dependent concentration of free electrons (m^{-3});

https://doi.org/10.56143/3030-3893-2026-3-113-117

- $n_t(t)$ is the time-dependent density of trapped electrons (m^{-3});
- $p(t)$ is the time-dependent hole concentration (m^{-3});
- C_n is the electron capture coefficient of the traps (m^3/s);
- N_t is the total effective trap density ($N_t = N_{t0} + N_{int}$);
- ν_0 is the thermal release frequency factor (attempt-to-escape frequency) (s^{-1});
- E_t is the trap activation energy (eV);
- R_r and R_{rt} are the recombination coefficients for free and trapped carriers, respectively (m^3/s).

2.2. Experimental and Measurement Methodology

- **PMMA/Al_2O_3 Nanocomposites:** Synthesized via *in-situ* polymerization of methyl methacrylate (MMA) monomer incorporated with 15--20 nm Al_2O_3 nanoparticles across a concentration range of 0.5--5.0 wt%. Ultrasonic dispersion at 40 kHz for 30 min was employed to ensure homogeneous particle dispersion.
- **Porous Al_2O_3 Matrix:** Fabricated via electrochemical anodization in a 0.3 M oxalic acid ($H_2C_2O_4$) electrolyte at $T = 10°C$ under an applied anodization potential of $U = 40$ V [10, 15].

Electrical and radiation measurements were conducted on samples with a thickness of $d = 100 \pm 5$ μm and an active silver-contact area of $S = 1.0$ cm^2. Radiation-induced conductivity was measured under ^{60}Co gamma (γ) radiation (0.1--10 Gy/s) using a Keithley 6517B electrometer/high-resistance meter. Thermally stimulated luminescence (TSL) spectra were acquired and interpreted according to the Randall–Wilkins trap model [4]. To ensure statistical validity, five identical samples were fabricated for each composition, and each measurement was repeated three times to determine mean values.

3. Results and Discussion

The modified Rose–Fowler–Nikolsky (RFN) system of differential equations (5) was solved numerically in MATLAB using the ode15s solver designed for stiff systems. The time-dependent drift radiation conductivity (σ_r) is related to the free electron density $n(t)$ via:

$$\sigma_r(t) = e \cdot n(t) \cdot \mu_0 \quad (6)$$

Where $e = 1.6 \times 10^{-19}$ C is the elementary charge, and μ_0 is the drift mobility of free electrons.

Numerical simulations reveal that the relaxation kinetics of radiation conductivity evolve through two distinct temporal regimes (Figure 2). During the initial non-stationary phase ($t < 10^{-6}$ s), a significant fraction of generated electrons is rapidly captured by localized interphase traps, resulting in dynamic conductivity growth. When dynamic equilibrium between generation, trapping, and recombination is established ($t \approx 10^{-6}$ s), the conductivity attains a steady-state value.

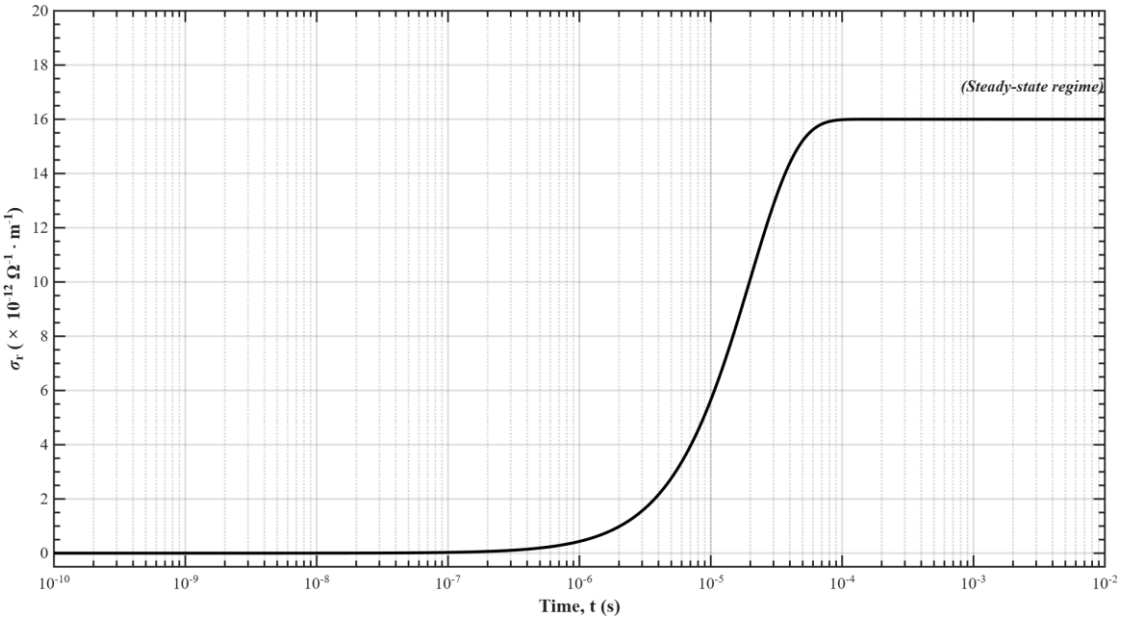


Fig. 2. Non-stationary relaxation kinetics of radiation-induced conductivity ($I = 1.0$ Gy/s, $T = 300$ K, $R = 15$ nm, $C = 3\%$, $d = 100$ μm). (Note: In the plot, the steady-state plateau is marked as "Steady-state regime" / "Stasionar rejim")

The filling kinetics of interphase traps (Figure 3) demonstrate that at $t \approx 10^{-3}$ s, the overwhelming majority of trap states become filled ($n_t \approx N_t$), causing the system to transition into a trap-filled saturation regime.

https://doi.org/10.56143/3030-3893-2026-3-113-117 A bridge between science and innovation

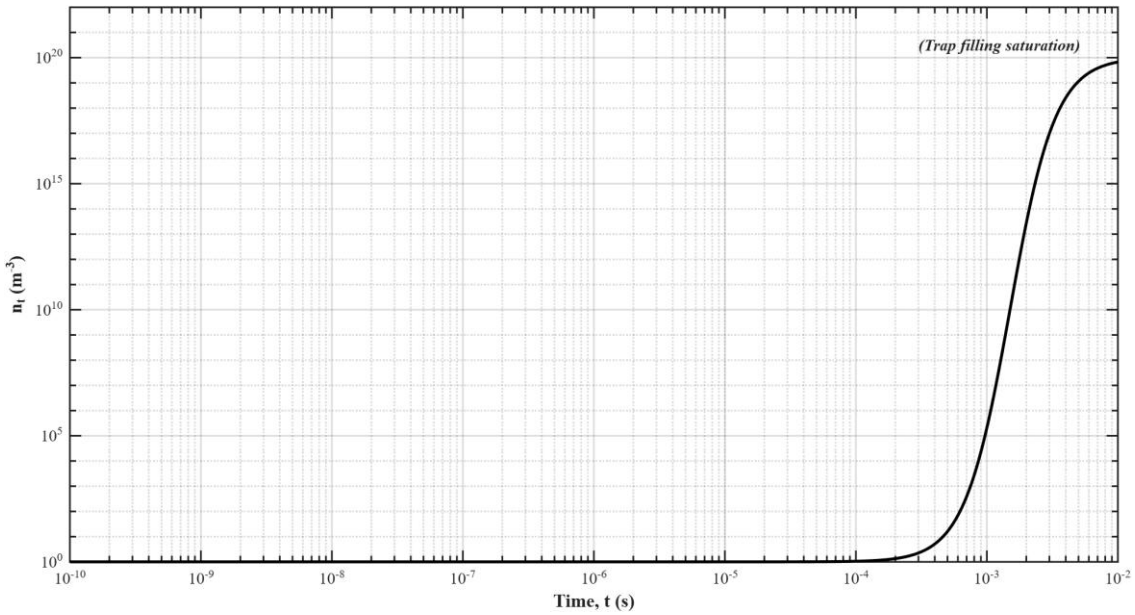


Fig.3. Electron trap-filling kinetics in interphase states ($I = 1.0$ Gy/s, $T = 300$ K, $R = 15$ nm, $C = 3\%$, $N_{int} \approx 10^{20}$ m^{-3}). (Note: In the plot, saturation is designated as "Trap filling" / "Tələlərin dolması")

Reducing the nanoparticle radius from $R = 50$ nm to $R = 15$ nm increases the specific surface area of the inclusions ($S_{sp} = 3C/R$) by approximately 3.3-fold. According to Eq. (3), the resulting increase in interphase trap density (N_{int}) significantly enhances the electron capture probability. MATLAB simulation outputs indicate that while the steady-state radiation conductivity is $\sigma_{r1} \approx 4.5 \times 10^{-11}\ \Omega^{-1} \cdot m^{-1}$ for $R = 50$ nm, it drops to $\sigma_{r2} \approx 1.6 \times 10^{-11}\ \Omega^{-1} \cdot m^{-1}$ for $R = 15$ nm. The ratio of these values ($\sigma_{r1}/\sigma_{r2} = 4.5/1.6 \approx 2.8$) demonstrates that the elevated interphase trap density achieved via nanoparticle downscaling reduces the steady-state radiation conductivity by exactly a factor of 2.8, thereby significantly improving the radiation hardness of the material.

To validate the numerical model, theoretical parameters were benchmarked against experimental I-V and TSL spectral data measured on 100 μm-thick PMMA/Al_2O_3 and porous Al_2O_3 samples (Table 1).

Table 1

Comparative analysis of theoretical and experimental results

Parameter / Indicator	**Theoretical (MATLAB Model)**	**Experimental Measurements**	**Relative Difference (%)**
PMMA-based Δ dose exponent	0.72	0.75 ± 0.02	4.0%
Al_2O_3-based Δ dose exponent	0.94	0.92 ± 0.03	2.1%
TSL Peak Temperature (T_{max})	520 K	512 K	1.5%
Steady-State Conductivity Relaxation Time	1.0×10^{-6} s	1.2×10^{-6} s	20.0%

As shown in Table 1, the model predictions exhibit close agreement with experimental data (within an error margin of 1.5%--4.0%). The 20.0% deviation observed in the relaxation time required to reach steady-state conductivity is attributed to the assumption of an ideally homogeneous matrix in the theoretical formulation. In real synthesized specimens, local electric field non-uniformities at micropore boundaries and energetic fluctuations of surface trap states induce slight kinetic delays (1.0×10^{-6} s theoretical vs. 1.2×10^{-6} s experimental) during the transition to the steady-state regime.

3. Conclusion

In porous polymer (PMMA) and metal-oxide (Al_2O_3) nanocomposites, the kinetics of charge carrier generation,

trapping, and recombination under ionizing radiation are strongly governed by the energetic spectrum of localized states within the matrix–nanoparticle interphase layer.

Numerical simulations carried out in MATLAB (ode15s) using the modified Rose–Fowler–Nikolsky model demonstrate that adjusting the nanoparticle radius (from $R = 50$ nm down to $R = 15$ nm) and volume concentration (C) increases interphase trap density, allowing steady-state radiation-induced conductivity to be suppressed by a factor of 2.8 and enhancing the radiation resistance of the material.

The simulation results correlate well with experimental I-V and TSL data, establishing a reliable theoretical and methodological foundation for predicting the electrophysical behavior of PMMA/Al_2O_3 porous nanocomposites in radiation environments and facilitating the engineering of radiation-hardened micro- and nanoelectronic components.

References

[1] Rose A. Concepts in Photoconductivity and Allied Problems. New York: Interscience Publishers, 1955, 168 p.

[2] Fowler J. F. X-ray induced conductivity in insulating materials. Proceedings of the Royal Society of London. Series A, 1956, vol. 236, no. 1207, pp. 464–480.

[3] Tyutnev A. P., Saenko V. S., Pozhidaev E. D., Kostyukov N. S. Dielectric Properties of Polymers in Ionizing Radiation Fields. Moscow: Nauka, 2005, 456 p. (in Russian).

[4] Randall J. T., Wilkins M. H. F. Phosphorescence and electron traps: I. The study of trap distributions. Proceedings of the Royal Society of London. Series A, 1945, vol. 184, no. 999, pp. 365–389.

[5] Khatipov S. A. Radiation-induced conductivity of polymers. Radiation Physics and Chemistry, 2001, vol. 60, no. 4–5, pp. 513–521.

[6] Cao G. Nanostructures and Nanomaterials: Synthesis, Properties and Applications. Imperial College Press, 2004, 448 p.

[7] Ibach H., Lüth H. Solid-State Physics: An Introduction to Principles of Materials Science. Springer Science & Business Media, 2009, 544 p.

[8] Elsgolts L. E. Differential Equations and the Calculus of Variations. Moscow: Nauka, 1974, 432 p. (in Russian).

[9] Tyutnev A. P., Ikhsanov R. S., Saenko V. S. Rose-Fowler-Nikolsky model revisited: numerical analysis and applicability limits. High Energy Chemistry, 2014, vol. 48, no. 6, pp. 423–429.

[10] Korotcenkov G. Porous Silicon: From Formation to Applications. CRC Press, 2016, vol. 1, 428 p.

[11] Poply A., Gupta M., Singh B. Radiation stability and dielectric behavior of nanocomposites: A review. Journal of Materials Science: Materials in Electronics, 2020, vol. 31, no. 12, pp. 9012–9028.

[12] Claeys C., Simoen E. Radiation Effects in Advanced Semiconductor Materials and Devices. Springer-Verlag, 2002, 420 p.

[13] Dang Z. M., Yuan J. K., Yao S. H., Tsubota T. Flexible nanodielectric materials with high permittivity for power energy storage. Advanced Materials, 2013, vol. 25, no. 9, pp. 1282–1294.

[14] Oldham T. R., McLean F. B. Total ionizing dose effects in MOS devices and circuits. IEEE Transactions on Nuclear Science, 2003, vol. 50, no. 3, pp. 483–499.

[15] Korotcenkov G., Cho B. K. Porous semiconductors: Synthesis, properties, and applications. Critical Reviews in Solid State and Materials Sciences, 2010, vol. 35, no. 3, pp. 153–178.

Information about the author

S.A. Cavadov

Azerbaijan State Oil and Industry University
Doctoral student of National Aerospace Agency
E-mail: sohrabcavadov2@gmail.com
Tel:+994103121307
https://orcid.org/0009-0005-9528-6770

Journal Engineer ISSN: 3030-3893 Volume:4| Issue:3| 2026

Received: 14 July 2026 | **Accepted:** 25 August 2026 | **Published:** 30 September 2026

Improving the reliability of the TD802 direct-current traction generator of the ChME3 shunting diesel locomotive through insulation replacement

O.R. Khamidov[1][a], Sh.A. Samatov[1][b], B.I. Gayratov[1][c], A.K. Djuraev[1][d]

[1]Tashkent state transport university, Tashkent, Uzbekistan

Abstract: This paper presents an analysis of the design and insulation system of the TD802 (TO802) direct-current traction generator installed on ChME3 shunting diesel locomotives operated on the railways of Uzbekistan, and substantiates a technology for improving its reliability through the replacement of that insulation. The study was carried out in three stages: an assembly-by-assembly analysis of the factory insulation system (armature winding, main and commutating pole coils, commutator, brush apparatus); identification of the physical mechanisms of insulation ageing and of their cumulative interaction; and development of a technological regulation for insulation replacement using modern heat-resistant materials. The proposed solution comprises vacuum-pressure impregnation (VPI) of the armature winding, replacement of asbestos gaskets with glass-mica and aramid-fibre materials, renewal of the commutator insulation, transition to a monolithic insulation system for the pole coils, and an upgrade of the insulation thermal class to H (180 °C). A quality-control procedure based on insulation resistance, absorption coefficient, polarization index, high-voltage testing, partial discharge monitoring and infrared thermography is proposed, together with a methodology for quantitative evaluation of the effect through the mean time between failures. It is shown that the proposed measures do not alter the design scheme of the machine and modernize only the insulating materials and the technology of their application, which makes them practically feasible at depot level.

Keywords: ChME3 shunting diesel locomotive, TD802 traction generator, insulation system, armature winding, vacuum-pressure impregnation, commutator, thermal ageing, insulation thermal class, reliability, mean time between failures

1. Introduction

Modernization of railway transport and improvement of the technical readiness of the traction rolling stock fleet are among the priority areas of state policy in the Republic of Uzbekistan. ChME3-series locomotives continue to occupy a significant share of the shunting locomotive fleet used for switching operations on the railways of Uzbekistan. These locomotives are equipped with a K6S310DR diesel engine rated at approximately 1350 hp, which converts mechanical energy into electrical energy through a TD802 traction generator — a ten-pole, self-ventilated direct-current machine with independent excitation rated at approximately 885 kW. The current produced by the generator is supplied to six TE-006 traction motors of 134 kW and 283 V each. The TD802 generator is therefore the central electrical machine of the locomotive traction system, and its technical condition directly determines the operational capability of the locomotive.

The majority of ChME3 locomotives have been in operation on the railways of Uzbekistan for more than 25–40 years. Over such an extended service period the electrical insulation system of the generator — in particular the armature winding, the main and commutating pole coils and the commutator insulation — gradually deteriorates under the combined effects of heat, vibration, moisture and mechanical loading. Depot maintenance experience shows that a substantial share of the unscheduled repairs of the TD802 generator is directly related to insulation faults: inter-turn short circuits, ground faults, and a drop of insulation resistance below the permissible threshold. Such failures usually occur unexpectedly and take the locomotive out of service for an extended period, since a complete generator rewind is a time- and resource-intensive operation.

The problem of maintaining the technical condition of locomotive equipment has been addressed in a number of studies. Intelligent and condition-based approaches to the diagnostics of traction electrical equipment have been developed for traction transformers and traction systems [1–7], including online monitoring architectures built on Internet of Things technologies [8]; the influence of insulation resistance and temperature on the condition of an electrical machine has been investigated using neural network models [9]. For diesel locomotives, fault analysis and diagnostic methods for power plant components have also been developed by the authors of this work [14–17]. However, these studies concentrate on the diagnostics of an existing insulation system rather than on the technology of its renewal, whereas for a machine that has been in service for several decades the decisive question is which materials the insulation is replaced with and by what technology.

For this reason, replacing the insulation system of the TD802 generator with modern materials and technologies, and thereby improving its reliability, is a matter of considerable scientific and practical importance for the railways of Uzbekistan. The aim of this paper is to analyze the factory insulation system of the TD802 generator, to identify the

[a] https://orcid.org/0000-0003-0821-5754
[b] https://orcid.org/0000-0002-4014-3845
[c] https://orcid.org/0009-0005-3957-337X
[d] https://orcid.org/0009-0007-2479-5134

causes of its deterioration, and to develop technological solutions for improving the reliability of the generator through the replacement of its insulation with modern heat-resistant materials.

The objectives of the study are as follows: to analyze the design and the factory insulation system of the TD802 generator for each major assembly (armature winding, main and commutating pole coils, commutator, brush apparatus); to substantiate the physical and technical mechanisms of insulation ageing; to develop a technological sequence for replacing the insulation with modern materials; to propose a methodology for quality control of the renewed insulation; and to assess the effect of the proposed solutions on the reliability and economic indicators of the machine.

2. Research methodology

The study was performed as an engineering-analytical investigation and is based on three groups of sources: the factory design documentation of the TD802 (TO802) generator, which provides the design dimensions of every assembly and the composition of its insulation; the regulatory documents governing the repair of locomotive traction electrical machines and the aggregated fault records of depot repairs, which make it possible to establish which assembly the insulation faults occur in; and the technical literature on traction electrical machines and on the diagnostics of locomotive equipment [1–17].

The analysis was carried out in three stages. In the first stage the factory insulation system was examined assembly by assembly — the main poles, the commutating poles, the armature core and winding, the commutator and the brush apparatus — and for each of them the insulating material, its method of application and its characteristic weak point were determined. In the second stage the physical mechanisms of insulation ageing (thermal, vibration, moisture and contamination, electrical, and mechanical wear) were identified, and their mutual reinforcement was evaluated rather than each factor being considered in isolation. In the third stage, on the basis of the weak points established in the first two stages, a technology for replacing the insulation with modern materials was developed, together with a technological regulation, a quality control procedure and a methodology for the quantitative assessment of the effect.

The criterion adopted for evaluating the effectiveness of the proposed solutions is the reliability of the generator in operation, expressed through the mean time between failures (MTBF) and the failure rate $\lambda = 1/\mathrm{MTBF}$, supplemented by the trend of the insulation resistance R60 and of the polarization index PI = R10/R1 recorded at successive inspections. A further condition imposed on the solution was that it must not require any change to the design scheme of the machine, so that it can be implemented within the existing depot repair process.

3. Results and Discussion

3.1. Design and factory insulation system of the TD802 generator

The TD802 generator (also referred to as TO802 in the factory documentation) is a ten-pole, self-ventilated direct-current machine with independent excitation and a starting winding. The generator frame is welded from steel sheet; one end is flange-mounted to the diesel engine housing, while the other is bolted to the locomotive frame by means of feet. The results of the assembly-by-assembly analysis of the factory insulation system are summarized in Table 1.

The generalized technical parameters of the generator and of the associated traction equipment are as follows: diesel engine — type K6S310DR, approximately 1350 hp; traction generator — TD802 (TO802), ten-pole, independently excited, self-ventilated, approximately 885 kW; traction motor — type TE-006, 134 kW, 283 V, six units per locomotive; auxiliary generator — type DT-701-4; exciter — type DT-706-4. These parameters determine the requirements placed on the insulation system, in particular the working voltage level and the current density, and must be taken into account when selecting insulating materials. The main dimensions of the commutator–armature assembly (a commutator diameter of 595 mm with 405 segments and 135 slots in the armature core) indicate that the machine operates at a relatively high surface speed at the commutator, which places particular demands on the commutator–brush assembly and the insulating elements adjacent to it: they must be resistant not only to electrical stress but also to mechanical and thermal loading.

Table 1

Factory insulation system of the TD802 generator by assembly and its characteristic weak points

№	Assembly	Factory insulation system	Characteristic weak point
1	Main poles (starting and independent excitation windings)	Riveted core of 1 mm electrical steel; 4 turns of 1×95 mm copper strip and ≈ 63.5 turns of 4.0×7.5 mm rectangular wire in eight stepped layers; layer-by-layer epoxy varnish coating	The varnish film becomes brittle under heat and vibration, cracks and delaminates — risk of inter-turn short circuits
2	Commutating poles (interpoles)	Coils of 2.2×50 mm copper busbar in two layers (5 and 4.5 turns, ≈ 9.5 turns in total); asbestos interlayer gaskets; coil filled with cast epoxy compound	Asbestos embrittles, accumulates dust, absorbs moisture and loses thermal conductivity; does not meet modern occupational safety requirements
3	Armature core and winding	Core of 0.5 mm varnished sheets, 135 slots, 72 ventilation holes; lap winding with equalizers, sections of six 2.8×9.0 mm conductors; five layers of mica tape in the slot and six layers of glass tape in the end portions; micanite sleeves	Multi-layer hand-applied insulation retains air voids between layers, which accelerates depletion of service life through partial discharges and moisture absorption

№	Assembly	Factory insulation system	Characteristic weak point
		and spacers; 2 mm steel wire banding, textolite wedges	
4	Commutator	Diameter 595 mm, 405 copper segments separated by 0.8 mm micanite spacers; risers silver-soldered; sleeve insulated by split-mica collars, clamped through a pressure ring	Mechanical wear together with the working surface and thermal cycling; the mica protrudes above the segments, causing poor brush contact and sparking — periodic undercutting required
5	Brush apparatus	Ten brush-holder yokes, five double brushes each (fifty double-brush positions); spring pressure 1.5–1.8 kgf; brush size 2(32×10×40) mm	Not an insulating element itself, but moisture and commutator dust penetrate through the brush-holder insulators and reduce the overall insulation resistance

3.2. Mechanisms of insulation deterioration

Under long-term operating conditions the factory insulation system described above deteriorates as a result of the following main factors:

– thermal ageing — the operating temperature of the generator, especially under high-load conditions, gradually breaks down the binding components of the insulating varnishes and of the mica tape; according to Montsinger's rule the insulation life is roughly halved for every 8–10 °C increase in operating temperature;

– vibration fatigue — locomotive motion and diesel engine vibration cause micro-movements between the insulation layers of the armature winding and of the pole coils, which leads to delamination;

– moisture and contamination — moisture and commutator dust entering the generator housing reduce the insulation resistance, particularly because asbestos gaskets and aged micanite readily absorb moisture;

– electrical ageing — partial discharges occurring in the air voids within the insulation layers gradually erode the insulating material from within;

– mechanical wear — wear of the commutator mica insulation together with the working surface, and accumulation of brush dust between the commutator segments, which results in surface tracking paths.

The combined effect of these factors causes the insulation resistance of the TD802 generator to fall below the normative threshold, which is typically required to remain above 1.5–2.0 MΩ, with the exact value specified in the depot regulatory documents; the machine may then be barred from operation or suffer an emergency shutdown.

Aggregated depot repair records allow the insulation-related faults of the generator to be grouped into three characteristic categories: inter-turn and ground faults in the armature winding, which occur mainly in the end windings owing to moisture accumulating under the banding; insulation breakdown in the pole coils, most often in the commutating pole coils, owing to embrittlement of the asbestos gaskets; and defects of the commutator insulation, namely undercutting problems and surface tracking paths between the segments. Each group has characteristic diagnostic signs, and recognizing them makes it possible to determine in advance which assembly requires particular attention during repair.

It should be emphasized that the ageing factors listed above do not act in isolation but reinforce one another. A contaminated ventilation system raises the internal temperature of the generator and thereby accelerates thermal ageing; thermally embrittled insulation cracks more readily under vibration; and cracked insulation admits moisture and dust more deeply, which accelerates electrical ageing through partial discharges. As a result of this chain reaction, the actual service life of the insulation is often considerably shorter than the theoretical value calculated from thermal ageing alone. This is precisely why insulation replacement must be approached comprehensively, taking all ageing factors into account together rather than addressing a single factor such as the heat-resistance class in isolation — this is the underlying logic of the solutions proposed below.

3.3. Technology for replacing the insulation

Replacing the generator insulation, whether partially or completely through rewinding, is a complex technological process carried out at the depot or at a repair plant, and its quality determines the reliable operation of the machine over the following eight to ten years or more.

The first stage of rewinding the armature is to remove the old winding from the core completely, clean the slots and inspect the core for mechanical and electrical defects such as inter-lamination short circuits. New conductors are then wound with modern glass-mica tape, a material that at equal thickness provides greater electrical and thermal strength than the traditional combination of mica tape and glass tape. After the winding has been placed in the slots, vacuum-pressure impregnation with a monolithic thermosetting resin is recommended instead of the traditional drip impregnation method. In the VPI process the winding is first evacuated in a vacuum chamber in order to remove air and moisture, after which the resin is forced under pressure into every microscopic void within the insulation layers and is then cured in a heating chamber. The result is a fully monolithic, non-hygroscopic insulation layer, which eliminates the air voids that give rise to partial discharges, increases resistance to moisture and to oil and fuel vapours, improves thermal conductivity so that heat is dissipated more efficiently from the conductor to the core, and prevents movement of the conductor within the slot under vibration together with the resulting abrasion of the insulation. For securing the end windings, glass-fibre banding tape is recommended in place of the traditional steel wire banding, and glass-fibre composite wedges in place of textolite wedges in the slot portions, since these materials are considerably more resistant to ageing and moisture.

When the main pole coils are rewound it is recommended to wrap the conductors with glass-mica tape and to impregnate the entire coil by the VPI method, which produces a more uniform and continuous insulation layer than the traditional layer-by-layer epoxy varnish coating applied by hand. In the commutating pole coils the asbestos gaskets should be replaced by modern glass-mica or aramid-fibre insulating materials of the Nomex type, which offer superior heat resistance and mechanical strength while producing no hazardous fibre residue. After the coil has been assembled it should be filled with monolithic resin under vacuum pressure rather than by casting epoxy compound, since this eliminates the microscopic air bubbles that typically form during compound pouring.

The insulation-related operations performed when repairing the commutator are the complete replacement of the micanite spacers between the segments if the commutator is fully reassembled, or the renewal of worn micanite by undercutting it 1.0–1.5 mm below the working surface; the replacement of the sleeve-to-commutator insulation, traditionally made of split mica collars, with monolithic glass-mica or epoxy-glass collars, which improves the mechanical strength and moisture resistance of the sleeve insulation; and thermal stabilization of the assembled commutator in a heating chamber, which relieves the internal stresses in the insulating materials and prevents the commutator from losing its roundness in service. After reassembly, precision turning and grinding of the commutator surface followed by mica undercutting ensures good commutator–brush contact from the moment the generator is returned to service.

The factory insulation system of the TD802 generator generally corresponds to thermal class B (130 °C) or F (155 °C). During rewinding it is recommended to replace all insulating materials with class H materials rated up to 180 °C. Even without any change to the actual operating temperature of the machine, this creates a thermal margin relative to the temperature limit of the material and substantially extends the service life of the insulation — an important consideration in the hot summer conditions of Uzbekistan, when both the ambient and the depot temperatures are elevated.

In order to realize the benefits of insulation replacement in full, a number of supplementary measures are also recommended: installing dust-protective filters in the ventilation channels so as to reduce contamination-related ageing; readjusting the brush spring pressure and the brush material, using electrographite-grade brushes matched to the new insulation system; and dynamically balancing the rotor in order to reduce the dynamic loading placed on the newly wound winding.

3.4. Technological regulation for insulation replacement

Replacement of the TD802 generator insulation at a depot or repair plant is recommended to follow the sequence of stages set out below. This regulation ensures that insulation quality is controlled at every stage of the repair and reduces the likelihood of random technological errors (Fig. 2).

– Stage 1. Remove the generator from the locomotive, clean external contamination and perform initial diagnostics — insulation resistance measurement and visual inspection;

– Stage 2. Disassemble the generator into its components — armature, pole coils, brush apparatus, bearing shields — washing and drying each assembly separately;

– Stage 3. Remove the old windings completely and inspect the core and the coil frames for mechanical and electrical defects;

– Stage 4. Prepare new conductors and wrap them with modern glass-mica insulating tape (armature sections, pole coils);

– Stage 5. Place the windings in their respective locations, install the micanite sleeves and spacers and fit the mechanical securing elements — banding and wedges;

– Stage 6. Impregnate the assembled windings in a vacuum-pressure chamber and cure them in a heating chamber according to the specified temperature–time regime;

– Stage 7. Reassemble the generator — mounting the pole coils to the frame and the armature to the bearing shields — inspect the commutator and renew its insulation if necessary;

– Stage 8. Turn and grind the commutator surface and undercut the mica;

– Stage 9. Install the brush apparatus, adjust the brush spring pressure and dynamically balance the rotor;

– Stage 10. Perform final diagnostics — insulation resistance, polarization index, high-voltage test and partial discharge monitoring;

– Stage 11. Run the generator under load on a test bench, perform thermographic monitoring, record the results in the technical passport and authorize installation on the locomotive.

The work performed and the measurement results obtained at each stage should be recorded in a repair log, which makes it possible to trace the insulation history of a particular generator in the future and to diagnose faults more rapidly should a problem arise.

3.5. Quality control and assessment of reliability indicators

Before a rewound generator is returned to service, the quality of its insulation system must be verified using the following indicators: the insulation resistance R60 and the absorption coefficient R60/R15 measured with a megohmmeter; the polarization index PI = R10/R1, which provides a deeper assessment of moisture content; a high-voltage test at 1.5–2 times the rated voltage, which reveals hidden defects; partial discharge monitoring, which characterizes the internal uniformity of the insulation; and infrared thermography during load testing, which identifies local hot spots such as poorly impregnated areas. These test results are entered in the technical passport of the generator and serve as a baseline for comparison during subsequent inspections.

The quantitative assessment of the effectiveness of insulation replacement should be based on reliability indicators derived from the operating statistics of the machine. The most widely used indicator is the mean time between failures (MTBF), defined as the total operating time between failures divided by the number of failures; the failure rate is its reciprocal, $\lambda = 1/\mathrm{MTBF}$. Calculating these indicators separately for the periods before and after insulation replacement and comparing them makes it possible to substantiate the real effectiveness of the proposed technological solutions. In addition, tracking the trend of the insulation resistance and of the polarization index over time, by recording in graphical form the values obtained at each inspection, is a practical method of forecasting the remaining insulation life. If the rate of decline of the insulation resistance per unit time between measurements exceeds a set threshold, this serves as a diagnostic indication that the generator requires an unscheduled inspection or repair. Unlike a strictly time-based repair schedule, this approach allocates maintenance

https://doi.org/10.56143/3030-3893-2026-3-118-124 A bridge between science and innovation

resources according to the actual technical condition of the machine, which is consistent with the condition-based diagnostic principles developed for traction electrical equipment [8; 9; 17].

Comparative Analysis

The differences between the factory insulating materials used in each major assembly of the TD802 generator and the modern materials proposed to replace them, together with the expected effect, are summarized in Table 2.

Table 2

Comparison of the factory and the proposed insulation systems of the TD802 generator

Aspect	Factory (existing) system	Proposed system	Expected effect
Armature winding	Mica tape (5 layers in the slot, 6 in the end portion) with glass tape; drip impregnation; steel wire banding; textolite wedges	Glass-mica tape; monolithic vacuum-pressure impregnation (VPI); glass-fibre banding tape; glass-fibre composite wedges	Higher resistance to partial discharges, sharply reduced moisture absorption, greater mechanical strength
Main pole coils	Layer-by-layer, hand-applied epoxy varnish coating in a stepped configuration	Continuous glass-mica insulation with VPI impregnation of the whole coil	Uniform insulation thickness, reduced dependence on manual technique
Commutating pole coils	Asbestos gaskets, cast epoxy compound	Glass-mica or aramid-fibre insulation (Nomex-type), VPI filling	Elimination of hazardous fibre residue, improved heat and moisture resistance
Commutator	0.8 mm micanite spacers, split-mica sleeve collars	Renewed micanite spacers or, in a full rebuild, monolithic glass-mica sleeve insulation; periodic mica undercutting	More stable commutator–brush contact, reduced sparking
Insulation thermal class	Class B (130 °C) or F (155 °C)	Class H (up to 180 °C)	Thermal margin relative to the temperature limit; important in the hot climate of Uzbekistan
Quality control	Mainly insulation resistance measurement	R60 and absorption coefficient R60/R15, polarization index R10/R1, high-voltage test, partial discharge monitoring, infrared thermography	Detection of hidden defects, a recorded baseline for tracking the ageing trend
Maintenance planning	Strictly time-based repair schedule	Condition-based planning using the trend of insulation resistance and polarization index, MTBF and failure rate $\lambda = 1/MTBF$	Repair resources allocated according to the actual technical condition of the machine

The comparison shows that the proposed changes do not fundamentally alter the design scheme of the generator but modernize the insulating material and the technology of its application in each assembly, which makes the solution relatively practical and economically justified for implementation at depot level. The key qualitative difference lies in the transition from a multi-layer, hand-applied insulation system, whose properties depend heavily on the skill of the operator, to a monolithic system formed under vacuum pressure, whose properties are determined by a controlled technological regime.

The economic effectiveness of replacing the insulation with modern materials consists of two main components: a reduction in the cost of unscheduled repairs owing to the extended fault-free operating life of the generator, and a reduction in the shunting work lost through locomotive downtime. Although modern insulating materials such as glass-mica tapes and VPI resin systems, as well as the vacuum-pressure equipment itself, require higher initial costs than the traditional materials, these costs are recouped over the full service life of the machine through its extended lifespan and the reduced number of emergency shutdowns. In order to assess the economic effectiveness accurately it is

recommended that each depot pilot the proposed technology on a limited number of generators and then compare their operating results — the number of failures, the intervals between repairs and the repair costs — with those of generators repaired using the traditional technology. On the basis of such a comparative analysis, a unified, technically and economically substantiated regulatory document for the repair of TD802 generators could be developed for use across the railways of Uzbekistan.

Replacing the insulation system of the TD802 generator with the modern materials and the VPI technology described above is expected to yield the following results: stabilization of the insulation resistance and polarization index values, with sustained readings above the normative thresholds; a reduction in the number of unscheduled repairs related to insulation faults; an extended mean time between failures owing to the upgraded thermal class; a lower probability of emergency shutdowns during seasonal transitions, particularly in high-humidity periods, owing to the improved moisture and dust resistance; and reduced sparking together with an extended commutator life owing to more stable commutator–brush contact. These results in turn contribute to a higher technical readiness rate for the ChME3 locomotive fleet equipped with TD802 generators, to optimized repair costs and to uninterrupted shunting operations.

4. Conclusion

Analysis of the design and of the factory insulation system of the TD802 (TO802) traction generator has shown that the traditional insulating materials used in its armature winding, pole coils and commutator — mica tape, micanite and asbestos gaskets — are subject to thermal, vibration-related and electrical ageing over long-term operation and constitute the primary cause of the unscheduled repairs of the machine. It has been established that these ageing factors do not act independently but reinforce one another, so that the actual service life of the insulation is shorter than the value calculated from thermal ageing alone; insulation replacement must therefore be approached comprehensively.

Complete replacement of this insulation with modern glass-mica materials, vacuum-pressure impregnation technology and materials of a higher thermal class can substantially improve the reliability of the generator, and the proposed eleven-stage technological regulation together with the quality control procedure makes it possible to implement the change within the existing depot repair process without altering the design scheme of the machine. Practical implementation of the proposed technological solutions at the depots of the railways of Uzbekistan, quantitative evaluation of their effectiveness on the basis of real operating statistics, and the subsequent development of unified technical guidelines for the repair of TD802 generators constitute the main direction of further research.

References

[1] Zhu, J., Chen, T., & Fu, Q. (2014). The research and application of WNN in the fault diagnosis technology of electric locomotive main transformer. In 7th IET International Conference on Power Electronics, Machines and Drives (pp. 1–6). Manchester.

[2] Zhu, J., Chen, T., Fu, Q., & Cheng, S. (2015). Detection of early failures within traction transformers based on Gaussian-PSO. In 3rd International Conference on Electric Power Equipment — Switching Technology (pp. 488–491). Busan.

[3] Zhu, J., Li, S., & Dong, H. (2021). Running status diagnosis of onboard traction transformers based on kernel principal component analysis and fuzzy clustering. IEEE Access, 9, 121835–121844.

[4] Zhu, J., Li, S., Liu, Y., & Dong, H. (2022). A hybrid method for the fault diagnosis of onboard traction transformers. Electronics, 11(5), 762.

[5] Li, M., Zhou, X., Qin, S., Bin, Z., & Wang, Y. (2023). Improved RAkEL's fault diagnosis method for high-speed train traction transformer. Sensors, 23(19), 8067.

[6] Wang, H., Li, Y.-F., & Ren, J. (2024). Machine learning for fault diagnosis of high-speed train traction systems: A review. Frontiers of Engineering Management, 11, 62–78.

[7] Zhong, K., Wang, J., Xu, S., Cheng, C., & Chen, H. (2023). Overview of fault prognosis for traction systems in high-speed trains: A deep learning perspective. Engineering Applications of Artificial Intelligence, 126, 106845.

[8] Wu, Z., Zhang, Z., Wang, W., Xing, T., & Xue, Z. (2022). Fault diagnosis algorithm of transformer and circuit breaker in traction power supply system based on IoT. Energies, 15(23), 8812.

[9] Lukovenko, A.S. (2016). Improving the reliability and quality of power supply to consumers of AC traction substations [Candidate's dissertation, KrIZhT — IrGUPS branch]. Krasnoyarsk.

[10] Dasarathy, B.V. (1997). Sensor fusion potential exploitation — innovative architectures and illustrative applications. Proceedings of the IEEE, 85(1), 24–38.

[11] Yusupov, D.T., Qutbidinov, O.M., Samatov, Sh.A., & Abdullaev, E.S. (2021). Investigation of factors influencing the operational characteristics of traction transformers. E3S Web of Conferences, 274.

[12] Kutbidinov, O.M., Yusupov, D.T., Samadov, Sh.A., & Abdullaev, E.S. (2021). Experimental research of utilized oils of traction transformers. International Journal of Advanced Research in Science, Engineering and Technology. India.

[13] Yusupov, D.T., Qutbidinov, O.M., Samatov, Sh.A., & Abdullaev, E.S. (2021). Investigation of winding faults of traction transformers. Earth and Environmental Science.

[14] Kudratov, S., Yusufov, A., Khamidov, O., & Samatov, S. (2025). Diesel locomotives — Fault analysis and problem solving. AIP Conference Proceedings, 3256(1), 060013. AIP Publishing LLC.

[15] Gayratov, B., Khamidov, O., Kudratov, S., & Samatov, S. (2026). The ANFIS anticipation of diesel locomotive engine on the improvement of lubricating oil analysis. AIP Conference Proceedings, 3447(1), 040008. AIP Publishing LLC.

Information about the author

Otabek Khamidov	Tashkent State Transport University, Department of Locomotives and Locomotive Engineering, Professor E-mail: otabek.rustamovich@yandex.ru Tel.:+99890 811 21 00 https://orcid.org/0000-0003-0821-5754
Shakhboz Samatov	Tashkent State Transport University, Department of Locomotives and Locomotive Engineering, Senior Lecturer E-mail: shaxbozbek4089525@gmail.com Tel.:+99894 408 95 25 https://orcid.org/0000-0002-4014-3845
Bakhodir Gayratov	Tashkent State Transport University, Department of Locomotives and Locomotive Engineering, PhD Student E-mail: bgayratoff@gmail.com Tel.:+99894 134 54 27 https://orcid.org/0009-0005-3957-337X
Abbos Djuraev	Tashkent State Transport University, Department of Locomotives and Locomotive Engineering, PhD Student Email: abbosjurayeviymona@gmail.com Tel.: +99888 854 40 00 https://orcid.org/0009-0007-2479-5134

Journal Engineer ISSN: 3030-3893 Volume:4| Issue:3| 2026

Received: 15 July 2026 | **Accepted:** 26 August 2026 | **Published:** 30 September 2026

Assessing the impact of integrating lean manufacturing methods into the quality management system on the efficiency of a mechanical engineering enterprise

U.M. Turdialiev[1][a], D.A. Boykishieva[1][b]

[1]Andijan state technical institute, Andijan, Uzbekistan

Abstract: This article presents the results of improving the quality management system in mechanical engineering enterprises based on the principles of lean manufacturing and evaluates the effectiveness of the proposed integrated management model. The study harmonized the requirements of ISO 9001 and IATF 16949 standards, the process approach, and lean manufacturing tools such as value stream mapping, 5S, Muda-Mura-Muri, 5Why, 4M, Kanban, just-in-time delivery, quick changeover, total productive maintenance, statistical process control, and failure mode and effects analysis. The effectiveness of the improvements was determined based on expert evaluation criteria covering the subsystems of strategic management, personnel activities, and production processes.

Keywords: quality management system, lean manufacturing, mechanical engineering, ISO 9001, IATF 16949, value stream mapping, 5S, process efficiency, expert assessment, Pearson correlation, Student's t-test, continuous improvement

1. Introduction

In the mechanical engineering industry, simultaneously ensuring product quality and production efficiency is a key factor that determines the competitiveness of enterprises. The growing complexity of modern engineering products, stricter requirements for technological precision, shorter delivery times, and rising consumer demands are limiting the ability to manage production processes solely through final product inspection. Such conditions require building quality directly into the production process, identifying potential defects before they occur, using resources rationally, and reducing non-value-adding activities.

The ISO 9001 standard stipulates that quality management should be organized based on a process approach, risk-based thinking, leadership accountability, and continuous improvement [1]. In automotive manufacturing and its component-producing enterprises, these requirements are further elaborated by the IATF 16949 standard [2]. However, the certification of a management system does not always automatically guarantee a reduction in production losses, shorter cycle times, or increased resource utilization efficiency.

The theoretical and practical foundations of the lean manufacturing concept are centered on eliminating activities from production processes that do not create value for the consumer. The Toyota Production System, formulated by T. Ohno, established the identification and reduction of waste as a crucial condition for increasing production efficiency [3]. J. Womack and D. Jones systemized the principles of value, value stream, continuous flow, pull production, and continuous improvement as the core components of lean manufacturing [4]. J. Liker, in turn, emphasizes that the effectiveness of this approach depends not only on individual technical tools but also on management culture, employee involvement, and continuous improvement [5].

Value stream mapping enables the systematic analysis of processes and the identification of non-value-adding operations [6]. Research by Shah and Ward has also shown that implementing lean manufacturing practices as a set of interconnected tools, rather than as separate methods, has a stronger impact on enterprise performance [7]. Holweg analyzed the evolution of lean manufacturing and substantiated its transformation from a simple set of production tools into a comprehensive management concept [8].

Recent research has focused on the issues of integrating quality management and lean manufacturing. Bacoup et al. demonstrated the need to harmonize loss reduction principles with standardized management mechanisms when transitioning from a quality management system to a lean quality management system [9]. Yadav and Desai substantiated the need for a systemic mechanism that combines organizational, technological, and human factors for the effective implementation of lean manufacturing [10]. It has also been noted that integrating ISO standards with lean management principles serves not only to ensure compliance with standard requirements but also to increase operational efficiency within an enterprise [11, 12].

Nevertheless, the issue of harmonizing the quality management system and lean manufacturing in machine-building enterprises, implementing them based on a unified management model, and comprehensively evaluating the results based on quality, process, and economic indicators has not been sufficiently systematized.

[a] https://orcid.org/0009-0005-9843-6340

[b] https://orcid.org/0009-0006-7238-1537

2. Research methodology

The study encompassed the production activities of machine-building enterprises, their quality management processes, and the mechanisms for applying lean manufacturing tools. The practical research was conducted on the cases of "Andijan Freight Car Building and Repair Plant" JSC, "Asaka Davr Butlovchi" LLC, and "Nawas" LLC. The impact of the proposed improvement model on production processes was analyzed in greater detail using the example of "Asaka Davr Butlovchi" LLC.

The research methodology was based on the requirements of the ISO 9001 and IATF 16949 standards. During the study, methods of analysis and synthesis, comparison, systematic and process-based approaches, expert assessment, observation, grouping, and mathematical statistics were utilized.

3. Results and Discussion

The initial expert assessment revealed that while elements of quality management were present in the machine-building enterprises, the principles of lean manufacturing had not been formed into a unified system across all management levels. Notably, the processes subsystem recorded the lowest result with 4.6 points. Strategic management was rated at 5.2 points, and employee performance at 5.5 points.

After the implementation of the improvement model, positive changes were observed across all subsystems.

Table 1

Results of the expert assessment before and after improvement

Subsystem	Previous state, score	Subsequent state, score	Absolute change	Post/Pre Index, %
Strategic management	5.19	7.03	+1.84	135.45
Employee performance	5.54	7.34	+1.80	132.49
Production Processes	4.60	6.76	+2.16	146.96

An increase in the strategic management assessment score from 5.19 to 7.03 points represents a relative improvement of 35.45%. Positive changes were noted in the areas of clarity of strategic direction, personal involvement of leadership, formation of key performance indicators, and systematic monitoring of consumer demand.

The average score for employee activities increased from 5.54 to 7.34 points. The involvement of employees in lean manufacturing, along with improvements to the motivation system, mechanisms for encouraging rationalization proposals, and the development of internal leaders, influenced this result.

The largest absolute change was observed in the production processes subsystem, where the average score increased from 4.60 to 6.76 points. This result demonstrates the effectiveness of practical measures aimed at 5S, visual management, waste identification, production flow coordination, and in-process quality control.

After the improvements, not only did the average values increase, but the dispersion of the assessment results also decreased significantly.

Table 2

Descriptive statistics of the expert assessment results

Subsystem	State	Mean	Variance	Standard deviation	Coefficient of variation, %
Strategic management	Before	5.19	1.88	1.37	26.33
Strategic management	After	7.03	0.62	0.79	11.25
Personnel	Before	5.54	1.77	1.33	24.04
Personnel	After	7.34	0.39	0.63	8.65
Processes	Before	4.60	0.92	0.96	20.77
Processes	After	6.76	0.64	0.80	11.89

In the strategic management subsystem, the dispersion decreased from 1.88 to 0.62, in the personnel subsystem from 1.77 to 0.39, and in the production processes subsystem from 0.92 to 0.64. The decrease in the coefficient of variation across all subsystems indicates that the evaluation results have stabilized. In particular, the reduction of the coefficient variation from 24.04% to 8.65% in the personnel subsystem signifies that the disparity in the development of system elements has substantially narrowed.

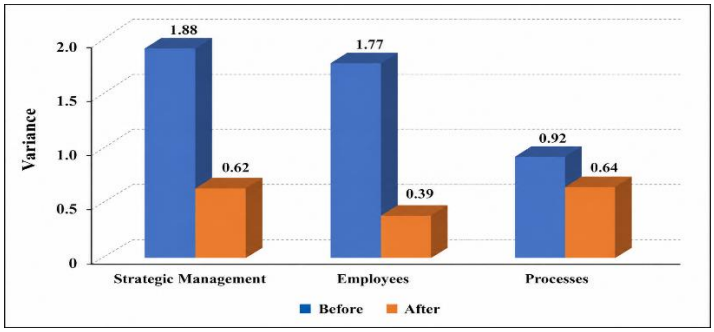


Fig. 1. Comparison of dispersion based on evaluation results

The Pearson correlation coefficient was calculated to determine the relationship between the previous and subsequent evaluations.

Table 3

Correlation between previous and subsequent expert evaluations

Subsystem	n	Pearson coefficient, r	Student's T-test, t	Result
Strategic management	7	0.9926	18.22	statistically significant
Personnel	5	0.9884	11.28	statistically significant
Processes	9	0.9334	6.88	statistically significant

For all subsystems (r>0.9), a very strong positive correlation was found between the previous and subsequent indicators. This indicates that the growth after the improvements was not due to random changes in individual indicators but rather occurred consistently across all evaluation items.

The calculated values from the student's t-test were higher than the critical values at the corresponding degrees of freedom, which confirmed the statistical significance of the identified correlations at the α=0.05 level.

The improvement model also had a positive effect on the direct technological indicators of production.

Table 4

Key Production Indicators After Model Implementation

Indicator	Before	After	Change
Operation time per part	9.5 minutes	8.7 minutes	-0.8 minutes
Share of defective products	1.8%	1.2%	-0.6 percentage points
Effectiveness of management decision-making	80%	90%	+10 percentage points

The reduction in operation time from 9.5 minutes to 8.7 minutes shows a time saving of approximately 8.4% per operation. The decrease in the share of defective products from 1.8% to 1.2% signifies a reduction of about 33.3% from the initial level. The effectiveness of management decision-making increased from 80% to 90%.

The economic efficiency of the model was achieved by shortening the production cycle time, reducing labor intensity, optimizing the volume of work-in-progress, and using material resources more efficiently.

Table 5

Economic Results of Implementing the Improvement Model

Enterprise	Economic benefit achieved	Payback period
"Nawas" LLC	130 million UZS	1.2 years
"Asaka Davr Butlovchi" LLC	138.4 million UZS	2.2 year's
"Andijan Freight Car Building and Repair Plant" JSC	146 million UZS	2.05 years

These results confirm that the proposed model is not limited to improving quality indicators but also has a positive effect on the economic efficiency of production processes.

DISCUSSION

The results obtained indicate that a quality management system and lean manufacturing should not be viewed as independent management approaches, but rather as interconnected elements of a single system. While a quality management system creates the institutional framework for regulating processes, defining responsibilities, monitoring results, and managing non-conformities, lean manufacturing complements this system by providing tools to identify waste, accelerate flows, and increase resource utilization efficiency.

This conclusion is consistent with the approach proposed by Shah and Ward, which advocates for applying lean manufacturing tools as a set of interconnected practices [7]. The study's finds that the process subsystem improved from 4.60 to 6.76 points-a higher rate of improvement compared to other subsystems-also demonstrates the direct impact of practical lean tools within the production environment.

However, the results also showed that the effectiveness of lean manufacturing is not determined solely by individual tools such as 5S, Kanban, or value stream mapping. Employee motivation, senior management involvement, the availability of key performance indicators, and a system for regular monitoring of results are crucial factors for the sustainable operation of the system. This aspect aligns with the concept, put forward by J. Liker, of viewing lean manufacturing in conjunction with management philosophy and corporate culture [5].

Another important feature of the proposed model is that it treats quality and efficiency not as separate outcomes but as mutually formative indicators. For example, 5S and standardization not only improve workplace organization but also reduce unnecessary movements, shorten operation times, and decrease the likelihood of errors. Value stream mapping, in addition to identifying waiting, excess inventory, and repetitive operations, also indicates at which points process control needs to be strengthened. While FMEA and statistical process control serve to enhance quality stability, Kanban and demand-driven management optimize the flow of materials.

The lean quality management approach proposed by Bacoup et al. also presents the integration of standardized management system mechanisms with lean manufacturing principles as a factor that enhances efficiency [9]. The concurrent improvement of research results at the strategic

https://doi.org/10.56143/3030-3893-2026-3-125-129 A bridge between science and innovation

management, personnel, and process levels suggests that this approach is also applicable to machine-building enterprises.

A key finding of the descriptive statistical analysis is that the improvements resulted not only in an increase in average scores but also in a decrease in the variance and coefficients of variation. This indicates that the gap between the strong and weak elements within the system has narrowed. For instance, the decrease in the coefficient of variation in the personnel activities subsystem from 24.04% to 8.65% signifies that activities, which were previously individual initiatives, have evolved into a more systematic management practice.

The Pearson correlation results further support this conclusion. The strong positive correlations in strategic management (r=0.9926), the personnel subsystem (r=0.9884), and processes (r=0.9334) indicate that their overall level has increased while preserving the relative structure of the pre-improvement evaluation items. Therefore, the model served not to artificially inflate specific indicators but to systematically elevate the existing management system to a higher level of development.

Changes in production indicators also confirm the consistency of expert evaluations with practical results. The reduction in operation time, decrease in the share of defective products, and increase in the effectiveness of management decisions show that the positive shifts in expert evaluation results are also reflected in real technological processes.

Thus, integrating the standardized requirements of a quality management system with the loss-reduction tools of lean manufacturing allows machine-building enterprises to enhance quality, efficiency, and economic outcomes within a single management framework.

4. Conclusion

The research, conducted based on the integration of the quality management system and lean manufacturing methods in machine-building enterprises, yielded the following scientific and practical results.

First, an improvement model was developed that harmonizes the requirements of ISO 9001 and IATF 16949 with the principles of lean manufacturing. This model encompasses process analysis, loss identification, determination of priority improvement areas, selection of appropriate tools, implementation, and monitoring of results.

Secondly, because of implementing the model, the average score for the strategic management subsystem improved from 5.2 to 7.0 points, employee performance from 5.5 to 7.3 points, and production processes from 4.6 to 6.7 points. The most significant change was observed in the production processes subsystem.

Thirdly, the decrease in variance, standard deviation, and coefficients of variation across all subsystems after the improvements indicates that the management system has stabilized and the development gap between its individual elements has narrowed.

Fourthly, a very strong positive correlation was identified between the initial and subsequent expert assessments. The following values were obtained: for strategic management (r=0.9926), for personnel (r=0.9884), and for processes (r=0.9334). Using the Student's T-test, it was confirmed that the correlations are statistically significant at a 95% confidence level.

Fifthly, because of the model's practical implementation, the operation time per part decreased from 9.5 to 8.7 minutes, the proportion of defective products fell from 1.8% to 1.2%, and the effectiveness of management decision-making increased from 80% to 90%.

Sixth, as a result of reducing production cycle time, labor intensity, and work-in-progress volume, as well as optimizing the use of material resources, an economic effect of 130 million sums was achieved at "Nawas" JV LLC, 138.4 million sums at "Asaka Davr Butlovchi" LLC, and 146 million sums at "Andijan Freight Car Construction and Repair Plant" JSC.

The research results showed that the complex integration of the quality management system and lean manufacturing tools is an effective mechanism for stabilizing quality, reducing waste, improving production processes, and increasing economic efficiency in machine-building enterprises.

References

[1] O'z DSt ISO 9001:2015. Quality management systems. Requirements.

[2] O'z DSt ISO/IATF 16949:2019. Quality management systems. Requirements for quality management systems for automotive production and relevant service part organizations.

[3] Ohno, T. The Toyota Production System: Beyond Large-Scale Production. - Moscow: Institute for Complex Strategic Studies, 2008. - 194 p.

[4] Womack, J.P., Jones, D.T. Lean Thinking: Banish Waste and Create Wealth in Your Corporation. - Moscow: Alpina Business Books, 2021. - 292 p.

[5] Liker, J. The Toyota Way: 14 Management Principles from the World's Greatest Manufacturer. - Moscow: Alpina Publisher, 2013. - 400 p.

[6] Rother M., Shook J. Learning to See: Value Stream Mapping to Add Value and Eliminate Muda. - Cambridge, MA: Lean Enterprise Institute, 1999. - 102 p.

[7] Shah R., Ward P.T. Lean manufacturing: Context, practice bundles, and performance // Journal of Operations Management. - 2003. - Vol. 21, No. 2. - P. 129-149.

[8] Holweg M. The genealogy of lean production // Journal of Operations Management. - 2007. - Vol. 25, No. 2. - P. 420-437.

[9] Bacoup P., Michel C., Habchi G., Pralus M. From a Quality Management System (QMS) to a Lean Quality Management System (LQMS) // The TQM Journal. - 2018. - Vol. 30, No. 1. - P. 1-25. DOI: 10.1108/TQM-06-2016-0053.

[10] Yadav G., Desai T.N. Development of a lean manufacturing framework to enhance implementation practices in companies // Journal of Cleaner Production. - 2020. - Vol. 258. - 120794. DOI: 10.1016/j.jclepro.2020.120794.

[11] Wirkus M., Chmielarz A. Integration of Lean Management with ISO management systems in enterprise // Management and Production Engineering Review. - 2018. - Vol. 9, No. 3. - P. 3-11.

[12] Fonseca L.M., Domingues J.P., Baylina-Machado P., Harder D. ISO 9001:2015 adoption: A multi-country

empirical research // Journal of Industrial Engineering and Management. - 2019. - Vol. 12, No. 1. - P. 27-50. DOI: 10.3926/jiem.2745.

Information about the author

Umid Turdialiev Rector of Andijan State Technical Institute
https://orcid.org/0009-0005-9843-6340
Tel: +998742234367

Dilnoza Boykishieva Researcher at the Andijan State Technical Institute
https://orcid.org/0009-0006-7238-1537
E-mail: islom26177@gmail.com
Tel: +998879832801

Journal Engineer ISSN: 3030-3893 Volume:4| Issue:3| 2026

Received: 15 July 2026 | **Accepted:** 26 August 2026 | **Published:** 30 September 2026

Use of mineral fillers for PVC-based linoleum production and investigation of their physical and mechanical properties

B.T. Sobirov[1][a], **N.Sh. Botirova**[1][b]

[1]Jizzakh Polytechnic Institute, Jizzakh, Uzbekistan

Abstract: Nowadays, the use of various polymer-based composite materials is increasing in the modern construction industry. In particular, polyvinyl chloride (PVC)-based floor covering materials are widely used in the construction of construction objects for various purposes due to their ease of use at the construction site, production in various sizes and designs, and high performance properties. This research paper presents the results of research on optimizing the raw material composition of PVC linoleum based on mineral fillers and improving its physicomechanical properties. During the research, the mechanisms of interaction of local mineral raw materials such as kaolin, bentonite, and calcium carbonate with the polymer matrix, their structure-forming properties, and the effect on the performance indicators of the finished material were analyzed. The optimal proportions of mineral fillers in the composition of the composition intended for linoleum were determined, and the possibility of developing a new economically efficient, abrasion-resistant, and thermally stable composite composition was substantiated.

Keywords: polyvinyl chloride, linoleum, composite material, raw material polymer matrix, filler, kaolin, bentonite, calcium carbonate, physical and mechanical properties, mineral filler, structure, formation

1. Introduction

The development of the modern construction industry is closely related to the creation of a new generation of composite materials used in various construction projects. Currently, the materials used in construction projects are subject to such requirements as high mechanical strength, long service life, resistance to aggressive environments, modern design, environmental safety and economic efficiency. Therefore, polymer-based composite materials are emerging as one of the most promising areas in the field of construction materials. In particular, rolled floor covering materials based on polyvinyl chloride (PVC) are widely used in modern construction practice due to their high performance characteristics. PVC-based linoleums are currently one of the most widely used floor covering materials in residential, administrative, industrial, educational, medical and commercial buildings [1].

At the same time, modern linoleum production technologies have technological problems related to raw materials, including ensuring its competitiveness due to the high cost of the product, dependence on some imported raw materials, and further improving physical and mechanical properties such as fire resistance. Therefore, one of the urgent scientific and practical tasks is to develop economically efficient and high-quality composite materials using mineral raw materials as fillers and saving expensive PVC.

The territory of Uzbekistan is rich in kaolin, bentonite, limestone and other mineral resources, and the use of these raw materials in polymer composite materials is of great economic and technological importance. The use of local resources reduces transportation costs, creates the opportunity to produce import-substituting products, and reduces production costs [2].

The main feature of polymer composite materials is that they consist of several components and have a single composite structure, which has high physical and mechanical and operational properties. Currently produced PVC-based linoleums consist of a polymer binder, plasticizer, stabilizer, pigment and mineral fillers. The interaction of these components forms the mechanical strength, elasticity, thermal stability and operational durability of the finished product [3]. From the point of view of modern materials science, mineral fillers are not a simple inert substance in the composition of the composite material, but an important structural element that controls the internal energy, deformation processes and interphase bonds of the polymer system. The physical and mechanical properties of composite materials largely depend on the type of mineral filler, its dispersion, surface energy, particle shape and the degree of interphase bonding with the polymer matrix. If the mineral filler is evenly distributed in the polymer system and provides high adhesion, the mechanical strength, abrasion resistance and operational stability of the material are significantly improved [4]. On the contrary, as a result of agglomeration of mineral particles or weak bonding with the polymer, microdefects, voids and internal stress centers are formed in the structure of the composite material. This reduces the service life of the finished product and leads to a deterioration in its operational properties. Kaolin, which is used as a mineral filler in PVC-based linoleums, is a white aluminosilicate clay of natural origin, characterized by high dispersibility, thermal stability and surface activity. Kaolin partially acts as a white pigment and stabilizer in polymer composite materials and improves the surface quality of the material [5]. Finely dispersed particles of kaolin form a

[a] https://orcid.org/0000-0003-3539-4612
[b] https://orcid.org/0009-0001-1685-7936

strong interfacial bond with the polymer matrix, increasing the mechanical strength of the material. In addition, kaolin increases the thermal stability of the composition and reduces deformation at high temperatures.

Bentonite, on the other hand, belongs to the group of clay aluminosilicate minerals composed of the mineral montmorillonite, and is distinguished by its layered structure and higher adsorption and dispersion properties compared to kaolinite. The layered structure of montmorillonite, which forms the basis of bentonite, is interconnected with the chains of the PVC polymer, which leads to the formation of an internal integral structure of the composite system [6]. The high surface activity of bentonite enhances the interfacial bonding between the polymer and mineral components, resulting in increased deformation resistance, abrasion resistance, and structural stability of the composite material.

Calcium carbonate is one of the most widely used mineral fillers in polymer-based composite materials. It is characterized by its low cost, widespread occurrence in nature in the form of natural rocks (e.g., limestone, chalk, and marl), and technological convenience. Calcium carbonate, along with reducing the cost of the product, serves to increase the hardness and density of the material [7]. At the same time, its excessive use leads to a decrease in the elasticity of the polymer-based composite material. Therefore, it is important to choose the optimal amount of calcium carbonate in the composition.

Scientific studies conducted in 2022-2025 show that the use of mineral fillers not separately, but in combination with other mineral fillers, gives a more effective result than individual components [8]. In particular, the combined use of kaolin, bentonite and calcium carbonate leads to structural compaction of the composite system, increased interaction between polymer chains and improved physical and mechanical properties of the composite material.

2. Research methodology

In this study, polyvinyl chloride (PVC) was used as the main polymer binder. PVC is a thermoplastic polymer with high mechanical strength, chemical stability, and service life.

Dioctyl phthalate (DOP, chemical formula: $C_{24}H_{38}O_4$) was used as a plasticizer. Dioctyl phthalate is a complex ester of phthalic acid and 2-ethylhexanol alcohol, a colorless or yellowish oily liquid. It is the most widely used classic plasticizer in the PVC industry. The main function of DOP is to penetrate between polymer chains, reduce intermolecular forces between them, and increase chain mobility. As a result, it significantly improves the elasticity, ductility, and cold resistance of the material, as well as reduces brittleness and processing temperature [9].

Metal-organic compounds (for example, Ca-Zn or Ba-Zn thermal stabilizers) were used as stabilizers. These stabilizers reduce the decomposition (destruction) of PVC at high temperatures and increase its thermal stability. Angren kaolin, Kattakurgan bentonite, and calcium carbonate from a limestone deposit in the Jizzakh region were used as mineral fillers.

Methodology for preparing and testing composite samples: Composite samples were prepared in laboratory conditions based on the following sequential technological stages:

1. Polymer matrix (PVC), plasticizer (DOP), stabilizer and mineral fillers in various ratios (kaolin, bentonite, calcium carbonate) were thoroughly mixed in a high-speed laboratory mixer (mixer) at a temperature of 80–100 °C until a homogeneous state was achieved.

2. The resulting dispersed mixture was plasticized at a temperature of 165–175 °C and brought to a state of slush (mass).

3. The heated mass was processed in a two-shaft laboratory roller mill (roller mill) at a temperature of 160–170 °C and brought to the form of a flat film/sheet.

4. Standard samples of a specified thickness were formed from the rolled films in a hydraulic press at a temperature of 170–175 °C and a pressure of 10–15 MPa and cooled under pressure.

The physical, mechanical and operational properties of the prepared composite samples were determined using the following standard test and analysis methods:

- Density: Using the hydrostatic weighing method (pycnometric method);
- Abrasion resistance: By measuring the mass loss of the sample due to abrasive friction in a drum or disc abrasive testing apparatus;
- Water absorption: By keeping the samples in distilled water for 24 hours and weighing the percentage of the increased mass;
- Flexural and tensile strength: By applying mechanical force to the sample in a universal tensile machine and measuring the fracture and deformation limits;
- Elasticity and hardness: By using a Shore hardness tester (Durometer, ShA/ShD) and methods for assessing ductility;
- Thermal stability: By determining the temperature and time of onset of PVC destruction by thermogravimetric analysis (TGA) and the Congo-roth indicator method[8].

3. Results and Discussion

The results of the study showed that the addition of kaolin significantly improved the surface quality of the material and increased the level of whiteness. The high dispersion of kaolin particles formed a strong interphase bond with the polymer matrix, increasing the mechanical strength of the material.

As a result of the use of bentonite, the internal structure of the composite system was densified and stabilized. The layered structure of bentonite interacted with the polymer chains, leading to improved resistance to deformation and friction. It was observed that the internal voids decreased in samples with the addition of bentonite and the structural integrity of the material increased[10].

The use of calcium carbonate in an optimal amount increased the hardness and dimensional stability of the material, while reducing the cost of the product. At the same time, it was confirmed that an excess of calcium carbonate leads to a decrease in elasticity[5].

During the study, it was found that the complex use of kaolin, bentonite and calcium carbonate gave the most effective results. The samples with this composition exhibited higher abrasion resistance, lower water absorption, better mechanical strength, and higher thermal stability compared to the control composition, which is explained by the synergistic effect of the mineral fillers.

https://doi.org/10.56143/3030-3893-2026-3-125-129 A bridge between science and innovation

4. Conclusion

The research, conducted based on the integration of the quality management system and lean manufacturing methods in machine-building enterprises, yielded the following scientific and practical results.

First, an improvement model was developed that harmonizes the requirements of ISO 9001 and IATF 16949 with the principles of lean manufacturing. This model encompasses process analysis, loss identification, determination of priority improvement areas, selection of appropriate tools, implementation, and monitoring of results.

Secondly, because of implementing the model, the average score for the strategic management subsystem improved from 5.2 to 7.0 points, employee performance from 5.5 to 7.3 points, and production processes from 4.6 to 6.7 points. The most significant change was observed in the production processes subsystem.

Thirdly, the decrease in variance, standard deviation, and coefficients of variation across all subsystems after the improvements indicates that the management system has stabilized and the development gap between its individual elements has narrowed.

Fourthly, a very strong positive correlation was identified between the initial and subsequent expert assessments. The following values were obtained: for strategic management (r=0.9926), for personnel (r=0.9884), and for processes (r=0.9334). Using the Student's T-test, it was confirmed that the correlations are statistically significant at a 95% confidence level.

Fifthly, because of the model's practical implementation, the operation time per part decreased from 9.5 to 8.7 minutes, the proportion of defective products fell from 1.8% to 1.2%, and the effectiveness of management decision-making increased from 80% to 90%.

Sixth, as a result of reducing production cycle time, labor intensity, and work-in-progress volume, as well as optimizing the use of material resources, an economic effect of 130 million sums was achieved at "Nawas" JV LLC, 138.4 million sums at "Asaka Davr Butlovchi" LLC, and 146 million sums at "Andijan Freight Car Construction and Repair Plant" JSC.

The research results showed that the complex integration of the quality management system and lean manufacturing tools is an effective mechanism for stabilizing quality, reducing waste, improving production processes, and increasing economic efficiency in machine-building enterprises.

References

[1] Callister W. D., Rethwisch D. G. Materials Science and Engineering: An Introduction. – 9th ed. – New York: John Wiley & Sons, 2014. – 984 p.

[2] Titow W. V. PVC Technology. – 4th ed. – London: Elsevier Applied Science Publishers, 1984. – 1240 p..

[3] Xanthos M. Functional Fillers for Plastics. – 2nd ed. – Weinheim: Wiley-VCH Verlag GmbH & Co. KGaA, 2010. – 489 p.

[4] Wickson E. J. Handbook of PVC Formulating. – New York: John Wiley & Sons, 1993. – 960 p.

[5] Малышев В. П. Физика композиционных полимерных материалов. – Москва: Химия, 2005. – 320 с.Сабиров Б.Т., Кадырова З.Р., Усманов Х.Л., Эминов А.М. Исследование бентонитов Узбекистана для разработки гидроизоляционных композиций // Теория композиционных строительных материалов и инновационные технологии: материалы Республиканской научно-практической конференции. – Ташкент: Ташкентский архитектурно-строительный институт, 2012. – С. 124–125.

[6] Murray H.H. Overview — clay mineral applications // Applied Clay Science. – 1991. – Vol. 5, Issues 5–6. – P. 379–395].Бектуров Э.А., Кудаибергенов С.Э. Полимерные композиционные материалы. – Алматы: Гйлйм, 2002.

[7] Тиллаев А.Т. Разработка технологии получения поливинилхлоридного линолеума с применением местных минеральных наполнителей и модифицсирующих добавок. – Ташкент, 1997.

[8] ГОСТ 7251–2016. Линолеум поливинилхлоридный на тепло- и звукоизоляционной основе. Технические условия.

[9] Мухторова Н.Б., Алиев Б.А., Сабиров Б.Т Исследование химико-минералогического состава шафирканской бентонитовой глины для получения новых сорбентов // International Scientific Journal "Science and Innovation". – 2022. – №3. – P. 168–175.

Information about the author

Bakhtiyor Sabirov	Jizzakh Polytechnic Institute Tel.: +998 97 716 00 37 https://orcid.org/0000-0003-3539-4612
Nodira Botirova	Jizzakh Polytechnic Institute E-mail: korreys95@gmail.com Tel.: +99891 195-98-87 https://orcid.org/0009-0001-1685-7936

Journal Engineer ISSN: 3030-3893 Volume:4| Issue:3| 2026

Received: 22 July 2026 | **Accepted:** 2 September 2026 | **Published:** 30 September 2026

Development of an artificial intelligence-based adaptive digital twin method for early fault detection and energy loss reduction in solar photovoltaic systems

G.N. Uzakov[1][a], M.A. Majidova[1][b]

[1]Karshi State Technical University, Karshi, Uzbekistan

Abstract: This article examines the scientific and conceptual foundations for developing an artificial intelligence-based adaptive digital twin method aimed at early fault detection and the reduction of associated energy losses in solar photovoltaic systems. An adaptive digital twin model is proposed by integrating real-time monitoring data, environmental parameters, electrical indicators, technical condition characteristics, and time-varying operational data into a unified information environment. The model is designed to enable early detection of operational deviations, forecasting of potential fault development, assessment of their impact on energy generation, and formulation of optimal technical decisions. The scientific novelty lies in dynamically updating the virtual model and integrating the sequence of "monitoring → early anomaly detection → fault forecasting → energy-loss assessment → technical decision" into a unified adaptive digital twin architecture.

Keywords: solar photovoltaic system, digital twin, artificial intelligence, adaptive model, early fault detection, energy losses, forecasting, technical diagnostics, predictive maintenance, monitoring

1. Introduction

The expanding application of photovoltaic (PV) systems in the energy sector is making the long-term, stable, and efficient operation of such systems an increasingly important scientific and practical challenge. During real-world operation, factors such as module degradation, partial shading, soiling, thermal effects, faults in electrical connections, and failures of inverters and other components can reduce the energy generation efficiency of photovoltaic systems. Therefore, rather than assessing system condition solely through periodic inspections, increasing attention is being paid to approaches based on monitoring data that enable early fault detection and predictive maintenance [1].

In recent years, digital twin technology has received considerable attention for monitoring the technical condition of photovoltaic systems, detecting faults, and forecasting their operational performance. A digital twin is a dynamic virtual representation of a physical object in a digital environment that can be used for condition monitoring, maintenance, and optimization of operating modes. Studies focusing on PV systems have identified the integration of digital twin technology with predictive maintenance, fault detection and diagnostics, the Internet of Things (IoT), and artificial intelligence (AI) as promising research directions [2].

However, the development of digital twins for photovoltaic systems has not yet reached full maturity. A systematic review of the literature on PV digital twins indicates that many existing studies do not adequately incorporate key characteristics of a fully developed digital twin, particularly bidirectional data exchange between the physical and virtual entities and the capability of the model to adapt itself to changing operating conditions. It has been reported that only 3.3% of the reviewed studies satisfied all of the proposed criteria for PV digital twins [4].

The development of artificial intelligence-based predictive maintenance and fault diagnosis methods is advancing this field to a new stage of research. Modern approaches enable the joint analysis of sensor, historical, meteorological, and electrical measurement data, thereby providing opportunities for early fault detection, assessment of fault severity, and prediction of potentially critical future conditions [3].

Accordingly, the aim of this study is to develop the scientific and methodological foundations of an adaptive digital twin method for photovoltaic systems that dynamically represents the system condition through AI-based processing of real-time monitoring data, environmental conditions, electrical and energy-related parameters, and technical-operational characteristics, while enabling early fault detection and contributing to the reduction of energy losses.

2. Research methodology

The present study is conducted using an analytical-conceptual methodology. The research materials consist of scientific publications and methodological approaches addressing fault detection in photovoltaic (PV) systems, condition assessment, digital twin development, artificial intelligence-based diagnostics, and monitoring of energy production losses [1–7].

The methodological framework of the study is based on an adaptive digital twin architecture incorporating the principles of **physical photovoltaic system → monitoring data → virtual model → artificial intelligence → feedback**. Data acquired from the physical system are used to continuously update the state of the virtual model, while the virtual model establishes the expected normal operating conditions of the system.

[a] https://orcid.org/0009-0005-7386-8075
[b] https://orcid.org/0009-0000-6078-5944

Deviations between the actual and predicted states are evaluated as potential indicators of faults [6].

For the purposes of the study, the collected data are classified into four principal groups:

1) Environmental parameters;
2) Electrical and energy-related parameters;
3) Technical condition parameters;
4) Time-series data.

At the initial stage of data processing, timestamp synchronization, identification of missing values, detection and separation of anomalous observations, and parameter normalization are performed [1,7].

The overall algorithmic sequence of the proposed method can be expressed as follows:

$$X(t) \rightarrow D(t) \rightarrow DT(t) \rightarrow \Delta(t) \rightarrow AI \rightarrow \hat{F}(t+\Delta t) \rightarrow \hat{L}E(t+\Delta t) \rightarrow Q. \quad (1)$$

Here, X(t) denotes the initial multivariate data; D(t) represents the processed data; DT(t) denotes the digital twin; Δ(t) represents the deviation between the actual and virtual results; AI denotes the artificial intelligence-based analysis and forecasting module; $\hat{F}(t+\Delta t)$ represents the predicted probability of a potential fault condition; $\hat{L}E(t+\Delta t)$ denotes the predicted energy loss; and Q represents the technical decision.

General criterion for fault assessment:

$$\Delta P(t) = P_{DT}(t) - P_{real}(t) \quad (2)$$

The energy loss is defined as:

$$L_E = \int_{t_1}^{t2} [PDT(t) - P_{real}(t)]dt \quad (3)$$

Here, L_e denotes the total energy loss; t_1 is the start time of the observation period; t_2 is the end time of the observation period; and dt represents an infinitesimal time interval.

For discrete monitoring data, the energy loss can be calculated as:

$$L_E \approx \sum i \ [PDT(ti) - Preal(ti)]\Delta t \quad (4)$$

These expressions represent conceptual assessment formulas and will be calibrated in subsequent experimental studies using real monitoring data.

3. Results and Discussion

The analysis of the literature and existing methodological approaches indicates that research on fault detection in photovoltaic (PV) systems has primarily developed in the areas of monitoring, anomaly detection, fault diagnosis, and predictive maintenance [1–7]. The main outcome of the present study is the development of a concept that integrates these individual research directions into a unified adaptive digital twin architecture.

Table 1

Comparative analysis of existing approaches for photovoltaic systems

No.	Approach	Task	Advantage	Limitation	Proposed Solution
1	Monitoring and anomaly detection [1]	Detection of deviations	Real-time operational monitoring	Not fully integrated with forecasting	Deviations are transferred to the AI module
2	AI-based fault diagnosis [5]	Identification of fault types	Detects complex relationships	Dependent on data quality	AI is integrated into the adaptive DT module
3	Digital Twin-based diagnostics [6]	Comparison of physical and virtual states	Evaluates expected system conditions	Adaptability may be limited	The model is continuously updated using real-time data
4	Predictive maintenance [3]	Assessment of fault development	Enables preventive maintenance	Energy consequences are not always incorporated	Energy-loss forecasting is integrated
5	Adaptive Digital Twin	Comprehensive system management	Integrates monitoring, diagnostics, and forecasting	Requires real-world validation	Model proposed in this study

Source: compiled by the authors based on [1]–[6].

The operational logic of the proposed model is based on the following sequential workflow:

Physical PV system → real-time monitoring → data preprocessing → digital twin → comparison of actual and virtual states → early anomaly detection → AI-based fault prediction → energy-loss assessment → technical decision.

https://doi.org/10.56143/3030-3893-2026-3-133-137

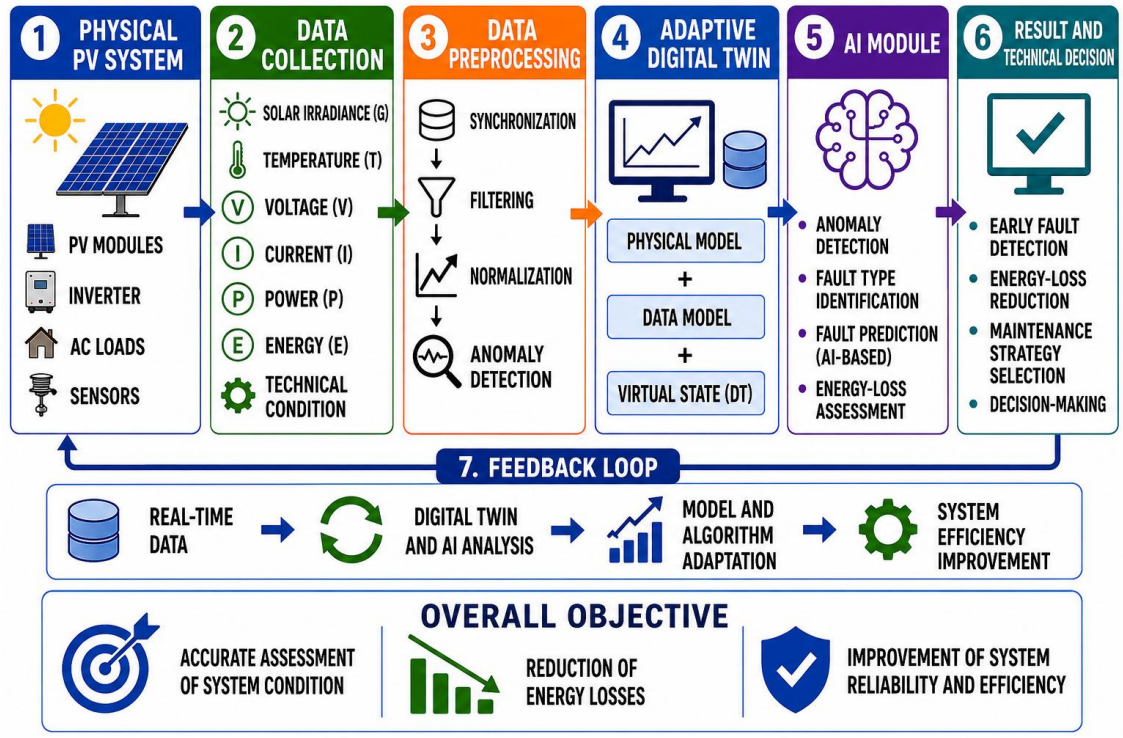


Fig. 1. Functional architecture of an artificial intelligence-based adaptive digital twin for photovoltaic systems

The central element of the proposed model is the **residual deviation indicator** between the physical system and its digital twin:

$$\varepsilon(t) = Y_{real}(t) - \hat{Y}DT(t). \quad (5)$$

If the value of ε(t) consistently exceeds the adaptive threshold, it is considered an early indication of a potential anomaly in the system. The threshold value is defined as an adaptive threshold that is dynamically updated according to solar irradiance, module temperature, ambient environmental conditions, and operating modes. The scientific novelty of the study is reflected in the following aspects: the environmental, electrical-energy, and technical-operational parameters of the PV system are integrated into a unified multivariate information model; the digital twin is dynamically updated using real-time monitoring data; the residual deviation between the physical and virtual systems is analyzed using artificial intelligence; and the predicted fault is linked to its corresponding energy-related consequences.

Table 2

Functional stages of the proposed adaptive digital twin method

Stage	Input Data	Main Operation	Output
1. Monitoring	Irradiance, temperature, current, voltage, power	Real-time data acquisition	Initial data stream
2. Data Preprocessing	Initial data	Synchronization and quality control	Reliable data set
3. Digital Twin	Multivariate data	Normal operating condition modeling	Expected system state
4. Early Detection	Actual and virtual outputs	Residual deviation analysis	Anomaly signal
5. AI-Based Forecasting	Deviations and time-series data	Fault prediction	Probable future state
6. Energy Assessment	Fault prediction	Estimation of potential energy loss	Energy-loss forecast
7. Decision-Making	Diagnostics and forecast results	Selection of maintenance strategy	Preventive maintenance decision

Source: developed by the authors based on [1]–[7].

https://doi.org/10.56143/3030-3893-2026-3-133-137 A bridge between science and innovation

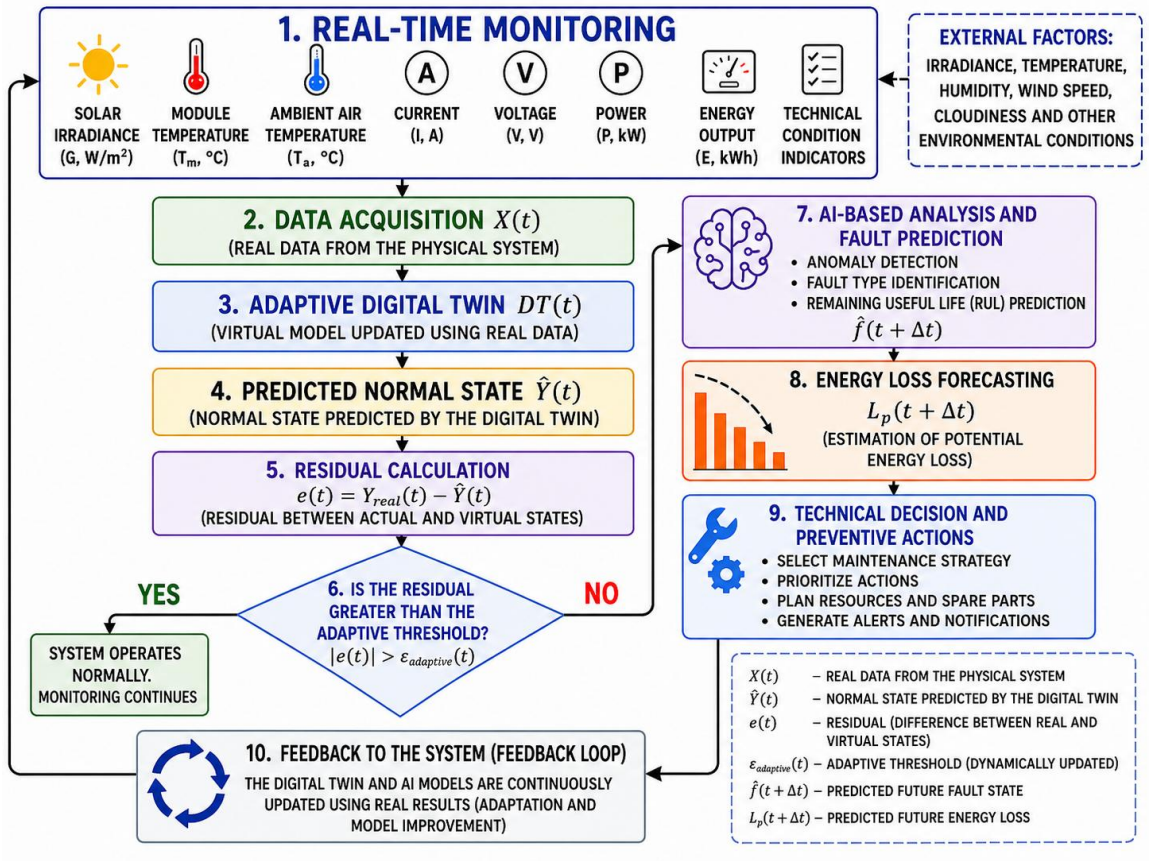


Fig. 2. Adaptive control cycle for early fault detection and energy-loss forecasting.

An important advantage of the proposed method is that the technical condition and energy performance are linked within a unified control cycle. Two anomalies of the same severity level may result in different amounts of energy loss under different operating conditions. Therefore, it is more appropriate to make technical decisions not solely on the basis of the presence of a fault, but also by considering its predicted energy-related consequences. In existing studies, AI-based predictive maintenance is regarded as a promising tool for optimizing maintenance strategies in PV systems [3,5]. In the proposed approach, predictive maintenance is integrated with the digital twin, forming the following decision-making chain: "condition assessment → cause evaluation → future-state forecasting → energy-loss estimation → decision-making." Systematic analyses of PV Digital Twin technologies identify adaptability and bidirectional data exchange as important directions for further development [4]. From this perspective, the main methodological contribution of the present study is the integration of a dynamically updated virtual model, continuously calibrated using real-world operational data, with AI-based diagnostic and energy-loss forecasting modules within a unified framework.

The scientific hypothesis of the study is formulated as follows:

If the digital twin of a photovoltaic system is adaptively updated using real-world operational data, and deviations between the physical and virtual states are analyzed over time using artificial intelligence, then the capability to detect faults before they cause a significant increase in energy losses and to forecast their potential energy-related consequences can be substantially enhanced.

4. Techno-economic justification and research gaps

The integration of Digital Twin (DT) models to enhance the autonomous reliability of photovoltaic (PV) systems is justified based on economic and operational criteria [5]. Unlike conventional monitoring systems, an intelligent DT architecture with bidirectional communication can contribute to reducing the levelized cost of electricity (LCOE) [1]. An autonomous digital twin system can reduce the LCOE through two major pathways: increasing energy yield and reducing operating expenditures (OPEX) [3]. By enabling the early detection of anomalous conditions and short-circuit faults using artificial intelligence [2], the system can minimize plant downtime through autonomous switching and self-healing of affected circuits without direct human intervention. On the other hand, in desert and semi-desert regions, decisions regarding PV panel cleaning can be made based on economic criteria. If the value of the recovered energy exceeds the cost of cleaning and no rainfall is expected in the near future, the system can automatically initiate waterless robotic cleaning operations. This approach can substantially reduce logistical and labor costs under water-scarcity conditions, thereby shortening the payback period of capital expenditures (CAPEX).

4.1. Critical research gaps

An analysis of fundamental research and international trends in the field has identified the following three critical research gaps at both global and regional levels: Lack of bidirectional data flow and control (Bidirectional Control). Only 3.3% of global PV Digital Twin (PVDT) studies have implemented genuine bidirectional communication [1]. Most existing models remain at the Digital Shadow stage, in which data flow primarily from the physical PV plant to its

virtual representation, without enabling autonomous feedback or control commands to be transmitted back to the physical system. Insufficient modeling of regional climatic factors. Existing digital twin frameworks and advanced AI algorithms have predominantly been developed and evaluated under European or temperate climatic conditions [4]. Consequently, they do not adequately account for climate-specific factors characteristic of Uzbekistan, particularly the Kyzylkum Desert and Aral Sea regions, such as the accumulation rate of saline dust, dust cementation phenomena, and long-term experimental measurements obtained from PV installations operating under comparable local environmental conditions. Limitations of hybrid modeling approaches. To reliably distinguish extreme climatic anomalies from physical system faults, there is a need for the parallel evaluation and integration of purely data-driven models with physics-based mathematical models. However, methodologies for developing such integrated, multi-domain hybrid architectures capable of combining physical knowledge with data-driven intelligence have not yet been sufficiently developed [1,5].

4. Conclusion

This study developed the scientific and methodological foundations of an artificial intelligence-based adaptive digital twin method aimed at the early detection of faults occurring in photovoltaic (PV) systems and the reduction of associated energy losses. Within the framework of the study, a functional architecture was proposed comprising the physical PV system, real-time monitoring, data preprocessing, an adaptive digital twin, comparison of actual and virtual states, AI-based fault prediction, and energy-loss assessment. The scientific novelty of the proposed approach lies in evaluating the residual deviation between the physical system and its virtual model using adaptive thresholds, integrating the processes from monitoring to technical decision-making within a unified architecture, and linking predicted fault conditions to their potential energy-loss consequences. The proposed approach provides a methodological basis for transitioning from periodic diagnostics to condition-based and predictive maintenance management. At the same time, the study is analytical and conceptual in nature; therefore, the quantitative performance of the proposed model should be experimentally validated at the next stage using long-term monitoring data from real photovoltaic power plants.

References

[1] IEA PVPS Task 13. The Use of Advanced Algorithms in PV Failure Monitoring. Report IEA-PVPS T13-19:2021. International Energy Agency Photovoltaic Power Systems Programme, 2021.

[2] Alao K. T., Gilani S. I. U. H., Sopian K., Alao T. O. A review on digital twin application in photovoltaic energy systems: challenges and opportunities // JMST Advances. 2024. Vol. 6. P. 257–282. https://doi.org/10.1007/s42791-024-00083-z

[3] Hamza A., Ali Z., Dudley S., Saleem K., Uneeb M., Christofides N. A multi-stage review framework for AI-driven predictive maintenance and fault diagnosis in photovoltaic systems // Applied Energy. 2025. Vol. 393. Art. 126108. https://doi.org/10.1016/j.apenergy.2025.126108

[4] Elnosh A., Calais M., Parlevliet D. A systematic literature review of digital twin research for photovoltaic systems: trends, challenges, and opportunities // Renewable and Sustainable Energy Reviews. 2026. Vol. 226. Art. 116326. https://doi.org/10.1016/j.rser.2025.116326

[5] Thakfan A., Bin Salamah Y. Artificial-intelligence-based detection of defects and faults in photovoltaic systems: a survey // Energies. 2024. Vol. 17, Iss. 19. Art. 4807. https://doi.org/10.3390/en17194807

[6] Hong Y.-Y., Pula R. A. Diagnosis of photovoltaic faults using digital twin and PSO-optimized shifted window transformer // Applied Soft Computing. 2024. Vol. 150. Art. 111092. https://doi.org/10.1016/j.asoc.2023.111092

[7] Montes-Romero J., Heinzle N., Livera A., Theocharides S., Makrides G., Sutterlueti J., Ransome S., Georghiou G. E. Novel data-driven health-state architecture for photovoltaic system failure diagnosis // Solar Energy. 2024. Vol. 279. Art. 112820. https://doi.org/10.1016/j.solener.2024.112820.

Information about the author

Gulom Uzakov	Karshi State Technical University, Doctor of Technical Sciences, Professor E-mail: uzoqov66@mail.ru https://orcid.org/0009-0005-7386-8075
Makhliyo Majidova	Karshi State Technical University, Assistant E-mail: maxliyomajidova106@gmail.com Tel.: +998 87 310 11 93 https://orcid.org/0009-0000-6078-5944

Journal Engineer ISSN: 3030-3893 Volume:4| Issue:3| 2026

Received: 22 July 2026 | **Accepted:** 2 September 2026 | **Published:** 30 September 2026

Precast–monolithic frame building system based on permanent reinforced concrete shell formwork: Analysis of world practice and experimental substantiation

U.D. Khamrokulov[1][a]

[1]Samarkand State University of technical named after Mirzo Ulugbek, Samarkand, Uzbekistan

Abstract: The paper examines the structural solutions of frame buildings erected by precast–monolithic technology in two consecutive stages — a systematic analysis of world practice and the author's own experimental verification. The objective is to identify the structural limits of the existing precast–monolithic frame systems, to substantiate the research gap they leave uncovered, and to verify experimentally a solution that fills this gap. More than seventeen foreign and CIS systems (KUB-2.5, ARKOS, RECON, UDS, Deltabeam, IMS, Structurapid, Thomas, RPS, BGK, Filigran and others) were compared against five criteria: the column solution, the beam solution, the floor solution, the detailing of the joint zone, and the limitation reported in the sources. The proposed solution was then tested under static loads on three types of two-bay, two-storey frame models designed at 1:4 scale by similarity theory. Four development directions of precast–monolithic technology were distinguished, and it was shown that none of them extends the principle of load-bearing formwork to the column cross-section. The ultimate load of the proposed solution exceeded that of the mon olithic reference by 2.8 % (134.12 kN against 130.50 kN) and the load at limiting deflection by 3.0 %, while the difference between the longitudinal strains of the shell and the core did not exceed 5 % in the elastic stage. The precast–monolithic frame system based on a permanent shell formwork column is therefore equal in strength and stiffness to monolithic technology and eliminates the joint-zone deficiencies identified in the existing systems.

Keywords: precast–monolithic concrete, permanent shell formwork, shell–core composite column, joint zone, comparative analysis, experimental substantiation

1. Introduction

More than 20–25 million m² of residential floor area is erected annually in the Republic of Uzbekistan, and 60–70 % of it falls on multi-storey buildings. Most of these buildings are built of monolithic reinforced concrete in removable formwork. The high cost of formwork operations, the extended construction period, the difficulty of controlling concrete quality on site and the dependence on weather conditions are the principal limitations of this technology. Precast–monolithic technology is regarded as a promising way of overcoming them: the frame elements are manufactured under factory conditions and are then united on site with cast-in-place concrete into a single spatial structure [1, 2].

Dozens of systems have been developed and certified worldwide in this direction. However, since each of them was formed around a particular structural idea, the set of systems covers not a continuous field but a number of areas that do not fully overlap. The systematic analysis carried out by Zoteyeva [3] revealed that the deficiencies of the most widespread solutions are concentrated precisely in the joint zone. Nevertheless, the literature review shows that no study has yet compared the structural limitations of the existing systems within a single set of criteria and linked the gap arising from that comparison directly with experimental verification.

The scientific basis of the present work was laid by the author's earlier studies: the influence of stage-by-stage erection and loading on the stress–strain state of multi-storey frame elements [20], the tests of columns made in permanent formwork [18] and the tests of precast hollow-core slab models [19]. The calculation apparatus relies on the nonlinear deformation model developed for flexural reinforced concrete members [21].

The objective of this paper is to compare the precast–monolithic frame systems used in world practice against a single set of criteria, to substantiate the research gap they leave uncovered, to formulate a structural solution filling that gap and to verify its performance experimentally. The novelty lies in the direct coupling of the two stages: every limitation identified at the first stage is answered by a measured indicator obtained at the second.

2. Research methodology

2.1. Method of the analytical part

The analysis covered the precast–monolithic frame systems that have been applied on an industrial scale in world and CIS practice. The sources were the official documents and series albums of the systems, the technical manuals of the manufacturers [4], the normative documents [5–8, 23] and the generalising studies [3, 9]. Each system was described against five criteria: (1) the column solution; (2) the beam solution; (3) the floor solution; (4) the detailing of the joint zone; (5) the principal limitation reported in the sources. The systems were then grouped by these criteria and a matrix of development directions was compiled; the empty cell of the matrix was interpreted as the research gap.

2.2. Method of the experimental part

[a] https://orcid.org/0009-0009-8061-3336

The solution filling the identified gap was verified on three types of frame model. The models were manufactured at 1:4 scale on the basis of similarity theory [10, 11]. Since the materials of the model and of the prototype were identical, the scale factors for stress and modulus of elasticity were taken as $k\sigma = kE = 1$; with a geometric scale $kl = 4$ this gives $kP = kl^2 = 16$ and $kf = kl = 4$. Each model was two-bay and two-storey with an axial grid of 1300×1200 mm. Model M-1 is the conventional monolithic reference; model M-2 has columns formed in permanent reinforced concrete shell formwork, U-shaped precast–monolithic beams and a monolithic floor; model M-3 has the same columns and beams as M-2 but a floor made of precast hollow-core slabs.

The concrete was of class B25. The auxiliary specimens were tested in accordance with GOST 10180-2012 [12] and GOST 24452-80 [13]; the following characteristics were obtained: $R_{bm} = 30.84$ MPa, $R_{bn} = 29.60$ MPa, $R_b = 22.77$ MPa, $R_{bt,n} = 1.85$ MPa and $E_b = 2.9 \cdot 10^4$ MPa. The longitudinal reinforcement was of class A400 ($\sigma_y = 690$ N/mm², $\sigma_u = 750$ N/mm², $\delta = 20$ %). All data were obtained in an accredited laboratory.

Loading was applied in stages by DG-25 hydraulic jacks in accordance with GOST 8829-94 [14] and the test procedure of Zalesov and Klimov [15]; the step of each stage was taken equal to 0.1 of the design ultimate load. Strains were measured by ICh-100 dial gauges with an accuracy of 0.01 mm and cracks were measured with an MPB-2 optical microscope (0.02 mm). Four characteristic states were recorded for each model: the formation of the first crack (P_{crc}), the attainment of the normative crack width ($a_{crc} = 0.3$ mm — P_{acrc}), the attainment of the limiting deflection ($f_{max} = L/200$ — P_f) and the loss of load-bearing capacity (P_u).

3. Results and Discussion

3.1. Comparative analysis of the precast–monolithic frame systems used in world practice

The results of the comparison against the five adopted criteria are given in Table 1. The systems are grouped not geographically but by their structural feature, which makes their limitations directly comparable with one another.

Table 1

Comparison of the precast–monolithic frame systems used in world practice against five criteria

System (country)	Column solution	Beam solution	Floor solution	Joint zone	Principal limitation identified
KUB-2.5 (Russia)	Precast multi-storey column	Beamless	Precast slab	“Slab–column” joint, monolithic ring	Frame performance depends on a single joint; no reserve of reliability
ARKOS (Belarus)	Precast column	Concealed beam inside the slab	Hollow-core slab	Keyed connection at the support	Support keys are executed without reinforcement
RECON (Russia)	Precast column	Beam with U-shaped loop bars	Hollow-core slab	Loop bars + monolithic key	Insufficient anchorage of the loop bars and insufficient key length (300 mm)
UDS (Russia)	Precast column	Precast–monolithic beam	Precast slab	Support joint	Support joint is not strengthened by additional reinforcement
Deltabeam (Finland)	Column with storey-wise slots	Steel–concrete composite Δ-beam	Hollow-core or monolithic slab	Welded steel connection	High steel consumption and amount of welding; dependence on a special factory product
IMS (former Yugoslavia)	Precast column	Post-tensioned beam	Precast slab	By post-tensioning	Special prestressing equipment and high qualification required
Structurapid (Italy)	Single-storey tubular column	T-shaped beam	Precast slab	Insertion into the column groove	Limited storey-to-storey connection of the tubular column
Thomas (USA)	1–3 storey column	Prestressed box-section beam	T-shaped slab + 76 mm topping	Lower corbel with steel collars	Large overall floor depth (0.95–0.99 m)
RPS (Bulgaria)	Precast column	Beamless	Two types of hollow-core slab	Through the groove at the slab end	Limited in-plane stiffness of the floor diaphragm
BGK (Ukraine)	Precast column	Beamless	Hexagonal slab	Mushroom-shaped capital	Punching of the slab in the capital zone governs the design
Filigran / Elementdecken -platten (Germany)	Wall system (no columns)	—	50–70 mm shell panels + monolithic core	Contact joint between shell and core	Wall rather than frame layout; free planning is restricted

https://doi.org/10.56143/3030-3893-2026-3-138-143 A bridge between science and innovation

Table 1 shows that in most systems the limitation is concentrated precisely in the joint zone, that is, at the place where the precast and the cast-in-place parts meet. The column, on the contrary, is treated in almost every system as a wholly factory-made product, and the composite action of precast and cast-in-place concrete within its cross-section is not used as a structural resource.

3.2. Development directions and the identified research gap

Generalisation of the data of Table 1 made it possible to distinguish four independent development directions of precast–monolithic technology: (1) beamless systems (KUB-2.5, RPS, BGK); (2) systems with concealed beams (ARKOS); (3) steel–concrete composite systems (Deltabeam); (4) wall and volumetric-block systems (Filigran, KOPE). The coverage of these directions with respect to the column, the beam and the floor is presented as a matrix in Table 2.

Table 2

Coverage of the development directions of precast–monolithic technology and the identified gap

Direction	Composite action of precast and cast-in-place concrete in the column	Composite action in the beam	Composite action in the floor	Formwork acting as part of the structure
1. Beamless (KUB-2.5, RPS, BGK)	—	no beam	+	—
2. With concealed beam (ARKOS)	—	+	+	—
3. Steel–concrete composite (Deltabeam)	—	+ (steel shell)	+	+ (in the beam only)
4. Wall / volumetric block (Filigran, KOPE)	no column	—	+	+ (in the wall only)
Proposed solution	+ (RC shell + monolithic core)	+ (U-shaped precast–monolithic beam)	+ (monolithic or precast–monolithic)	+ (in column, beam and floor)



Fig. 1. The proposed precast–monolithic frame structural solution and its joint zone

Table 2 shows the coverage and, at the same time, the gap: in none of the existing directions is the principle of load-bearing formwork extended as far as the column cross-section. In the Deltabeam system this principle is realised only in the beam (a steel shell), and in the Filigran system only in the wall. In other words, the concept of a column formed inside thin-walled permanent reinforced concrete shell formwork, acting as a single composite section together with its inner monolithic core and working jointly with a U-shaped precast–monolithic beam and a precast floor, has not been developed. This gap defines the subject of the present study.

3.3. The proposed structural solution

In order to fill the identified gap, a solution consisting of the following three elements was formulated. The column is a thin-walled reinforced concrete shell formwork, reinforced with basalt bars, whose wall thickness is about one eighth of the cross-sectional dimension and whose interior is filled with cast-in-place concrete on site. Having performed the function of formwork, the shell becomes a working part of the cross-section and confines the core concrete laterally. The beam is a precast–monolithic member whose lower part is manufactured in the factory with a U-shaped section and whose upper part is cast together with the floor; the U-shaped shell remains open for placing the reinforcement, so that the contact joint lies within the effective depth of the section and not in the tensile zone. The floor is either a monolithic slab (variant M-2) or a topping cast over precast hollow-core slabs (variant M-3).

3.4. Experimental verification of the proposed solution

In all three models the failure developed in accordance with the theory of limit states: cracks first appeared in the tensile zone of the beams and in the joint zones, then the tensile reinforcement reached its yield limit, and finally the concrete of the compressed zone was crushed [16, 17]. In models M-2 and M-3 the columns behaved as two-layer composite members: no signs of slip were observed at the interface between the shell and the core, and in the elastic stage (load $\leq 0.5 \cdot P_u$) the difference between their longitudinal strains did not exceed 5 %. This confirms that the shell and the core work as a single composite section in a regime of equal strains.

The characteristic loads determined for the three models and their ratios are given in Table 3.

https://doi.org/10.56143/3030-3893-2026-3-138-143

Table 3

Results of testing the frame models under static loads

Indicator	M-1 (reference, monolithic)	M-2 (shell-formwork column, monolithic floor)	M-3 (shell-formwork column, precast floor)
Cracking load P_{crc}, kN	43.62	36.38	43.62
Load at a_{crc} = 0.3 mm, P_{acrc}, kN	94.30	94.30	94.30
Load at limiting deflection P_f, kN	122.15	125.84	104.42
Ultimate load P_u, kN	130.50	134.12	119.64
P_{acrc} / P_u	0.723	0.703	0.788
P_u relative to M-1, %	100	102.8	91.7
P_f relative to M-1, %	100	103.0	85.5
P_{crc} relative to M-1, %	100	83.4	100
Deflection at P = 101.54 kN relative to M-1, %	100	108…117	149…189



Fig. 2. "Load–deflection" relationships for the three models and comparison of the ultimate loads

When the model parameters were converted to the prototype building by means of the adopted scale factors, the column section became 400×400 mm, the shell wall thickness 50 mm, the core section 300×300 mm, the hollow-core slab thickness 220 mm (void diameter 160 mm) and the longitudinal reinforcement 4Ø32 A400 — all of which correspond exactly to the dimensions of standard products in current use. The ratio of the limiting deflections was 24.0/6.0 = 4, that is, exactly equal to the adopted factor *kf*. This independently confirms that the similarity conditions were satisfied.

Discussion

The principal result of the study is the link between the analytical and the experimental stage: every limitation identified in Table 1 can be answered by a measured indicator from Table 3. This correspondence is summarised in Table 4.

Table 4

Limitations identified in the existing systems and the response of the proposed solution

Identified limitation (system)	Structural response in the proposed solution	Experimental confirmation
Unreinforced key at the support joint (ARKOS)	The joint zone is reinforced inside the U-shaped shell of the beam; the key is crossed by reinforcement	Horizontal cracks appeared in the joint zone only at the final loading stages; Pacrc was identical in all three models (94.30 kN)
Insufficient anchorage of the loop bars (RECON)	The beam reinforcement is carried continuously inside the U-shaped shell; loop bars are not required	Failure was governed by yielding of the reinforcement, not by anchorage
Frame performance depends on a single joint, no reserve (KUB-2.5)	The column–beam–floor triad forms three consecutive independent connections	Failure developed gradually, in a ductile manner and with warning cracks
High steel consumption and amount of welding (Deltabeam)	The shell is made of thin-walled reinforced concrete rather than steel; basalt reinforcement is used; welding is not required	P_u = 134.12 kN — 2.8 % higher than the reference, without a steel shell
Composite action of precast and cast-in-place concrete in the column section is not used (all systems)	The shell becomes a working part of the section and confines the core laterally	The difference between the longitudinal strains of shell and core is ≤ 5 %; no slip was observed

https://doi.org/10.56143/3030-3893-2026-3-138-143 A bridge between science and innovation

The crack resistance of model M-2 requires a separate comment: its first crack was recorded at a load 16.6 % lower than that of the reference (36.38 kN). This is explained by the fact that in the M-2 beam the horizontal contact joint between the precast and the cast-in-place layers lies in the upper part of the tensile zone and that the first crack was localised precisely along this joint [22]. It is essential, however, that this did not adversely affect the ultimate load-bearing capacity: the load corresponding to the normative crack width was the same in all three models (94.30 kN), which means that under normal service conditions all three solutions are equally reliable.

Variant M-3 gave a result 8.3 % lower in terms of ultimate load and 14.5 % lower in terms of the load at limiting deflection, and its deflections were 1.5–1.9 times greater than those of the reference. The reason is the more hinge-like connection of the precast hollow-core slabs to the beams and the lower stiffness of the floor diaphragm. This independently confirms the conclusion recorded in Table 1 for beamless systems and systems with precast floors, namely the limited in-plane stiffness of the diaphragm. Accordingly, M-2 was adopted as the principal recommended solution and M-3 as an alternative one.

The results obtained do not contradict the principles of shear resistance along the contact joint set out in Section 10 of EN 1992-1-1 [5], in the provisions of ACI 318-19 concerning precast structures [6, 23] and in fib Model Code 2010 [7]: the absence of slip at the shell–core interface indicates that the roughened-surface condition required by these documents was satisfied. At the same time, the current national normative documents [8] contain no direct provisions for assessing the crack resistance and the stiffness of such composite sections; the present results may serve as an initial basis for filling this gap.

Limitations of the study. The investigation was restricted to static loads; behaviour under seismic (cyclic) actions requires a separate study. In addition, at a scale of 1:4 the bond law between the reinforcement and the concrete does not obey complete similarity, and therefore the results concerning crack spacing and crack width should be extrapolated by means of correction factors.

4. Conclusion

1. The precast–monolithic frame systems used in world and CIS practice were compared against five criteria, and it was established that their limitations are concentrated mainly in the joint zone, that is, at the place where the precast and the cast-in-place parts meet, whereas the column section is treated in almost every system as a wholly factory-made product.

2. Four development directions of precast–monolithic technology were distinguished, and it was shown that in none of them is the principle of load-bearing formwork extended as far as the column section. To fill this gap, a solution comprising a column in thin-walled permanent reinforced concrete shell formwork, a U-shaped precast–monolithic beam and a precast–monolithic floor was proposed.

3. Variant M-2 of the proposed solution gave a result 2.8 % higher than the monolithic reference in terms of ultimate load (134.12 kN against 130.50 kN) and 3.0 % higher in terms of the load at limiting deflection, while its deflections differed from those of the reference by only 8–17 %.

4. In the composite column with permanent shell formwork the shell and the monolithic core act jointly and without slip in the elastic stage — the difference between their longitudinal strains did not exceed 5 %. This experimentally justifies taking the shell into account as a working part of the cross-section.

5. The load corresponding to the normative crack width was 94.30 kN in all three models. Hence, under normal service conditions all three structural solutions are equally reliable.

6. When converted to the prototype building, the model parameters coincided exactly with the dimensions of standard products in current use, and the ratio of the limiting deflections was equal to $kf = 4$. This confirms that the similarity conditions were satisfied and makes it possible to transfer the results to real buildings.

References

[1] Golyshev A.B., Polishchuk V.P., Sungatullin Ya.G., Bachinsky V.Ya. et al. Design and manufacture of precast–monolithic structures / ed. by A.B. Golyshev. – Kyiv: Budivelnyk, 1982. – 152 p.

[2] Mordich A.I., Belevich V.N., Simbirkin V.N., Navoy D.I. Experience of practical application and results of full-scale tests of the BelNIIS precast–monolithic frame // Bulletin of Construction Engineering. – 2004. – No. 8. – pp. 8–12.

[3] Zoteyeva E.E. Complex assessment and improvement of structural and technological solutions of civil monolithic and precast–monolithic buildings: Cand. Tech. Sci. diss.: 05.23.08. – Yekaterinburg: Ural Federal University, 2018. – 148 p.

[4] Peikko Group. DELTABEAM® Composite Beam. Technical Manual. – Lahti: Peikko Group Corporation, 2023.

[5] EN 1992-1-1:2004. Eurocode 2: Design of concrete structures. Part 1-1: General rules and rules for buildings. – Brussels: CEN, 2004. – 226 p.

[6] ACI 318-19. Building Code Requirements for Structural Concrete and Commentary. – Farmington Hills, MI: American Concrete Institute, 2019. – 624 p.

[7] fib Model Code for Concrete Structures 2010. – Berlin: Ernst & Sohn, 2013. – 434 p.

[8] ShNK 2.03.01-24. Concrete and reinforced concrete structures. – Tashkent: Ministry of Construction of the Republic of Uzbekistan, 2024.

[9] Jasienko J., Oleinik A., Pisznyak I. Theory of strengthening and restoration of precast-monolithic buildings using permanent formwork // Archives of Civil and Mechanical Engineering. – 2010. – Vol. 10.

[10] Buckingham E. On physically similar systems; illustrations of the use of dimensional equations // Physical Review. – 1914. – Vol. 4, No. 4. – pp. 345–376.

[11] Sabnis G.M., Harris H.G., White R.N., Mirza M.S. Structural modeling and experimental techniques. – Englewood Cliffs, NJ: Prentice-Hall, 1983. – 585 p.

[12] GOST 10180-2012. Concretes. Methods for strength determination using reference specimens. – Moscow: Standartinform, 2013. – 30 p.

[13] GOST 24452-80. Concretes. Methods of prismatic compressive strength, modulus of elasticity and Poisson's

ratio determination. – Moscow: Publishing House of Standards, 1980. – 16 p.

[14] GOST 8829-94. Reinforced concrete and concrete factory-made building products. Loading test methods. – Moscow: Standartinform, 1997. – 26 p.

[15] Zalesov A.S., Klimov Yu.A. Strength of reinforced concrete structures under the action of transverse forces. – Kyiv: Budivelnyk, 1989. – 104 p.

[16] Gvozdev A.A. Calculation of the load-bearing capacity of structures by the limit equilibrium method. – Moscow: Gosstroyizdat, 1949. – 280 p.

[17] Murashev V.I. Crack resistance, stiffness and strength of reinforced concrete. – Moscow: Mashstroyizdat, 1950. – 268 p.

[18] Khamrokulov U.D., Madatov I.A., Kamoliddinov D. Experimental studies on testing columns made in permanent formwork // Problems of Architecture and Construction. – 2025. – No. 2. – pp. 75–77.

[19] Khamrokulov U.D. Determination of the load-bearing capacity of a precast hollow-core slab model // Problems of Architecture and Construction. – 2025. – No. 3. – pp. 58–60.

[20] Khamrokulov U.D. The influence of stage-by-stage erection and loading on the stress–strain state of multi-storey frame building elements: PhD diss. – Samarkand: SamSUACE, 2022. – 142 p.

[21] Usmanov V.F. Strength, crack resistance and deformation of flexural bar elements of reinforced concrete structures: Doct. Tech. Sci. (DSc) diss. – Samarkand: SamSUACE, 2023. – 268 p.

[22] Smolyago G.A. Deformability and crack resistance of flexural reinforced concrete elements: monograph. – Belgorod: BSTU named after V.G. Shukhov, 2009. – 224 p.

[23] PCI Design Handbook: Precast and Prestressed Concrete. 8th ed. – Chicago: Precast/Prestressed Concrete Institute, 2017.

Information about the author

Ulugbek Khamrokulov
Samarkand State Technical University named after Mirzo Ulugbek, Department of Civil engineering, DSc student, PhD
E-mail: midimin@mail.ru
Tel.: +998 91 552-96-64
https://orcid.org/0009-0009-8061-3336

Journal Engineer ISSN: 3030-3893 Volume:4| Issue:3| 2026

Received: 23 July 2026 | **Accepted:** 3 September 2026 | **Published:** 30 September 2026

Mechanically induced surface modification of diabase aggregate for high-performance concrete

Z. Kurbonov[1][a], S. Bozorboev[1]

[1]Jizzakh Polytechnic Institute, Jizzakh, Uzbekistan

Abstract: This study investigates the effect of pre-treatment of diabase sand in an aqueous medium on the mechanical properties of concrete. A submerged processing device equipped with two vertically arranged counter-rotating rotors was used to treat the mineral aggregate directly inside an open mixing vessel. Diabase sand from the Uzunbulak-II deposit with a particle size of 0.16–1.25 mm was used as the mineral component, while technical lignosulfonate was applied as a chemical additive. The treatment was performed for 30 min at a relative working-element velocity of 34.6 m/s and a rotor gap of 5 mm. Particle-size analysis showed that the content of particles smaller than 0.05 mm increased from 0.5% to 5%, while the main 0.16–0.63 mm fraction changed only slightly. Concrete produced using the treated aggregate achieved a 28-day compressive strength of 47.8 MPa, representing an 18.9% increase compared with the untreated control mixture. The obtained results indicate that pre-treatment of mineral aggregates in an aqueous medium can be considered a promising approach for improving the strength characteristics of concrete.

Keywords: diabase sand, mineral aggregate, mechanical treatment, surface modification, aqueous medium, lignosulfonate, concrete, compressive strength, particle-size distribution, mechanical processing

1. Introduction

Concrete is one of the most widely used construction materials due to its high compressive strength, durability, availability of raw materials, and adaptability to different structural applications. The performance of concrete is determined not only by the properties of cement and water but also by the characteristics of mineral aggregates, which constitute the major volume fraction of the composite. Therefore, improving the interaction between aggregate particles and the cementitious matrix is an important approach for enhancing the mechanical performance and durability of concrete.

Mineral aggregates are generally considered relatively inert components of concrete; however, their surface characteristics have a significant influence on the formation of the interfacial transition zone between aggregate particles and cement paste. Surface roughness, particle morphology, specific surface area, and the presence of weak surface films can affect mechanical interlocking and adhesion within the cement matrix. Consequently, controlled modification of aggregate surfaces and particle-size characteristics can provide an opportunity to improve the structure and mechanical properties of cement-based composites.

Diabase and basalt aggregates are characterized by high hardness, strength, and resistance to environmental influences, which makes them suitable for use in concrete and other construction materials. At the same time, the relatively dense and mechanically stable structure of these mineral materials limits the possibility of modifying their surface characteristics using conventional mixing procedures. Intensive mechanical treatment can increase the specific surface area, alter particle morphology, remove weak surface layers, and generate additional active surfaces. However, excessive grinding may result in unnecessary energy consumption and excessive formation of fine particles.

An alternative approach is the treatment of mineral aggregates directly in an aqueous suspension. In such a system, mechanical impact, shear deformation, particle–particle interaction, and hydrodynamic effects can occur simultaneously. The presence of a liquid medium facilitates the circulation of fine particles and provides favorable conditions for the interaction of freshly generated mineral surfaces with dissolved chemical additives. In particular, lignosulfonate-based additives can be adsorbed onto newly formed particle surfaces during mechanical processing, potentially affecting particle dispersion and their subsequent interaction with the cementitious matrix.

The efficiency of mechanical treatment depends strongly on the configuration and operating parameters of the processing system. Counter-rotating working elements can generate a localized zone of intense shear and impact within the suspension. Such a configuration provides relative movement between the working elements and promotes repeated interaction of mineral particles with the processing zone. When the treatment is performed directly inside an open mixing vessel, the need for a separate closed grinding chamber and forced material-transfer system can also be reduced.

The use of an immersed processing system is particularly relevant for concrete production because aggregate treatment can be integrated into the preparation of the concrete mixture. This approach may allow mineral particles to be processed together with water and a chemical additive before the introduction of cement and coarse aggregate. As a result, the treated suspension can be directly incorporated

[a] https://orcid.org/0000-0002-1491-4044

into the subsequent concrete mixing process without an additional drying or transportation stage.

Despite the potential advantages of intensive mechanical treatment of mineral aggregates, the relationship between treatment conditions, particle-size modification, and the resulting strength of concrete requires further experimental investigation. In particular, it is important to determine whether intensive treatment can improve the properties of the aggregate without causing excessive grinding of the original particle fraction.

Therefore, the objective of this study was to investigate the effect of in-situ mechanical treatment of diabase sand in an aqueous medium on its particle-size characteristics and on the compressive strength of concrete. The study focused on diabase sand with a particle size of 0.16–1.25 mm treated using a submerged counter-rotating rotor system in the presence of technical lignosulfonate. The influence of the treatment process was evaluated by comparing the particle-size distribution of untreated and treated sand and by determining the 7- and 28-day compressive strength of concrete prepared using the treated aggregate.

The results obtained in this study provide an experimental basis for evaluating the applicability of in-situ mechanical treatment of mineral aggregates as a technological approach for improving the mechanical performance of concrete while maintaining the main fraction of the original aggregate.

Literature Review. The mechanical performance of concrete is strongly influenced by the characteristics of its mineral aggregates and by the quality of the contact zone between aggregate particles and the cementitious matrix. Although aggregates are generally regarded as relatively inert components, their particle size distribution, morphology, surface roughness, and surface condition can substantially affect the packing structure and mechanical interaction within hardened concrete.

Mechanical treatment of mineral materials is widely considered an effective approach for modifying particle characteristics. During intensive mechanical processing, particles can undergo impact, shear, abrasion, and fracture, resulting in changes in particle-size distribution and surface morphology. The formation of newly exposed surfaces may improve mechanical interlocking between aggregate particles and cement paste. However, excessive grinding is undesirable because it increases energy consumption and may lead to an excessive amount of fine material.

Particular attention has been given to the treatment of mineral materials in liquid media. Compared with dry processing, treatment in an aqueous suspension provides continuous particle circulation and facilitates the removal and dispersion of fine particles. Simultaneous mechanical and hydrodynamic effects can promote the destruction of weak surface layers and modification of the external surface of mineral grains.

The use of chemical additives during mechanical treatment may further influence the dispersion process. Lignosulfonate-based additives are capable of interacting with mineral surfaces and can facilitate particle dispersion in aqueous systems. When mechanical treatment continuously generates fresh mineral surfaces, adsorption of the dissolved additive may occur simultaneously with surface renewal. This provides a potential mechanism for controlling particle agglomeration and improving the subsequent interaction between mineral particles and the cementitious matrix.

Another important factor is the hydrodynamic regime generated within the treatment zone. Counter-rotating working elements can produce a localized region characterized by high relative velocity, shear, and repeated particle movement. In comparison with a single rotating element, the counter-rotating configuration provides a greater relative velocity between opposing working elements at the same peripheral velocity. The resulting mechanical environment can intensify particle–particle and particle–working-element interactions.

The technological integration of aggregate treatment directly into a concrete mixer is also of practical interest. A submerged processing system eliminates the need for separate drying and grinding stages and allows the mineral suspension to be treated immediately before concrete production. Such an approach can potentially reduce material handling operations and simplify the technological process.

Previous approaches to mechanical activation of mineral materials have predominantly focused on intensive grinding and the production of highly dispersed powders. The present study considers a different technological objective: controlled modification of the surface and particle-size characteristics of a relatively coarse mineral aggregate while retaining a substantial portion of its initial fraction. This distinction is important because the objective is not complete grinding of the diabase but selective mechanical treatment that can improve its interaction with the cementitious matrix.

Based on these considerations, the present study evaluates the effect of aqueous mechanical pre-treatment of diabase sand on particle-size distribution and concrete compressive strength. The experimental approach combines mechanical processing, aqueous suspension treatment, and simultaneous addition of lignosulfonate.

2. Research methodology

Diabase sand obtained from the Uzunbulak-II deposit in the Jizzakh Region of the Republic of Uzbekistan was selected as the mineral aggregate. The initial particle-size range was 0.16–1.25 mm. According to the experimental description, the diabase had a Mohs hardness of approximately 6–7 and a density of 2.9–3.0 g/cm³.

Technical lignosulfonate (LST) was used as a chemical additive during aqueous treatment. In the experimental procedure, the additive dosage was 0.17% of the mass of the mineral aggregate.

For the concrete mixture, M400 cement, diabase crushed stone with a particle size of 5–20 mm, water, and the treated diabase sand were used. The concrete composition was maintained constant for the comparative tests.

Mechanical Pre-Treatment System

The mineral aggregate was treated using a submerged mechanical processing system equipped with two vertically oriented counter-rotating rotors. The working module consisted of two parallel vertical shafts positioned 90–190 mm apart. Disk-shaped rotors with diameters of 100–200 mm were mounted on the shafts.

In the basic experimental configuration, the rotor diameter was 110 mm, the shaft spacing was 100 mm, and the disks were vertically displaced by 55 mm. Each disk was equipped with six rod-shaped working elements having a length of 50 mm and a square cross-section of 10 × 10 mm.

The working elements of the upper rotor were directed downward, whereas those of the lower rotor were directed

upward. During operation, the working elements of one rotor passed through the spaces between the working elements of the opposite rotor without direct mechanical contact. The gap between the opposing elements was maintained at 5 mm.

The electric motor had a rated power of 3 kW and a rotational speed of 3000 rpm. The working module was immersed directly into the mineral suspension at a depth of approximately 25 cm. This configuration enabled treatment of the suspension directly inside the concrete mixer.

Preparation and Treatment of the Mineral Suspension

The suspension was prepared by sequentially introducing 45 kg of water, 60 kg of diabase sand, and 100 g of technical lignosulfonate into the mixing vessel. The initial water temperature was 18–20 °C. The resulting suspension had a total mass of approximately 105.1 kg, with a solid-to-total mass ratio of approximately 57%.

Before mechanical treatment, the components were preliminarily mixed for 2–3 min at a mixer rotation speed of approximately 20 rpm.

Particle-Size Analysis

The particle-size distribution of the diabase sand was determined before and after mechanical treatment. The initial aggregate consisted primarily of particles within the 0.16–1.25 mm range.

For comparative evaluation, the material was divided into four particle-size groups:

- 0.63–1.25 mm;
- 0.16–0.63 mm;
- 0.05–0.16 mm;
- <0.05 mm.

The changes in the proportion of these fractions were used to evaluate the degree of selective mechanical fragmentation.

Concrete Preparation and Strength Testing

After completion of the 30-min treatment, the working module was removed from the suspension. The treated diabase sand and the water contained in the suspension were subsequently used directly for concrete preparation.

The concrete mixture contained:

- M400 cement — 480 kg/m³;
- treated diabase sand — 720 kg/m³;
- diabase crushed stone, 5–20 mm — 1104 kg/m³;
- total mixing water — 180 L/m³.

The control mixture had the same basic proportion of cement, sand, coarse aggregate, and water but was prepared using untreated diabase sand.

The concrete specimens were tested for compressive strength at 7 and 28 days. The experimental procedure was based on the requirements specified in GOST 10180. The obtained strength values were compared with those of the control concrete.

The principal indicators used for evaluating the effectiveness of the treatment were the change in particle-size distribution and the increase in compressive strength of concrete relative to the untreated control composition.

3. Results and Discussion

The mechanical pre-treatment of diabase sand in an aqueous medium resulted in a measurable change in its particle-size distribution. The initial material obtained from the Uzunbulak-II deposit was characterized by a particle-size range of 0.16–1.25 mm. After 30 min of treatment at a relative working-element velocity of 34.6 m/s and a rotor gap of 5 mm, an increase in the fine-particle fraction was observed.

The particle-size distribution before and after treatment is presented in Table 1.

Table 1

Particle-size distribution of diabase sand before and after aqueous mechanical treatment

Sample	0.63–1.25 mm	0.16–0.63 mm	0.05–0.16 mm	<0.05 mm
Control	46.0%	53.5%	–	0.5%
Treated	30.5%	49.5%	15.0%	5.0%

The results demonstrate that the proportion of particles smaller than 0.05 mm increased from 0.5% in the untreated material to 5.0% after treatment. At the same time, the main 0.16–0.63 mm fraction remained relatively stable, decreasing from 53.5% to 49.5%.

The proportion of the 0.63–1.25 mm fraction decreased from 46.0% to 30.5%, accompanied by the appearance of 0.05–0.16 mm particles at a proportion of 15%. This indicates that the treatment caused selective fragmentation of the larger particles rather than complete grinding of the original aggregate.

The observed changes are consistent with the intended operating principle of the processing system, in which mineral particles are subjected to repeated impact, shear, and abrasive interactions within the treatment zone. The formation of additional fine particles indicates that the mechanical treatment was sufficiently intensive to modify the particle-size distribution while retaining a considerable proportion of the original aggregate fractions.

Effect of Treated Diabase Sand on Concrete Strength

The treated diabase sand was subsequently used directly in concrete production. The concrete mixture was prepared using the same basic proportion of cement, sand, coarse aggregate, and water for both the experimental and control compositions.

The compressive strength results obtained at 7 and 28 days are summarized in Table 2.

Table 2

Compressive strength of concrete containing untreated and treated diabase sand

Group	Cement: Sand: Coarse aggregate	W/C	7-day strength, MPa	28-day strength, MPa	Increase relative to control
Control	1:1.5:2.3	0.40	28.4	40.2	–
Treated	1:1.5:2.3	0.40	36.2	47.8	+18.9%

The concrete containing the treated diabase sand demonstrated a 7-day compressive strength of 36.2 MPa compared with 28.4 MPa for the control mixture. This corresponds to an increase of approximately 27.5% at the early-age testing stage.

At 28 days, the compressive strength of the experimental concrete reached 47.8 MPa, whereas the control concrete achieved 40.2 MPa. Thus, the use of mechanically pre-treated diabase sand resulted in an increase of 7.6 MPa, corresponding to an improvement of 18.9% relative to the control composition.

The results also show that the treated concrete developed strength more rapidly during the early curing period. Its 7-day strength reached approximately 75.7% of its 28-day strength, while the corresponding value for the control concrete was approximately 70.6%.

Relationship between Particle-Size Modification and Concrete Strength

The increase in concrete strength was accompanied by changes in the particle-size distribution of the diabase sand. The treatment generated an additional fine fraction while preserving a substantial proportion of the original 0.16–0.63 mm fraction.

The formation of finer particles may improve the packing of the granular skeleton and reduce the size of voids between larger aggregate particles. In addition, mechanical treatment can modify the external surface of mineral particles, potentially improving mechanical interlocking with the cementitious matrix.

The experimental results therefore indicate a relationship between controlled modification of the aggregate and the resulting mechanical performance of concrete. However, the present experimental data do not allow the contribution of individual mechanisms—such as surface roughness, particle packing, shear effects, or chemical adsorption—to be quantified separately. These mechanisms should therefore be considered as possible contributing factors rather than independently verified causes.

Practical Effectiveness of the Treatment

One of the important features of the investigated approach is that the mineral aggregate was treated directly in the aqueous medium and subsequently used for concrete production without a separate drying stage. The treatment was performed for 30 min using a submerged counter-rotating rotor system.

The experimental configuration provided a relative working-element velocity of 34.6 m/s, a 5 mm inter-rotor gap, and a treatment duration of 30 min. Under these conditions, the fine fraction below 0.05 mm increased tenfold in relative terms, from 0.5% to 5.0%.

At the same time, the principal concrete performance indicator—the 28-day compressive strength—increased from 40.2 to 47.8 MPa. The combined particle-size and strength results demonstrate that controlled aqueous pre-treatment of diabase sand has the potential to improve the mechanical performance of concrete.

It should be emphasized that the reported experimental results are based on the specific processing conditions and concrete composition investigated in this study. Further experiments with different treatment durations, rotor velocities, gap sizes, additive dosages, and aggregate fractions are required to determine the optimal processing conditions and establish the reproducibility of the observed strength improvement.

Discussion

The obtained results demonstrate that aqueous mechanical pre-treatment can significantly modify the particle-size characteristics of diabase sand and positively affect the compressive strength of concrete. The increase in the fraction of particles smaller than 0.05 mm from 0.5% to 5.0% indicates that the treatment promotes selective fragmentation of the larger particles. At the same time, the main 0.16–0.63 mm fraction was largely preserved, suggesting that the process does not result in complete grinding of the aggregate.

The improvement in concrete strength can be associated with the combined effect of particle-size modification and changes in the surface condition of the mineral aggregate. The formation of additional fine particles may improve packing within the cementitious system, while mechanical treatment can enhance the physical interaction between the aggregate surface and cement paste. Under the investigated conditions, the 28-day compressive strength increased from 40.2 MPa for the control concrete to 47.8 MPa for concrete containing treated diabase sand, corresponding to an 18.9% improvement.

An important technological advantage of the investigated method is the possibility of treating the mineral aggregate directly in an aqueous suspension and subsequently using the treated suspension for concrete preparation. This eliminates the need for an additional drying stage and may simplify the overall production process. However, the contribution of individual mechanisms, including surface modification, particle packing, shear effects, and additive adsorption, requires further experimental verification.

4. Conclusion

The study demonstrated the effectiveness of aqueous mechanical pre-treatment of diabase sand for improving the mechanical performance of concrete. Under the investigated conditions, treatment at a relative working-element velocity of 34.6 m/s, a 5 mm rotor gap, and a duration of 30 min resulted in a substantial modification of the particle-size distribution.

The proportion of particles smaller than 0.05 mm increased from 0.5% to 5.0%, while a considerable part of the original aggregate structure was retained. The use of the treated diabase sand increased the 7-day compressive strength of concrete from 28.4 to 36.2 MPa and the 28-day strength from 40.2 to 47.8 MPa. The resulting 18.9% increase in 28-day compressive strength confirms the potential of the proposed pre-treatment approach.

The investigated technology can be considered a promising method for improving mineral aggregate performance directly within an aqueous medium. Further studies should focus on optimizing treatment duration, rotor velocity, inter-rotor gap, and chemical additive dosage, as well as on evaluating the durability and microstructural characteristics of the resulting concrete.

References

[1] Egamberdiyev, I. B. o‘g‘li, Zafarov, O. XXX, & Qurbonov, Z. H. (2026). Aggressiv muhit ta’siriga bardoshli beton konstruksiyalarni tayyorlash uchun mo‘ljallangan

beton qorishmasining tarkibi. Uzbekistan Patent IAP 8635, application No. IAP 20260314, July 6, 2026.

[2] Elahi, M., Shearer, C. R., Naser, A., & Reza, A. N. R. (2021). Improving the sulfate attack resistance of concrete by using supplementary cementitious materials (SCMs): A review. Construction and Building Materials, 281, 122628. DOI: 10.1016/j.conbuildmat.2021.122628.

[3] Liang, N., Mao, J., Yan, R., Liu, X., & Zhou, X. (2022). The damage evolution behavior of polypropylene fiber reinforced concrete subjected to sulfate attack based on acoustic emission. Frontiers of Structural and Civil Engineering, 16(3), 316–328. DOI: 10.1007/s11709-022-0810-8.

[4] A. K. Akhrarovich, A. R. Nazirbayevich, and Q. Z. Hamidulloyevich, “Analysis of the thermal insulation properties of expanded clay concrete with mineral additives,” Universum: Technical Sciences, no. 10(139), pp. 61–64, 2025, doi: 10.32743/UniTech.2025.139.10.20967.

[5] N. Parsaeva and Z. H. Kurbanov, “Study of the process of determination of chemically contained water in the concentration of additional cement made on the basis of peroxide waste,” AIP Conference Proceedings, vol. 2789, no. 1, Art. no. 020012, 2023, doi: 10.1063/5.0145712.J

[6] Z. H. Kurbanov and N. Parsaeva, “Strong grinding based on local raw materials getting stones,” AIP Conference Proceedings, vol. 2432, no. 1, Art. no. 030104, 2022, doi: 10.1063/5.0089995.

[7] Z. H. Kurbanov, Dry Building Mixtures Based on Cement, Advances in Materials Science Research, vol. 60. New York, NY, USA: Nova Science Publishers, 2024, pp. 283–286.

[8] GOST 31384-2017. Protection of Concrete and Reinforced Concrete Structures Against Corrosion. General Technical Requirements. Moscow, Russia, 2017.

[9] O. B. Berdiyev, Z. H. Kurbanov, E. Tilavov, N. Rasulova, S. Boboqulova, I. Jumanov, and B. Botirov, “The calculation of reinforced concrete conical dome shells considering concrete creep,” E3S Web of Conferences, vol. 587, Art. no. 03001, 2024, doi: 10.1051/e3sconf/202458703001.

[10] Egamberdiyev, I. B. o‘g‘li, & Zafarov, O. XXX. (2026). Temirbeton mahsulotlarini tayyorlash uchun mo‘ljallangan beton qorishmasi. Uzbekistan Patent IAP 8623, application No. IAP 20260313, registered June 29, 2026.

[11] Zhang, C., Li, J., Yu, M., et al. (2024). Mechanism and performance control methods of sulfate attack on concrete: A review. Materials, 17(19), 4836. DOI: 10.3390/ma17194836.

Information about the author

Zavkiddinjon Kurbonov	Associate Professor, Department of Construction Materials and Structures, Jizzakh Polytechnic Institute, PhD in Technical Sciences E-mail: zavaclash@gmail.com Tel.:+998880950999 https://orcid.org/0000-0002-1491-4044
Sirojiddin Bozorboev	"KARAKALPAK SEMENT" LLC, Sample Collector, Laboratory

Journal Engineer ISSN: 3030-3893 Volume:4| Issue:3| 2026

Received: 24 July 2026 | **Accepted:** 4 September 2026 | **Published:** 30 September 2026

Optimization of fine-grained concrete composition for hydraulic structures using chemical admixtures

Z. Kurbonov[1][a], S. Bozorboev[1], I. Egamberdiev[1]

[1]Jizzakh Polytechnic Institute, Jizzakh, Uzbekistan

Abstract: This study investigates the improvement of the physical, mechanical, and technological properties of fine-grained concrete intended for use in hydraulic structures. Portland cement M500 D20 produced in the Jizzakh region was used as the binder, while crushed diabase-based material and natural sand were used as mineral aggregates. To regulate the properties of the concrete mixture, Sika 4336 and Sika 908 chemical admixtures were incorporated at dosages of 0.3, 0.5, 0.7, and 0.9% by cement mass. The average density, workability, and compressive strength of the concrete were investigated at curing ages of 3, 7, and 28 days. The experimental results demonstrated the high efficiency of the concrete composition containing Sika 4336. At 28 days, the average compressive strength reached 55.93 MPa, which was 11.5% higher than that of the concrete containing Sika 908. The slump of the concrete mixture containing Sika 4336 reached 24 cm, while its workability was maintained for approximately two hours. Based on the comprehensive analysis of the physical, mechanical, technological, and economic characteristics, the B30 (M400) fine-grained concrete composition was recommended as an optimal composition for hydraulic structures. The obtained results demonstrate the potential of locally available diabase aggregate combined with an effective polycarboxylate-based chemical admixture for producing high-performance fine-grained concrete for hydraulic engineering applications.

Keywords: fine-grained concrete, hydraulic structures, diabase, Portland cement, superplasticizer, Sika 4336, Sika 908, concrete mixture, compressive strength, density, water permeability, concrete composition

1. Introduction

Hydraulic structures are among the most important elements of water-management infrastructure, and their reliability largely depends on the durability and performance of the concrete used in their construction. Concrete in hydraulic structures is subjected to prolonged exposure to water, moisture, hydrostatic pressure, temperature variations, and other environmental factors. Therefore, ensuring sufficient compressive strength, density, water resistance, frost resistance, and long-term durability is an important requirement for concrete used in hydraulic engineering. The analysis presented in the dissertation indicates that improving the strength, water resistance, and long-term durability of fine-grained concrete for hydraulic structures is one of the relevant directions in modern construction materials technology.

Fine-grained concrete has attracted considerable attention because its properties can be effectively controlled through the selection and optimization of cement, fine aggregate, water-to-cement ratio, mineral fillers, and chemical admixtures. The absence of conventional coarse aggregate or its limited use results in a material whose structure is strongly influenced by the characteristics of the fine aggregate and cement matrix. Consequently, the granulometric composition, density, water absorption, and strength of the aggregate become important factors in determining the physical and mechanical properties of the resulting concrete.

For hydraulic engineering applications, the use of locally available mineral materials is particularly important. The investigated concrete compositions were prepared using Portland cement, natural sand, and mineral fillers based on diabase. The dissertation research established that diabase aggregates characterized by high density and strength can contribute to improving the physical and mechanical properties of fine-grained concrete. Concrete specimens obtained during the experimental investigations had densities within the range of 2427–2450 kg/m³, confirming the formation of a relatively dense concrete structure.

Another important approach to improving the performance of fine-grained concrete is the application of modern chemical admixtures. Chemical admixtures can modify the rheological properties of fresh concrete, improve workability, reduce water demand, and contribute to the formation of a denser hardened structure. In the present study, Sika 4336 and Sika 908 were selected for experimental investigation. According to the research data, Sika 4336 is a high-performance superplasticizer based on polycarboxylate ether, intended to increase concrete workability and reduce water consumption. Sika 908 was investigated as an additional chemical modifier aimed primarily at improving durability and corrosion resistance of reinforced concrete structures.

The chemical admixtures were introduced into the concrete mixtures at dosages of 0.3, 0.5, 0.7, and 0.9% by cement mass. Their influence on the workability, density, and compressive strength of fine-grained concrete was experimentally evaluated. The experimental results demonstrated that the use of Sika 4336 provided particularly favorable results. At 28 days, the average compressive strength of the concrete containing Sika 4336 reached 55.93

[a] https://orcid.org/0000-0002-1491-4044

MPa, exceeding the corresponding result obtained with Sika 908 by 11.5%. Furthermore, the slump of the concrete mixture containing Sika 4336 reached 24 cm and remained almost unchanged for approximately two hours.

The obtained results indicate that the combined optimization of the mineral composition and chemical modification of fine-grained concrete can provide a technically effective material for hydraulic structures. The development of B22.5 (M300), B25 (M350), and B30 (M400) compositions and their comparative evaluation showed that the B30 (M400) composition provided the most favorable combination of strength, workability, and operational characteristics and was therefore recommended for hydraulic structures.

Thus, the purpose of this study was to investigate the effect of diabase-based mineral aggregate and chemical admixtures on the physical, mechanical, and technological properties of fine-grained concrete and to determine an optimal composition suitable for hydraulic structures. The study focuses particularly on the comparative effectiveness of Sika 4336 and Sika 908 and on establishing the optimal admixture dosage for obtaining concrete with improved performance characteristics.

Literature Review. Concrete used in hydraulic structures is exposed to a complex combination of environmental and mechanical actions, including prolonged contact with water, hydrostatic pressure, moisture variation, temperature fluctuations, and freeze–thaw cycles. Therefore, the development of concrete with adequate compressive strength, density, water resistance, and long-term durability is an important research direction in modern construction materials technology. In particular, the optimization of concrete composition is considered an effective approach for improving the performance and service reliability of hydraulic structures.

Fine-grained concrete has received increasing attention because its physical and mechanical properties can be controlled through the rational selection of cement, fine aggregates, water-to-cement ratio, mineral fillers, and chemical admixtures. Unlike conventional concrete containing a significant proportion of coarse aggregate, the structure of fine-grained concrete is strongly influenced by the characteristics and particle-size distribution of the fine aggregate and cement matrix. Consequently, aggregate grading, particle packing, density, water absorption, and strength play an important role in determining the final properties of the concrete.

The use of locally available mineral materials is particularly relevant for the production of construction materials. Local aggregates can reduce transportation costs, increase the economic efficiency of concrete production, and provide an opportunity to utilize regional mineral resources. Dense and strong crushed-rock aggregates can contribute to the formation of a compact concrete structure and improve its mechanical performance. In this context, diabase-based mineral materials are of particular interest because of their suitable physical and mechanical characteristics. The experimental materials used in the present study included diabase-based crushed material and natural sand, which were selected as mineral components of the fine-grained concrete.

Another important approach to improving concrete performance is the incorporation of chemical admixtures. Modern chemical admixtures are widely used to regulate the rheological properties of fresh concrete, increase workability, reduce water demand, and improve the structure of hardened concrete. Superplasticizers are especially effective because they enable a high level of workability to be achieved at a reduced water content. A lower water-to-cement ratio generally promotes the formation of a denser cementitious matrix, which can contribute to increased compressive strength and improved resistance to water penetration.

Polycarboxylate-based superplasticizers are among the most effective chemical admixtures used in modern concrete technology. Their dispersing action promotes better separation of cement particles and improves the efficiency of water utilization within the concrete mixture. As a result, the required workability can be maintained with a lower water content. However, the effectiveness of a chemical admixture depends not only on its chemical composition but also on its dosage, cement characteristics, aggregate properties, water-to-cement ratio, and overall concrete composition.

The determination of an optimum admixture dosage is therefore an important part of concrete mix optimization. An insufficient dosage may not provide the required improvement in workability or strength, whereas an excessive dosage may negatively affect the stability and setting characteristics of the concrete mixture. For this reason, experimental evaluation of several admixture dosages is necessary to establish the most effective range for a particular combination of cement and aggregates.

For hydraulic structures, high compressive strength alone cannot be considered a sufficient criterion for selecting an optimal concrete composition. The concrete should also possess appropriate density, workability, water resistance, and durability characteristics. Consequently, a comprehensive assessment of physical, mechanical, technological, and operational properties is required when developing concrete mixtures for hydraulic engineering applications.

Previous research approaches indicate that the combined optimization of mineral composition and chemical modification can significantly improve the performance of fine-grained concrete. The use of high-density mineral aggregates together with efficient chemical admixtures provides an opportunity to obtain a compact concrete structure while maintaining adequate workability of the fresh mixture. Such an approach is particularly relevant when locally available mineral resources are incorporated into the concrete composition.

The present study focuses on the comparative evaluation of Sika 4336 and Sika 908 chemical admixtures in fine-grained concrete containing Portland cement, natural sand, and diabase-based mineral materials. The admixtures were investigated at dosages of 0.3, 0.5, 0.7, and 0.9% by cement mass. Their effects on the workability, density, and compressive strength of concrete were evaluated at curing ages of 3, 7, and 28 days.

The experimental program considered B22.5 (M300), B25 (M350), and B30 (M400) concrete compositions. Comparative evaluation of control and chemically modified mixtures made it possible to determine the influence of chemical admixtures on the development of concrete properties. According to the experimental results, the use of Sika 4336 demonstrated particularly favorable performance, including improved workability and increased 28-day compressive strength.

Based on the reviewed approaches and the results obtained in the present investigation, the optimization of

fine-grained concrete for hydraulic structures should be based on the integrated consideration of aggregate characteristics, cement content, water demand, chemical admixture dosage, workability, and strength development. The combination of locally available diabase-based mineral materials with an effective chemical admixture represents a promising approach for producing dense and high-performance fine-grained concrete suitable for hydraulic engineering applications.

2. Research methodology

The experimental investigation was carried out using Portland cement, fine mineral aggregates, natural sand, water, and chemical admixtures. M500 D20 Portland cement was used as the main binder. The physical and mechanical properties of the cement were determined in accordance with the relevant standard requirements, including GOST 310.2-76, GOST 310.3-76, GOST 310.4-81, and GOST 31108-2020, which are included among the standards used in the research.

Diabase-based mineral material was used as the principal mineral component. The crushed diabase aggregate and diabase screening material were selected because of their suitable physical and mechanical characteristics. The aggregate properties were evaluated using methods specified in GOST 8267-93 and GOST 8269.0-97.

Natural sand from two local sources was investigated. The first was sand supplied by “NEW NERUD” LLC, with a fineness modulus of 1.8 and bulk density of 1603 kg/m³. The second was sand supplied by “ZARHAL QUM” LLC, with a fineness modulus of 2.6 and bulk density of 1598 kg/m³. The particle-size distribution, moisture content, clay and dust content, and bulk density of the sands were determined according to GOST 8735-88 and GOST 8736-2014.

Two chemical admixtures, Sika 4336 and Sika 908, were used to modify the concrete mixtures. The admixtures were introduced at dosages of 0.3, 0.5, 0.7, and 0.9% by cement mass. The influence of the admixtures on fresh concrete workability and hardened concrete strength was subsequently evaluated.

The experimental compositions were developed for concrete classes B22.5 (M300), B25 (M350), and B30 (M400). The compositions were adjusted according to cement consumption and the required design strength.

For the B30 concrete composition containing Sika 908, for example, the mixture consisted of 350 kg of cement, 849 kg of diabase screenings (0–5 mm), 212 kg of Chinaz sand, 832 kg of diabase aggregate (5–20 mm), 180 L of water, and 3.15 kg of Sika 908, corresponding to 0.9% of the cement mass. The slump of this mixture was 22 cm.

The experimental program also included concrete specimens without chemical admixtures, which were used as control compositions. This made it possible to determine the relative influence of chemical modification on the development of concrete strength.

Experimental Testing

The fresh concrete mixtures were evaluated primarily in terms of average density and workability. The workability was characterized by the slump of the concrete mixture.

Hardened concrete specimens were tested at 3, 7, and 28 days. Compressive strength was determined using laboratory testing equipment, and the obtained instrumental values were processed using a 0.95 measurement coefficient. The concrete strength was then classified according to the corresponding strength class.

For the control compositions without chemical admixtures, the measured average 28-day compressive strengths were 46.1 MPa for B22.5 (M300), 55.7 MPa for B25 (M350), and 60.1 MPa for B30 (M400).

For the chemically modified compositions, the corresponding physical and mechanical characteristics were determined under comparable laboratory conditions. The concrete specimens were maintained at laboratory conditions of approximately 21–22°C and 69–72% relative humidity during the experimental period.

The experimental program was based on the relevant standards governing cement, aggregates, concrete mixtures, and chemical admixtures. The principal standards considered in the study included:

GOST 310.2-76 — determination of cement fineness;

GOST 310.3-76 — determination of normal consistency, setting time, and volume stability of cement;

GOST 310.4-81 — determination of cement strength in bending and compression;

GOST 31108-2020 — general construction cements, technical specifications;

GOST 8267-93 — crushed stone and gravel from dense rocks for construction;

GOST 8269.0-97 — methods for physical and mechanical testing of crushed stone and gravel;

GOST 8735-88 — test methods for construction sand;

GOST 8736-2014 — technical specifications for construction sand;

GOST 7473-2010 — concrete mixtures, technical specifications;

GOST 26633-2015 — heavy and fine-grained concrete, technical specifications;

GOST 24211-2003 — admixtures for concrete and construction mortars.

The experimental methodology therefore combined characterization of the initial raw materials, preparation of control and modified concrete mixtures, determination of fresh concrete properties, and evaluation of strength development at different curing ages. This approach allowed the effectiveness of the investigated chemical admixtures to be assessed and the most suitable fine-grained concrete composition for hydraulic structures to be identified.

3. Results and Discussion

The experimental investigation was conducted to evaluate the effect of chemical admixtures on the physical and mechanical properties of fine-grained concrete intended for hydraulic structures. The concrete compositions were prepared using Portland cement, diabase-based mineral aggregates, natural sand, water, and chemical admixtures. The influence of the admixtures was evaluated through the density and compressive strength of concrete specimens at curing ages of 3, 7, and 28 days.

The experimental program included concrete compositions of B22.5 (M300), B25 (M350), and B30 (M400). Both chemically modified and control compositions without chemical admixtures were investigated. The admixtures were incorporated at different dosages, while the experimental results showed that a dosage of 0.5% by cement mass provided favorable strength, density, and water-resistance characteristics.

https://doi.org/10.56143/3030-3893-2026-3-149-154 A bridge between science and innovation

Properties of Concrete with Chemical Admixture

The results obtained for the concrete specimens containing chemical admixtures are presented in Table 4. The specimens demonstrated average densities in the range of approximately 2380–2422 kg/m³, depending on the concrete grade and curing age. The compressive strength increased considerably with curing age, demonstrating active strength development between 3 and 28 days.

Table 1

Physical and mechanical properties of concrete specimens with chemical admixtures

Concrete grade	Age, days	Average density, kg/m³	Average compressive strength, MPa
B22.5 (M300)	3	2394	21.5
B22.5 (M300)	7	2383	36.7
B22.5 (M300)	28	2396	51.0
B25 (M350)	3	2405	39.4
B25 (M350)	7	2405	48.7
B25 (M350)	28	2402	58.3
B30 (M400)	3	2407	39.6
B30 (M400)	7	2416	51.7
B30 (M400)	28	2416	61.4

The results show that the compressive strength increased systematically with curing age. For the B22.5 composition, the average strength increased from 21.5 MPa at 3 days to 51.0 MPa at 28 days. For B25 concrete, the corresponding increase was from 39.4 to 58.3 MPa, while B30 concrete demonstrated an increase from 39.6 to 61.4 MPa.

The increase in strength with curing age indicates continued development of the cementitious matrix and formation of a denser hardened structure. The B30 composition exhibited the highest 28-day strength among the investigated concrete grades. To evaluate the effectiveness of chemical modification, the obtained results were compared with control concrete specimens prepared without chemical admixtures. The control specimens demonstrated lower compressive strength values at the corresponding curing ages.

Table 2

Compressive strength of concrete without chemical admixtures

Concrete grade	3 days, MPa	7 days, MPa	28 days, MPa
B22.5 (M300)	19.6	33.0	46.3
B25 (M350)	26.8	43.4	55.5
B30 (M400)	33.8	46.1	60.6

The comparison indicates that the chemically modified compositions generally demonstrated higher strength than the corresponding control mixtures. The effect was particularly evident at early and intermediate curing ages.

For example, the B22.5 concrete with chemical admixture reached approximately 36.7 MPa at 7 days, compared with approximately 33 MPa for the control composition. At 28 days, the corresponding values were approximately 51.0 and 46.3 MPa, respectively.

For B25 concrete, the 28-day strength increased from approximately 55.5 MPa for the control composition to approximately 58.3 MPa for the chemically modified composition.

The results therefore confirm that chemical modification contributes to improved strength development of the fine-grained concrete.

Particular attention was given to comparing the performance of Sika 4336 and Sika 908. According to the experimental research, the specimens containing Sika 4336 demonstrated the most favorable overall results.

The average compressive strength of the concrete containing Sika 4336 at 28 days reached 55.93 MPa. This value was reported to be 11.5% higher than the corresponding result obtained for the composition containing Sika 908.

Table 3

Comparative performance of Sika 4336 and Sika 908

Parameter	Sika 4336	Sika 908
Chemical admixture dosage investigated	0.3–0.9%	0.3–0.9%
Selected optimum dosage	**0.5%**	**0.5%**
Slump, cm	**24**	22
28-day average compressive strength, MPa	**55.93**	Lower by 11.5%
Workability retention	Approximately 2 h	Lower than Sika 4336
Overall assessment	**More effective**	Effective

The superiority of Sika 4336 was also observed in the fresh concrete properties. The slump of the mixture containing Sika 4336 reached 24 cm, and the mixture retained its workability for approximately two hours.

This characteristic is important for hydraulic construction because maintaining workability during transportation and placement facilitates concrete handling and improves the quality of compaction.

Technical and Economic Assessment. The economic analysis showed that the calculated cost of 1 m³ of concrete containing Sika 4336 was 631,270 UZS, while the corresponding composition containing Sika 908 had a calculated cost of 628,270 UZS.

Table 4

Estimated cost of concrete compositions

Composition	Estimated cost of 1 m³, UZS
Concrete with Sika 4336	**631,270**
Concrete with Sika 908	**628,270**
Difference	3,000

Although the Sika 4336 composition had a slightly higher calculated cost, its higher mechanical performance and improved workability provide important technical advantages. Therefore, the selection of the optimal

composition should be based not only on initial material cost but also on strength, workability, durability, and expected service performance.

Overall, the experimental results demonstrate that the use of diabase-based aggregate together with Sika 4336 provides a technically effective solution for producing fine-grained concrete for hydraulic structures. The highest efficiency was obtained with the B30 (M400) composition, which demonstrated high strength and favorable workability characteristics.

4. Conclusion

The experimental investigation demonstrated that the performance of fine-grained concrete for hydraulic structures can be significantly improved through the combined optimization of mineral aggregates and chemical admixtures. The main conclusions of the study are as follows:

Diabase-based mineral aggregate proved to be suitable for producing dense and high-strength fine-grained concrete due to its favorable physical and mechanical characteristics.

The incorporation of Sika 4336 and Sika 908 chemical admixtures improved the technological and mechanical properties of the investigated concrete mixtures. The admixtures enabled better control of fresh concrete workability and contributed to strength development.

The Sika 4336-based concrete demonstrated the most favorable overall performance. Its average compressive strength at 28 days reached 55.93 MPa, which was 11.5% higher than that of the concrete containing Sika 908.

The use of Sika 4336 significantly improved the workability of the fresh concrete mixture. The slump reached 24 cm, while the mixture retained its workability for approximately 2 hours, providing favorable conditions for transportation, placement, and compaction.

The experimental program resulted in the development and evaluation of B22.5 (M300), B25 (M350), and B30 (M400) fine-grained concrete compositions. Comparative analysis showed that the B30 (M400) composition provided the most favorable combination of strength and technological performance for hydraulic engineering applications.

The optimal dosage of Sika 4336 was determined to be 0.5% of the cement mass, providing an effective balance between concrete workability and mechanical performance.

The obtained results confirm that the combined use of locally available diabase aggregate and Sika 4336 chemical admixture is a promising technological approach for producing high-performance fine-grained concrete for hydraulic structures.

The developed concrete composition can be considered a technically effective material for hydraulic engineering structures where high strength, dense structure, improved workability, and reliable long-term performance are required.

References

[1] Talipov N.Kh., Rasulova N., Ortikulov D. Adhesive Mortars Based on Low-Water-Consumption Cements. Me'morchilik va qurilish muammolari, 2023, No. 1, pp. 56–58.

[2] Kurbonov Z.Kh., Talipov N.Kh. Adhesion Properties of Adhesive Mortars Based on Low-Water-Consumption Cements. In: Advances in Materials Science, Vol. 62. Nova Science Publishers, 2023, pp. 211–217. ISBN 979-8-88697-777-6.

[3] Talipov N.Kh., Kurbonov Z.Kh., Ortikkulov D. Adhesion Properties of Adhesive Mortars Based on Low-Water-Consumption Cements. Yangi O'zbekiston: Ilm Qaldirg'ochlari, II Republican Scientific-Practical Conference, 2023, pp. 362–366.

[4] Kurbonov Z.Kh., Talipov N.Kh., Eshkulov N., Berdiev O. Dry Building Mixtures Based on Cement. In: Innovative Solutions to Technical and Engineering-Technological Problems of Production. Jizzakh, 2022, pp. 127–129.

[5] Berdiev O.B., Kurbonov Z.Kh., Talipov N.H., Sauganova G.R., Daribay A.G. Application of Fine-Ground Cement in the Production of Adhesive Dry Building Mixtures. Proceedings of the X International Conference "Industrial Technologies and Engineering" (ICITE–2023), Vol. I, 2023, pp. 145–149.

[6] Talipov N.Kh., Kurbonov Z.Kh. Tile Adhesive Based on Low-Water-Consumption Cement. Proceedings of the International Scientific-Practical Conference Innovative Technologies in the Digitalization Environment of Higher Education: Problems and Solutions–2024, 14–15 March 2024, pp. 45–48.

[7] Domanskaya I.K. Problems and Methods of Selecting the Composition of Dry Building Mixtures. Dry Building Mixtures, 2010, No. 5, pp. 22–23.

[8] Savelyev A.A. Innovative Solution for the Modification of Dry Building Mixtures. Dry Building Mixtures, 2012, No. 4, pp. 52–53.

[9] Zozulya P.V. Optimization of the Particle-Size Distribution and Properties of Aggregates and Fillers for Dry Building Mixtures. Proceedings of the III International Conference Dry Building Mixtures for the 21st Century: Technology and Business, Saint Petersburg, 2003, pp. 12–13.

[10] Korneev V.I., Zozulya P.V. Dry Building Mixtures: Composition and Properties. Moscow: RIF "Stroymaterialy", 2010, 320 p.

[11] GOST 31357–2007. Dry Building Mixtures Based on Cement Binder. General Technical Specifications. Moscow: Standartinform, 2008.

[12] GOST 58277–2018. Dry Building Mixtures Based on Cement Binder. Test Methods. Moscow: Stroyizdat, 2019, 28 p.

Information about the author

Zavkiddinjon Kurbonov

Associate Professor, Department of Construction Materials and Structures, Jizzakh Polytechnic Institute, PhD in Technical Sciences
E-mail: zavaclash@gmail.com
Tel.:+998880950999
https://orcid.org/0000-0002-1491-4044

Sirojiddin Bozorboev "KARAKALPAK SEMENT" LLC, Sample Collector, Laboratory

Ikhtiyor Egamberdiyev Head of the Laboratory, "ULTRA BETON" LLC

Received: 25 July 2026 | **Accepted:** 5 September 2026 | **Published:** 30 September 2026

An automated system for assessing the seismic resistance of buildings and structures using regulatory documents

D.A. Bekmirzaev[1], I. Mirzaev[2,3], R.R. Yuldoshev[2]

[1]Institute of Mechanics and Seismic Stability of Structures named after M.T. Urazbaev, Tashkent, Uzbekistan

[2]National Research Institute for Seismic Safety and Resilient Construction under Tashkent Institute of Architecture and Civil Engineering, Tashkent, Uzbekistan

[3]Tashkent State Transport University, Tashkent, Uzbekistan

Abstract: This paper proposes an automated system that compares building information with applicable construction requirements. The aim is to make preliminary seismic assessment easier to understand, repeat and review. The method combines a digital building record, an approved list of regulatory rules, engineering calculations and a report that identifies the source of each result. Every applicable check has one of three outcomes: pass, fail or not checked because evidence is insufficient. Four equations describe the demand-to-capacity ratio, storey drift, assessment coverage and the pass rate of completed checks. A synthetic example contains five checks: two pass, one fails and two remain unresolved. Coverage is therefore 60%, while the pass rate is 66.7%. These percentages describe the checklist, not the probability of surviving an earthquake. The main contribution is a transparent decision process that keeps confirmed deficiencies separate from missing evidence. The example demonstrates the method; field validation and a qualified engineer's final assessment are still required.

Keywords: seismic resistance, existing buildings, regulatory requirements, automated checking, building passport, structural assessment

1. Introduction

Seismic resistance is the ability of a structure to meet a specified performance requirement under earthquake loading. It cannot be determined from the construction year or the number of storeys alone. Engineers need information about the site, structural system, materials, connections, foundations and existing damage. ISO 13822 provides a general basis for assessing existing structures [5]. ASCE/SEI 41-23 provides a performance-based framework for seismic evaluation [6]. Rapid visual screening serves a more limited purpose: it helps identify buildings that need further investigation [7].

In many building inventories, information is stored in a building passport: a digital record containing the building's identity, location, dimensions, structural characteristics and inspection documents.
A passport is useful, but it is not a complete structural model. The supplied manuscript describes a system for searching regulatory documents using such records [11]. The present study develops that idea into a clearly defined checking procedure.

The research question is how to turn building data and regulatory text into a result that another engineer can verify. Earlier studies show the importance of translating requirements into explicit computer rules [8, 9]. Here, the proposed system links every result to its input evidence and regulatory source. Document search helps find the requirement; an approved calculation or comparison determines the result.

2. Research methodology

Documents used in the proposed system

A regulatory document is an official standard or rule that defines an applicable technical requirement. For Uzbekistan, the proposed rule database starts with the documents in Table 1. QMQ 2.01.03-19 is identified in the reference list of ShNQ 1.04.01-23 [1, 2]. The latter also addresses technical investigation and monitoring of existing buildings. Material-specific requirements are obtained from the relevant concrete or masonry standard [3, 4].

Table 1

Main documents and the information they support

Document	Subject	Use in the system
QMQ 2.01.03-19 [1]	Construction in seismic regions	Seismic requirements and analysis basis
ShNQ 1.04.01-23 [2]	Technical investigation and monitoring	Inspection evidence and condition assessment
ShNQ 2.03.01-24 [3]	Concrete and reinforced-concrete structures	Applicable material and member checks
ShNQ 2.03.07-21 [4]	Masonry and reinforced masonry	Applicable masonry checks

https://doi.org/10.56143/3030-3893-2026-3-155-158 A bridge between science and innovation

Source: official records and cross-references [1–4]. English document titles are translations.

Table 1 is a starting point, not a complete assessment checklist. A real project may also require standards for loads, soils, foundations and nonstructural elements. Each document must be checked for its scope, effective edition and amendments. A recent publication date alone does not prove that a document applies to a particular building. International references [5–7] provide methodological guidance; their numerical limits must not be mixed with national rules without an approved assessment basis.

Building information and rule preparation

The minimum input includes building identification, location, use, storey count, dimensions, structural system, material test results and inspection findings. Where a calculation is needed, the system also requires a suitable structural model and the relevant loading and foundation information. Each value is stored together with its unit, source document, observation date and verification status. An unverified statement is not treated as a measured property.

Before a requirement is automated, an engineer prepares a rule record. This record states the document and clause, the buildings to which it applies, the required inputs, the comparison to perform and the explanation to show. For example, a member-strength rule compares the calculated force with the corresponding design resistance. The program must use compatible units and the same assessment basis for both values.

The supplied material does not provide an independently verified set of building calculations and expert decisions. This paper therefore presents a proposed method and a synthetic example, not a measured accuracy study. Exact clause-specific limits must be taken from the approved full text before the system is used on real buildings.

Assessment method and equations

For each requirement, the system first checks applicability and evidence. It then returns pass if the requirement is satisfied, fail if reliable evidence shows a violation, or not checked if the evidence is insufficient. Requirements outside the building's scope are excluded only after the reason is recorded. A missing test result must never be counted as a pass.

Demand-to-capacity ratio

For a force-controlled strength check, the calculated demand is divided by the corresponding design resistance:

$$\rho_j = \frac{E_{d,j}}{R_{d,j}}, \qquad R_{d,j} > 0 \tag{1}$$

Here, ρ_j is the demand-to-capacity ratio for check j; $E_{d,j}$ is the calculated force or moment; and $R_{d,j}$ is the corresponding design resistance. Use a nonnegative demand magnitude, a positive resistance and matching units. A value of $\rho_j \leq 1$ satisfies this strength check; $\rho_j > 1$ indicates that demand exceeds resistance. For example, 180 kN divided by 200 kN gives 0.90. The result applies only to that check, not to the whole building.

Demand and resistance must come from suitable engineering calculations, with the load combinations, material properties and factors required by the selected assessment method. Equation (1) does not replace deformation, detailing, foundation or stability checks.

Storey drift ratio

Storey drift describes the relative horizontal movement between two adjacent floors:

$$\theta_i = \frac{|\Delta_i|}{h_i} \tag{2}$$

Here, θ_i is the drift ratio of storey i; Δ_i is its relative horizontal displacement from the structural analysis; and h_i is the storey height. Displacement and height must have the same units. The result is compared with the applicable limit, θ_{lim}. For example, 9 mm divided by 3,000 mm equals 0.003, or 0.3%. The allowable limit depends on the selected code and performance requirement [1, 6].

What the two summary percentages mean

Assessment coverage shows how many applicable checks have enough reliable evidence to be completed:

$$C = \frac{N_e}{N_a} \times 100\% \tag{3}$$

N_a is the number of applicable checks in the approved checklist, and N_e is the number completed. Both passed and failed checks are completed checks. The pass rate considers only the completed checks:

$$P = \frac{N_p}{N_e} \times 100\% \tag{4}$$

N_p is the number of passed checks. Coverage C is undefined when $N_a = 0$; pass rate P is undefined when $N_e = 0$. These are unweighted reporting indicators, not a safety class or an earthquake-survival probability. Every failed check remains visible even if P is high. Unknown applicability must be resolved before the summary is used.

Proposed system operation

The system has four main tasks: collect the building evidence, find the applicable requirement, carry out the check and explain the result. The supplied manuscript describes the document-search component [11]. The checking procedure below is the proposed extension; the screenshot alone does not demonstrate that this procedure has been implemented or validated.

Data collection. The operator selects a building record and attaches drawings, inspection reports and test results. The system checks units and flags empty or contradictory fields. An engineer confirms whether the information is suitable for the intended assessment.

Rule selection. Document search retrieves relevant clauses. Retrieval-augmented generation means finding supporting text before drafting an answer [10]. In this system, it helps explain the source; it does not create an engineering requirement or decide that a building is safe.

Checking and reporting. Approved rules compare verified values or engineering calculation results. The report lists the evidence, document and clause, calculation, outcome and required follow-up. If evidence is missing, it names the missing information. A qualified engineer reviews the report and determines any further investigation.

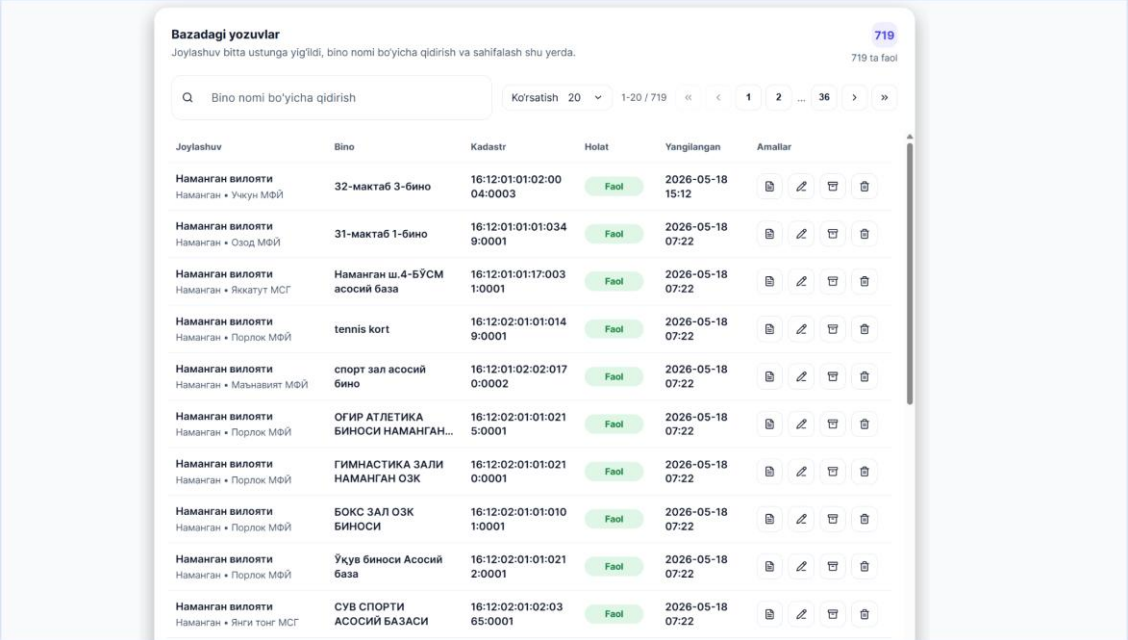


Fig. 1. Supplied building-inventory interface. The displayed 719 active records describe the inventory, not validated seismic-assessment results

In Figure 1, the green label "Faol" means that a database record is active. It must not be interpreted as a positive seismic assessment. Administrative status and engineering status should be stored and displayed separately.

Illustrative results and discussion

A five-check example

Consider a hypothetical two-storey reinforced-concrete building. To demonstrate the method, five checks are selected from a larger assessment checklist. All numerical values in Table 2 are invented, and the drift limit of 0.004 is an assumption for this example, not a quoted Uzbek code limit. No result in the table describes a building shown in Figure 1.

Table 2

Synthetic inputs and results for the selected checks

Check	Input values	Calculation	Outcome
Column shear	Demand: 180 kN Resistance: 200 kN	ρ = 0.90	Pass
Beam shear	Demand: 90 kN Resistance: 80 kN	ρ = 1.125	Fail
First-storey drift	Movement: 9 mm Height: 3,000 mm Assumed limit: 0.004	θ = 0.003	Pass
Beam-column joint	Detailing not verified	Not calculated	Not checked
Foundation	Soil report unavailable	Not calculated	Not checked

Source: illustrative values selected for this paper; not field measurements or a complete building assessment.

The column check passes because 180/200 = 0.90. The beam check fails because 90/80 = 1.125: its assumed demand is 12.5% greater than its assumed resistance. The drift check passes against the example's assumed limit because 9/3,000 = 0.003 < 0.004. The other two checks cannot be completed. Missing joint or soil information does not itself prove a physical defect.

For this five-check subset, $N_a = 5$, $N_e = 3$ and $N_p = 2$. Equation (3) gives C = 3/5 × 100% = 60%. Equation (4) gives P = 2/3 × 100% ≈ 66.7%. In plain terms, three checks were completed and two of those passed. The building cannot be described as "66.7% earthquake-resistant."

The report should state: one strength check failed, and two checks require additional evidence. The next steps are engineering review of the beam result, verification of joint detailing and investigation of foundation conditions. The confirmed failure and the missing evidence are reported separately because they call for different actions.

Interpretation and validation needs

A simple sensitivity check illustrates why both percentages are needed. If the assumed beam resistance is changed to 100 kN, its ratio becomes 0.90 and all three completed checks pass. P rises to 100%, but C stays at 60%. The unresolved joint and foundation checks still prevent a

complete conclusion. This is a second synthetic scenario, not evidence of a real repair.

Before practical deployment, the rules should be tested against independent engineer calculations, including values at the acceptance boundary, missing inputs and conflicting document editions. Any accuracy or time-saving claim requires a documented validation dataset. The present example demonstrates arithmetic and reporting logic only.

3. Conclusion

A useful automated seismic-assessment system must do more than retrieve regulatory text. It must identify the applicable requirement, use verified building evidence, perform an approved comparison and explain the result. The proposed method gives each check a clear outcome and preserves the distinction between a detected deficiency and insufficient information.

The four equations have separate purposes: demand-to-capacity and drift ratios support engineering checks, while coverage and pass rate describe the progress and results of the selected checklist. Neither percentage is a seismic safety certificate. The synthetic example shows how a failed check and missing evidence remain visible. Further work should validate the rules on real buildings using approved regulatory texts and independent expert review. Final decisions about seismic resistance remain the responsibility of qualified structural engineers.

References

[1] Ministry of Construction of the Republic of Uzbekistan. QMQ 2.01.03-19: Construction in Seismic Regions. Tashkent; 2019.

[2] Ministry of Construction, Housing and Communal Services of the Republic of Uzbekistan. ShNQ 1.04.01-23: Procedure for Studying and Monitoring the Technical Condition of Buildings and Structures. Approved by Order No. 01/2-19 of 16 May 2024, as amended in 2025. LexUZ.

[3] Ministry of Construction, Housing and Communal Services of the Republic of Uzbekistan. ShNQ 2.03.01-24: Concrete and Reinforced-Concrete Structures. Approved by Order No. 01/2-22 of 20 June 2024. LexUZ.

[4] Ministry of Construction, Housing and Communal Services of the Republic of Uzbekistan. ShNQ 2.03.07-21: Masonry and Reinforced-Masonry Structures. Approved by Order No. 01/2-30 of 15 July 2024. LexUZ.

[5] International Organization for Standardization. ISO 13822:2010: Bases for Design of Structures — Assessment of Existing Structures. 2nd ed. Geneva: ISO; 2010. ISO catalogue.

[6] American Society of Civil Engineers. ASCE/SEI 41-23: Seismic Evaluation and Retrofit of Existing Buildings. Reston, VA: ASCE; 2023. ASCE catalogue.

[7] Federal Emergency Management Agency. Rapid Visual Screening of Buildings for Potential Seismic Hazards: A Handbook. 3rd ed. FEMA P-154. Washington, DC: FEMA; 2015. FEMA publication.

[8] Eastman C, Lee JM, Jeong YS, Lee JK. Automatic rule-based checking of building designs. Automation in Construction. 2009;18(8):1011–1033. doi:10.1016/j.autcon.2009.07.002.

[9] Solihin W, Eastman C. Classification of rules for automated BIM rule checking development. Automation in Construction. 2015;53:69–82. doi:10.1016/j.autcon.2015.03.003.

[10] Lewis P, Perez E, Piktus A, et al. Retrieval-augmented generation for knowledge-intensive NLP tasks. Advances in Neural Information Processing Systems. 2020;33:9459–9474. NeurIPS proceedings.

[11] Bekmirzaev DA, Mirzaev I, Yo‘ldoshev RR. Adaptive Hybrid AI-Based Retrieval-Augmented Generation for Construction and Seismic Regulatory Question Answering. Manuscript; n.d.

Information about the author

Diyorbek Bekmirzaev	Institute of Mechanics and Seismic Stability of Structures named after M.T. Urazbaev E-mail: diyorbek_84@mail.ru
Ibrakhim Mirzaev	National Research Institute for Seismic Safety and Resilient Construction under Tashkent Institute of Architecture and Civil Engineering, Tashkent State Transport University E-mail: ibrakhim.mir@mail.ru
R. Yuldoshev	National Research Institute for Seismic Safety and Resilient Construction under Tashkent Institute of Architecture and Civil Engineering E-mail: aloqa@suvoriy.com

Journal Engineer ISSN: 3030-3893 Volume:4| Issue:3| 2026

Received: 30 July 2026 | **Accepted:** 10 September 2026 | **Published:** 30 September 2026

Types and properties of mineral fillers used in the production of ceramzit concrete

R.N. Ametov[1][a], J.R. Mustafakulov[2]

[1]Jizzakh Polytechnic Institute, Jizzakh, Uzbekistan

[2]Tashkent University of Architecture and Civil Engineering, Tashkent, Uzbekistan

Abstract: This article analyzes the types, physical, mechanical and chemical properties of mineral fillers used in the production of expanded clay concrete. The effect of industrial waste-based and natural mineral additives included in the composition of expanded clay concrete on the strength, density, thermal conductivity and long-term service properties of concrete is studied. The role of microsilica, ash, slag, peroxynite sand, perlite, vermiculite and other mineral fillers in improving the structure of expanded clay concrete is also shown. The study highlights the significance of the granulometric composition, porosity, bulk density, and granular characteristics of mineral aggregates in determining the structure and quality parameters of expanded-clay concrete. It also analyzes the effective use of local mineral raw materials in lightweight concrete production, their technical and economic advantages, and opportunities for optimizing the concrete mix design. The research findings demonstrate that the required strength, density, and thermal insulation properties of expanded-clay concrete can be achieved through the proper selection of mineral aggregates. The obtained data can be utilized in the production of energy-efficient and high-performance construction materials.

Keywords: expanded clay concrete, mineral filler, microsilica, fly ash, peroxynite sand, peroxynite, perlite, vermiculite, aerated concrete, strength, thermal insulation, thermal analysis, cement, pozzolanic activity, contact zone, calcium silicate gel, mass loss

1. Introduction

Today, the rapid development of the construction industry, the rational use of energy resources and the creation of environmentally friendly building materials are of urgent importance worldwide. In modern construction, one of the main tasks is to increase the energy efficiency of buildings and structures, reduce the mass of structures and ensure their long service life. Therefore, scientific research is being carried out on a large scale on the production of lightweight concrete, in particular expanded clay concrete, and on improving its properties.

The physical and mechanical properties of expanded clay concrete largely depend on the quality of the binder, large and small aggregates, and mineral additives that make up its composition. In particular, in recent years, the use of various mineral aggregates in concrete technology has gained particular importance. Mineral aggregates allow improving the microstructure of cement stone, reducing the porosity of concrete, increasing its strength, reducing water permeability, and improving its thermal and technical characteristics.

The building materials industry uses a wide range of mineral fillers of natural and man-made origin. In particular, microsilica, ash from thermal power plants, blast furnace slag, perlite, vermiculite, limestone flour and other mineral materials are added to expanded clay concrete, significantly improving its quality indicators. Most of these materials are industrial waste, and their effective use makes it possible to reduce environmental problems, reduce waste volume and reduce production costs.

Studying the mechanisms of action of mineral fillers in the composition of expanded clay concrete, determining their optimal amount and assessing their impact on the physical and mechanical properties of the material is an important scientific and practical issue. In particular, reducing cement consumption while maintaining or improving the strength and operational properties of concrete is one of the main directions of modern concrete technology.

The purpose of this article is to analyze the types of mineral fillers used in the production of expanded clay concrete, to study their physical, chemical and mechanical properties and to assess their impact on the quality indicators of expanded clay concrete.

Literature review

Analysis of scientific research shows that representatives of Uzbekistan and neighboring scientific schools have extensively studied the issues of modifying concrete and cement compositions based on mineral and chemical additives. In particular, the possibilities of controlling the structure and contact zone of concrete using mineral additives such as fly ash, zeolite, microsilica, and polycarboxylate superplasticizers are scientifically substantiated.

In this regard, lightweight concretes made from local raw materials, including expanded clay concrete, play an important role in increasing the thermal and technical efficiency of buildings. However, the high water absorption of the expanded clay filler, porosity in the contact zone (ITZ), and the balance between strength and density create

[a] https://orcid.org/0000-0002-8135-5019

the need to improve these concretes with mineral and chemical additives [1].

In the research conducted by Uzbek scientists, great attention is paid to the issues of improving the physical, mechanical and operational properties of concrete and cement compositions using mineral additives. The research mainly focuses on the use of industrial waste and natural mineral resources.

Materials such as ash and slag waste from thermal power plants, metallurgical slag, phosphogypsum and microsilica have been studied as active and inert mineral additives in cement compositions. It has been found that these additives, while reducing clinker consumption, serve to densify the microstructure of cement stone, enhance secondary hydration processes and, as a result, increase strength [2].

Studies on natural aluminosilicate raw materials, in particular kaolin, alunite and zeolites, have confirmed the pozzolanic activity of these materials [3]. Studies on microsilica, due to its high dispersibility and pozzolanic activity, confirm that it reduces capillary porosity in the cement matrix, and has a positive effect on strengthening the contact zone, especially in lightweight concretes [4].

Chemical additives play an important role in concrete technology in controlling the rheological properties of the mixture and increasing the strength of hardened concrete. In scientific research conducted in Uzbekistan, the effectiveness of plasticizers and superplasticizers, especially additives based on polycarboxylate esters, has been widely studied [5].

Polycarboxylate superplasticizers allow reducing water consumption in the concrete mixture by 20–35%, which leads to an increase in strength due to a decrease in the water-cement ratio. When used in combination with mineral additives, these additives ensure a uniform distribution of particles and improve the microstructural stability of concrete [6].

Chemical additives are of particular importance for expanded clay concrete, as they serve to compensate for the excess water consumption caused by the high water absorption of expanded clay grains. As a result, the strength and thermal performance of concrete are improved without increasing its density.

The use of mineral and chemical additives is carried out on the basis of regulatory documents. The classification, technical requirements and areas of application of additives for concrete and mixtures are established in GOST 24211 and relevant national standards. Based on these documents, the effect of additives on the properties of concrete is evaluated in laboratory and pilot-industrial conditions [7].

2. Research methodology

This study investigated the types, physicochemical and mechanical properties of mineral fillers used in the production of expanded clay concrete, as well as their influence on the quality indicators of expanded clay concrete. The research work was carried out based on theoretical analysis, laboratory tests and statistical processing of results.

At the first stage of the study, domestic and foreign scientific sources, regulatory documents and scientific articles were analyzed. The composition and properties of mineral fillers widely used in expanded clay concrete, such as microsilica, thermal power plant ash, blast furnace slag, perlite, vermiculite and limestone flour, were studied.

In the second stage, Portland cement, expanded clay gravel, natural sand and various mineral fillers were used to prepare expanded clay concrete samples. Mineral fillers were added in certain percentages relative to the cement mass, and control and experimental compositions were developed. Concrete mixtures were prepared in laboratory conditions, standard-sized samples were poured into molds and stored under normal hardening conditions for a specified period.

During the study, the average density, compressive strength, water absorption and thermal conductivity of concrete samples were determined. The tests were carried out in accordance with the requirements of current state standards and regulatory documents. The results obtained were compared with the indicators of the control composition and the effect of mineral fillers on the properties of expanded clay concrete was evaluated.

The methods of comparison, analysis and statistical evaluation were used in the processing of the research results. The average values of the obtained indicators for each composition were determined and the patterns of their change were analyzed. Also, the role of mineral fillers in improving the microstructure of concrete and their effectiveness were scientifically substantiated.

The main goal of the research methodology was to determine the optimal type of mineral fillers used in the composition of expanded clay concrete and to assess the possibilities of improving the physical and mechanical properties of concrete.

3. Results and Discussion

In the research, industrial waste from local enterprises and factories and secondary active mineral additives were used to save cement consumption. Active mineral additives are substances with extremely fine grinding, high specific surface area and high reaction permeability, which are added in an amount of 5 to 20% of the cement mass. Currently, industrial waste also serves as a source of mineral additives, the volume of which reaches one million tons per year. These include waste from thermal power plants, metallurgical industries, and chemical industries.

The results of scientific research show that the introduction of 10-28% of fine, low-activity and inert fillers ensures the full use of the clinker fraction of cement, increases the density of concrete, reduces its deformation, shrinkage, and volume change, increases its resistance to the effects of aggressive waters, and reduces the cost of cement [8,9].

Main Observations. Microsilica powder: the chemical composition of the microsilica obtained for the study is presented in Table 1 below.

Table 1

Chemical composition of microsilica

	SiO_2	Al_2O	Fe_2O	CaO	SO_3	MgO	Na_2	K_2O	TiO_2	Mn_2	PPP	Σ
										0	1	2
	87,9	1,28	1,43	0,92	0,04	0,84	0,25	0,41	0,03	0,60	2,64	96,4

	89,02	1,32	1,43	0,88	0,03	0,86	0,25	0,41	0,04	0,608	2,62	97,52
	88,56	1,25	1,33	1,02	0,03	0,8	0,28	0,42	0,04	0,601	2,62	97,01
Averag	88,50	1,28	1,40	0,94	0,03	0,83	0,26	0,41	0,04	0,61	2,63	96,98

Note: P.P.P – Loss on Incineration.

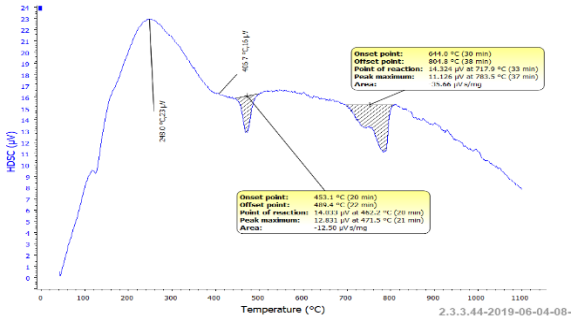


Fig. 1. Thermal analysis result (DSC-TGA) of cement stone with microsilica added

Today, as the ferroalloy production workshop of Uzmetkobinat JSC expands in activity and increases in product production, a large amount of microremnezium is being released as waste in the technological process and tends to accumulate on the territory of the enterprise.

The addition of microsilica increases the thermochemical stability of the cementitious composite, reduces the amount of portlandite, and ensures the formation of additional C–S–H gel. This, in turn, improves the strength and thermal resistance of the material [10, 11].

Fly ash. The chemical composition of fly ash and the results of thermal analysis (DSC-TGA) of cement stone with fly ash addition are presented in accordance with GOST 25818-2017 [12].

Fly ash is demonstrated by the traditional method in terms of its ability to absorb lime from the mortar, improves water permeability, reduces the water-cement ratio, and increases the long-term strength of concrete. It does not contain chlorine or other components that cause corrosion when used in reinforced concrete, and is fully suitable for use in concrete [13].

Table 2

Chemical composition of fly ash

Naming	Oxide content, % by mass							
	SiO_2	Al_2O_3	Fe_2O_3	CaO	MgO	SO_3	Na_2O+K_2O	Total
Fly ash	35,00	18,45	15,20	18,20	4,15	3,80	3,70	100

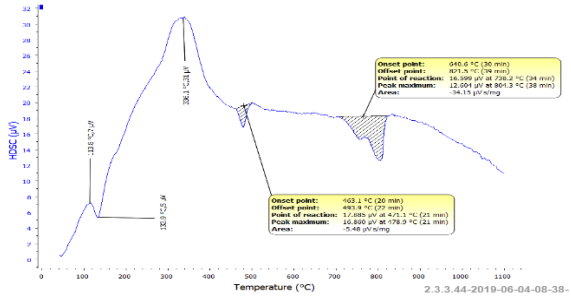


Fig. 2. Thermal analysis result (DSC-TGA) of cement stone with fly ash addition

4. Conclusion

Based on the conducted research, it can be concluded that the use of mineral fillers in the production of expanded clay concrete significantly improves the physical, mechanical, and operational properties of the material. The analyzed fillers - microsilica, fly ash, blast furnace slag, perlite, vermiculite, and limestone flour - play an important role in optimizing the structure of cement stone and increasing the overall efficiency of lightweight concrete.

The experimental results demonstrated that microsilica, due to its high content of amorphous SiO_2 and extremely fine particle size, actively participates in pozzolanic reactions, leading to the formation of additional C–S–H gel. This process densifies the cement matrix, reduces the amount of free portlandite, improves thermochemical stability, and enhances both compressive strength and durability of expanded clay concrete.

Fly ash also showed positive effects on the properties of concrete. Its use improved workability, reduced the water-cement ratio, decreased permeability, and contributed to the growth of long-term strength. In addition, the absence of harmful chloride compounds makes fly ash suitable for reinforced concrete applications and environmentally safe for construction practice.

The study confirmed that the incorporation of 10–28% finely dispersed mineral fillers allows for more efficient utilization of cement clinker, reduction of cement consumption, decrease in shrinkage and deformation, and improvement in resistance to aggressive environmental influences. At the same time, the use of industrial by-products and waste materials contributes to solving environmental problems by reducing industrial waste accumulation and lowering production costs.

Thus, the optimal selection and dosage of mineral fillers in expanded clay concrete technology make it possible to obtain energy-efficient, durable, and economically viable building materials. The obtained results can serve as a scientific basis for further development of lightweight concrete compositions using local raw materials and industrial waste resources.

References

[1] Xusniyarov M.X., Timoxin A.L. Yengil betonlarning strukturaviy xossalari. // Qurilish materiallari. - 2018.

[2] Malhotra V.M. Supplementary Cementing Materials. // Ottawa, 2006.
[3] Dvorkin L.I. Puzolanik qo‘shimchalar va betonlar. // Kiev, 2015.
[4] Bentur A., Cohen M.D. Effect of silica fume // Cement and Concrete Research. // 1987 years.
[5] Aïtcin P.-C. High Performance Concrete. // London, 1998.
[6] Plank J. Superplasticizers in concrete // Cement International. // 2016.
[7] ГОСТ 24211-2008. Добавки для бетонов и строительных растворов. // Общие технические условия. Москва. Стандартинформ 2010.
[8] Баранова А.А., Савенков А.И. Пенобетон, модифицированный микрокремнеземом ЗАО «Кремний» // №8 (91), 2014. С. 78-81.
[9] Исследование влияния количества добавки микрокремнезема на свойства карбидкремниевых огнеупоров на глиноземсодержащей связке // Збірник наукових праць ПАТ «УКРНДІ ВОГНЕТРИВІВ ІМ. А.С. БЕРЕЖНОГО», 2012, № 112. С. 53.
[10] Турсунов Б.А. Кўп компонентли цементларнинг кимёвий таркибларини ўрганиш//Меъморчилик ва қурилиш муаммоари СамДАҚИ, 2021,№4,132-133 б.
[11] Исследование влияния количества добавки микрокремнезема на свойства карбидкремниевых огнеупоров на глиноземсодержащей связке // Збірник наукових праць ПАТ «УКРНДІ ВОГНЕТРИВІВ ІМ. А.С. БЕРЕЖНОГО», 2012, № 112. – С. 53.
[12] ГОСТ 25818-2017 Золы-уноса тепловых электростанций для бетонов. Технические условия. Дата введения 2018-08-01.
[13] Akramov X.A., Ametov R.N., Qurbonov Z.X. // Анализ теплоизоляционных свойств керамзитобетона с минеральными добавками. // Universum: технические науки // Научный журнал // Выпуск: 10(139), Москва Октябрь 2025, Часть 9. (02.00.00 №1) https://7universum.com/ru/tech/archive/item/20967
[14] Akramov Kh.A., Ametov R.N. // Physicochemical analysis of expanded clay concrete modified with mineral and chemical additives. // International scientific journal «Engineer», Special Issue 2026, Vol. 1 No. 1, E-ISSN 3030-3893 39-43 page. (05.00.00; 30.11.2024, 364/5-son.) https://doi.org/10.56143/3030-3893-2026-1S-39-43
[15] Ametov R.N., Djurayeva H.F. Mahalliy xom ashyolardan tayyorlangan keramzitbeton ishlab chiqarishning texnologiyasini takomillashtirish va foydalanish istiqbollari. // Central asian journal of education and innovation // 24-yanvar 2024-yil. https://doi.org/10.5281/zenodo.10559440.

Information about the author

Rasul Ametov	Jizzakh Polytechnic Institute, Assistant of the Department of Construction Materials and Structures, PhD in Technical Sciences E-mail: Ametovrasul44@gmail.com Tel.: +998913951414 https://orcid.org/0000-0002-8135-5019
Javohir Mustafakulov	Doctoral Researcher, Tashkent University of Architecture and Construction Tel.: +998995570666

Journal Engineer ISSN: 3030-3893 Volume:4| Issue:3| 2026

Received: 30 July 2026 | **Accepted:** 10 September 2026 | **Published:** 30 September 2026

Structure, magnetostructural transformations and magnetocaloric properties of Heusler alloys and the MnAs compound: a review

F. Khasanov[1][a]

[1]Tashkent State Transport University, Tashkent, Uzbekistan

Abstract: The review systematises current views on the relationship between the crystal structure, the magnetic ordering and the magnetocaloric effect in two groups of promising functional materials — Heusler alloys of the Ni–Mn–Z (Z = Ga, In, Sn) families and the MnAs compound. Two principal approaches to the quantitative evaluation of the effect are discussed: the indirect one, based on the application of the Maxwell relations to magnetisation and heat-capacity data, and the direct one, which implies an immediate measurement of the adiabatic temperature change. It is shown that indirect methods are convenient for the screening of materials, but in the region of first-order phase transitions, where the conditions of applicability of the Maxwell relations are violated, the error of the calculated quantity may reach tens of per cent. The structural transformations in MnAs are considered separately — the first-order transition from the ferromagnetic hexagonal $B8_1$-type phase to the paramagnetic orthorhombic B31-type phase near 317 K and the subsequent second-order transition to the hexagonal paramagnetic phase near 394 K — together with the form of the magnetic phase diagram of this compound in steady fields. It is concluded that the combination of a high sensitivity of the magnetostructural transition to the external field with the proximity of the transition temperature to room temperature makes these materials the most realistic candidates for the working body of solid-state magnetic refrigerators.

Keywords: magnetocaloric effect, Heusler alloys, MnAs, magnetostructural phase transition, adiabatic temperature change, isothermal entropy change, Curie point, magnetic refrigeration, shape memory effect

1. Introduction

The development of functional materials whose physical properties change abruptly under a small external stimulus remains one of the actively developing directions of solid-state physics. Practically significant effects in such materials are, as a rule, realised near phase transitions, where the system becomes unstable with respect to weak perturbations. A characteristic example is the thermoelastic martensitic transformation observed in a number of intermetallic compounds, primarily nickel-containing ones: the rearrangement of the twin structure of martensite during such a transformation is accompanied by a considerable reversible change of the shape and dimensions of the specimen, which is known as the shape memory effect. Shape memory materials have found application in medical devices, instrument engineering and actuator systems.

Fundamentally new possibilities arise in those compounds in which the structural transformation occurs inside a magnetically ordered phase. In the Heusler alloy Ni_2MnGa the martensitic transition is realised in the ferromagnetic state, and as a consequence the lattice and the spin subsystems become rigidly coupled. Such a magnetostructural transformation can be induced not only by temperature but also by a magnetic field or by a mechanical stress, and it leads to a simultaneous change of the structure, the magnetisation, the electrical resistivity and the entropy of the specimen. It is with this strong spin–lattice coupling that the giant magnetoresistance, the magnetically driven shape memory effect [14] and the magnetocaloric effect observed in these materials are associated.

The present work is a critical review of published data on the structure, the character of the phase transformations and the magnetocaloric properties of Heusler alloys of the Ni–Mn–Z families and of the MnAs compound. The aim of the review is to compare the results obtained by direct and by indirect methods and to outline the range of problems that require further experimental study in high magnetic fields. The paper reports no new experimental data; its contribution consists in the systematisation of published results and in the identification of the quantitative discrepancy between the two measurement approaches, which is essential for the correct screening of candidate materials.

2. Research methodology

2.1. Scope of the review and selection of sources

The review covers publications devoted to three groups of questions: the thermodynamics and the measurement of the magnetocaloric effect; Ni–Mn–Z (Z = Ga, In, Sn) Heusler alloys together with their cobalt-doped quaternary modifications; and the MnAs compound with its substituted analogues. Preference was given to works that report either a direct measurement of the adiabatic temperature change or a joint analysis of magnetisation, heat-capacity and structural data, since only such works make a comparison of the two approaches possible. Lattice parameters and phase compositions are quoted as reported by the original authors. The quantities compared throughout the review are the adiabatic temperature change ΔT_{ad}, the isothermal change of the magnetic part of the entropy ΔS_m, the transition temperature and the width of the hysteresis loop.

[a] https://orcid.org/0009-0004-6301-9822

https://doi.org/10.56143/3030-3893-2026-3-163-167 A bridge between science and innovation

ENGINEER

2.2. The magnetocaloric effect: definitions and thermodynamic background

The magnetocaloric effect consists in a change of the temperature of a magnetic material upon an adiabatic change of the external magnetic field or, under isothermal conditions, in the release or absorption of heat by the material. Accordingly, the effect is characterised by two interrelated quantities: the adiabatic temperature change ΔT_{ad} and the isothermal change of the magnetic part of the entropy ΔS_m. The sign of ΔT_{ad} allows the direct ($\Delta T_{ad} > 0$) and the inverse ($\Delta T_{ad} < 0$) magnetocaloric effect to be distinguished; the latter is typical of Heusler alloys with an inverse martensitic transformation, in which switching the field on stabilises the phase with the lower lattice entropy [12, 15].

The physical nature of the effect is related to the redistribution of entropy between the magnetic, the lattice and the electronic subsystems. Near the Curie point, that is, at a second-order phase transition, the field suppresses the fluctuations of the spin system and reduces the magnetic entropy; at a first-order transition the latent heat of the structural transformation is added to this, which is what provides the so-called giant magnetocaloric effect [4, 16].

2.3. Direct and indirect methods of evaluating the effect

Experimentally, the magnetocaloric effect is studied in two ways. The direct method implies the measurement of ΔT_{ad} by a thermocouple or a resistance thermometer attached to the specimen upon a rapid insertion of the specimen into the field or its rapid withdrawal. The indirect method is based on the calculation of ΔS_m from magnetisation isotherms by means of the Maxwell relation and, if heat-capacity data in a field are available, on the subsequent calculation of ΔT_{ad}. The indirect approach is less demanding with respect to instrumentation and therefore dominates in the literature, which makes it a convenient tool for the primary screening of materials [16, 17].

In the region of a first-order phase transition, however, where the magnetisation undergoes a discontinuity and the state of the specimen depends on its history, the applicability of the Maxwell relation is limited and the calculated values may be overestimated; according to published estimates, the discrepancy with direct measurements reaches 20–30 % [16, 17]. The spread of direct measurements is hindered by the absence of standardised procedures, by the difficulty of ensuring adiabatic conditions and by the limited availability of high fields: most works have been performed in fields of up to 2 T produced by permanent-magnet systems. For Heusler alloys and for MnAs, however, a field of 2 T is not sufficient for the complete completion of the first-order transition, and as a result the measured ΔT_{ad} turns out to be lower than the potentially attainable value. This circumstance determines the relevance of direct measurements in fields above 5–10 T.

3. Results and Discussion

3.1. Realisation of the effect in a refrigeration device

The practical realisation of the effect in a cooling device is as follows. The working body, being in a thermally insulated state, is introduced into the region of a strong field and is heated owing to the direct magnetocaloric effect; the excess heat is removed by a heat-transfer fluid to the hot heat exchanger. The working body is then withdrawn from the field, is demagnetised and cools below the initial temperature, after which it absorbs heat from the object to be cooled. Upon completion of the cycle the sequence is repeated, and the material operates as a magnetic heat pump. It is essential that a single change of the field produces a comparatively small temperature span; the widening of the working interval is achieved by regenerative schemes, in particular by the active magnetic regenerator (AMR) cycle, in which the temperature gradient is accumulated along the packed bed over many cycles [16, 17].

3.2. Heusler alloys of the Ni–Mn–Z families

Heusler alloys of composition Ni–Mn–Z (Z = Ga, In, Sn) and their quaternary modifications doped with cobalt are attractive because the temperature of the martensitic transition in them can be shifted towards room temperature by varying the composition, while the transition itself possesses a high sensitivity to the magnetic field. In the Ni–Mn–Sn and Ni–Mn–In–Co systems an inverse magnetocaloric effect is observed [12]; for the composition $Ni_{45.7}Mn_{36.6}In_{13.5}Co_{4.2}$ a direct measurement yielded $\Delta T_{ad} \approx -8$ K in a field of 1.95 T, which is one of the largest values of the inverse effect in moderate fields [13]. Alloys of the Ni–Mn–Ga family, on the contrary, exhibit predominantly a direct magnetocaloric effect, and it is in these alloys that the magnetically driven strain caused by the field-induced reorientation of martensite variants is realised [14].

The practical application of these materials is hindered by the hysteresis of the first-order transition, which lowers the reversibility of the effect upon cycling, and also by their brittleness and comparatively low thermal conductivity. Current research is therefore directed both at narrowing the hysteresis loop by means of alloying and heat treatment and at studying the irreversible component of the effect under repeated field cycling.

3.3. Structural and magnetic transformations in MnAs

The MnAs compound is a model object for the study of the spin–lattice interaction. At room temperature it is ferromagnetic and has a hexagonal structure of the $B8_1$ type (space group $P6_3/mmc$, α phase). On heating to $T \approx 317$ K a first-order transition to the paramagnetic orthorhombic phase of the B31 type (space group Pnma, β phase) takes place, in which the magnetic ordering disappears simultaneously with the change of the lattice symmetry. The transformation is accompanied by a giant magnetostriction of the order of 2 % and by the release of a considerable latent heat. A further increase of the temperature to ≈ 394 K leads to a second-order displacive transition and to the restoration of the hexagonal symmetry, but now in the paramagnetic state (γ phase).

X-ray diffraction studies give for the hexagonal phase the lattice parameters $a \approx 3.730$ Å and $c \approx 5.700$ Å. In the region of the first-order transition temperature a coexistence of the phases is observed: according to quantitative phase analysis, at $T = 317$ K the fraction of the hexagonal phase is about 56 % and that of the orthorhombic phase about 44 %, which is typical of first-order transformations with a wide two-phase interval. The parameters of the orthorhombic phase are $a \approx 5.720$ Å, $b \approx 3.692$ Å, $c \approx 6.35$ Å.

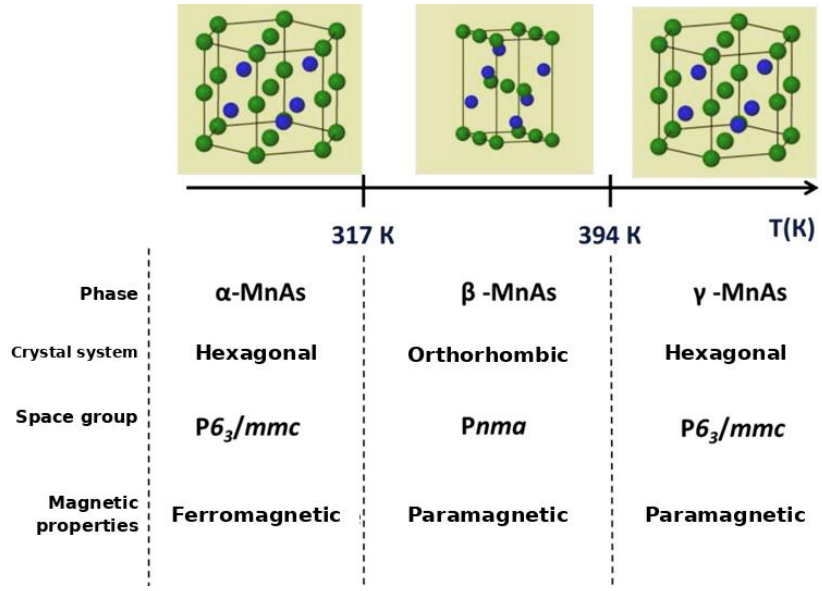


Fig. 1. Scheme of the structural and magnetic transformations in the MnAs compound

The theoretical description of the α → β transition has a long history. The first phenomenological model, proposed by Bean and Rodbell, started from an explicit dependence of the Curie temperature on the volume of the unit cell: for a sufficiently strong magnetoelastic coupling the transition changes from second order to first order with a jump of the volume [5]. Later an alternative mechanism was proposed which relates the transformation to a transition of the manganese ions from the high-spin to the low-spin state induced by a lattice distortion [6]. A subsequent treatment within the framework of the Landau theory with two coupled order parameters — the magnetisation and the lattice strain — made it possible to describe both transitions in a unified way and to reproduce the phase diagram with the lines of the first- and second-order transitions, including the influence of the field. The β → γ transition is thereby interpreted as a stabilisation of the hexagonal phase upon an increase of the volume caused by thermal expansion. Taken together, these results indicate the decisive role of lattice distortions and of the strong spin–lattice coupling in MnAs.

The magnetic phase diagram of the compound in a steady field has been constructed from magnetisation and volume-effect data. The region of existence of the orthorhombic paramagnetic phase is bounded in the (T, μ₀H) plane by fields of approximately up to 9 T: the line of the first-order transition, which starts from the point T ≈ 317 K at H = 0, and the line of the second-order transition, which starts from the point T ≈ 394 K, converge at a tricritical point near 370 K. The presence of a tricritical point means that the very character of the transformation can be controlled by an external field, converting it from first order into second order — a circumstance of fundamental importance for reducing the hysteresis in practical applications.

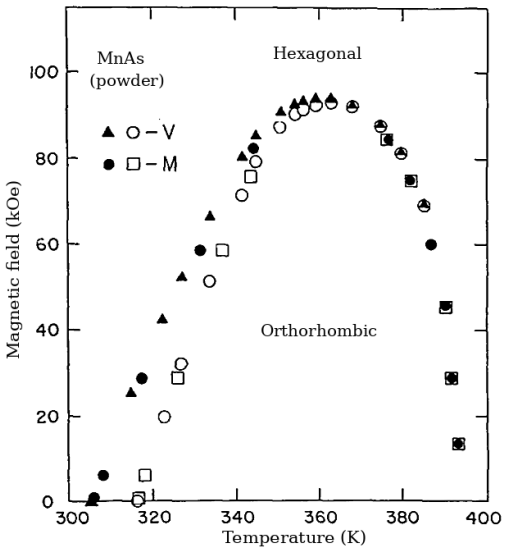


Fig. 2. Magnetic phase diagram of MnAs in a steady magnetic field, constructed from the magnetisation M and the volume V of the crystal lattice. Filled symbols denote the transition from the orthorhombic to the hexagonal structure, open symbols the reverse transition

https://doi.org/10.56143/3030-3893-2026-3-163-167

3.4. Development of magnetocaloric research and the current state of the problem

The effect was discovered by E. Warburg in 1881 [1]. The practical use of magnetic cooling was first demonstrated in 1933 by Giauque and MacDougall, who by the method of adiabatic demagnetisation of gadolinium sulfate reached a temperature of about 0.25 K, a record low value for that time [2]. The possibility of operation near room temperature was shown by Brown in 1976 [3]: using metallic gadolinium and up to fifty successive magnetisation–demagnetisation cycles in fields of up to 7 T, he obtained a temperature span between the hot and the cold ends of the device of about 47 K, that is, approximately three times larger than the ΔT_{ad} of gadolinium for a single change of a field of the same magnitude.

A qualitatively new stage began in 1997 with the discovery of the giant magnetocaloric effect in the compound $Gd_5Si_2Ge_2$, caused by a first-order magnetostructural transition [4]. Subsequently the giant effect was found in $La(Fe,Si)_{13}$ compounds and their hydrides [10, 11], in $MnFeP_{1-x}As_x$ compounds [9], in MnAs and its substituted analogues [7, 8], in Heusler alloys of various families [12, 13] and in $MnCoGeB_x$ systems. The effect is also studied intensively in manganites, where it serves as a sensitive probe of the critical behaviour near the magnetic ordering temperature [18].

The interest in this subject over the last three decades is due to two circumstances. From the fundamental point of view the magnetocaloric effect is a sensitive tool for the investigation of magnetic and magnetostructural transformations, since it is directly related to the entropy of the system. From the applied point of view, a significant share of the world consumption of electric energy falls on the production of artificial cold and on air conditioning, and the transition to solid-state magnetic cooling technologies that do not use gaseous refrigerants with a high greenhouse potential could yield a gain both in energy efficiency and in environmental safety [16, 17].

3.5. Comparative assessment and open questions

The comparison of the two groups of materials shows that they are limited by different factors. In Ni–Mn–Z Heusler alloys the transition temperature is controlled over a wide range by the composition, but the reversibility of the effect is restricted by the hysteresis and by the brittleness of the intermetallic compound. In MnAs the transition lies close to room temperature by its very nature and the field sensitivity of the transformation is high, but the working point can be shifted only by substitution or by external pressure. Common to both groups is the principal methodological problem: the values of ΔS_m obtained from the Maxwell relation cannot be regarded as a reliable characteristic of a first-order transition, and the published values of ΔT_{ad} have been measured, for the most part, in fields that are insufficient to complete the transition. Consequently, a direct comparison of materials from data of different origin is at present of limited validity, and the cyclic rather than the single-shot value of the effect should be adopted as the criterion of practical suitability.

4. Conclusion

1. The analysis of published data shows that the most realistic candidates for the role of the working body of a room-temperature magnetic refrigerator remain materials with a first-order magnetostructural transition near 300 K that combine a high sensitivity of the transition temperature to the field with a moderate hysteresis. These requirements are met to the greatest extent by Heusler alloys of the Ni–Mn–Z families and by the MnAs compound.

2. The indirect method based on the Maxwell relation is convenient for the primary screening of materials, but in the region of a first-order transition it may overestimate the effect by 20–30 %; the values obtained in this way should therefore be verified by direct measurements.

3. Most of the published direct measurements have been performed in fields of up to 2 T, which is insufficient for the complete completion of the transition in the materials considered; the accumulation of direct ΔT_{ad} data in fields above 5–10 T is a priority experimental task.

4. Since the suitability of a material for a device is determined by the cyclic and not by the single-shot value of the effect, the study of the reversibility of the effect under repeated field cycling should be regarded as an equally necessary part of the characterisation of a magnetocaloric material.

References

[1] Warburg E. Über die thermische und elektrische Nachwirkung. Annalen der Physik. 1881;13:141–164.

[2] Giauque W.F., MacDougall D.P. Attainment of temperatures below 1° absolute by demagnetization of $Gd_2(SO_4)_3 \cdot 8H_2O$. Physical Review. 1933;43:768.

[3] Brown G.V. Magnetic heat pumping near room temperature. Journal of Applied Physics. 1976;47:3673–3680.

[4] Pecharsky V.K., Gschneidner K.A. Giant magnetocaloric effect in $Gd_5(Si_2Ge_2)$. Physical Review Letters. 1997;78:4494–4497.

[5] Bean C.P., Rodbell D.S. Magnetic disorder as a first-order phase transformation. Physical Review. 1962;126:104–115.

[6] Goodenough J.B., Kafalas J.A. Comparison of the properties of MnAs and $MnAs_{1-x}P_x$. Physical Review. 1967;157:389–395.

[7] Wada H., Tanabe Y. Giant magnetocaloric effect of $MnAs_{1-x}Sb_x$. Applied Physics Letters. 2001;79:3302–3304.

[8] Gama S. et al. Pressure-induced colossal magnetocaloric effect in MnAs. Physical Review Letters. 2004;93:237202.

[9] Tegus O. et al. Transition-metal-based magnetic refrigerants for room-temperature applications. Nature. 2002;415:150–152.

[10] Hu F.X. et al. Influence of negative lattice expansion and metamagnetic transition on magnetic entropy change in the compound $LaFe_{11.4}Si_{1.6}$. Applied Physics Letters. 2001;78:3675–3677.

[11] Fujita A. et al. Itinerant-electron metamagnetic transition and large magnetocaloric effects in $La(Fe_xSi_{1-x})_{13}$ compounds. Physical Review B. 2003;67:104416.

[12] Krenke T. et al. Inverse magnetocaloric effect in ferromagnetic Ni–Mn–Sn alloys. Nature Materials. 2005;4:450–454.

[13] Liu J. et al. Giant magnetocaloric effect driven by structural transitions. Nature Materials. 2012;11:620–626.

[14] Ullakko K. et al. Large magnetic-field-induced strains in Ni_2MnGa single crystals. Applied Physics Letters. 1996;69:1966–1968.

[15] Tishin A.M., Spichkin Y.I. The Magnetocaloric Effect and its Applications. Bristol: CRC Press, 2003.

[16] Franco V. et al. Magnetocaloric effect: from materials research to refrigeration devices. Annual Review of Materials Research. 2012;42:305–342.

[17] Lyubina J. Magnetocaloric materials for energy efficient cooling. Journal of Physics D: Applied Physics. 2017;50:053002.

[18] Batdalov A.B. et al. Magnetocaloric effect and features of the critical behaviour in manganites. Journal of Experimental and Theoretical Physics. 2016;149(5):1011.

Information about the author

Fozil Khasanov Tashkent State Transport University, PhD, Associate Professor
E-mail: fozilhasanov777@gmail.com
https://orcid.org/0009-0004-6301-9822

Journal Engineer ISSN: 3030-3893 Volume:4| Issue:3| 2026

Received: 31 July 2026 | **Accepted:** 11 September 2026 | **Published:** 30 September 2026

Complex chemical admixture intended for improving the properties of concrete mixture

O. Berdiev[1][a], O. Zafarov[1], E. Urishbaev[2]

[1]Jizzakh Polytechnic Institute, Jizzakh, Uzbekistan

[2]Tashkent Institute of Architecture and Civil Engineering, Tashkent, Uzbekistan

Abstract: This paper presents the results of an experimental study on the composition and performance of a multifunctional admixture developed for concrete mixtures using an S-3 superplasticizer based on polynaphthalene sulfonates. The proposed admixture incorporates S-3 superplasticizer, ferrosilicon production waste, a blend of B115 technical-grade tall pitch and oleic acid, calcium hydrosulfoaluminate, and basalt powder. The study evaluates the effect of the developed composite admixture on the workability and water demand of fresh concrete mixtures, as well as on the physical and mechanical performance of hardened concrete. The obtained results demonstrate that the incorporation of the admixture improves the workability of the concrete mixture and reduces its water requirement, while contributing to the formation of a denser cementitious structure. The use of the developed composition provides favorable conditions for increasing concrete strength and improving its long-term performance characteristics. In addition, incorporating industrial by-products into the admixture offers a practical approach to the more efficient utilization of secondary raw materials and supports resource-efficient concrete production.

Keywords: concrete, concrete mixture, multifunctional admixture, S-3 superplasticizer, polynaphthalene sulfonate, ferrosilicon production waste, tall pitch, oleic acid, calcium hydrosulfoaluminate, basalt powder, workability, water demand, concrete strength, performance characteristics

1. Introduction

Nowadays, the rapid development of transport infrastructure in the Republic of Uzbekistan, as well as the expansion of activities related to the construction, reconstruction, and major rehabilitation of highways, is regarded as one of the important priorities of state policy. The construction of modern highways, major transport routes, bridges, and other artificial structures aimed at improving transport and logistics capabilities across the country is placing increasingly stringent requirements on the quality of materials used in road construction. In particular, the use of cement concretes with high strength, resistance to water and freeze–thaw effects, abrasion resistance, and long-term service stability is becoming increasingly important. The service life and operational reliability of road pavements largely depend on the structural characteristics of concrete, the raw-material components used, and the interaction between the admixture components. Therefore, the scientifically based optimization of concrete composition, utilization of the combined effects of mineral and chemical components, optimization of cement consumption, and improvement of the physical–mechanical and performance characteristics of concrete are among the pressing scientific and practical challenges of today. In particular, the use of complex admixtures provides an opportunity to produce high-quality pavement concrete by improving the workability of the concrete mixture, reducing its water demand, and controlling the setting and compaction processes. Under the sharply continental climatic conditions of Uzbekistan, road pavements are exposed to various natural and operational factors throughout the year. Sharp fluctuations in air temperature, repeated wetting and drying cycles, freeze–thaw cycles, atmospheric precipitation, solar radiation, as well as repeated dynamic and static loads generated by vehicular traffic may cause various deformation processes within the structure of concrete pavements. In addition, the movement of heavy vehicles, abrasive wear, and exposure to certain aggressive environments may adversely affect the strength, structural integrity, and service life of concrete. Therefore, the development of new concrete compositions and technologies capable of ensuring the resistance of pavement concrete to high loads and climatic effects is of particular scientific importance [1]. Efficient utilization of local mineral raw materials and industrial wastes, including their incorporation into concrete as active or functional components, is another important approach to addressing these challenges. Such an approach not only makes it possible to improve specific properties of concrete but also promotes the rational utilization of secondary resources, reduces production costs, and enhances the environmental efficiency of construction-material production. From this perspective, the development of a new generation of road concretes based on complex mineral–chemical admixtures represents a relevant research direction [2].

A number of regulatory and legal documents aimed at modernizing the construction sector in the Republic, introducing modern and innovative technologies, efficiently utilizing the local raw-material base, and increasing the production volume and quality of construction materials have been adopted. In particular, the Presidential Decree of

[a] https://orcid.org/0009-0009-9656-2350

the Republic of Uzbekistan No. PF-60 dated January 28, 2022, entitled **"On the Development Strategy of New Uzbekistan for 2022–2026,"** and Presidential Decree No. PF-6119 dated November 27, 2020, entitled **"On Approval of the Strategy for Modernization, Accelerated and Innovative Development of the Construction Sector for 2021–2025,"** define priority tasks to be implemented in these areas. Accordingly, improving the composition of concrete used in road construction, determining the effect of complex admixtures on physicochemical processes in cementitious systems, and evaluating their influence on the strength and performance characteristics of concrete constitute important scientific and practical objectives. In particular, the development and practical implementation of complex admixtures capable of improving the technological properties of fresh concrete mixtures while simultaneously increasing the density, strength, water impermeability, freeze–thaw resistance, and abrasion resistance of hardened concrete offer considerable potential [3].

Theoretical and experimental studies in this field are being conducted at the accredited scientific laboratory **"Testing of Construction Products"** of Jizzakh Polytechnic Institute and at the research laboratories of the **Department of Construction Materials and Products**. Comprehensive research activities are being carried out in these laboratories to investigate the composition and properties of construction materials, develop new composite materials, and determine the effects of mineral and chemical admixtures on the properties of concrete. As a result of the theoretical investigations and experimental studies conducted, a number of scientific developments have been developed aimed at improving the composition of concrete intended for road construction, increasing the efficiency of complex admixtures, and enhancing the principal physical–mechanical and performance characteristics of concrete. These developments provide a scientific and practical basis for increasing the strength and service life of modern road pavements, efficiently utilizing local and secondary raw materials, and improving construction-material production technologies.

Literature review

Increasing the strength, durability, and operational stability of concrete is one of the key directions in modern construction materials science. In particular, concretes intended for highways require higher performance indices compared to conventional concretes due to operating under constant traffic loads, moisture, freeze-thaw cycles, repeated temperature fluctuations, and abrasive actions. In this regard, numerous scientific studies have been conducted on modifying concrete composition using chemical and mineral additives [4].

Superplasticizers based on polycondensation products, notably S-3 type additives based on polynaphthalenesulfonate, play a significant role in improving the technological properties of concrete mixtures. These superplasticizers reduce the mutual attraction of cement particles and help maintain them in a dispersed state. Consequently, the workability of the concrete mixture increases, making it possible to reduce the water content while maintaining a consistent consistency. The reduction in the water-cement ratio serves to decrease the capillary porosity of the hardened cement paste, thereby improving the strength and density characteristics of the concrete.

The use of mineral additives is noted in the literature as one of the effective methods for controlling the structure formation process of concrete. In particular, finely dispersed materials rich in silicon dioxide react with calcium hydroxide formed during cement hydration, leading to the formation of additional calcium-silicate-hydrate compounds. Such a process can lead to the densification of the concrete structure, a reduction in porosity, and an increase in strength. From this perspective, utilizing mineral waste generated from metallurgy and ferroalloy production enterprises as secondary raw materials in concrete composition is considered one of the promising directions.

The issue of utilizing ferrosilicon production waste in the composition of building materials has also been widely studied in recent years. The fine dispersity of these waste products and the active siliceous components in their mineral composition make it possible to use them in cementitious composites. The introduction of such materials into the cement system can fill the gaps between particles, increase structural density, and influence the formation process of hydration products. At the same time, the use of industrial waste is important from the standpoint of reducing the demand for natural mineral resources and increasing the efficiency of waste recycling.

The use of organic components with hydrophobic properties to increase the resistance of concrete to moisture has also been extensively covered in scientific literature. Specifically, substances based on higher fatty acids can affect the capillary structure of cementitious materials, restricting the penetration of water into the concrete. The presence of organic compounds in tall oil pitch shows the possibility of using it in combination with oleic acid as a component that regulates the hydrophobic properties of the concrete composition. However, determining the optimal amount of such organic components is important, as their excessive application can negatively affect the strength indices of the concrete.

Components based on calcium hydrosulfoaluminate belong to the category of mineral modifiers that actively influence the setting and structure formation processes of cement. As a result of their reactions in the cement system, hydration products with a crystalline structure can be formed, and the densification of the cement paste can be observed. The use of such components makes it possible to control the early-age curing process of concrete, accelerate structural formation, and in some cases limit deformation processes.

The role of basalt-based mineral powders in the concrete composition also deserves special attention. The high mechanical stability and mineral composition of basalt allow it to be crushed and used as a finely dispersed component. Basalt powder can act as a micro-filler in the concrete composition, reducing voids in the cement matrix and increasing the density of the composite structure. At the same time, the use of basalt-based materials expands the opportunities for the efficient use of local mineral raw materials [5].

As seen from the analyzed scientific sources, the individual effects of superplasticizers, mineral additives, and hydrophobic components on concrete properties have been sufficiently studied. However, research combining several functional components within a single complex additive, determining their interaction, and their combined effect on the structural and operational properties of concrete is relatively scarce. In particular, a comprehensive evaluation of the effectiveness of a multi-component system consisting of S-3 superplasticizer, ferrosilicon production waste, a

https://doi.org/10.56143/3030-3893-2026-3-168-174 A bridge between science and innovation

mixture of tall oil pitch and oleic acid, calcium hydrosulfoaluminate, and basalt powder for road concretes remains a pressing issue.Therefore, this study focuses on investigating the possibilities of improving the technological properties of concrete mixtures, reducing water demand, densifying the concrete structure, and increasing its strength and operational performance by combining components with various functional properties within a single complex additive. This approach has both scientific and practical significance, not only in terms of obtaining high-quality road concretes, but also in reusing industrial waste and efficiently utilizing local mineral resources.

2. Research methodology

In order to develop a complex additive composition for high-strength and high-operational-stability heavyweight concrete, a modified concrete mixture based on an interrelated system of mineral and chemical components was prepared. Components that control the rheological, structural, and operational properties of the concrete mixture through various mechanisms were introduced into the complex additive composition [7]. The components used in the study and their mass fractions in the complex additive were determined as follows:

- **S-3 superplasticizer based on polynaphthalenesulfonates — 52%.** This component serves to increase the workability of the concrete mixture, reduce water demand, and optimize the water-cement ratio by improving the dispersion of cement particles. As a result, conditions are created for reducing the capillary porosity of the hardened cement paste and increasing the density and strength of the concrete structure;

- **Ferrosilicon production waste — 25%.** This component actively participates in the cement system as a finely dispersed mineral additive, promoting the formation of additional binding compounds due to pozzolanic reactions. As a result, the microstructure of the cement paste becomes denser, porosity decreases, and the strength, water impermeability, and resistance of concrete to aggressive environments are improved;

- **Calcium hydrosulfoaluminate — 12%.** This component influences the hydration and hardening processes of cement, helping to balance volumetric changes occurring during the curing period. As a result, favorable conditions are created for reducing internal stresses, limiting the formation of microcracks, and forming an integrated structure of the cement paste;

- **Dust waste from basalt production — 8%.** This material, with particle sizes ranging from 0.1 to 100 μm, was used as a micro-filler component. Its finely dispersed particles fill the voids in the cement matrix, ensuring a dense packing of particles. Consequently, conditions are created for increasing the density, structural integrity, and mechanical strength of concrete;

- **A mixture of B115 technical grade tall oil pitch and oleic acid — 3%.** The mixture was prepared in a 7:3 mass ratio and used as a hydrophobic component in the concrete composition. This component is aimed at restricting the penetration of moisture through the capillary channels of concrete, reducing water absorption, and increasing the resistance of concrete to water and freeze-thaw cycles.

The total mass fraction of the components in the complex additive is 100%. The structural components were selected taking into account not only their individual functional properties, but also their mutual compatibility and combined effect. While the S-3 superplasticizer serves to control the water demand of the concrete mixture, the mineral components increase the microstructural density of the cement matrix. The hydrophobic component, in turn, is aimed at limiting the penetration of moisture into the concrete structure. Thus, the complex additive is designed to simultaneously affect the technological, physico-mechanical, and operational indices of concrete.

In obtaining heavy concretes with high operational properties, controlling the internal structure and porosity indices of concrete is of great importance. The presence of excess water in the concrete composition leads to an increase in the number of capillary pores during the hardening process of the cement paste. This situation, in turn, reduces the strength and density of concrete, facilitating the penetration of moisture and aggressive environments into the material. Consequently, the destruction of the concrete structure under the influence of freeze-thaw cycles, wetting-drying processes, and repeated mechanical loads can accelerate.

Therefore, the main direction of the research methodology consisted of optimizing the amount of water in the concrete mixture, ensuring effective dispersion of cement particles, reducing porosity using mineral micro-fillers, and limiting capillary wetting through a hydrophobic component. The functional roles of the components making up the complex additive were selected in a mutually complementary manner, aimed at simultaneously improving several important properties of concrete [6].

Most traditional chemical or mineral additives are aimed at improving a specific property of concrete. When it is necessary to control several indicators simultaneously, the need arises to use various additives separately. Such an approach can complicate the technology of introducing additives into the concrete composition, require ensuring compatibility between components, and affect the economic efficiency of the production process.

To eliminate this problem, the principle of combining components with various functional properties within a single finely dispersed complex additive was adopted in the study. The proposed composition is aimed at reducing the water demand of the concrete mixture, improving workability, densifying the microstructure of the cement paste, lowering capillary porosity, and increasing the strength and water resistance indices of hardened concrete.

In evaluating the effectiveness of the complex additive, the workability and water demand of the concrete mixture, as well as the density, compressive strength, water absorption, water impermeability, and frost resistance of the hardened concrete were adopted as the main control indicators. By comparing the experimental results with the control concrete composition, the effect of the complex additive on each indicator was determined.

The developed complex additive is designed to combine the mechanisms of chemical plasticization, mineral modification, micro-filling, volumetric stabilization, and hydrophobization. This approach creates a technological basis for obtaining high-strength heavyweight concrete with a dense structure and stability against external environmental influences. In addition, the use of ferrosilicon and basalt production waste makes it possible to involve secondary raw materials in the production process of building materials and efficiently utilize resources.

3. Results and Discussion

As a result of the experimental studies conducted, it was determined that the developed complex additive has a positive effect on the technological properties of the concrete mixture as well as the physical-mechanical and operational indices of the hardened concrete. As a result of the effective dispersion of cement particles by the S-3 superplasticizer in the complex composition, the mobility and workability of the concrete mixture increased, making it possible to reduce water consumption by 20–25% while maintaining the required consistency. The decrease in the water-cement ratio leads to a reduction in the volume of capillary pores formed in the hardened cement paste and the formation of a denser microstructure.

As a result of the densification of the cement matrix, along with an increase in the compressive strength of concrete, its resistance to water penetration and repeated freeze-thaw cycles also improves. At the same time, the formation of a dense and low-porosity structure increases the resistance of concrete to external environmental influences, creating conditions for the long-term stable operation of structures [7].

In the studies, it was observed that the combined use of the S-3 superplasticizer with components that control the hardening process has a positive effect on the initial hydration processes of cement. As a result, the rate of strength formation of concrete at an early age increases. This feature makes it possible to shorten the duration of the technological cycle, release molds faster, and increase production efficiency in the manufacture of precast reinforced concrete products. At the same time, the intensification of the technological process creates an opportunity to use energy resources more efficiently by reducing the need for heat treatment.

Based on laboratory experiments, 52% of the S-3 superplasticizer in the complex additive composition was determined as the optimal value. At this ratio, the required workability of the concrete mixture is ensured, and along with a decrease in water consumption, it was observed that the most optimal results are achieved in the strength, water impermeability, and frost resistance indices of the hardened concrete. However, an increase in the amount of S-3 beyond the optimal value should be evaluated taking into account its interaction with other components of the complex system.

The other components of the complex additive also perform an important functional role in geological and structural formation. While the participation of ferrosilicon production waste as a finely dispersed mineral component helps to densify the cement matrix, basalt dust serves as a micro-filler to reduce voids between particles. Calcium hydrosulfoaluminate is aimed at ensuring the volumetric stability of the structure during the hardening process, whereas the mixture of B115 tall oil pitch and oleic acid acts as a hydrophobic component limiting the capillary wetting of concrete.

The functional complementarity of the components within the complex additive makes it possible to control the technological properties of oaths/concrete mixtures and improve the operational indices of the hardened concrete. The proposed composition creates favorable conditions for reducing the water demand of the mixture, ensuring the necessary workability, increasing the density of the cement matrix, and forming a high-strength structure.

The obtained results show that it is possible to improve the quality indices of high-strength heavy concretes through the use of the complex additive. In particular, as a result of the decrease in the water-cement ratio, the effect of finely dispersed mineral components as a micro-filler and active additive, and the restriction of moisture penetration by the hydrophobic component, a complex action mechanism is formed to increase the density and operational stability of concrete. These results demonstrate the prospects of applying the developed additive in the production of highways, reinforced concrete structures, and concrete products operating under high operational loads.

Proposed Compositions of the Complex Admixture for Concrete Mixtures

During the experimental studies, several compositional variants of a complex admixture intended for high-strength heavy concrete were developed. The main objective of the study was to determine the changes in the technological properties of the concrete mixture, as well as in the physical, mechanical, and performance characteristics of hardened concrete, resulting from variations in the mass proportions of the admixture components.

The complex admixture investigated in this study consisted of an S-3 superplasticizer based on polynaphthalene sulfonates, ferrosilicon production waste, calcium hydrosulfoaluminate, finely dispersed dust waste generated during basalt production, as well as a mixture of B115-grade tall pitch and oleic acid. These components were incorporated to perform specific functional roles, including improving the workability of the concrete mixture, reducing water demand, increasing the density of the cement matrix, limiting capillary porosity, and enhancing the resistance of concrete to environmental effects.

In the experimental program, the mass proportions of the components were varied within specified ranges, and their effects on the workability and water–cement ratio of the concrete mixture, as well as on the compressive strength, water impermeability, and frost resistance of hardened concrete, were evaluated. The results obtained for each composition were compared, providing a basis for determining the optimum composition of the complex admixture [8].

The experimental compositions of the complex admixture and the mass proportions of their individual components are presented in Table 1. Based on a comprehensive analysis of the obtained results, Composition 3 was identified as the most appropriate variant in terms of improving the technological properties of the concrete mixture and the physical, mechanical, and performance characteristics of hardened concrete.

In the identified optimum composition, the synergistic interaction of the components ensured the required workability of the concrete mixture, reduced water consumption, and promoted the formation of a denser cement matrix. At the same time, this composition created favorable conditions for increasing the strength, water impermeability, and frost resistance of concrete. Therefore, Composition 3 was adopted as the optimum complex admixture composition recommended for producing heavy concrete with enhanced performance characteristics.

https://doi.org/10.56143/3030-3893-2026-3-168-174 A bridge between science and innovation

Table 1

Samples of the Proposed Complex Admixture Compositions for Concrete Mixtures

Composition No.	Components, wt. %				
	S-3 Superplasticizer	Ferrosilicon Production Waste	Calcium Hydrosulfoaluminate	Basalt Dust Waste (0.1–100 μm))	B115 Tall Pitch–Oleic Acid (7:3)
1	48	28	12	9	3
2	50	26	12	9	3
3 (optimal)	52	25	12	8	3
4	54	24	11	8	3
5	56	22	11	8	3
H1	45–60	20–30	10–15	5–10	2–5

Table 2

Physical, Mechanical, and Performance Properties of Concrete with the Proposed Complex Admixture

Parameters	Mix 1	Mix 2	Mix 3	Mix 4	Mix 5
Concrete mixture slump, cm	15	16	17	16	15
Compressive strength, MPa (28 days)	68.5	71.2	74.8	72.4	70.6
Flexural strength, MPa	7.2	7.6	8.1	7.8	7.4
Water impermeability grade	W12	W14	W16	W14	W12
Frost resistance, cycles	F300	F400	F500	F400	F300
Water absorption, %	3.8	3.4	3.1	3.3	3.6

Test results of concrete samples modified with a complex additive. During the experimental tests, concrete samples modified with a complex additive were prepared based on various compositions given in Table 2. The prepared samples were tested under established laboratory conditions, and their main physical-mechanical and operational indicators were compared. In the research, compressive and bending strength of concrete, water impermeability, water absorption, and frost resistance were adopted as the main evaluation criteria.

A comprehensive analysis of the obtained experimental results showed that composition No. 3 provided the most optimal results. This composition consists of a mixture of 52% S-3 superplasticizer, 25% ferrosilicon production waste, 12% calcium hydrosulfoaluminate, 8% basalt dust, and 3% tall pitch-oleic acid of brand B115.

It was found that when using this composition, the compressive and bending strength indicators of concrete increased, the water impermeability property improved, and water absorption decreased. Also, the resistance of concrete to repeated freeze-thaw effects increased, and a higher result was recorded compared to other compositions in terms of frost resistance indicator [9].

The high efficiency of composition No. 3 is explained by the mutually complementary effect of the complex additive components. While the S-3 superplasticizer increased the workability of the concrete mixture and allowed for a reduction in the water-cement ratio, the fine disperse particles of ferrosilicon waste and basalt dust reduced the voids in the cement matrix, serving to form a denser structure. Calcium hydrosulfoaluminate helped ensure structural stability during the hardening process, while the mixture of tall pitch and oleic acid enhanced the hydrophobic properties of the concrete.

Based on the experimental results, composition No. 3 was accepted as the optimal complex additive composition for obtaining heavy concrete with high strength and improved operational properties. The use of this composition is considered promising for the production of high-durability concretes for road pavements, transport structures, and concrete structures subject to complex environmental influences.

Physical and mechanical properties of concrete prepared on the basis of the complex additive. In order to determine the effect of the proposed complex additive on the physical-mechanical and operational indicators of concrete, experimental tests of concrete samples were carried out according to compositions numbered 1–5. In the research, standard-sized samples were prepared to evaluate the main strength and operational properties of concrete [10].

To determine the compressive strength of concrete, cube-shaped samples with dimensions of 100×100×100 mm were prepared and kept under normal hardening conditions for 28 days. Experimental tests were organized in accordance with the requirements of current regulatory documents GOST 10180-2012, GOST 10181-2014, GOST 12730.5-2018, GOST 12730.3-2020, and GOST 10060-2012. The workability of the concrete mixture was determined based on the slump test indicator.

Evaluation of compressive strength was carried out using a MATEST C109N hydraulic press. The water impermeability properties of concrete were determined using a MATEST C435 testing device, and frost resistance indicators using an ARCTIKO LAF 700 freezing chamber. When it was necessary to study the microstructural state of concrete and the interaction mechanism of complex additive components with the cement stone in more depth, a TESCAN MIRA3 scanning electron microscope (SEM) was used.

Analysis of the experimental results showed that the use of the complex additive, alongside improving the technological properties of the concrete mixture, also has a positive effect on the structural state of the hardened concrete. In particular, due to the dispersing effect of the S-3 superplasticizer in the additive, the workability of the concrete mixture improved, creating the opportunity to reduce the water-cement ratio while maintaining the required consistency. This limited the formation of capillary pores in the cement stone, creating conditions for the formation of a relatively dense and stable microstructure.

The fine disperse particles of mineral components helped fill the voids in the cement matrix and densify the structure. As a result, the compressive strength and water impermeability properties of the concrete improved. Furthermore, as a result of the effect of the hydrophobic component, it was observed that the water absorption of concrete decreased, and the penetration of moisture into the material through capillary paths was restricted. These factors also created favorable conditions for increasing the resistance of concrete to the effects of freeze-thaw cycles.

Among the tested compositions, concrete samples prepared on the basis of composition No. 3 demonstrated the highest indicators. In this composition, the mutually coordinated effect of the S-3 superplasticizer, ferrosilicon production waste, calcium hydrosulfoaluminate, basalt dust, and the mixture of B115 tall pitch–oleic acid was observed. As a result, concrete samples of this composition recorded high compressive strength and water impermeability indicators, while water absorption recorded relatively low values. Also, in terms of frost resistance, this composition showed superior results compared to other experimental variants [11].

The experimental test results confirmed that the developed complex additive allows for the comprehensive improvement of the physical-mechanical and operational properties of concrete by controlling the workability of the concrete mixture, reducing the water-cement ratio, and densifying the microstructure of the cement stone. Based on the obtained results, composition No. 3 was recommended as the most optimal composition for heavy concretes where high strength and operational stability are required.

4. Conclusion

Based on the conducted theoretical research and experimental tests, the composition of a complex additive aimed at improving the physical-mechanical and operational properties of high-strength heavy concretes was developed, and its effectiveness was evaluated. The study utilized an S-3 superplasticizer based on polynaphthalenesulfonates, ferrosilicon production waste, calcium hydrosulfoaluminate, fine disperse dust waste from basalt production, and a mixture of brand B115 tall pitch and oleic acid.

During the experimental process, five composition variants were compared, and their impact on the workability of the concrete mixture and the main physical-mechanical and operational indicators of the hardened concrete was determined. According to the research results, composition No. 3—consisting of a complex additive composed of 52% S-3 superplasticizer, 25% ferrosilicon production waste, 12% calcium hydrosulfoaluminate, 8% basalt dust, and 3% of a mixture of brand B115 tall pitch-oleic acid—was designated as the most optimal composition.

The application of this composition allowed for the formation of a denser microstructure of the cement stone, along with improving the workability of the concrete mixture and reducing the water-cement ratio. As a result, the compressive strength of the concrete reached up to 74.8 MPa, and the bending strength up to 8.1 MPa. Furthermore, the water impermeability grade of the concrete was increased to W16, the frost resistance indicator to F500, and water absorption was reduced to 3.1%. These indicators demonstrate the effectiveness of the complex additive in increasing the density, strength, and resistance of concrete to external environmental influences.

The research results showed that the components of the complex additive have a functionally complementary effect. The S-3 superplasticizer served to improve the rheological properties of the concrete mixture and reduce water demand, the ferrosilicon waste and basalt dust to densify the cement matrix, calcium hydrosulfoaluminate to ensure structural stability, and the tall pitch-oleic acid mixture to increase the hydrophobic properties of the concrete. As a result, the formation of a high-density, strong, and durable concrete structure resistant to external environmental impacts was achieved.

It is promising to apply the developed complex additive in the preparation of road and airfield pavements, transport and hydraulic structures, bridge structures, and reinforced concrete elements operating under high mechanical and climatic loads. Especially in structures operating under the influence of temperature fluctuations, moisture, and repeated traffic loads, the use of this concrete composition can serve to increase their operational reliability.

Also, the use of ferrosilicon and basalt production waste in the composition of the complex additive makes it possible to involve industrial waste as a secondary raw material in the production process of building materials. This is of significant practical importance in terms of reducing the use of natural resources, optimizing material compositions, mitigating the problem of waste disposal, and increasing the ecological and economic efficiency of concrete production. The research results showed that the proposed complex additive is an effective technological solution for obtaining heavy concretes requiring high strength, water impermeability, and frost resistance. The indicators of 74.8 MPa compressive strength, 8.1 MPa bending strength, W16 water impermeability, and F500 frost resistance confirm the high operational potential of the developed concrete composition.

References

[1] Berdiyev O., Kurbanov Z., Tilavov E., Rasulova N., Boboqulova S., Jumanov I., Ametov R., O‘Roqboyev O., Parsaeva N., Botirov B. The calculation of reinforced concrete conical dome shells considering concrete creep. E3S Web of Conferences. 2024. Vol. 587. Article 03001. DOI: 10.1051/e3sconf/202458703001

[2] Rakhimov M.A., Rakhimova G.M., Suleimbekova Z.A. Modification of Concrete Railway Sleepers and Assessment of Its Bearing Capacity. International Journal of GEOMATE. 2021. Vol. 20, Issue 77. P. 40-48.

[3] Asmatulayev B., Asmatulayev R., Asmatulayev N., Bakirbayeva A. Construction of durable road rolled concrete based on belite slag cement and binders. International Journal of GEOMATE. 2023. Vol. 24, Issue 104. P. 27-35.

[4] GOST 10181–2014. Concrete mixes. Test methods. - M.: Standartinform, 2015. - 36 p.
[5] GOST 24211–2008. Additives for concretes and mortars. General specifications. - M.: Standartinform, 2009. - 20 p.
[6] GOST 7473-2010. Concrete mixes. Specifications. - M.: Standartinform, 2012. - 18 p.
[7] Hong Y., Tian W., Dong H., Li J. Research on Crack Classification Method of Cement Concrete Pavement. Journal of Physics: Conference Series. 2020. Vol. 1622. Article 012120. DOI: 10.1088/1742-6596/1622/1/012120.
[8] GOST 10060-2012. Concretes. Methods for determination of frost resistance. - M.: Standartinform, 2013.
[9] GOST 12730.3-2020. Concretes. Methods for determination of water absorption. - M.: Standartinform, 2020.
[10] GOST 12730.5-2018. Concretes. Methods for determination of water impermeability. - M.: Standartinform, 2019.
[11] GOST 10180-2012. Concretes. Methods for determination of strength using control samples. - M.: Standartinform, 2013.

Information about the author

Oblokul Berdiev	Candidate of Technical Sciences, Professor at the Department of Building Materials and Structures, Jizzakh Polytechnic Institute https://orcid.org/0009-0009-9656-2350
Olmos Zafarov	Doctor of Technical Sciences, Professor, Head of the Department of Building Materials and Structures, Jizzakh Polytechnic Institute
Elbek Urishbaev	Basic Doctoral Student at the Tashkent Institute of Architecture and Civil Engineering E-mail: elbek.uzb.1990@gmail.com Tel.:+99891 566 49 49

Received: 3 August 2026 | **Accepted:** 14 September 2026 | **Published:** 30 September 2026

A risk-oriented approach to the development of transport systems with embedded information technologies

I.N. Kavaliova[1][a], A.N. Panov[2][b], E.Yu. Romashova[2][c], U.A. Ziyamukhamedova[3][d], L.N. Marchenko[4][e], Y.S. Podgornaya[5][f], V.V. Podgornaya[6][g]

[1]The State Scientific Institution "V. A. Belyi Metal-Polymer Research Institute of National Academy of Sciences of Belarus", Gomel, Belarus

[2]Mechanical Engineering Research Institute of the Russian Academy of Sciences (IMASH RAN), Moscow, Russia

[3]Tashkent State Transport University, Tashkent, Uzbekistan

[4]Francisk Skorina Gomel State University, Gomel, Belarus

[5]State Scientific Institution "Institute of Mathematics of the National Academy of Sciences of Belarus", Minsk, Belarus

[6]Higher Educational Establishment of the Federation of Trade Unions of Belarus «International University «MITSO» Gomel Branch, Gomel, Belarus

Abstract: The article explores the process of transformation of methodological approaches to ensure safety and reliability of transport systems - from deterministic, tolerance, statistical and probabilistic paradigms to a complex risk-oriented concept, integrated into the life cycle of creating transport objects. The proposed approach aims to achieve a balanced "quality - cost - risk" ratio, which creates the preconditions for increasing the competitiveness of the machine complex products through increased efficiency of intellectual activity in the design stages, production and operation of technical systems. The analysis of current problems was carried out, prospective directions of methodology were considered, as well as models and methods for justifying the permissibility of design-technological risks. Examples of the implementation of risk-oriented strategies and tactics at different stages of the life cycle of transport systems are given.

Keywords: risk-oriented concept, life cycle, digital twins, mathematical model, rail transport, technological systems, information technology

1. Introduction

The development of rail transport as an integral part of the system of machine science and mechanical engineering has historically focused on solving a complex of interconnected tasks: optimizing resource consumption in all stages of the creation of machinery, Ensuring the required level of reliability and safety of technical systems and technological processes, studying cause-and-effect relationships of degradation phenomena (including analysis of damage mechanisms of both individual elements and complex technical complexes), as well as automating the processing of datasets to reduce the time to market for new products. The creation and application of intelligent systems is of particular importance in modern times, which inevitably generates new classes of risk and requires the development of adequate methods to manage them [1-4].

As a priority for the development of transport systems, and in particular its key component - rail transport, the further development and implementation of a risk-based approach is currently being considered. The evolution of methodology, which has been in full development since the early 2000s, involves a gradual shift from traditional deterministic, tolerant, statistical, and probabilistic methods (including predictions of reliability) to holistic risk assessment and management. This paradigm has been reflected in both basic scientific research and applied industry development - from the implementation of unique projects to the organization of serial production within the full life cycle of technical objects [4].

The particular relevance and specificity of a risk-based approach for the railway industry is due to:

- increased requirements for the safety of the transport process;
- the complexity and interdependence of infrastructure facilities and rolling stock;
- Long service life and the need for risk management at all stages of the life cycle: from conception, design and manufacturing to repair and disposal;
- the existence of a regulatory framework based mainly on deterministic and statistical paradigms, with the simultaneous need to optimize maintenance costs.

[a] https://orcid.org/0000-0002-8098-0568
[b] https://orcid.org/0009-0000-3791-551X
[c] https://orcid.org/0009-0002-5052-9319
[d] https://orcid.org/0000-0001-5005-0477
[e] https://orcid.org/0000-0003-2425-1720
[f] https://orcid.org/0009-0008-4299-4265
[g] https://orcid.org/0009-0008-3597-5648

https://doi.org/10.56143/3030-3893-2026-3-175-179

The aim of this work is to analyze existing methods and develop conceptual models and methodologies for applying a risk-based approach in order to ensure an acceptable level of risks when increasing the productivity of intellectual activities in the process of building transport systems. The solution to this problem aims at optimizing the "quality-cost-risk" relationship and achieving an acceptable level of risk (i.e. acceptable probability and integral damage) for failures at different stages of the life cycle of transport systems.

2. Research methodology

The following areas of study are identified in the context of the life cycle of transport systems and related risks [4]:

- normalization and standardization of terminology, including the conceptual range in the field of artificial intelligence, as well as regulating the application of information systems at all stages of the life cycle;
- numerical modeling of physical processes as a tool to reduce resource costs and accelerate the preparation of new technology production;
- the duality of risks arising from the interaction of hardware and information subsystems;
- risk management based on the application of built-in monitoring systems for degradation processes.

There is now an intensive introduction of integrated information systems in the technical complex [3, 5] as a means to increase the productivity of intellectual activity - both during the design phase and during operation. The main source of risks leading to natural, man-made and social damage is inappropriate or insufficiently reliable information (figure 1).

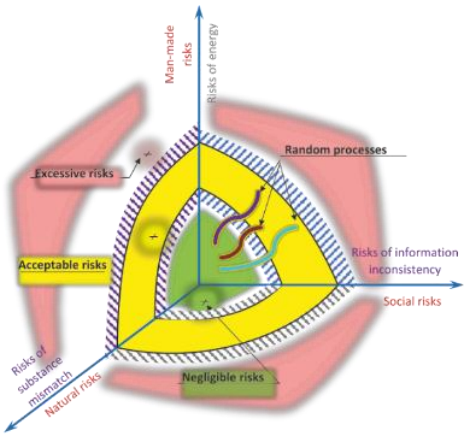


Fig. 1. Presentation of the risk analysis structure of a process using a hybrid system based on a risk-based design and process approach: challenges, threats, vulnerabilities and damages

To implement risk-oriented thinking, a hyperbolic model developed by the authors is proposed that describes the relationship between potential damage and an acceptable probability of non-compliance (figure 2). The underlying principle is that significant damage should be less likely to materialize than less significant damage. This ensures that an acceptable or required probability of identified damage is achieved. To facilitate risk analysis in practical activities, including management of the life cycle of a socio-technical system, continuous hyperbolic dependence can be presented as a step function (score on the parameters "probability - priority/damage significance"), which allows for the ranking of priorities and their corresponding acceptable probabilities of discrepancies. Accordingly, a system for identifying the scores of significance of consequences is introduced in the design and technology and other documentation.

With a view to harmonizing and ensuring the universal application in managed environments of information systems for "second nature" objects - techniques and technologies - a series of international and national standards are being developed, defining:

— Terminology and conceptual provisions (for example ISO/IEC 22989:2022);

— Impact assessment processes (ISO/IEC 38507:2022);

— Requirements for the organization's management system (ISO/IEC FDIS 42001);

— Risk identification methodology (ISO/IEC 22894:2022).

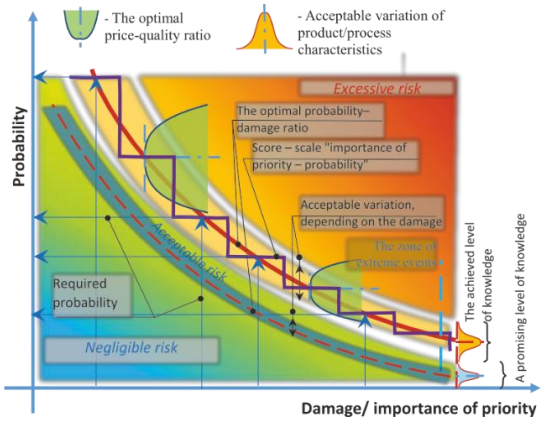


Fig. 2. Fundamental five-component model of optimization of "probability - damage" - "quality - value" - "variation - damage" dependencies

National standards are also being developed to apply terms and definitions correctly. In particular, GOST R 57188 presents a terminology apparatus for modeling physical processes, and GOST R 57412 identifies applicable electronic models in the processes of product development, production and operation. Standards are developed in the supply chain to ensure that technical systems with embedded software complete their life cycle stages efficiently and effectively. Thus, the GOST series P 57700 regulates software certification and validation systems.

2.1 Regulatory framework and standardization of modelling

It should be noted that the methods of interlinked risk management of physical and information systems are still insufficient for widespread practical application. Moreover, the term "artificial intelligence" (AI) is still not definitively defined even in ISO/IEC 22989. In the standards STB 1694 and STB 2582 (developed with the authors of this article) for the English term "artificial intelligence" is proposed the phrase "means of supporting intellectual activity" (MSIA), which, in our view, more accurately reflects the essence of this concept. This interpretation is not misleading, as it is with AI as a kind of "miracle," but makes a valid analogy with the means to support human physical activity - the creation of machines (such as machine tools) and tools that enhance productivity.

Currently, to reduce development and production lead times [1-4], for example, within the GOST series P 15,000,

a set of standards regulating the implementation of numerical modeling of technical products has been developed. An analysis of these documents leads to the following conclusions.

The GOST series R 57700 defines requirements for numerical modeling systems, including software certification and validation processes. In particular, GOST R 57700.10 regulates the processes of verification and validation of numerous models of complex structural elements in the elastic area, as well as requirements for software of computer models used in product development and acceptance, qualification, series and other tests, as well as at later stages of the life cycle.

The classification of computer models is presented in GOST R 57700.22, general provisions on the use of digital twins of articles - in GOST R 57000.37. This standard introduces the following key concepts:

— Model adequacy - compliance of the model with the modelled article (process, phenomenon) according to the substantiated list of characteristics;

— Digital product model - a system of mathematical and computer models, as well as electronic product documents, describing the structure, functionality, and behavior of a product being developed or operated at various stages of the life cycle, for which, based on the results of digital and (or) other tests for GOST 16504 have been evaluated for compliance with the requirements;

— Digital product twins - a system consisting of the digital model of the product and bilateral information links with the product (if any) and/or its component parts;

— Model is the entity that reproduces a real-world phenomenon, object, or property of an object;

— Mathematical model - a model in which information about the modeling object is presented as mathematical characters and expressions.

2.2 Hybrid systems risk analysis issues

Because all socio-technical systems are subject to degradation processes, the entire life cycle - from marketing research to disposal - should be considered in assessing adequacy risks. Risk analysis includes steps to assess threat, damage and vulnerability scenarios. To ensure universal application, a series of international and national standards are being developed that define the terminology apparatus, concepts, impact assessment processes, management system requirements, and risk identification methodology for information technology applications.

The full risk analysis of technical systems using electronic models requires further development of appropriate methodologies and methods that take into account the stages of assessing threat, damage and vulnerability scenarios.

At the present stage of development, experimental tests are partly replaced or supplemented by calculation models. The use of such models makes it possible to predict the behavior of machines and systems in service conditions, assess their strength, durability, energy efficiency and safety, and conduct scenario analysis without the need to perform expensive or potentially dangerous physical tests.

The most important task is to define the conditions of use of digital twins, which allow experiments to be replaced by calculated models, taking into account the completeness, accuracy, and reliability of the results obtained. The key point is to select an appropriate criterion for evaluating model results. Researchers have pointed out the lack of a hierarchical framework for regulatory and technical documents that allow and regulate the application and scope of digital technologies. Thus, there is an objective need to describe the conditions of application of calculation models in regulatory and technical documentation, justification and legitimization of digital tests. Decisions to replace physical tests with calculation models must be made based on identification of local damage zones using documents in which risk indicators depend on assigned points (figure 2), to determine the significance of risks in deciding whether to conduct a physical experiment, computational simulation, or a combination thereof. The risk assessment for a point system is based on conventional approaches but requires verification and analysis of the effects of changing operating conditions [3, 6].

In order to achieve an acceptable level of risks for technical systems with embedded software, a graphical process risk analysis model using a hybrid (material and information) system based on a risk-oriented project-processing approach has been proposed (figure 3). The model takes into account challenges, threats, vulnerability and damage. Each of the subsystems - physical (machinery, design) and information (software) - is characterized by its own risks of non-compliance.

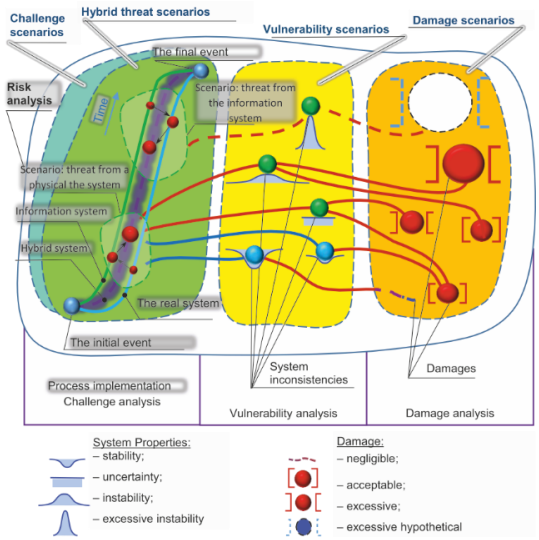


Fig. 3. Graphical risk analysis model of the technical system with hybrid - material and information - subsystem

It is necessary to consider a series of scenarios for identifying both the individual vulnerabilities of the hardware and information subsystems, and their mutual vulnerability due to the mutual influence of threats and vulnerabilities in each. A separate issue is the need to re-perform risk analysis because information systems may have adaptive functions; moreover, both stakeholder requirements and regulatory requirements change in the operation of technical systems. As a result, the vulnerabilities of hybrid systems are also transforming, necessitating a reassessment of whether an acceptable level of risk has been reached. For risk management of technical systems with built-in software, it is proposed to use the series of standards STB 1506, STB 2582 developed with the participation of authors, as well as the methodology of risk analysis FMEA.

In implementing a risk-based approach, the most important step is to synthesize design and engineering activities in the supply chain to reduce vulnerability. The

https://doi.org/10.56143/3030-3893-2026-3-175-179 A bridge between science and innovation

decision to allocate resources for technological improvements is determined by the degree of unacceptability of potential damage. The relationship between risk management at the strategic, operational, programmatic and project levels should be considered, since the acceptability of integrated risks is determined by the configurator, i.e. a system of a higher level than the one under consideration [7-10].

Risk-oriented thinking allows for the consideration of ways to reduce product and process risks by diagnosing and monitoring degradation processes, thereby preventing critical situations from occurring. Thus, acceptable risk is achieved without increasing product strength inventories - at the expense of timely prevention of adverse events. Figure 4 presents a developed model for achieving acceptable damage by preventing excessive risk through diagnostics and monitoring.

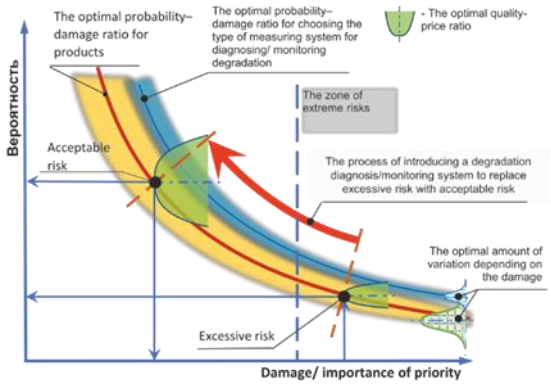


Fig. 4. Model for preventing excessive damage by diagnosing and monitoring degradation processes by changing the significance of consequences

Excessive damage can be prevented and reduced to an acceptable or negligible level by diagnosing and monitoring degradation processes using appropriate types and variations of measurement systems. The extrinsic hyperbolic "probability-damage" dependence is characteristic of a monitoring system. The parabolic dependence "quality - value" depends on the size of the damage and its significance, with the steepness of this dependence increasing as the significance of the damage increases. The acceptability of variation in product or process characteristics is reduced depending on the significance of damage and priorities. In conditions of high uncertainty, congestion and service life, an additional system of diagnostics and monitoring can reduce the cost of product creation and achieve replacement of excessive operational risk with acceptable.

3. Conclusion

The analysis confirms that the shift to a risk-oriented paradigm in transport engineering, and particularly in the railway industry, is an objective necessity. This necessity stems from the increasing complexity of technical systems, the integration of intelligent components, and the need to optimize costs while maintaining safety. Development of the methodological base, including harmonization of terminology, improvement of normative documentation and development of practical methods for risk assessment and management of hybrids (material-information) systems, provides a framework for achieving acceptable risk levels at all stages of the life cycle. Especially important are the validation and verification of digital models, the definition of conditions for their application in place of field tests, as well as the consideration of risk dualism when interaction between physical and information components. The models and approaches proposed in the work, including the hyperbolic "probability-damage" dependence, a point system for assessing the significance of risks and the concept of preventing excessive damage by means of monitoring, can serve as a basis for further research and practical implementation of risk-oriented design in transport engineering.

Acknowledgments

This work was supported by the framework of the State Program for Scientific Research 6.1.08 of the MPRI NASB and under the state assignment project FFGU-2024-0024 IMASH RAN

References

[1] N. A. Makhutov et al., Bezopasnost' Rossii. Pravovye, sotsial'no-ekonomicheskie i nauchno-tekhnicheskie aspekty. Tematicheskiy blok «Bezopasnost' zheleznodorozhnogo transporta». Nauchnye osnovy funktsional'noy bezopasnosti zheleznodorozhnogo transporta [Safety of Russia. Legal, Socio-Economic and Scientific-Technical Aspects. Thematic Block "Safety of Railway Transport". Scientific Foundations of Functional Safety of Railway Transport]. Moscow: MGOF "Znanie", 2023, p. 560 (in Russian).

[2] A. L. Kazakov and A. V. Dudakova, “Primenenie ontologicheskogo podkhoda dlya sozdaniya intellektual'noy sistemy upravleniya na zheleznodorozhnom transporte” [Application of an Ontological Approach to Create an Intelligent Control System in Railway Transport], Vestnik Ural'skogo gosudarstvennogo universiteta putey soobshcheniya [Herald of the Ural State University of Railway Transport], no. 3, pp. 33–41, 2019 (in Russian).

[3] A. N. Panov, I. I. Osmola, I. V. Shkadretsov, V. B. Lovkis, and L. A. Marinich, Nauchno-metodicheskie osnovy proektirovaniya: sistemnoe obespechenie priemlemykh riskov v avtotraktorosel'khozmashinostroenii [Scientific and Methodological Foundations of Design: System Ensuring of Acceptable Risks in Automotive, Tractor and Agricultural Engineering]. Minsk: BGATU, 2009, p. 486 (in Russian).

[4] M. Iansiti, “Technology integration: Managing technological evolution in a complex environment,” Research Policy, vol. 24, no. 4, pp. 521–542, Jul. 1995.

[5] L. N. Marchenko, I. N. Kavaliova, and V. V. Podgornaya, "Selection of a Base Vegetable Oil for the Development of a Biodegradable Lubricant Using the TOPSIS Method," Journal of Machinery Manufacture and Reliability, vol. 53, 2024, pp. 313-320.

[6] A. N. Panov and E. Yu. Romashova, "Osnovy metodologii risk-orientirovannogo proektirovaniya v mashinostroenii" [Fundamentals of the Methodology of Risk-Based Design in Mechanical Engineering], Mashinostroenie i inzhenernoe obrazovanie [Mechanical Engineering and Engineering Education], no. 1–2, pp. 8–16, 2024 (in Russian).

[7] A. Gill, "Non-Standard Risk Model for Applications in Railway Transport," Scientific Journal of Silesian University of Technology. Series Transport, vol. 124, pp. 63–76, 2024. doi: 10.20858/sjsutst.2024.124.5

[8] E. Nedeliakova, L. Lizbetinova, R. Stasiak-Betlejewska, and A. Sperka, "Application of the Reason model within risk management on railway crossings – A case study," Scientific Journal of Silesian University of Technology. Series Transport, vol. 109, pp. 129–140, 2020. doi: 10.20858/sjsutst.2020.109.12

[9] M. Bulakh, A. Okorokov, and D. Baranovskyi, "Risk System and Railway Safety," IOP Conf. Series: Earth and Environmental Science, vol. 666, no. 4, p. 042074, 2021. doi: 10.1088/1755-1315/666/4/042074

[10] F. Dinmohammadi, M. Shafiee, and B. Alkali, "A Risk-based Model for Inspection and Maintenance of Railway Rolling Stock," in Risk, Reliability and Safety: Innovating Theory and Practice, L. Walls, M. Revie, and T. Bedford, Eds. London: CRC Press, 2016, pp. 1165–1172. doi: 10.1201/9781315374987.

Information about the author

Inna Kavaliova	The State Scientific Institution "V. A. Belyi Metal-Polymer Research Institute of National Academy of Sciences of Belarus", Candidate of Engineering Sciences (Ph.D. in Eng.), Associate Professor E-mail: kavaliova@mpri.org.by, innakov2@mail.ru Tel.: +375297310096 https://orcid.org/0000-0002-8098-0568
Alexander Panov	Mechanical Engineering Research Institute of the Russian Academy of Sciences (IMASH RAN), Candidate of Engineering sciences (Ph.D. in Eng.), Laboratory of Digital Methods for Managing the Life Cycle of Engineering Products E-mail: aleksandrnikolayevich.panov@mail.ru Tel.: +7 9099905778 https://orcid.org/0009-0000-3791-551X
Ekaterina Romashova	Mechanical Engineering Research Institute of the Russian Academy of Sciences (IMASH RAN), Laboratory of Digital Methods for Managing the Life Cycle of Engineering Products, Researcher E-mail: romashova@imash.ru Tel.: +7 9099931759 https://orcid.org/0009-0002-5052-9319
Umida Ziyamukhamedova	Tashkent State Transport University, Department of Materials Science and Mechanical Engineering, Doctor of Technical Sciences (D.Sc.), Professor E-mail: z.umida1973@yandex.ru Tel.: +998911915665 https://orcid.org/0000-0001-5005-0477
Larysa Marchenko	Francisk Skorina Gomel State University, Candidate of Engineering Sciences (Ph.D. in Eng.), Associate Professor E-mail: lmarchenko@gsu.by, lamarchenko2309@gmail.com Tel.: +375296182928 https://orcid.org/0000-0003-2425-1720
Yuliya Podgornaya	State Scientific Institution "Institute of Mathematics of the National Academy of Sciences of Belarus", Master of Applied Mathematics and Computer Science E-mail: julipodgornaya652@gmail.com, julipodgornayafff@mail.ru Tel.: +375293988637 https://orcid.org/0009-0008-4299-4265
Victoriya Podgornaya	Higher Educational Establishment of the Federation of Trade Unions of Belarus «International University «MITSO» Gomel Branch, Ph.D. in Physical and Mathematical Sciences, Associate Professor E-mail: vvpodgornaya@mail.ru Tel.: +375293118104 https://orcid.org/0009-0008-3597-5648

Received: 6 August 2026 | **Accepted:** 17 September 2026 | **Published:** 30 September 2026

Development and localization of a manufacturing technology for cast center plates for 1520 mm gauge freight wagons

Y.Y. Abdukhalikov[1], T.T. Urazbaev[2][a], B.A. Abdunazarov[3], O.Kh. Achildiev[3]

[1]State Institution "Center for Improving the Efficiency of Projects and Procurement" under the Agency for Industrial Cooperation and Public Procurement, Tashkent, Uzbekistan

[2]Tashkent State Transport University, Tashkent, Uzbekistan

[3]JSC "Foundry and Mechanical Plant", Tashkent, Uzbekistan

Abstract: The present study addresses the scientific and engineering problem of developing and localizing a manufacturing technology for cast center plates for freight railway wagons operating on 1520 mm gauge railways, based on the production facilities of JSC "Foundry and Mechanical Plant" (Tashkent). The relevance of the research is determined by the need to establish local manufacturing of safety-critical freight wagon components using the available production equipment and commercially available grades of cast steel while ensuring compliance with the requirements of the applicable regulatory and technical documentation. According to GOST 34468-2018, the manufacture of cast center plates and center-plate seats is specified using steel grades 20FL, 20G1FL, 20GL, 20L, and 25L in accordance with GOST 977. For steel grade 25L, the carbon content shall not exceed 0.25%. The mechanical properties of cast center plates shall comply with the requirements of GOST 977. For cast center plates manufactured from the specified steel grades, the bearing and thrust surfaces shall have a hardness of at least 143 HB. In the present study, steel grades 20L and 25L are considered as the primary materials for localized production. These grades are characterized by lower cost compared with 20FL, 20G1FL, and 20GL, provided that the finished components meet the requirements of GOST 34468-2018 and GOST 977. The selection of a casting process is обусловлен by the absence of dedicated forging or stamping facilities for center plate production at JSC "Foundry and Mechanical Plant" and by the availability of an operating foundry capable of manufacturing center plates in sand-clay moulds. The technological capabilities of the plant include a 6-ton-capacity induction furnace manufactured by Otto Junker, an automatic moulding line manufactured by Kunkel Wagner, a normalizing furnace manufactured by JSC "Kerammash," laboratory equipment for quality control of the metal and finished castings, as well as metal-cutting equipment for subsequent machining operations. The objective of the study is to develop and provide a scientific and engineering justification for a localized manufacturing technology for cast center plates made of steel grades 20L and 25L using the existing production facilities of JSC "Foundry and Mechanical Plant" while ensuring compliance with the requirements of GOST 34468-2018. Particular attention is paid to the selection of the appropriate steel grade, optimization of the gating and feeding system, ensuring adequate mould filling and controlled solidification of the casting, minimizing the risk of casting defects, development of appropriate heat-treatment parameters, and experimental verification of the manufactured components against the applicable regulatory requirements.

Keywords: center plate, freight railway wagon, 1520 mm gauge, production localization, 20L steel, 25L steel, casting, sand-clay mould, induction furnace, gating and feeding system, heat treatment, mechanical properties, GOST 34468-2018

1. Introduction

Railway transport is one of the key components of the transport infrastructure supporting large-scale freight transportation. The reliability and operational safety of the freight wagon fleet largely depend on the quality and service reliability of critical components subjected to significant static and dynamic loads. [3]

One of the critical components of a freight wagon's central support assembly is the center plate. This component provides interaction between the wagon body and the bogie, transfers operational loads, and enables mutual rotation of the running-gear elements as the wagon moves through curved sections of track. [4]

For freight wagons operating on 1520 mm gauge railways, the technical requirements for center plates are regulated by GOST 34468-2018, "Center Plates for Freight Wagons of 1520 mm Gauge Railways. General Technical Conditions." The standard specifies requirements for the design, materials, manufacturing quality, acceptance, and inspection methods for center plates and center-plate seats. [1]

An important task in modern railway vehicle manufacturing and wagon repair is to reduce dependence on external supplies of critical spare parts and to establish local manufacturing technologies. For the Republic of

[a] https://orcid.org/0009-0006-1808-489X

Uzbekistan, this task is particularly important in developing an independent production base to support the maintenance and operation of the freight wagon fleet for 1520 mm gauge railways.

This study examines the feasibility of localizing center-plate production at JSC "Foundry and Mechanical Plant" in Tashkent. The enterprise has an operating foundry equipped with modern melting, moulding, heat-treatment, laboratory, and metal-cutting equipment. The existing production base provides the prerequisites for mastering center-plate manufacturing without establishing a separate stamping facility.

A major factor in selecting the manufacturing technology is the absence of stamping equipment required for producing forged or stamped center plates at the enterprise. At the same time, the plant has the technological capability to produce steel castings in sand-clay moulds. Therefore, a cast design of the center plate is proposed for production localization.

The choice of the casting technology is determined not only by the availability of appropriate equipment but also by the requirements of the regulatory documentation. GOST 34468-2018 permits the manufacture of cast center plates and center-plate seats from steel grades 20FL, 20G1FL, 20GL, 20L, and 25L in accordance with GOST 977. Thus, the casting method is normatively permissible, provided that the specified requirements for material, mechanical properties, hardness, geometry, and component quality are satisfied. [1]

Of particular interest is the possibility of using the relatively inexpensive cast-steel grades 20L and 25L instead of 20FL, 20G1FL, and 20GL. From the standpoint of production localization, the use of 20L and 25L may reduce the cost of the metallic charge and the finished component; however, the economic advantage must be considered together with compliance with the regulatory requirements for the quality and operational performance of the center plate.

The use of 25L steel requires particular control of its chemical composition, since GOST 34468-2018 limits the carbon content of this grade to no more than 0.25%. The mechanical properties of cast center plates shall comply with GOST 977. [2]

Accordingly, the main scientific and engineering problem is not merely the selection of a less expensive steel grade, but also establishing whether a cast center plate made of 20L and 25L steels can be produced that satisfies the requirements of GOST 34468-2018 using the existing equipment of JSC "Foundry and Mechanical Plant".

A 6-ton-capacity Otto Junker induction furnace is proposed for melting. Moulding is to be performed on an automatic Kunkel Wagner moulding line using sand-clay moulds. After casting, normalization is proposed in a furnace manufactured by JSC "Kerammash", followed by machining using the plant's existing metal-cutting equipment.

For quality assurance, the enterprise has laboratory facilities capable of analyzing the chemical composition and physical and mechanical characteristics of the metal and monitoring the quality of finished products. The availability of this equipment makes it possible to establish a complete manufacturing cycle for the center plate directly at the local production site.

An essential element in technology development is ensuring the quality of the cast metal. In the production of large steel castings, the possibility of shrinkage cavities and porosity, gas defects, non-metallic inclusions, hot cracks, and other defects must be considered. Therefore, the technology should account for the relationship between the chemical composition of the steel, melting parameters, pouring temperature, gating and feeding system design, mould-filling conditions, and solidification behavior. [6, 7, 8]

Particular attention should be paid to optimizing the gating and feeding system of the center plate. The component geometry, massive sections, and changes in cross-section may produce thermal nodes where conditions favorable for shrinkage defects can develop. Consequently, the rational design of metal delivery and feeding should be substantiated by analytical and experimental methods. [6, 7, 8]

Computer simulation of mould filling and metal solidification is a modern tool for addressing this problem. A computational approach makes it possible, before manufacturing a pilot batch, to evaluate the temperature field, filling sequence, solidification direction, and potential zones of shrinkage-defect formation. [9, 10]

Thus, the development of a localized center-plate manufacturing technology should be based on a comprehensive investigation of the following interrelationships: [6, 8, 9]

steel grade → chemical composition → melting parameters → pouring temperature → gating and feeding system → mould filling → solidification → casting defects → heat treatment → microstructure → mechanical properties → finished-component quality.

Research Objective

The objective of the study is to develop and scientifically and technically substantiate a localized technology for manufacturing cast center plates for 1520 mm gauge freight wagons from 20L and 25L steels at JSC "Foundry and Mechanical Plant" (Tashkent), using the existing foundry, heat-treatment, laboratory, and machining equipment while ensuring compliance with GOST 34468-2018.

Research Tasks

To achieve this objective, the following tasks must be addressed:

1. Analyze the structural and regulatory requirements for center plates of 1520 mm gauge freight wagons.
2. Analyze the requirements of GOST 34468-2018 and GOST 977 for materials used in cast center plates.
3. Substantiate the feasibility of using 20L and 25L steels as the primary materials for localized production.
4. Conduct a comparative analysis of 20L, 25L, 20FL, 20G1FL, and 20GL steels in terms of cost, chemical composition, castability, and required mechanical properties.
5. Develop a technological flow for manufacturing the center plate at JSC "Foundry and Mechanical Plant".
6. Determine rational melting parameters for 20L and 25L steels in the 6-ton Otto Junker induction furnace.
7. Develop or optimize the gating and feeding system for casting the center plate in a sand-clay mould.
8. Investigate mould filling and metal solidification.
9. Identify potential zones for shrinkage and other casting defects.
10. Develop heat-treatment schedules for the castings using the JSC "Kerammash" normalization furnace.

https://doi.org/10.56143/3030-3893-2026-3-180-185

11. Investigate the chemical composition, microstructure, and mechanical properties of 20L and 25L steels after casting and heat treatment.
12. Determine the hardness of the bearing and thrust surfaces of the center plate.
13. 13. Perform dimensional and non-destructive inspection of finished components.
14. Experimentally verify compliance of the manufactured center plates with GOST 34468-2018.
15. Conduct a technical and economic comparison of the localized casting technology with alternative stamped-center-plate manufacturing.
16. Determine the economic efficiency of using 20L and 25L steels under localized production conditions.

2. Research methodology

Analysis of GOST 34468-2018 Requirements for Center-Plate Materials and Manufacturing Method

GOST 34468-2018 provides for the manufacture of center plates by various methods, including cast production. For cast center plates and center-plate seats, the standard specifies steel grades 20FL, 20G1FL, 20GL, 20L, and 25L in accordance with GOST 977. For 25L steel, the carbon content shall not exceed 0.25%. The mechanical properties of cast center plates shall comply with GOST 977. Thus, the regulatory framework permits the use of 20L and 25L steels for the component under consideration. At the same time, inclusion of a steel grade in the list specified in GOST 34468-2018 does not, by itself, mean that every manufactured component automatically meets all requirements of the standard. Compliance must be confirmed by inspection and test results for the specific products. [2]

Accordingly, this study considers the use of 20L and 25L steels as the principal scientific hypothesis: with an appropriate selection of chemical composition, melting parameters, gating and feeding system, and heat treatment, 20L and 25L steels may be used to produce cast center plates complying with GOST 34468-2018 while reducing the material component of production cost.

Rationale for Selecting the Casting Technology

The selection of the casting technology for manufacturing the center plate is determined by a combination of technical and economic factors. [4, 5]

JSC “Foundry and Mechanical Plant” has an operating foundry comprising:

- a 6-ton Otto Junker induction furnace;
- an automatic Kunkel Wagner moulding line;
- equipment for producing and preparing sand-clay moulds;
- a normalization furnace manufactured by JSC “Kerammash”;
- laboratory equipment for metal quality control;
- metal-cutting equipment for machining castings.

Thus, implementation of the casting technology does not require the establishment of a fundamentally new production unit.

The proposed technological sequence is as follows: preparation of charge materials → charge loading → melting in the induction furnace → chemical-composition control → composition adjustment → temperature control → metal tapping → preparation of the sand-clay mould → mould assembly → pouring → solidification → shakeout → casting cleaning → visual and instrumental inspection → normalization → machining → final center-plate inspection.

The use of the automatic Kunkel Wagner moulding line makes it possible to ensure stable mould geometry and reproducibility of moulding parameters. The existing 6-ton Otto Junker induction furnace enables industrial melting of steel for pilot and subsequent serial production of center plates. The availability of the JSC “Kerammash” normalization furnace allows heat treatment to be incorporated into a single localized production cycle.

Rationale for Selecting 20L and 25L Steels

The main focus of the study is to assess the feasibility of using 20L and 25L steels instead of the more expensive grades 20FL, 20G1FL, and 20GL. [4, 6]

In accordance with GOST 34468-2018, all of the listed grades are specified for the manufacture of cast center plates. Therefore, the comparison should be based on a combination of operational and economic indicators.

The economic advantage of 20L and 25L steels should not be assessed solely by the cost per tonne of steel, but by the final cost of the center plate:

$C_{cp} = C_{met} + C_{melt} + C_{mould} + C_{heat} + C_{mach} + C_{ins} + C_{ovh}$,

where C_{cp} is the cost of the finished center plate; C_{met} is the cost of the metallic charge; C_{melt} is melting cost; C_{mould} is moulding cost; C_{heat} is heat-treatment cost; C_{mach} is machining cost; C_{ins} is inspection cost; and C_{ovh} is overhead cost.

This approach will make it possible to quantify the economic effect of production localization.

Production Facilities of JSC “Foundry and Mechanical Plant”

The study uses the existing production infrastructure of JSC “Foundry and Mechanical Plant”.

Table 1

Technological Equipment Used for Production Localization

Technological Operation	Equipment	Primary Purpose
Melting	Otto Junker induction furnace, 6 t	Steel melting
Moulding	Kunkel Wagner automatic moulding line	Production of sand-clay moulds
Heat treatment	JSC “Kerammash” normalization furnace	Normalization of castings
Inspection	Laboratory equipment	Chemical composition and properties
Machining	Metal-cutting machines	Achieving final dimensions
Non-destructive testing	To be specified	Inspection of internal/surface defects

Thus, the proposed process assumes maximum utilization of the plant’s existing equipment.

This is one of the key principles of localization: the technology is developed not by establishing an entirely new production facility, but by adapting the existing technological infrastructure to manufacture a new safety-critical component.

Materials and Methods

The study involves two principal steel grades—20L and 25L. At the first stage, the chemical composition of each heat is determined. For 25L steel, particular attention must be paid to carbon content because GOST 34468-2018 limits it to no more than 0.25%.

The analysis should include carbon, silicon, manganese, sulfur, phosphorus, chromium, nickel, copper, and other elements in accordance with the applicable requirements for the selected steel grade. [2]

After obtaining pilot castings, the following characteristics are to be investigated: chemical composition, mechanical properties, hardness, microstructure, geometric parameters, surface quality, internal defects, and the results of heat treatment.

Proposed Experimental Research Methodology

The study should be conducted according to the following sequence.

Stage 1. Investigation of the Existing Technology

The following parameters are determined:

- casting mass;
- mass of gating elements;
- mass of risers;
- yield of sound castings;
- pouring temperature;
- chemical composition;
- moulding parameters;
- existing gating-system design;
- type and quantity of rejected castings.

Stage 2. Simulation

The following are calculated:

- mould filling;
- temperature field;
- solidification time;
- solidification direction;
- potential shrinkage zones;
- probability of porosity formation.

Stage 3. Optimization

Based on the simulation results, the following parameters are adjusted: [9, 10]

- gating-channel dimensions;
- number of feeders;
- riser locations;
- metal-entry locations;
- dimensions of system elements.

Stage 4. Manufacture of Pilot Castings

Pilot center plates are manufactured from 20L and 25L steels.

Stage 5. Heat Treatment

The castings are subjected to normalization using the JSC “Kerammash” furnace.

Stage 6. Property Characterization

The following properties are determined:

- ultimate tensile strength;
- yield strength;
- elongation;
- reduction of area;
- impact toughness;
- hardness;
- microstructure.

Stage 7. Finished-Component Inspection

The following inspections are performed:

- dimensional inspection;
- visual inspection;
- surface inspection;
- non-destructive testing;
- inspection of working surfaces.

Stage 8. Comparison with GOST Requirements

The obtained results are compared with the regulatory requirements of GOST 34468-2018 and GOST 977. [1, 2]

Scientific Hypothesis

The scientific hypothesis of this study is that the use of 20L and 25L steels in combination with an optimized casting technology using sand-clay moulds, a rational gating and feeding system, and normalization will make it possible to produce a center plate for a 1520 mm gauge freight wagon that complies with GOST 34468-2018. At the same time, the use of the less expensive 20L and 25L grades compared with 20FL, 20G1FL, and 20GL is expected to reduce the material component of the product cost. This hypothesis requires experimental verification based on a comprehensive set of indicators: [6, 7]

$$H_0: \begin{cases} C \le C_{\text{ГОСТ}}, \\ \sigma_B \ge [\sigma_B], \\ \sigma_T \ge [\sigma_T], \\ \delta \ge [\delta], \\ KCU \ge [KCU], \\ HB \ge 143, \\ D_{\text{факт}} \le D_{\text{доп}}. \end{cases}$$

where the normative values of mechanical properties and geometric tolerances shall be determined from the relevant sections of GOST 34468-2018 and GOST 977 for the specific center-plate design.

Expected Scientific Novelty

The expected scientific novelty of the study consists in:

1. establishing rational parameters for manufacturing center plates from 20L and 25L steels in sand-clay moulds;
2. determining the relationship between gating and feeding system parameters and defect formation in the cast preform;
3. determining the effect of melting and heat-treatment parameters on the structure and mechanical properties of the center-plate metal; [4, 5]
4. experimentally confirming the feasibility of producing a center plate from 20L and/or 25L steel that complies with GOST 34468-2018;
5. developing a technological basis for localized center-plate production using the existing production facilities of JSC “Foundry and Mechanical Plant”. [4, 5]

Practical Significance

The practical significance of the study lies in establishing a technological basis for organizing the production of cast center plates for 1520 mm gauge freight wagons in the Republic of Uzbekistan.

The use of the existing equipment of JSC “Foundry and Mechanical Plant” minimizes the need for capital investment in a new production complex.

The technology based on the available:

- 6-ton Otto Junker induction furnace; [4, 5]
- automatic Kunkel Wagner moulding line;
- JSC “Kerammash” normalization furnace;

https://doi.org/10.56143/3030-3893-2026-3-180-185 A bridge between science and innovation

- laboratory facilities;
- metal-cutting equipment

makes it possible to organize the complete technological cycle for manufacturing the component at a single production site.

The expected economic effect may be achieved through:

- use of more readily available steel grades;
- use of existing foundry equipment;
- elimination of the need to establish stamping production;
- reduction of external supplies;
- reduction of transportation costs;
- shorter delivery times;
- organization of serial production.

3. Conclusion

The study addresses the scientific and engineering problem of localizing the production of center plates for 1520 mm gauge freight wagons at JSC "Foundry and Mechanical Plant" in Tashkent.

The principal technological solution considered is the manufacture of the center plate by casting in a sand-clay mould, followed by normalization and machining.

The choice of the casting method is determined by the availability of the required production facilities at the enterprise and the absence of stamping production. At the same time, cast center plates are provided for by GOST 34468-2018, which allows this method to be considered normatively permissible when the specified requirements for the finished component are met. [1]

20L and 25L steels were selected as the principal materials for the study. Their use for manufacturing cast center plates is provided for by GOST 34468-2018. For 25L steel, particular attention must be paid to compliance with the carbon-content limit of no more than 0.25%. [1, 2]

The proposed technology is oriented toward maximum utilization of the plant's existing equipment: the 6-ton Otto Junker induction furnace, the automatic Kunkel Wagner moulding line, the JSC "Kerammash" normalization furnace, laboratory equipment, and metal-cutting machines.

The main direction of further research is experimental verification of the feasibility of producing high-quality cast center plates from 20L and 25L steels that comply with GOST 34468-2018, as well as determination of their production cost-effectiveness. [6, 7, 11]

A final assessment of the proposed technology should be based on a comparative analysis of the chemical composition, mechanical properties, hardness, microstructure, dimensional accuracy, surface quality, internal defects, and cost of the manufactured components. [6, 11]

References

[1] GOST 34468-2018. Center Plates for Freight Wagons of 1,520 mm Gauge Railways. General Technical Conditions.

[2] GOST 977. Steel Castings. General Technical Conditions.

[3] GOST 33211-2014. Freight Main-Line Railway Wagons. Strength and Dynamic Performance Requirements.

[4] Olshevskiy A., Kim C.W., Yang H., Olshevskiy A. Wear simulation for the centre plate arrangement of a freight car // Vehicle System Dynamics. 2015. Vol. 53, No. 6. P. 856–876. DOI: 10.1080/00423114.2015.1023319.

[5] Muradian L.A., Podosonov D.O. Improving TBO of freight car bogies. Geometry model of center pad wear // Science and Transport Progress. 2017. DOI: 10.15802/stp2017/92533.

[6] Makino T., Shimokawa Y., Yamamoto M. Fatigue Property and Design Criterion of Cast Steel for Railway Bogie Frames // Materials Transactions. 2019. Vol. 60, No. 6. P. 950–958. DOI: 10.2320/matertrans.Z-M2019814.

[7] Yu L.Y., Zhao Y.X. Fatigue Limit Measurement of the Cast Steel for Chinese Railway Rolling Wagon Bogie Frames // Advanced Materials Research. 2010. Vols. 118–120. P. 121–125. DOI: 10.4028/www.scientific.net/AMR.118-120.121.

[8] Campbell J. Complete Casting Handbook: Metal Casting Processes, Metallurgy, Techniques and Design. 2nd ed. Oxford: Butterworth-Heinemann, 2015. 1054 p. ISBN 978-0-444-63509-9. DOI: 10.1016/C2014-0-01548-1.

[9] Campbell J. Casting Practice: Guidelines for Effective Production of Reliable Castings // ASM Handbook. Vol. 15: Casting. ASM International, 2008. P. 497–505. DOI: 10.31399/asm.hb.v15.a0005277.

[10] DasGupta R. Common Defects in Various Casting Processes // ASM Handbook. Vol. 15: Casting. ASM International, 2008. P. 1192–1202. DOI: 10.31399/asm.hb.v15.a0005344.

[11] Poweleit D. Selection and Evaluation of Steel Castings // ASM Handbook. Vol. 15: Casting. ASM International, 2008. P. 975–986. DOI: 10.31399/asm.hb.v15.a0005330.

[12] Shape Casting of Steel // ASM Handbook. Vol. 15: Casting. ASM International, 2008. P. 926–948. DOI: 10.31399/asm.hb.v15.a0005299.

Information about the author

Yerdaulet Abdukhalikov	Lead Specialist, State Institution "Center for Improving the Efficiency of Projects and Procurement" under the Agency for Industrial Cooperation and Public Procurement E-mail: ye.abduxalikov@expertcenter.uz Tel.: +998998410859
Talgat Urazbaev	Associate Professor, Department of Materials Science and Mechanical Engineering, Tashkent State Transport University, PhD E-mail: talgat_1988.26@mail Tel.: +998974301088 https://orcid.org/0009-0006-1808-489X
Bakhtiyor Abdunazarov	Head of the Foundry Complex, JSC "Foundry and Mechanical Plant"

E-mail: baxa_863@mail.ru
Tel.: +998 91 166 23 34

o.a._surxon@mail.ru
Tel.: +998 77 371 40 49

Odil Achildiev Chief Metallurgist, JSC "Foundry and Mechanical Plant"
E-mail:

https://doi.org/10.56143/3030-3893-2026-3-180-185

Received: 6 August 2026 | **Accepted:** 17 September 2026 | **Published:** 30 September 2026

Study of the impact of heavy trucks on the smoothness of asphalt concrete pavement

A. Urakov[1][a], E. Ashurov[2][b]

[1]Tashkent State Transport University, Tashkent, Uzbekistan

[2]Termez State University of Engineering and Agrotechnologies, Termez, Uzbekistan

Abstract: This article examines the significant increase in traffic flow on the 1315–1458 km section of the M-39 “Almaty–Bishkek–Tashkent–Shahrisabz–Termez” highway located in the southern region of the republic, and investigates the effect of heavy freight vehicles on the smoothness of asphalt concrete pavement, particularly the formation of wheel-path rutting. The study analyses the elastic and plastic deformations occurring in the pavement under heavy truck loads, the deterioration of pavement smoothness and the reduction in pavement service life. The longitudinal roughness of the 1360–1425 km section was surveyed in both directions with the “TRASSA” mobile road laboratory complex and evaluated against the International Roughness Index (IRI). The mean measured index is 1.76 m/km in the Tashkent–Termez direction and 1.49 m/km in the Termez–Tashkent direction, while 8.4 % and 3.7 % of the surveyed length respectively exceed the permissible value of 3 m/km established for category I roads; the maximum recorded value reaches 8.08 m/km. On this basis engineering recommendations were developed to improve the transport and operational condition of the pavement.

Keywords: asphalt concrete pavement, smoothness, heavy truck, deformation, IRI, deflection, traffic flow

1. Introduction

At present, the increasing traffic volume on highways, especially the growth in the number of heavy trucks, has a significant impact on the operational condition of road pavements. The axle loads of heavy freight vehicles operating on national and international roads cause various deformations in asphalt concrete pavements, leading to a deterioration of the pavement smoothness indicators.

The smoothness of a road pavement depends on several factors and is one of the main parameters determining traffic safety, fuel consumption, driving speed and passenger comfort. The deterioration of pavement smoothness results in increased vehicle operating costs and a reduction of the pavement service life [1].

Therefore, investigating the impact of heavy trucks on the smoothness of asphalt concrete pavement is considered one of the urgent scientific and practical issues in the field of highway engineering. The aim of the present work is to determine, from field measurements on an operating international highway, how the share of heavy trucks in the traffic flow is reflected in the longitudinal roughness of the asphalt concrete pavement, and to compare the measured values with the permissible standard indicators.

2. Research methodology

The methodology of this study is aimed at determining the impact of heavy trucks within the traffic flow on the smoothness of asphalt concrete pavement, evaluating the deformations formed in the pavement, and identifying the patterns of change in the smoothness indicators.

The smoothness of the asphalt concrete pavement was evaluated on the basis of the International Roughness Index (IRI). A number of scholars have conducted research in this field, including O.A. Krasikov, E.V. Uglova, F.B. Matvienko, A.K. Birulya, A.P. Vasilev, I.S. Sadikov, A.X. Urakov and A.G. Yunusov [3].

Smoothness is a transport-operational indicator that characterises the levelness of a road pavement surface. Pavement smoothness is evaluated through the vertical vibrations generated during vehicle movement. In international practice, pavement smoothness is mainly determined using the IRI (International Roughness Index) indicator [2].

The longitudinal smoothness of highway pavements is assessed in accordance with IQN 05-2011 “Rules for diagnostics and evaluation of highway conditions” by comparing the measured values with the permissible standard indicators (Table 1); the road categories themselves are assigned in accordance with ShNQ 2.05.02-07 [6]. If the actual value of the smoothness indicator is less than or equal to the allowable value, the pavement is considered to meet the required operational standards in terms of smoothness [5].

[a] https://orcid.org/0000-0001-8404-3013

[b] https://orcid.org/0009-0005-5885-0133

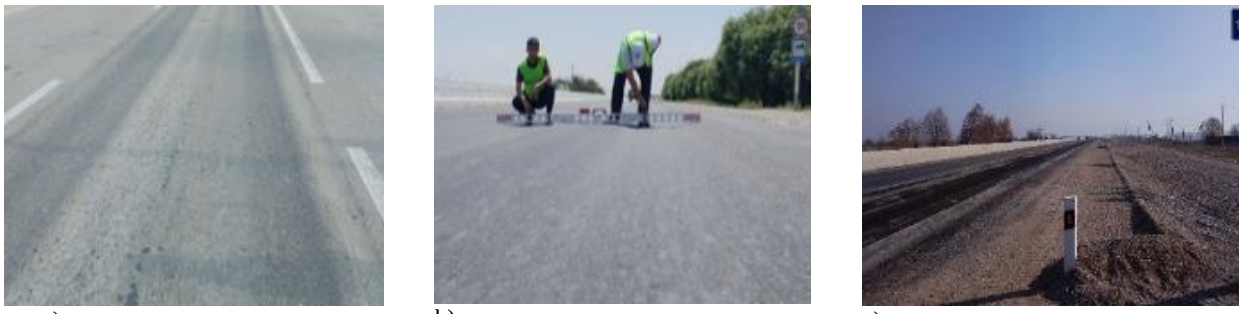
Table 1

Permissible values of the longitudinal roughness index according to IQN 05-2011

Traffic intensity, veh/day	Road category	Pavement type	Longitudinal roughness index based on IRI, m/km
more than 7000	I	Capital	3.0
3000–7000	II	Capital	3.5
1000–3000	III	Capital	4.0
1000–3000	III	Lightweight	4.5
500–1000	IV	Lightweight	5.0
200–500	IV	Transitional	5.5
less than 200	V	Lower	6.0

The reconstruction project of the 1315–1458 km (143 km) section of the international M-39 "Almaty–Bishkek–Tashkent–Shahrisabz–Termez" highway, passing through the Surkhandarya region in the southern part of the republic, was implemented with international investment funds [9, 10]. Currently, the traffic flow along this road section is increasingly composed of foreign-made vehicles with high dynamic characteristics.

In this area, the Sherabad Cement Plant and several Sherabad construction material quarries are located. The excessive axle loads of the transported cargo, which exceed the permissible axle load standards, as well as the formation of wheel-path rutting on the pavement surface, have resulted in noticeable pavement roughness and unevenness [4].



a) b) c)

Fig. 1. Wheel-path rutting and pavement roughness deformations on the 1400–1420 km section of the M-39 "Almaty–Bishkek–Tashkent–Shahrisabz–Termez" highway

The process of the development of pavement smoothness deformations under the impact of heavy trucks within the traffic flow is occurring very rapidly on these highways.

During the experimental studies carried out on the research section, investigations were conducted using the "TRASSA" mobile road laboratory complex, which is designed to evaluate the transport-operational characteristics of highways. The pavement condition was assessed on the basis of the International Roughness Index (IRI) indicator [2].



a) b) c)

Fig. 2. "TRASSA" mobile road laboratory complex: a) general view; b) operator workstation; c) measuring equipment

Using the FORD "TRASSA" mobile road laboratory complex, monitoring studies were conducted on the 1360–1425 km (65 km) section of the M-39 "Almaty–Bishkek–Tashkent–Shahrisabz–Termez" highway. As a result of these investigations, the following parameters were measured,

https://doi.org/10.56143/3030-3893-2026-3-186-190 A bridge between science and innovation

evaluated and simultaneously analysed in an electronic database:

– geometric parameters (longitudinal and transverse smoothness, traveled road length);

– longitudinal smoothness based on the International Roughness Index (IRI);

– pavement structural strength using the DINA 4 (FWD) dynamic loading device, in accordance with MKN 52-2008 [7] and GOST 32729–2014 [8];

– traffic intensity and traffic flow composition.

3. Results and discussion

The results of the monitoring studies conducted on the 1360–1425 km section of the M-39 "Almaty–Bishkek–Tashkent–Shahrisabz–Termez" highway showed that as the proportion of heavy trucks in the traffic flow increases, the smoothness indicators of the asphalt concrete pavement deteriorate. The measurements cover 67.7 km of carriageway in each direction with a recording step of 100 m.

Particularly in the southern regions, under high summer temperatures, the softening of the asphalt concrete pavement accelerates the formation of longitudinal ruts (wheel-path rutting). On roads with a high daily volume of heavy trucks, pavement deflection increases significantly. According to the results, the increase in the number of freight vehicles accelerates pavement unevenness and deformation processes [4].

Table 2

Longitudinal roughness indicators measured on the 1360–1425 km section of the M-39 "Almaty–Bishkek–Tashkent–Shahrisabz–Termez" highway

Indicator	Tashkent–Termez	Termez–Tashkent
Surveyed length, km	67.7	67.7
Mean IRI, m/km	1.76	1.49
Median IRI, m/km	1.54	1.31
Maximum IRI, m/km	8.08	5.44
Length with IRI > 3 m/km, %	8.4	3.7
Length with IRI > 4 m/km, %	3.1	0.9
Length with IRI > 5 m/km, %	1.2	0.3

The measured roughness profiles are presented in Figures 3–5. In the Tashkent–Termez direction the mean value of the index is 1.76 m/km and 8.4 % of the surveyed length exceeds the permissible value of 3 m/km established for category I roads; in the Termez–Tashkent direction the corresponding values are 1.49 m/km and 3.7 %. The maximum recorded value, 8.08 m/km, is 2.7 times the permissible one. The asymmetry between the two directions corresponds to the predominant direction of loaded heavy vehicles moving from the Sherabad quarries and cement plant.

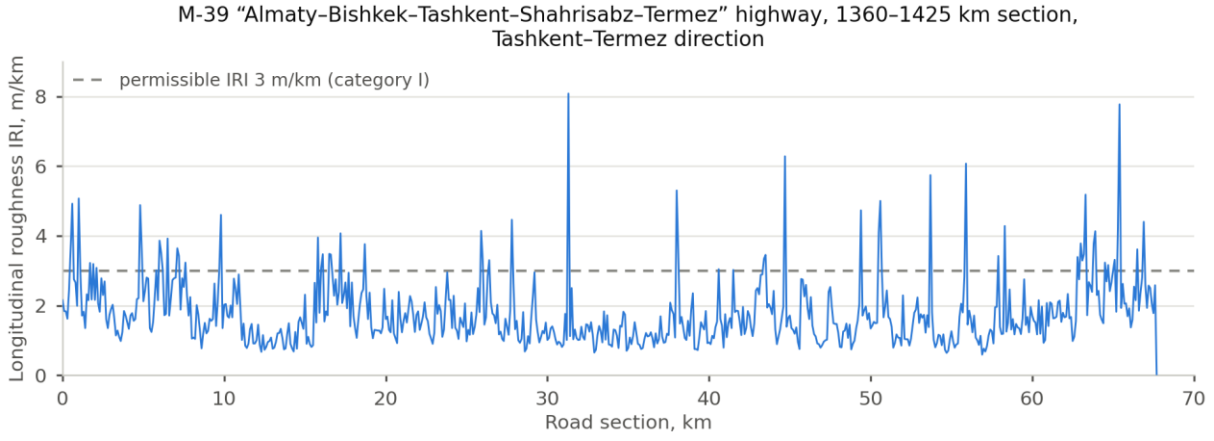


Fig. 3. Longitudinal roughness along the Tashkent–Termez direction on the 1360–1425 km section of the M-39 "Almaty–Bishkek–Tashkent–Shahrisabz–Termez" highway

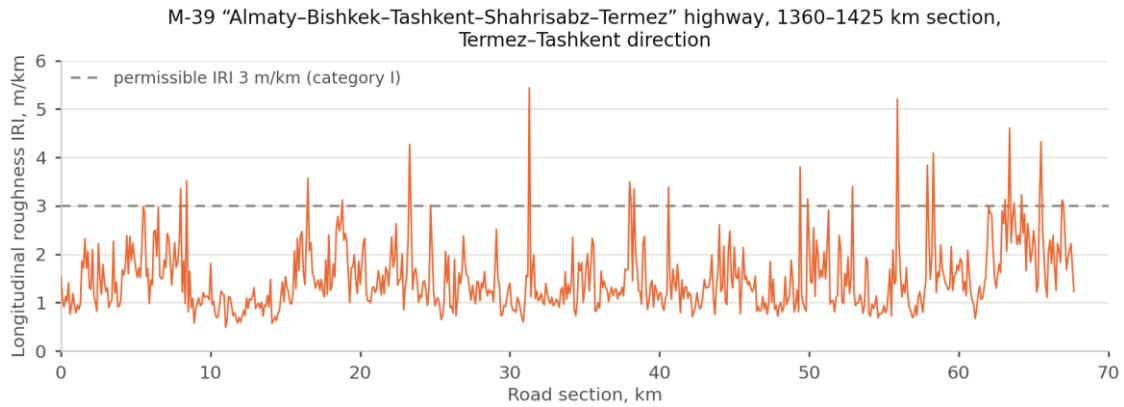


Fig. 4. Longitudinal roughness along the Termez–Tashkent direction on the 1360–1425 km section of the M-39 “Almaty–Bishkek–Tashkent–Shahrisabz–Termez” highway

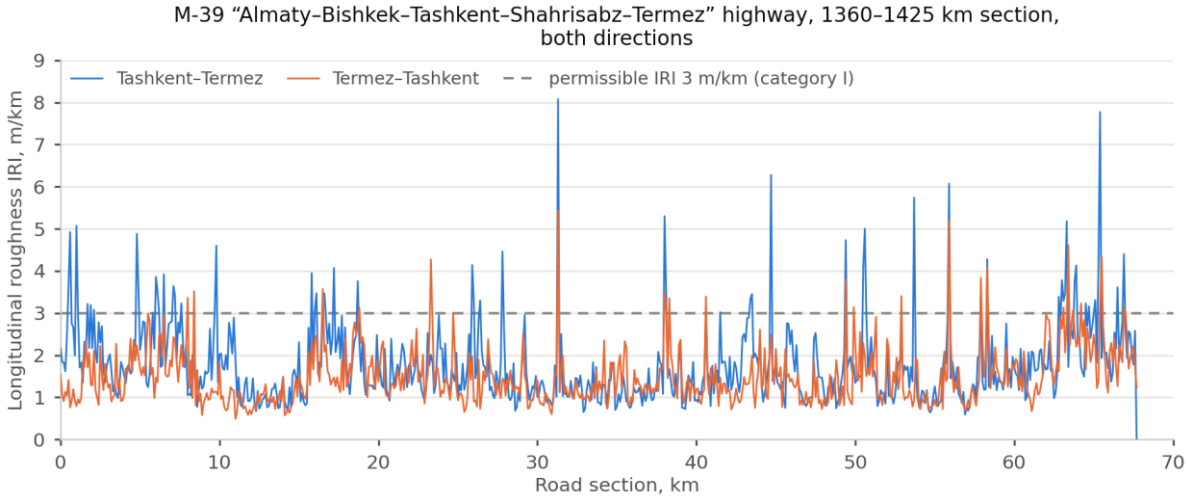


Fig. 5. Comparison of the longitudinal roughness in both directions on the 1360–1425 km section of the M-39 “Almaty–Bishkek–Tashkent–Shahrisabz–Termez” highway

The pavement smoothness of the carriageway was evaluated against the required International Roughness Index values, and the corresponding permissible limits are shown in Figures 3–5 as a dashed line. The sections where the measured index systematically exceeds this limit are concentrated in the zones of intensive heavy-vehicle loading, which confirms the connection between the traffic flow composition and the rate of deterioration of the pavement smoothness.

4. Conclusion

1. The research findings revealed that the increasing longitudinal pavement irregularities (wheel-path rutting) observed on the 1360–1425 km section of the M-39 “Almaty–Bishkek–Tashkent–Shahrisabz–Termez” highway indicate the negative impact of heavy trucks within the traffic flow on the smoothness of the asphalt concrete pavement. Repeated exposure to high axle loads causes elastic and plastic deformations in the pavement structure, resulting in the deterioration of the pavement smoothness indicators.

2. In the Tashkent–Termez direction 8.4 % of the surveyed length, and in the Termez–Tashkent direction 3.7 %, do not meet the permissible roughness value of 3 m/km for category I roads; the mean values are 1.76 and 1.49 m/km respectively. The difference between the directions reflects the predominant direction of the loaded heavy vehicle flow.

3. The studied highway is located in a hot climatic region, where not only the intensity of heavy freight transportation is increasing, but pavement deflection and deformation are also becoming more severe under such conditions. Therefore, during the design and operation of highways, it is essential to take into account the composition of the traffic flow, particularly the proportion of heavy trucks.

4. For the sections where the permissible roughness value is exceeded, it is advisable to carry out axle-load control of heavy vehicles, to plan levelling layers within the maintenance programme, and to repeat the IRI survey after the repair works in order to evaluate their effectiveness.

References

[1] Sodikov I.S. Transport and operational performance indicators of highways. Textbook. Tashkent: TAYLQEI, 2019. https://library.samdpi.uz/ebooks/view?id=15478

[2] Urakov A.X. Technologies for maintenance and repair of highways. Textbook. Tashkent: TAYLQEI, 2019. https://unilibrary.uz/literature/50239

[3] Yunusov A.G., Xoliqov B.A., Soataliev R.R. Modern methods for evaluating the transport and operational indicators of road pavements. Study guide. Tashkent: TAYLQEI, 2020. https://unilibrary.uz/literature/104344

[4] Urakov A.X., Ashurov E.T. Problems caused by heavy truck traffic on asphalt concrete pavement surfaces. https://www.researchgate.net/publication/394724693

[5] IQN 05-2011. Rules for diagnostics and evaluation of highway conditions. Tashkent, 2012.

[6] ShNQ 2.05.02-07. Highways. Tashkent: Davarxitektqurilish, 2008. https://lex.uz/docs/4444014

[7] MKN 52-2008. Guidelines for assessing the strength of flexible pavements and calculating their strengthening. https://lex.uz/docs/1331535

[8] GOST 32729–2014. Automobile roads of general use. Method for measuring the elastic deflection of flexible pavement structures to determine strength. Moscow: Standartinform, 2014.

[9] Committee for Roads of the Republic of Uzbekistan. Official site. https://gov.uz/oz/uzavtoyul

[10] “Surxondaryo avtomobil yo‘llari” unitary enterprise. Official site. https://www.surxondaryoavtoyul.uz/.

Information about the author

Asliddin Urakov	Tashkent State Transport University, Faculty of Road Engineering, Doctor of Technical Sciences (DSc), Professor Tel.: +998 97 784 26 08 https://orcid.org/0000-0001-8404-3013
Elyor Ashurov	Termez State University of Engineering and Agrotechnologies, Department of Road Engineering, Assistant E-mail: ashurovelyor18@gmail.com Tel.: +998 90 247 33 90 https://orcid.org/0009-0005-5885-0133

CONTEXT / MUNDARIJA

Kh. Tuychiev, Kh. Tuychiev
Assessment and improvement of constructive safety of the Damas light passenger vehicle.....**5**

A. Azizov, F. Sindarov
Comparison of the switch control circuit with main supply and central supply circuit, and analysis of the sequence of operation of the HTIC block.....**10**

O. Khamidov, B. Gayratov, Sh. Kudratov, F. Djuraev
An intelligent diagnostic approach based on oil analysis for assessing the technical condition of diesel locomotive engines.....**14**

O. Shokirov
Scientific and practical justification of safe vehicle speeds in mountainous areas of the M-39 highway of international importance.....**18**

M. Sobirov, A. Hamidov
Security analysis of windows local authentication recovery techniques and defensive mechanisms.....**24**

U. Ziyamukhamedova, J. Nafasov, E. Turgunaliev, B. Nematov, D. Akhmedova
Investigation of the tribological properties of modified composite materials used under abrasive wear conditions **28**

J. Djumanov, M. Sobirov
A multi-layer information model and adaptive algorithms for monitoring hybrid energy supply in IoT-based telecommunication networks **33**

D. Yusupov, O. Kutbidinov, B. Avazov
Assessment of the technical condition of a transformer based on the operational parameters of its oil using the fuzzy logic method.....**38**

E. Abdurahmanova
Application of artificial intelligence in modeling non-stationary oil filtration in multilayer porous media and data reliability issues.....**46**

K. Musulmanov, U. Sangirov, M. Abdullaeva
Assessment of cycling infrastructure and bikeability in Tashkent city.....**50**

D. Yusupov, B. Avazov, O. Kutbidinov
Assessment of the technical condition of a transformer based on the operational parameters of its oil using the fuzzy logic method.....**54**

CONTENT / MUNDARIJA

T. Alimov, J. Shukurov, Y. Ergashev, N. Abdujabarov
An integrated framework for multidisciplinary design optimization of unmanned aerial vehicles……..**61**

E. Khujamkulov
Digital national microprocessor-based semi-automatic interlocking system for improving the throughput capacity of Uzbekistan Railways……..**67**

O. Mukhitdinov, S. Khudaykulov, D. Kaniev
Energy equations of a channel suspension-carrying flow with full account for the work of interphase interaction forces……..**71**

Mu Zhendi
Network diagnosis and governance-coupled optimization in seaport–dry port multimodal transport corridors under the Maritime Silk Road……**78**

N. Sotivoldieva
Scientific and theoretical foundations of resource management in ensuring product quality and safety at light industry (sewing and knitting) enterprises……..**87**

B. Botirov
Experimental investigation of mechanical properties of A-III reinforcing steel bars with a diameter of 10 mm……..**92**

Kh. Abduvokhidov, Z. Juraev
Practical principles for reducing risks arising from measurement parameters in equipment operation (on the example of an artificial lung ventilation apparatus) ……..**96**

O. Khamidov, Sh. Samatov, B. Gayratov, A. Djuraev
Analysis of artificial neural network applications for assessing the technical condition of traction transformers in electric locomotives……..**105**

I. Makhamataliev, V. Soy, N. Mukhammadiev, F. Abdukayumov, N. Erdanov, Sh. Uzakov, A. Jumageldiev
Concrete based on low-strength carbonate rocks……..**109**

S. Cavadov
Investigation of ionizing radiation-induced conductivity and relaxation kinetics in porous polymer and metal-oxide nanocomposites……..**113**

CONTEXT / MUNDARIJA

O. Khamidov, Sh. Samatov, B. Gayratov, A. Djuraev
Improving the reliability of the TD802 direct-current traction generator of the ChME3 shunting diesel locomotive through insulation replacement……118

U. Turdialiev, D. Boykishieva
Assessing the impact of integrating lean manufacturing methods into the quality management system on the efficiency of a mechanical engineering enterprise……125

B. Sobirov, N. Botirova
Use of mineral fillers for PVC-based linoleum production and investigation of their physical and mechanical properties……130

G. Uzakov, M. Majidova
Development of an artificial intelligence-based adaptive digital twin method for early fault detection and energy loss reduction in solar photovoltaic systems……133

U. Khamrokulov
Precast–monolithic frame building system based on permanent reinforced concrete shell formwork: Analysis of world practice and experimental substantiation……138

Z. Kurbonov, S. Bozorboev
Mechanically induced surface modification of diabase aggregate for high-performance concrete……144

Z. Kurbonov, S. Bozorboev, I. Egamberdiev
Optimization of fine-grained concrete composition for hydraulic structures using chemical admixtures……149

D. Bekmirzaev, I. Mirzaev, R. Yuldoshev
An automated system for assessing the seismic resistance of buildings and structures using regulatory documents……155

R. Ametov, J. Mustafakulov
Types and properties of mineral fillers used in the production of ceramzit concrete……159

F. Khasanov
Structure, magnetostructural transformations and magnetocaloric properties of Heusler alloys and the MnAs compound: a review……163

CONTEXT / MUNDARIJA

O. Berdiev, O. Zafarov, E. Urishbaev
Complex chemical admixture intended for improving the properties of concrete mixture……168

I. Kavaliova, A. Panov, E. Romashova, U. Ziyamukhamedova, L. Marchenko, Y. Podgornaya, V. Podgornaya
A risk-oriented approach to the development of transport systems with embedded information technologies……175

Y. Abdukhalikov, T. Urazbaev, B. Abdunazarov, O. Achildiev
Development and localization of a manufacturing technology for cast center plates for 1520 mm gauge freight wagons……180

A. Urakov, E. Ashurov
Study of the impact of heavy trucks on the smoothness of asphalt concrete pavement……186